



**Chemical Synthesis and Pharmacological Testing of
Novel CXCL12 Inhibitors with Characterisation of
Signalling Pathways Regulating CXCL12
Expression in Bone Cancer**

By

MOHAMMED SINJAR FARHAN

**A thesis submitted in the fulfilment of the requirements for the degree of
Doctor of Philosophy**

2025

Strathclyde Institute of Pharmacy and Biomedical Sciences (SIPBS), Glasgow,
UK

Author's Declaration

This thesis is the result of the author's original research. It has been composed by the author and has not been previously submitted for examination, which has led to the award of a degree.

The copyright of this thesis belongs to the author under the terms of the United Kingdom Copyright Act, as qualified by the University of Strathclyde Regulation 3.50. Due acknowledgment must always be made to the use of any material contained in or derived from this thesis.

Signed: *Mohammed Sinjar*

Date: 01/08/2025

Dedication

I dedicate this thesis, the fruit of long days and nights of labour in pursuit of knowledge, to my beloved parents, who stood by me at every moment and supported me with their prayers to face the challenges during my PhD journey. I pray to God to preserve them and grant them long life.

To the light of my eyes and the beat of my heart, my dear wife Fatimah, and our children Essa, Noor, Abdullah, and Samer, who stood by me through the most difficult circumstances of my Ph.D. journey. Your constant prayers and unwavering support filled me with strength and positive energy.

I dedicate this thesis to you as a rose in your beautiful garden, which is your pure heart. I pray to God to preserve you for me, grant you a long life, and fulfil your hopes. I also dedicate this work to my dear brothers and sisters; I pray to God to preserve and protect them. To my childhood friend (Osama), who died of cancer, I will never forget you and pray to God to rest in peace.

I feel grateful to have such a wonderful family stand with me during this journey. No words can express appreciation.

Acknowledgements

First and foremost, I would like to thank Allah (God) for giving me the power to believe in myself and pursue my dreams. I could never have done this without the faith I have in you.

“Nightmare,” “happy,” “lost,” “homesick,” “sad,” “stress,” “fun,” “crazy,” “excitement,” “overtime working,” “joy,” and “why didn’t it work this time” and “what did I do to myself” were the most common words and phrases I used during my Ph.D. There were many people who gave me endless advice and support to make it easier for me. Firstly, I would like to express my sincere and profound gratitude to my fantastic supervisor, Robin for giving me the opportunity to finish my study at his Lab. Thank you for spending a significant amount of time discussing and providing feedback on my writing, presentation and poster preparation, which has really improved my presentation and writing skills. If there was an Oscar prize for the best supervisor, you would get one. Also, I would like to thank my second supervisor, Craig for giving me the opportunity to do my chemistry study at his Lab, who always helped me with his team and made things easier for me.

Also, I would like to thank everyone from the Plevin and Paul laboratory who helped me in the lab work. Thank you to Ashley, Haidar, Yosra, Mohammed, and Natalia who have given me a lot of advice and sharing ideas with me. Thank you, Kirsty, for being my partner and best friend during crazy moments in the lab. I will always miss your lovely singing in the lab.

Special thanks to the Ibrahim Khadra Lab, and to Dr. Lina for her help and support with HPLC analysis and writing revisions. A huge thank you to Dr. Katy for teaching me statistics, transfection, and lab techniques, and for always being available to answer my questions and help me at any time. You are a professional and wonderful lady. I would also like to thank my best friend, “Martyn Henry” from Jamieson Lab for his invaluable help and support in the chemistry Lab, writing revisions and responding to any questions. A big thank you to my beautiful wife, words cannot express how grateful I am to have you in my life. I cannot imagine that without her sacrifices, continuous encouragement, and support, I will be able to achieve my goals. Thank you to everyone who had helped me during my Ph.D. journey.

My acknowledgments also go to the Ministry of Higher Education in Iraq and the University of Anbar for awarding me the scholarship and allowing me to study abroad to undertake my Ph.D. degree in the United Kingdom.

Abstract

The chemokine, CXCL12 (SDF-1), is produced by diverse cell types and promotes cancer progression within the tumour microenvironment through its effects. A number of inhibitors for the CXCL12 receptor, CXCR4, have been developed for the treatment of certain cancers. However, these drugs have limited clinical success and toxicity issues, raising concerns about long-term effects. Studies have shown the essential role of MAPK and NF- κ B pathways in the regulation of chemokine production. Therefore, the current study aimed to investigate the role of MAPK and the NF- κ B pathway in the regulation of CXCL12 induced by IL-1 β in the human osteosarcoma cell line (U2OS) model. Furthermore, a preliminary study of 5000 commercial compounds assessed for inhibition of IL-1 β -induced CXCL12 reporter activity identified a number of hits. Thus, an additional part of the thesis aimed to synthesise and pharmacologically evaluate novel CXCL12 inhibitors and examine their mechanism (s) of inhibition.

Initially, the target KM compounds were successfully synthesised, and thermal stability analysis showed constant temperature stability. These compounds were candidates for pharmacological studies following assessment of signalling cascades in IL-1 β -induced CXCL12 expression in the latter part of the thesis

In validating candidate signalling pathways studies showed no role for JNK and p38 MAPK in CXCL12 regulation. IL-1 β strongly stimulated the IKK α -dependent NF κ B pathway, which aligns with previous research. Pharmacological inhibition of TAK-1 and IKK alpha implicated IKK alpha in CXCL12 induction, with no discernible role of IKK β -dependent NF κ B pathway. However, molecular experiments using siRNA knockdown confirmed that whilst siRNA IKK α plays an essential role in non-canonical pathway regulation, it does not impact CXCL12 induction. This suggests that with respect to CXCL12 regulation, the compounds SU1261 and 5Z-7-oxo exhibit off-target effects. Surprisingly, MEKK3, which has no regulatory involvement in any IL-1 β -induced MAPK or NF κ B pathway was implicated in CXCL12 induction.

Synthesised CXCL12 inhibitors were characterised, two compounds, KM8 and KM11, showed significant inhibition of CXCL12 production stimulated by IL-1 β . For these compounds, inhibition of CXCL12 induction did not correlate with any effects on MAPK or NF κ B pathways, which were not

affected. This implies inhibition of another pathway leading to CXCL12 induction, possibly MEKK3 or another axis.

Posters and Oral Presentation

Oral Presentations

Mohammad Farhan, Kirsty Tinto, Margaret R Cunningham, Kathryn A McIntosh, and Robin Plevin (2023). TAK-1 inhibition prevents cytokine-mediated CXCL12 production in a bone cancer cell line. 19th World Congress of basic and clinical Pharmacology WCP2023, Glasgow, UK. <https://bpspubs.onlinelibrary.wiley.com/doi/epdf/10.1111/bph.16110>.

Mohammad Farhan, Kirsty Tinto, Margaret R Cunningham, Kathryn A McIntosh, and Robin Plevin. Elucidating the Signalling Pathways Mediating CXCL12 Induction by IL-1 β in Bone Cancer Cells and Testing of Novel Chemical Compounds. Postgraduate Research Day, University of Strathclyde. 6th June 2024. Glasgow UK

Posters Presentation

Mohammad Farhan, Kirsty Tinto, Martyn Henry, Kathryn A McIntosh, Craig Jamieson, and Robin Plevin. Chemical Synthesis and pharmacological testing of novel CXCL12 inhibitors in bone cancer. Postgraduate Research Day, University of Strathclyde. 2nd February 2023. Glasgow UK

Abbreviations

AcoH	Acetic acid
Ac ₂ O	Acetic Anhydride
Ar	Aromatic
AP1	Activator protein 1
ANOVA	Analysis of variance
AKT	Serine/threonine-protein kinase
APS	Ammonium persulphate
ATF-3/5	Activating transcription factor 3/5
ATP	Adenosine triphosphate
BAFF	B-cell activation factor
BCL2L1	B-cell lymphoma 2-like 1
Bid	BH3-interacting domain death agonist
TBid	Truncated BH3-interacting domain death agonist
BLC	B lymphocyte chemoattractant
br	Broad
Boc	<i>tert</i> -Butyloxycarbonyl
BSA	Bovine serum albumin
CD40L	Cluster of differentiation-40 ligand
c-IAP	Cellular inhibitor of apoptosis protein
COX	Cyclooxygenase
CTLA-4	Cytotoxic T-Lymphocyte-Associated Protein 4
CTLs	Cytotoxic T-Lymphocytes
CTGF	Connective tissue growth factor
CXCL-12	Chemokine (C-X-C motif) ligand
CXCR4	Chemokine (C-X-C) receptor 4
d	Doublet
DCM	1,2-Dichloromethane
DMF	Dimethylformamide
DMSO	Dimethylsulfoxide
DN	Dominant negative
DPP4	Dipeptidyl peptidase 4
DTT	Dithiothreitol
DIC	<i>N, N</i> -Diisopropyl carbodiimide
equiv.	Equivalents
ESI	Electrospray ionisation
Et	Ethyl
ECL	Enhanced Chemiluminescence
ECM	Extracellular matrix
EGFR	Epidermal growth factor receptor
EMT	Epidermal-mesenchymal transition
ERK	Extracellular regulated kinase
ESC	European Screening Centre
FASL	Fas Ligand
FCS	Foetal calf serum

FGF	Fibroblast growth factor
g	Grams
GAPDH	Glycerlaldehyde-3-phosphate dehydrogenase
GPCR	G-protein coupled receptors
GR	Glucocorticoid receptor
GSK3	Glycogen synthase kinase 3
h	Hour
HER2	Human epidermal growth factor receptor2
HES	Hairy/Enhancer-of-Split
H ₂ O ₂	Hydrogen peroxide
HIF1 α	Hypoxia-inducible factor 1-alpha
HLH	Helix-loop-helix
HPLC	High-performance liquid chromatography
Hz	Hertz
HUVEC	Human umbilical vein endothelial cells
IC ₅₀	Half maximal inhibitory concentration
ICAM-1	Intracellular adhesion molecule-1
IL-1 β	Interleukin-1 beta
IL-1R	Interleukin-1 receptor
IL-8	Interleukin-8
I κ B α	Inhibitory kappa B alpha
IKK	Inhibitory kappa B kinase
<i>J</i>	Coupling constant
kDa	kilo-Dalton
KRAS	Kirsten rat sarcoma viral oncogene homolog
LAG-3	Lymphocyte-Activation Gene 3
LIGHT	Lymphotoxin-like, exhibits Inducible expression, and competes with HSV Glycoprotein D for HVEM, a receptor expressed by T lymphocytes
LOD	Limit of detection
LOQ	Limit of quantification
LT α 1 β 2	Lymphotoxin alpha 1 beta 2
MMP	Matrix metalloproteinase
MAPK	Mitogen-activated protein kinase
MEF	Mouse Embryonic Fibroblast
β -ME	β -mercaptoethanol
Me	Methyl
MHz	Megahertz
min	Minutes
mol	Moles
MTT	3-(4,5-dimethylthiazol-2-yl)-2,5-diphenyltetrazolium bromide
MyD88	Myeloid differentiation primary response 88
<i>m/z</i>	Mass to charge ratio
NMR	Nuclear magnetic resonance
NF κ B	Nuclear factor kappa B
NEMO	NF κ B essential modulator
NIK	NF κ B-inducing kinase
NK	Natural killer cells
Nov	Nephroblastoma overexpressed

PAGE	Polyacrylamide gel electrophoresis
PBS	Phosphate buffered saline
PDL-1	Programmed Death-Ligand 1
PI3K	Phosphoinositide-3 kinase
PIK3CA	PI3K catalytic subunit α
PKC	Protein kinase C
Ph	Phenyl
ppm	Parts per million
q	Quartet
rt	Room temperature
RANK	Receptor activator of NF κ B
RANKL	Receptor activator of NF κ B ligand
RIP1	Receptor-Interacting Protein 1
RT-qPCR	Real-time quantitative Polymerase Chain Reaction
s	Singlet
SAR	Structural activity relationship
SCC	Squamous cell carcinomas
SDF1	Stromal cell-derived factors-1 α
SDS	Sodium dodecyl sulphate
Sp1	Specificity protein 1
SAR	Structure-Activity Relationship
siRNA	Small interfering RNA
shRNA	Short hairpin interfering RNA
SNAr	Nucleophilic aromatic substitution
t	Triplet
TAB-2	TAK-1 binding protein 2
TAK-1	Transforming growth factor β -activated kinase 1
TAZ	Transcriptional co-activators with PDZ binding motifs
^t Bu	Tertiary butyl
TEMED	<i>N,N,N,N</i> -tetramethylenediamine
TGF β	Transforming growth factor β receptor
TLR	Toll-like receptor
TNF α	Tumour necrosis factor alpha
TNFR	TNF-receptor
TRAF	TNF receptor-associated factor
TRAIL	TNF-related apoptosis-inducing ligand
TFA	Trifluoroacetic acid
THF	Tetrahydrofuran
TLC	Thin-layer chromatography
TMS	Trimethylsilyl
UV	Ultraviolet
VCAM-1	Vascular cell adhesion molecule 1
VCP/p97	Valosin-containing protein
VEGF	Vascular endothelial growth factor
XIAP	X-linked inhibitor of apoptosis protein
PTEN	Phosphatase and tensin homology

List of Tables

Chapter One

Table 1. 1 The Main CXCR4 Antagonists Used in Cancer Treatment.....	46
---	----

Chapter Two

Table 2. 1 Antibodies Used in Western Blots and Their Optimal Conditions.....	62
---	----

Table 2. 2 siRNA Transfection Target Gene, siRNA Target Sequences, and Origin.....	69
--	----

Chapter Three

Table 3. 1 Screened chemical compounds and in-house KM compounds with <i>in vitro</i> inhibitory potency IC ₅₀ , Cytotoxicity, and calculated Drug-likeness.....	73
---	----

Table 3. 2 Details of the Mobile phase used in HPLC Analysis.....	82
---	----

Table 3. 3 Calibration data of KM10	100
---	-----

Table 3. 4 Calibration data of KM11	103
---	-----

Table 3. 5 Calibration data of KM6	106
--	-----

List of Figures

Chapter One

Figure 1.1 The expected numbers of new cases and cancer-related deaths worldwide in 2022 for both genders. A) Incidence, B) Mortality. Figure adapted from (Bray et al., 2024).	3
Figure 1. 2 Signs/Hallmarks of cancer cells.	9
Figure 1. 3 The structure of NF- κ B and I κ B family protein members.	14
Figure 1. 4 Structure of IKKs, IKK α , IKK β and IKK γ (NEMO).	15
Figure 1. 5 The NF- κ B pathways, the Canonical and Non-canonical pathways.	20
Figure 1. 6 The relationship between inflammation and cancer development.	26
Figure 1. 7 The cells of origin for OS.	28
Figure 1. 8 The Main Signalling Pathways in Osteosarcoma and Their Inducing Factors.	30
Figure 1. 9 Structure of Chemokine Types. Figure adapted from (Cuesta-Gomez et al., 2021).	34
Figure 1. 10 Schematic Representation of Chemokine System Organisation	35
Figure 1. 11 CXCL12 Structure and Splice Isoforms.	38
Figure 1. 12 Diagram representation of CXCL12-mediated signalling pathways.	41
Figure 1. 13 Chemical Structures and Names of Selected CXCL12 Inhibitors.	52
Figure 1. 14 Chemical Structures and Names of Targeted CXCL12 Inhibitors (KM).	53

Chapter Two

Figure 2. 1 A diagrammatic representation of the SDS-PAGE and Western blotting workflow.	61
---	----

Chapter Three

Figure 3. 1 Calibration curve of KM10 by HPLC	100
Figure 3. 2 Short-term thermal stability study for 7 days at 25 °C, 37 °C, and 50 °C for KM10 .	101

Figure 3. 3 Calibration curve of KM11 by HPLC	103
Figure 3. 4 Short-term thermal stability study for 7 days at 25 °C, 37 °C, and 50 °C for KM11105	
Figure 3. 5 Calibration curve of KM6 by HPLC	106
Figure 3. 6 Short-term thermal stability study for 7 days at 25 °C, 37 °C, and 50 °C for KM6	108

Chapter Four

Figure 4. 1 Effect of IL-1 β on CXCL12 expression in U2OS cells.....	112
Figure 4. 2 Time course of IL-1 β -induced phosphorylation of ERK and c/EBP β in U2OS cells...	114
Figure 4. 3 Time course of IL-1 β -induced phosphorylation of pJNK in U2OS cells.....	115
Figure 4. 4 Time course of IL-1 β -induced phosphorylation of p38 in U2OS cells.	116
Figure 4. 5 Time course of IL-1 β -induced I κ B α degradation and p65 phosphorylation in U2OS cells.	117
Figure 4. 6 Time course of IL-1 β -induced p100 phosphorylation in U2OS cells.	119
Figure 4. 7 Effect of IKK2 X1 on IL-1 β -induced cellular I κ B α degradation in U2OS cells.	120
Figure 4. 8 Effect of SU1261 on IL-1 β -induced p100 phosphorylation in U2OS cells.	121
Figure 4. 9 The effect of IKK α siRNA on IKK α expression in U2OS cells.	123
Figure 4. 10 The effect of IKK β siRNA on IKK β expression in U2OS cells.	124
Figure 4. 11 The effect of IKK α siRNA upon IL-1 β -mediated phosphorylation of p100 in U2OS cells.	126
Figure 4. 12 The effect of IKK β siRNA upon IL-1 β -mediated cellular degradation of I κ B α in U2OS cells.	127
Figure 4. 13 The effect of IKK α and IKK β siRNA double knockdown upon IL-1 β -mediated p100 phosphorylation and cellular I κ B α degradation in U2OS cells.	129
Figure 4. 14 The effect of combined IKK β siRNA and IKK α inhibition upon IL-1 β -mediated cellular I κ B α degradation in U2OS cells.	130
Figure 4. 15 Effect of TAK1 inhibitor 5Z-7oxo on IL-1 β -induced phosphorylation of JNK in U2OS cells.	131

Figure 4. 16 Effect of the TAK1 inhibitor 5Z-7oxo on IL- 1 β -mediated cellular I κ B α degradation in U2OS cells.	133
Figure 4. 17 Effect of TAK1 inhibitor 5Z-7-oxo on IL-1 β induced phosphorylation of p100 in U2OS cells.	134
Figure 4. 18 The effect of siRNA TAK1 on TAK1 expression in U2OS cells.	136
Figure 4. 19 The effect of TAK1 siRNA upon IL-1 β -mediated phosphorylation of JNK in U2OS cells.	137
Figure 4. 20 The effect of TAK1 siRNA upon IL-1 β -mediated phosphorylation of p38 in U2OS cells.	138
Figure 4. 21 The effect of TAK1 siRNA upon IL-1 β -mediated cellular I κ B- α loss and p65 phosphorylation in U2OS cells.	140
Figure 4. 22 The effect of TAK1 siRNA upon IL1 β -mediated phosphorylation of p100 in U2OS cells.	141
Figure 4. 23 The effect of TAK1 siRNA upon IL-1 β -mediated phosphorylation of IKK α / β in U2OS cells.	142
Figure 4. 24 The effect of siRNA MEKK3 on MEKK3 expression in U2OS cells.	144
Figure 4. 25 The effect of MEKK3 siRNA upon IL-1 β -mediated phosphorylation of JNK in U2OS cells.	145
Figure 4. 26 The effect of MEKK3 siRNA upon IL-1 β -mediated p100 phosphorylation and cellular I κ B- α loss in U2OS cells.	147
Figure 4. 27 The effect of combined TAK1 and MEKK3 siRNA upon IL-1 β -mediated phosphorylation of JNK in U2OS cells.	149
Figure 4. 28 The effect of combined TAK1 and MEKK3 siRNA upon IL-1 β -mediated cellular I κ B α loss in U2OS cells.	151
Figure 4. 29 The effect of combined TAK-1 and MEKK3 siRNA upon IL-1 β -mediated phosphorylation of p100 and IKK α / β in U2OS cells.	153
Figure 4. 30 Effect of SP600125 on IL-1 β -induced phosphorylation of JNK in U2OS cells.	155
Figure 4. 31 Effect of MAPK inhibitors upon IL-1 β -mediated CXCL12 activity in U2OS cells.	156
Figure 4. 32 The effect of NF- κ B inhibitors upon IL-1 β -mediated CXCL12 activity in U2OS cells.	157

Figure 4. 33 The effect of siRNA IKK α and IKK β on IL-1 β -induced CXCL12 activity in U2OS CXCL12 cells.....	158
Figure 4. 34 The effect of siRNA IKK α and IKK β double knockdown on IL-1 β -induced CXCL12 activity in U2OS CXCL12 cells.	159
Figure 4. 35 The effect of combined SU1261 with siRNA IKK α and IKK β on IL-1 β -induced CXCL12 activity in U2OS CXCL12 cells.....	161
Figure 4. 36 Effect of AMG548 on IL-1 β -induced cellular I κ B α loss and p65 phosphorylation in U2OS cells.	162
Figure 4. 37 Effect of AMG548 on IL-1 β -induced phosphorylation of p100 in U2OS cells.....	164
Figure 4. 38 Effect of AMG548 on IL-1 β -induced phosphorylation of pJNK in U2OS cells.	165
Figure 4. 39 The effect of AMG548 upon IL-1 β stimulated CXCL12 induction in U2OS cells. ...	166
Figure 4. 40 Effect of AMG548 on U2OS cell viability using MTT Assay.....	167
Figure 4. 41 The effect of TAK1 inhibitor, 5Z-7oxo upon IL-1 β -induced CXCL12 activity in U2OS cells.	169
Figure 4. 42 Effect of TAK1 inhibitor, 5Z-7oxo on U2OS cell viability.	170
Figure 4. 43 The effect of TAK1 inhibitor, Takinib, upon IL-1 β -induced CXCL12 activity in U2OS cells.	171
Figure 4. 44 The effect of siRNA TAK1 on IL-1 β -induced CXCL12 activity in U2OS CXCL12 cells.	173
Figure 4. 45 Time course of IL-1 β induction of CXCL12 in U2OS cells.	174
Figure 4. 46 The effect of TAK-1 siRNA upon CXCL12 protein levels in U2OS cells.....	175
Figure 4. 47 Time course of IL-1 β induction of IL-8 in U2OS cells.....	176
Figure 4. 48 The effect of TAK-1 siRNA upon IL-8 protein levels in U2OS cells.....	177
Figure 4. 49 The effect of siRNA MEKK3 on IL-1 β -induced CXCL12 activity in U2OS-CXCL12 cells.	179
Figure 4. 50 The effect of MEKK3 inhibitor, Ponatinib upon IL-1 β -mediated CXCL12 activity in U2OS cells.	181
Figure 4. 51 The effect of MEKK3 siRNA upon CXCL12 protein levels in U2OS cells.....	182

Figure 4. 52 The effect of MEKK3 siRNA upon IL-8 protein levels in U2OS cells.	183
---	-----

Chapter Five

Figure 5.1 The effect of KM compounds upon IL-1 β -induced CXCL12 activity in U2OS-CXCL12 cells.	195
Figure 5. 2 The effect of KM compounds upon IL-1 β -induced CXCL12 activity in U2OS cells. .	196
Figure 5. 3 Effect of KM compounds KM2, KM5, and KM6 on U2OS cell viability.	197
Figure 5. 4 The effect of KM8 upon IL-1 β -induced CXCL12 activity in U2OS cells.	199
Figure 5. 5 The effect of KM11 upon IL-1 β -induced CXCL12 activity in U2OS cells.	200
Figure 5. 6 The effect of KM compounds on luciferase enzyme activity in U2OS Cells.	201
Figure 5. 7 Effect of KM8 on U2OS cell viability.	202
Figure 5. 8 Effect of KM11 on U2OS cell viability.	203
Figure 5. 9 The effect of KM8 upon CXCL12 protein levels in U2OS cells.	204
Figure 5. 10 The effect of KM11 upon CXCL12 protein levels in U2OS cells.	205
Figure 5. 11 The effect of KM8 upon IL-8 protein levels in U2OS cells.	206
Figure 5. 12 The effect of KM11 upon IL-8 protein levels in U2OS cells.	207
Figure 5. 13 Effect of KM8 on IL-1 β -induced phosphorylation of JNK in U2OS cells.	209
Figure 5. 14 Effect of KM8 on IL-1 β -induced cellular I κ B α loss and phosphorylation of p65 in U2OS cells.	210
Figure 5. 15 Effect of KM8 on IL-1 β -induced phosphorylation of p100 in U2OS cells.	212
Figure 5. 16 Effect of KM11 on IL-1 β -induced phosphorylation of JNK in U2OS cells.	213
Figure 5. 17 Effect of KM11 on IL-1 β -induced cellular I κ B α loss and phosphorylation of p65 in U2OS cells.	214
Figure 5. 18 Effect of KM11 on IL-1 β -induced phosphorylation of p100 in U2OS cells.	215

Chapter Six

Figure 6. 1 A schematic diagram shows the effect of IL-1 β -induced CXCL12 expression via the MAPK, NF- κ B, and MEKK3 pathways—role of KM compounds in inhibiting CXCL12 activity in U2OS cells.233

Table of Contents

Dedication	ii
Acknowledgements.....	iii
Abstract.....	iv
Posters and Oral Presentation	vi
Abbreviations.....	vii
List of Tables	x
List of Figures.....	xi
Table of Contents	xvii
Chapter One	1
1.1 Cancer	2
1.2 Hallmarks of cancer	3
1.2.1 Sustaining Proliferative Signalling	3
1.2.2 Evading Growth Suppressors.....	4
1.2.3 Resistance to Apoptosis.....	4
1.2.4 Enabling Replicative Immortality.....	5
1.2.5 Inducing Angiogenesis.....	5
1.2.6 Induction of Invasion and Metastasis	6
1.2.7 Evading the Immune System.....	6
1.2.8 Genomic Instability	7
1.2.9 Abnormal Metabolism	7
1.2.10 Inflammation.....	8
1.3 Signalling Pathways in Cancer	9

1.3.1 The Ras/Raf/ MAPK Signalling Pathway	10
1.3.2 The PI3K/AKT Signalling Pathway.....	10
1.3.3 NF-κB Signalling Pathway.....	11
1.3.3.1 Structure of NF-κB Family Members.....	12
1.3.3.2 Structure of Inhibitory-kappa B (IκB) Family Members	12
1.3.3.3 Structure and Function of the Inhibitory Kappa B Kinases (IKKs)	15
1.3.3.4 Activation of NF-κB p100/p52	16
1.3.3.5 The Molecular Activation of IκBα in the Canonical NF-κB Pathway.....	16
1.3.4 Signalling Pathways of NF-κB.....	17
1.3.4.1 Receptor Coupling to the Canonical NF- κ B Pathway.....	17
1.3.4.2 The Non-Canonical NF- κ B Pathway.....	18
1.3.4.3 The Role of the NF- κ B Pathway in Cancer	20
1.4 The Role of Inflammation in the Tumour Microenvironment	22
1.5 Osteosarcoma.....	27
1.5.1 Subtypes of Osteosarcoma	28
1.5.1.1 Classical Osteosarcoma	28
1.5.1.2 Surface Osteosarcoma	29
1.5.1.3 Telangiectatic Osteosarcoma	29
1.5.1.4 Small Cell Osteosarcoma	29
1.5.2 Signalling Pathways in Osteosarcoma	29
1.5.2.1 The MAPK Signalling Pathways.....	30
1.5.2.2 The NF- κ B Signalling Pathway.....	31
1.5.3 Osteosarcoma Treatment.....	32

1.6 Chemokines.....	33
1.6.1 Role of Chemokines in Cancer	35
1.7 Stromal Cell-derived Factor-1 (SDF-1) CXCL12	36
1.7.1 Structural Features and Components of CXCL12.....	37
1.7.2 CXCL12 Production.....	39
1.7.3 Cellular Mechanisms Activated by CXCL12.....	39
1.7.4 Signalling Functions of CXCR7	41
1.7.5 Role of CXCL12 in Cancer Development	42
1.7.6 CXCR4 Antagonists	44
1.7.7 Challenges in Developing CXCL12/CXCR4 Inhibitors	47
1.7.8 Cellular factors that regulate CXCL12 expression	48
1.7.9 Pharmacological and Molecular Inhibition of CXCL12 Production.....	50
1.8 Aims of the Study	51
Chapter Two	54
2.1 General Reagents for Biological Assay.....	55
2.1.1 Anti-bodies	56
2.1.2 Pharmacological Agonists	57
2.1.3 Target Compounds	57
2.2 Chemical Synthesis.....	58
2.3 Cell Culture.....	58
2.3.1 Culture of Human Osteosarcoma (U2OS) Cells	59
2.3.2 Trypsinisation and Subculture	59
2.4 Western Blotting.....	59

2.4.1 Quiescing Cells.....	59
2.4.2 Preparation of Whole-Cell Extracts	59
2.4.3 SDS-Polyacrylamide Gel Electrophoresis (SDS-PAGE).....	60
2.4.4 Electrophoretic Transfer of Proteins onto Nitrocellulose Membrane	60
2.4.5 Immunological Detection of Proteins.....	61
2.4.6 Re-probing and Stripping of Nitrocellulose Membrane	63
2.4.7 Scanning Densitometry and Analysis of Expression Levels	64
2.5 Promoter-Linked Reporter Assay	64
2.5.1 CXCL12 Gene Promoter-Linked Luciferase Reporter Activity Assay	64
2.6 MTT Toxicity Assay.....	65
2.7 Enzyme-Linked Immunosorbent Assay (ELISA)	65
2.7.1 Preparation and Treatment of U2OS Cells.....	65
2.7.2 Measurement of Human CXCL12/SDF1-alpha.....	66
2.7.3 Measurement of Human IL-8 (CXCL8).....	66
2.8 Treatment of Bone Cancer Cell Line	67
2.8.1 Testing Compounds.....	67
2.8.2 siRNA-mediated Silencing of Target Genes (TAK1, IKKα, IKKβ, and MEKK3) in Cells.....	67
2.9 Data Analysis	69
Chapter Three	70
3.1 Introduction	71
3.2 Results and Discussion	75
3.2.1 Synthesis of ethyl 5-(2-(1<i>H</i>-indol-3-yl)acetamido)-3-methylthiophene-2-carboxylate (KM6).....	75

3.2.2 Synthesis of <i>N</i>-(2-(4-((5-methyl isoxazole 3yl) methyl) piperazine-1-yl)-2-oxoethyl)-[1,1'-biphenyl]-4-carboxamide (KM10).....	76
3.2.3 Synthesis of <i>N</i>-allyl-<i>N</i>-(4-(4-cyclohexylphenyl)thiazol-2-yl)acetamide (KM11)	78
3.2.4 Synthesis of AMG-548 (NLK/p38 inhibitor)	78
3.3 Experimental data for KM compounds	80
3.3.1 General Experimental	80
3.3.2 Stability Analysis Study using High-Performance Liquid Chromatography (HPLC)	82
3.3.2.1 Preparation of Stock and Standard Solutions for KM Compounds.....	83
3.3.2.2 Method Development and Partial Validation	83
3.3.3 Synthesis of Ethyl 5-amino-3-methylthiophene-2-carboxylate	85
3.3.4 Synthesis of Ethyl 5-(2-(1<i>H</i>-indol-3-yl)acetamido)-3-methylthiophene-2-carboxylate (KM6).....	86
3.3.5 Synthesis of methyl ([1,1'-biphenyl]-4-carbonyl) glycinate (1A).....	87
3.3.6 Synthesis of [1,1'-biphenyl]-4-carbonyl) glycine (1B)	88
3.3.7 Synthesis of <i>tert</i>-butyl 4-(([1,1'-biphenyl]-4carbonyl) glycy) piperazine-1-carboxylate (1C).....	88
3.3.8 Synthesis of <i>N</i>-(2-oxo-2-(piperazin-1-yl) ethyl)-[1,1'-biphenyl]-4-carboxamide (1D)89	
3.3.9 Synthesis of <i>N</i>-(2-(4-((5-methylisoxazol 3yl) methyl) piperazin-1-yl)-2-oxoethyl)-[1,1'-biphenyl]-4-carboxamide (KM10)	90
3.3.10 Synthesis of 4-(4-cyclohexylphenyl)thiazol-2-amine	91
3.3.11 Synthesis of <i>N</i>-(4-(4-Cyclohexylphenyl)thiazol-2-yl)acetamide.....	92
3.3.12 Synthesis of <i>N</i>-Allyl-<i>N</i>-(4-(4-cyclohexylphenyl)thiazol-2-yl)acetamide (KM11)	93
3.3.13 Synthesis of <i>tert</i>-Butyl (<i>S</i>)-(1-cyano-2-phenylethyl)carbamate	94
3.3.14 Synthesis of <i>tert</i>-Butyl (<i>S</i>)-(1-amino-3-phenylpropan-2-yl)carbamate	95

3.3.15 Synthesis of 3-Methyl-2-(methylthio)-5-(naphthalen-2-yl)-6-(pyridin-4-yl)pyrimidin-4(3 <i>H</i>)-one	96
3.3.16 Synthesis of 3-Methyl-2-(methylsulfonyl)-5-(naphthalen-2-yl)-6-(pyridin-4-yl)pyrimidin-4(3 <i>H</i>)-one	97
3.3.17 Synthesis of (<i>S</i>)-2-((2-Amino-3-phenylpropyl)amino)-3-methyl-5-(naphthalen-2-yl)-6-(pyridin-4-yl)pyrimidin-4(3 <i>H</i>)-one (AMG-548)	98
3.4 Analysis of Compound Stability Intended for Pharmacological Testing.....	99
3.4.1 Results and Discussion	99
3.4.1.1 Quantitative HPLC Analysis and Calibration Curve of KM10	99
3.4.1.2 Quantitative HPLC Analysis and Calibration Curve of KM11	102
3.4.1.3 Quantitative HPLC Analysis and Calibration Curve of KM6	105
3.5 Conclusion.....	109
Chapter Four	110
4.1 Introduction	111
4.1.1 The effect of IL-1 β on CXCL12 expression in U2OS cells.....	111
4.2 IL-1 β Induces MAP Kinase Signalling Pathways in U2OS Cells	112
4.2.1 The effect of IL-1 β on Phosphorylated ERK in U2OS Cells	113
4.2.3 The effect of IL-1 β on Phosphorylated p38 in U2OS Cells.....	115
4.3 IL-1 β -mediated activation of canonical NF- κ B signalling in U2OS cells.....	116
4.3.1 The effect of IL-1 β on Cellular I κ B- α and p65 Phosphorylation in U2OS Cells	116
4.4 IL-1 β Induces Non-Canonical NF- κ B Signalling in U2OS Cells	118
4.4.1 The effect of IL-1 β on p100 phosphorylation and p52 Formation in U2OS Cells...	118
4.5 Effect of NF- κ B Inhibition upon Cellular Signalling mediated by IL-1 β in U2OS Cells	119
4.5.1 Effect of IKK- β Inhibition upon Canonical NF- κ B signalling induced by IL-1 β in U2OS Cells	119

4.5.2 Effect IKKα- Inhibition upon Canonical NF-κB Signalling Induced by IL-1β in U2OS Cells.....	121
4.5.3 Effect of siRNA-mediated silencing of cellular IKKα and IKKβ expression on NF-κB signalling pathways in U2OS Cells	122
4.5.3.1 Knockdown efficiency of siRNA-mediated silencing of IKKα and IKKβ in U2OS Cells.....	122
4.5.3.2 The effect of IKKα siRNA Silencing on IL-1β-Induced Phosphorylation of p100 in U2OS Cells	125
4.5.3.3 The effect of IKKβ siRNA Silencing on IL-1β-Induced Cellular IκBα loss in U2OS Cells.....	127
4.5.3.4 The effect of IKKα and IKKβ siRNA Double Knockdown on IL-1β-Induced p100 Phosphorylation in U2OS Cells.....	128
.....	130
4.6 Effect of TAK1 Inhibition on IL-1β-Induced Cellular Signalling in U2OS Cells	131
4.6.1 Effect of 5Z-7oxozeaenol (5Z-7oxo) on IL-1β-induced JNK phosphorylation in U2OS cells.....	131
4.6.2 Effect of 5Z-7oxo on IL- 1β- Induced Cellular IκBα Degradation and p65 Phosphorylation in U2OS Cells.....	132
4.6.3 Effect of 5Z-7oxo on IL-1β-Induced p100 Phosphorylation in U2OS Cells.....	134
4.6.4 Effect of siRNA-mediated silencing of cellular TAK1 on signalling pathways stimulated by IL-1β in U2OS Cells	135
4.6.4.1 Knockdown Efficiency of siRNA-mediated Silencing of TAK1 in U2OS Cells	135
4.6.4.2 The effect of TAK1 siRNA silencing on IL-1β-Induced JNK phosphorylation in U2OS Cells	137
4.6.4.3 The effect of TAK1 siRNA silencing on IL-1β-Induced p38 phosphorylation in U2OS Cells	138
4.6.4.4 The effect of TAK1 siRNA Silencing on IL-1β-Induced cellular IκB-α Degradation and p65 Phosphorylation in U2OS Cells	139
4.6.4.5 The effect of TAK1 siRNA Silencing on IL-1β-Induced p100 phosphorylation in U2OS cells.....	141

4.6.4.6 The effect of TAK1 siRNA silencing on IL-1β-induced phosphorylation of IKKα/β in U2OS cells	142
4.7 Effect of Mitogen-Activated Protein Kinase Kinase Kinase 3 (MEKK3) inhibition on IL-1β-induced cellular signalling in U2OS cells	143
4.7.1 Effect of siRNA-mediated silencing of cellular MEKK3 expression on IL-1β - stimulated signalling Pathways in U2OS cells	143
4.7.1.1 Knockdown efficiency of siRNA-mediated silencing of MEKK3 in U2OS cells...	143
4.7.1.2 The effect of MEKK3 siRNA Silencing on IL-1β-Induced JNK Phosphorylation in U2OS Cells	145
4.7.1.3 The effect of MEKK3 siRNA Silencing on IL-1β-Induced Phosphorylation of p100 and Cellular IκB-α Degradation in U2OS Cells	146
4.8 Effect of Combined TAK-1/MEKK3 siRNA Silencing upon IL-1β-Inducing Signalling Pathways in U2OS Cells	148
4.8.1 Effect of combined TAK-1 and MEKK3 siRNA silencing on IL-1β-induced MAPK signalling.....	148
4.8.2 The effect of combined TAK1 and MEKK3 siRNA silencing on IL-1β-induced cellular IκB-α degradation in U2OS Cells	150
4.8.3 The effect of combined TAK-1 and MEKK3 SiRNA silencing on IL-1β-induced p100 and IKKα/β phosphorylation in U2OS cells.....	152
4.9 Identification of the signalling pathway (s) involved in IL-1β-induced CXCL12 activity in U2OS-CXCL12 cells.....	154
4.9.1 Effect of MAP Kinase Inhibition upon Cellular Signalling Stimulated by IL-1β in U2OS Cells	154
4.9.1.1 Effect of JNK inhibition upon ppJNK induced by IL-1β in U2OS cells.....	154
4.9.1.2 Effect of MAPK inhibitors on IL-1β-induced CXCL12 luciferase activity in U2OS-CXCL12 Cells	155
4.9.1.3 Effect of NF-κB inhibitors on IL-1β-induced CXCL12 induction in U2OS cells ..	156
4.9.2 Characterisation of the role of IKKα and IKKβ in the regulation of IL-1β-induced CXCL12 activity in U2OS-CXCL12 cells.....	158

4.9.3 The effect of combined p38/NLK inhibition on IL-1β-induced cellular signalling and CXCL12 induction in U2OS Cells.....	162
4.9.3.1 The effect of combined p38/NLK inhibition on IL-1 β -induced cellular I κ B α degradation and p65 phosphorylation in U2OS Cells	162
4.9.3.2 The effect of Combined p38/NLK Inhibition on IL-1 β -induced p100 phosphorylation in U2OS Cells.....	163
4.9.3.3 The effect of combined p38/NLK inhibition on IL-1 β -induced JNK phosphorylation in U2OS Cells.....	164
4.9.3.4 Effect of combined MAPK p38/NLK inhibiton on IL-1 β -induced CXCL12 reporter activity in U2OS Cells.....	165
4.9.4 Effect of TAK1 Inhibitors on IL-1β-induced CXCL12 Activity in U2OS Cells	167
4.9.4.1 The effect of TAK-1 siRNA on IL-1 β - induced CXCL12 activity in U2OS-CXCL12 cells.....	172
4.10 Regulation of CXCL12 production by ELISA	174
4.10.1 Detection of CXCL12 Protein Expression in U2OS Cells using ELISA Assay.....	174
4.10.1.1 Effect of TAK-1 siRNA on IL-1 β induced CXCL12 Protein Expression using ELISA in U2OS Cells.....	175
4.10.2 Detection of CXCL8 (IL-8) Protein Expression in U2OS Cells using ELISA Assay	176
4.10.2.1 Effect of TAK-1 siRNA silencing on IL-1 β induced IL-8 protein expression in U2OS-cells.....	177
4.10.3 The role of MEKK3 in the regulation of IL-1β- stimulated CXCL12 induction in U2OS cells.....	178
4.10.4 The role of MEKK3 in the regulation of IL-1β-induced CXCL12 protein expression using ELISA in U2OS cells	182
4.10.5 Effect of MEKK3 SiRNA Silencing on IL-1β induced IL-8 Protein Expression in U2OS-Cells	183
4.11 Discussion.....	184
Chapter Five	192

5.1 Introduction	193
5.2 The effect of novel KM compounds on IL-1β-induced CXCL12 luciferase activity in U2OS cells	194
5.3 Effect of novel KM compounds on luciferase enzyme activity	201
5.4 Effect of novel CXCL12 inhibitors on U2OS cell viability using MTT assay.....	202
5.5 Effect of novel CXCL12 inhibitors on IL-1β-induced CXCL12 protein expression in U2OS cells	204
5.5.1 Effect of KM8 on IL-1β-Induced CXCL12 Protein Expression using ELISA in U2OS cells.....	204
5.5.2 Effect of KM11 Compound on IL-1β-Induced CXCL12 Protein Expression using ELISA in U2OS cells.	205
5.5.3 Effect of Novel CXCL12 Inhibitors on IL-1β-Induced IL8 Protein Expression in U2OS Cells	206
5.5.3.1 Effect of KM8 on IL-1 β -induced IL8 protein expression in U2OS Cells.....	206
5.5.3.2 Effect of KM11 Compound on IL-1 β -Induced IL8 Protein Expression in U2OS Cells	207
5.6 Effect of Novel CXCL12 Inhibitors (KM Compounds) on IL-1β-induced MAPK Signalling in U2OS Cells.....	208
5.6.1 Effect of KM8 Compound on IL-1β-Induced JNK Phosphorylation in U2OS Cells	208
5.6.2 Effect of novel CXCL12 inhibitors upon IL-1β-Induced Canonical NF-κB Signalling in U2OS Cells	209
5.6.2.1 Effect of KM8 Compound on IL-1 β -Induced Cellular I κ B- α loss and Phosphorylation of p65 in U2OS Cells.....	209
5.6.3 Effect of Novel CXCL12 Inhibitors on IL-1β-Induced Non-Canonical NF-κB Signalling in U2OS Cells.	211
5.6.3.1 Effect of KM8 Compound on IL-1 β -Induced p100 Phosphorylation and p52 Formation in U2OS Cells	211
5.7 Effect of KM11 on IL-1β-Induced signalling pathways in U2OS cells.....	213

5.7.1 Effect of KM11 on IL-1β-induced JNK phosphorylation in U2OS cells	213
5.7.2 Effect of KM11 on IL-1β-induced NFκB pathway in U2OS Cells	214
5.7.3 Effect of KM11 on IL-1β-Induced p100 phosphorylation and p52 Formation in U2OS cells	215
Chapter Six	219
6.1 General Discussion and Future Work.....	221
6.2 Conclusion.....	233
References	234
Appendix Seven	272

Chapter One

General Introduction

1. Introduction

1.1 Cancer

Cancer is the uncontrolled proliferation of cells that can affect any body organ. This abnormal condition causes differentiation to be compromised and cell growth to take over, resulting in tumour formation and spread to other organs (Hanahan & Weinberg, 2000). In a study conducted by Siegel and others, cancer has been classified as the first or second leading cause of death in individuals under the age of 70 in 183 countries (Cause & Age, 2020). The American Cancer Society report estimates that more than 600,000 deaths and 1.9 million newly diagnosed cancer-related cases occurred in the United States in 2022 (Siegel et al., 2022). Similarly, cancer statistics for England demonstrated a 25% increase in the overall cancer incidence rate in men, higher than in women in the population in 2022 (Baker & Mansfield, 2023).

A recent report from the World Health Organisation (WHO) in 2024, provided by the International Agency for Research on Cancer, estimates a 77% increase in cancer incidence from 22 million cancer cases in 2022 to 35 million cancer cases in 2050, with increasing cancer-related deaths (Bray et al., 2024). Importantly, three major cancer types accounted for two-thirds of diagnosed cases and cancer-related deaths globally in 2022: lung cancer, which is predominant in men; breast cancer, which is predominantly found in women; and colorectal cancer (based on studies by the Global Cancer Observatory, 2022). Figure 1.1 illustrates the expected incidence and mortality rates for men and women globally regarding the four predominant malignancies in 2022 (Bray et al., 2024).

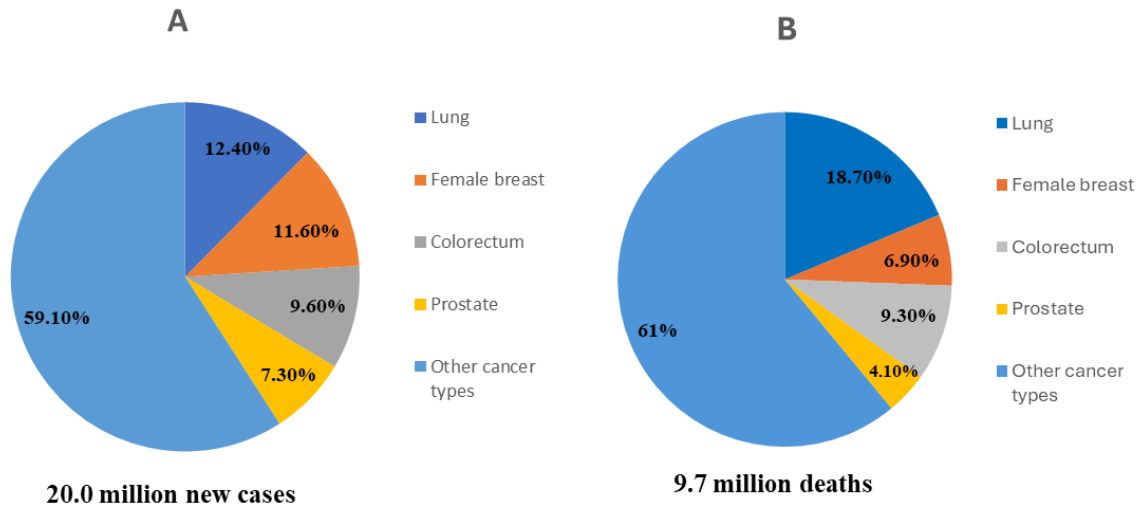


Figure 1.1 The expected numbers of new cases and cancer-related deaths worldwide in 2022 for both genders. A) Incidence, B) Mortality. Figure adapted from (Bray et al., 2024).

1.2 Hallmarks of cancer

Over the last 30 years, cancer research has developed extensive knowledge, revealing it to be a disease involving dynamic changes in the genome. These changes result from somatic genetic modifications in normal cells to produce cancer cells. In 2000, Weinberg and Hanahan highlighted the six main hallmarks of cancer cells as shown in Figure 1.2, which will be detailed below, which were further developed in 2011 to include four additional hallmarks (Hanahan & Weinberg, 2000, 2011).

1.2.1 Sustaining Proliferative Signalling

Normal tissues regulate the production of growth-promoting factors responsible for cell growth and division, thereby maintaining their function. Similarly, cancer cells can sustain proliferative signalling by different pathways, such as the autocrine pathway, which involves producing growth factor ligands that bind to cognate receptors, resulting in stimulation of the normal cells to further supply them with multiple growth factors (Cheng et al., 2008). Another regulatory factor is paracrine-induced

overexpression of receptors on the cancer cell surface or structural modifications in receptor molecules, resulting in growth factor production and downstream signalling pathway stimulation. Hyperactivation of the signalling pathway itself is underpinned by somatic mutation (Hanahan & Weinberg, 2011). These mutations were observed in the B-Raf protein mutation in human melanoma, mediating sustained activation of the Mitogen-Activated Protein kinase (MAPK) pathway and constant activation of proliferative signals (Davies & Samuels, 2010). Similarly, Jiang & Liu demonstrated that mutations in the phosphoinositide 3-kinase (PI3-kinase) isoforms hyperactivated the Akt/PKB signalling cascades in different types of cancer (Jiang & Liu, 2009). Moreover, studies on negative regulatory mechanisms have identified Phosphatase and tensin homolog (PTEN), whose inactivation further enhances proliferative signalling (Sudarsanam & Johnson, 2010; Wertz & Dixit, 2010).

1.2.2 Evading Growth Suppressors

There are multiple tumour suppressor genes that inhibit or limit cancer cell growth and proliferation. Normally, these genes act together during a certain stage in the cell cycle and function to maintain genomic integrity. Defects or mutations in these suppressor genes, such as RB (retinoblastoma-associated) and p53 proteins, enable the cancerous cells to persist in growth and proliferation (Burkhart & Sage, 2008; Deshpande et al., 2005). For instance, mutations in the p53 tumour suppressor gene and the RB1 gene result in enhanced uncontrolled cell division due to their inactivation and the accumulation of genetic abnormalities that drive cancer progression (Ghebranious & Donehower, 1998).

1.2.3 Resistance to Apoptosis

Normally, apoptosis or programmed cell death is caused by many processes, such as inflammation or cell damage. Two main pathways, an effector and a regulator, produce the apoptotic signals through intrinsic and extrinsic programs controlled by family members of Bcl-2. Initially, the extrinsic pathway is activated via death receptor ligation, such as Fas/CD95, leading to activation of initiator Caspase-8 or -10, and this activates effector Caspase-3 and -7 (Hanahan & Weinberg, 2011; Mohammad et al., 2015). The intrinsic pathway is activated via intracellular stress such as oncogene activation and DNA damage, inducing mitochondrial signals that form an apoptosome, which activates Caspase-9, which in turn activates the effector Caspases-3 and -7 (Hanahan & Weinberg, 2011; Neophytou et al., 2021).

Apoptosis can be inhibited by suppressing the proapoptotic proteins (Bax and Bak) via the anti-apoptotic Bcl-2 (Adams & Cory, 2007). Mutation of the tumour suppressor TP53 protein, increasing the expression of anti-apoptotic Bcl-2 or enhancing the survival signals, and downregulating proapoptotic factors, interrupting the extrinsic apoptosis pathway (Hanahan & Weinberg, 2011). For example, overexpression of anti-apoptotic family members Bcl-2 blocked the mitochondrial signals and prevented apoptosome formation, which is necessary for effector Caspase activation downstream, mediating intrinsic signalling (Mohammad et al., 2015). Furthermore, somatic mutation in caspase genes, such as Caspase-8, which frequently occur in some malignancies such as colorectal cancer, can reduce the caspase activity or catalytic ability, which decreases the effector function and reduces apoptosis (Neophytou et al., 2021). Inactivation of Caspases-3 and -7, aids resistance of cancer cells to apoptosis induced by death receptors such as Fas and TRAIL receptors (DR4/5) (Mohammad et al., 2015; Neophytou et al., 2021).

1.2.4 Enabling Replicative Immortality

The healthy cells undergo senescence and crisis or apoptosis stages during their life cycle, controlled by telomere function that has a crucial role in the limitation of the chromosomal DNA ends (Blasco, 2005). It has been found that senescence resistance and cell death in cancer cells are linked to an extension of the telomeric DNA segments, which can occur after telomerase stimulation, resulting in immortalised cells with malignant progression in some cancer types, like breast cancer (Raynaud et al., 2010). Inhibiting telomerase activity or disrupting the lengthening of the telomerase pathway could limit the replicative potential of cancer cells, leading to their senescence and death.

1.2.5 Inducing Angiogenesis

Hanahan and Folkman in 1996 illustrated that cancer cells are similar to normal cells and need essential nutrients and oxygen for cellular metabolic processes, which are enhanced via pro-angiogenic factors such as FGF and VEGF. Normal cells can be provided with nutrients during the early life cycle by generating new endothelial cells and vessels via angiogenesis (Hanahan & Folkman, 1996). In contrast, the development of vasculature remains triggered in cancer with continuous production of vessels through the release of many angiogenic stimuli such as thrombospondin-1 (TSP-1), VEGF-A, and FGF (Baeriswyl & Christofori, 2009; Hanahan & Weinberg, 2011). Other studies

showed that supporting cells (pericytes) and cells derived from bone marrow were essential in tumour angiogenesis development (Qian & Pollard, 2010; Raza et al., 2010). Drugs that target these factors have been developed, such as VEGF inhibitors. Bevacizumab has been shown to be an effective drug for VEGF-induced angiogenesis in colorectal cancer (Pavlidis & Pavlidis, 2013).

1.2.6 Induction of Invasion and Metastasis

Many studies have shown the complexity of mechanisms implicated in cancer invasion and migration. Metastasis starts from the intracellular migration of cancer cells from the local invasion through blood or lymphatic vessels to other tissues as macro tumours and colonies. One of these essential factors that regulates cancer development is E-cadherin, which through the adhesion of cells together and prevents migration, and any mutation or reduction in this regulator can enhance the tumour hallmark (Berx & Van Roy, 2009). Other experiments elucidated the involvement of epithelial-mesenchymal transition (EMT) in cell invasion and migration, including epithelial cells and inflammatory cells, to mediate cancer invasion and metastasis, as well as activation of associated transcription factors (Friedl & Wolf, 2008, 2010; Micalizzi et al., 2010).

1.2.7 Evading the Immune System

It is now recognised that immune cell function is a significant factor in cancer development. Under normal conditions, abnormal cells are recognised and killed through coordinating innate and adaptive mechanisms involving CTLs and NK cells (Mohammad et al., 2015; Neophytou et al., 2021). However, cancer cells have the ability to avoid detection due to genetic mutation and do not present as foreign cells and thereby evade destruction by the immune system. They also attenuate or deactivate specific cellular processes responsible for the immune protection against cancer cells, producing prolonged survival for them (Hanahan & Weinberg, 2011). For example, by releasing TGF- β and other suppressing factors that subdue CD8⁺ T cell differentiation into regulatory T cells (Tregs), which suppress the immune responses towards tumour cells, as reported in mouse tumour models (Yang et al., 2010). Natural killer cells were also involved in this regulatory system by reducing receptor activation on T-cells, such as NKG2D (Natural Killer Group 2D) and NKp30 (Natural cytotoxicity triggering receptor 3), and/or enhancing inhibitory signals resulting in downregulation of death ligands or reduction in cytotoxic components release (perforin/granzymes),

evading the immune system destruction (Mamessier et al., 2011; Neophytou et al., 2021). Furthermore, recent experiments revealed that cancer cells, such as breast cancer, can evade the immune defence through the recruitment of immune-suppressive Tregs within the tumour microenvironment (TME) (Plitas & Rudensky, 2020). Myeloid-derived suppressor cells were found to be involved in immune response inhibition in cancer through inhibiting the activity of CTLs (Lu et al., 2024). This is particularly important for the tumour microenvironment.

1.2.8 Genomic Instability

Cancer cells have specific characteristics with respect to the genome and genomic instability. Cancer cells can detect and fix any genetic defects at a rate higher than normal cells, which have selectivity for these functions; thus, uncontrolled development of the genetic mutation can occur, resulting in the accumulation of this mutation at an accelerated rate with the increasing oncogene activation and tumour suppressor gene inactivation (Hanahan & Weinberg, 2011). Genomic instability not only drives tumorigenesis but also contributes to heterogeneity, which can lead to therapeutic resistance and disease recurrence (Turner & Reis-Filho, 2012).

1.2.9 Abnormal Metabolism

Abnormal metabolism is a unique feature of cancer cells through the reprogramming of cellular nutrition and energy production through a glycolysis-dependent rather than an oxidative phosphorylation pathway. This enables the cancer cells to produce ATP and metabolic intermediates required for proliferation and TME adaptation. Yang and co-workers demonstrated that disturbing the Tricarboxylic acid cycle enhanced cancer cell metabolism both *in vitro* and *in vivo*, which resulted from a lactate overflow that promotes energy release. This enables the survival of cancer cells and hypoxia resistance by metabolic adaptation, a hallmark of solid tumours (Yang et al., 2024).

More recently, studies have shown the importance of crosstalk between metabolic and epigenetic modifications in tumour cells, such as noncoding RNA, chromatin remodelling, histone lactylation, and DNA methylation. The findings demonstrate the complexity with respect to reprogramming the metabolism of cancer cells to survive, replicate, and evade treatment (Xu et al., 2023).

1.2.10 Inflammation

Tumours and inflammation have long been linked. Inflammation can create a supportive environment for cancer growth and development. The inflammatory response includes a number of immune cells, cytokines, and chemokines that can contribute to converting normal cells into cancerous ones. For example, chronic inflammation can lead to DNA damage and genomic instability, thus providing a good condition for mutation and clonal expansion of mutant cells. Such alterations were clearly identified in chronic hepatitis, *H. pylori*-induced gastritis, or inflammation induced by schistosoma, which enhanced liver, stomach, or bladder cancers, respectively. Similarly, inflammatory cells can release nitrogen species and reactive oxygen species, which can cause further DNA damage and mutations (Hanahan & Weinberg, 2011).

In addition, cytokines and growth factors produced in the inflammatory medium can promote cell proliferation, survival, and angiogenesis through regulating several cellular pathways such as NF κ -B and MAPK signalling cascades, all of which are essential for tumour development and metastasis (DeNardo et al., 2010; Grivennikov et al., 2010). It has been found that chemical inhalation of asbestos and tobacco triggered IL-1 β expression and other inflammatory signalling cascades, which increased the risk of lung cancer and malignant mesothelioma (Kadariya et al., 2016; Takahashi et al., 2010). Recent studies demonstrated that inflammation-induced obesity could also promote the risk of developing various cancers (Quail & Dannenberg, 2019). Others have shown the essential role of chemokines in tumour growth and metastasis through the recruitment of immune and non-immune cells and regulating TME (Kortlever et al., 2017; Liao et al., 2019).

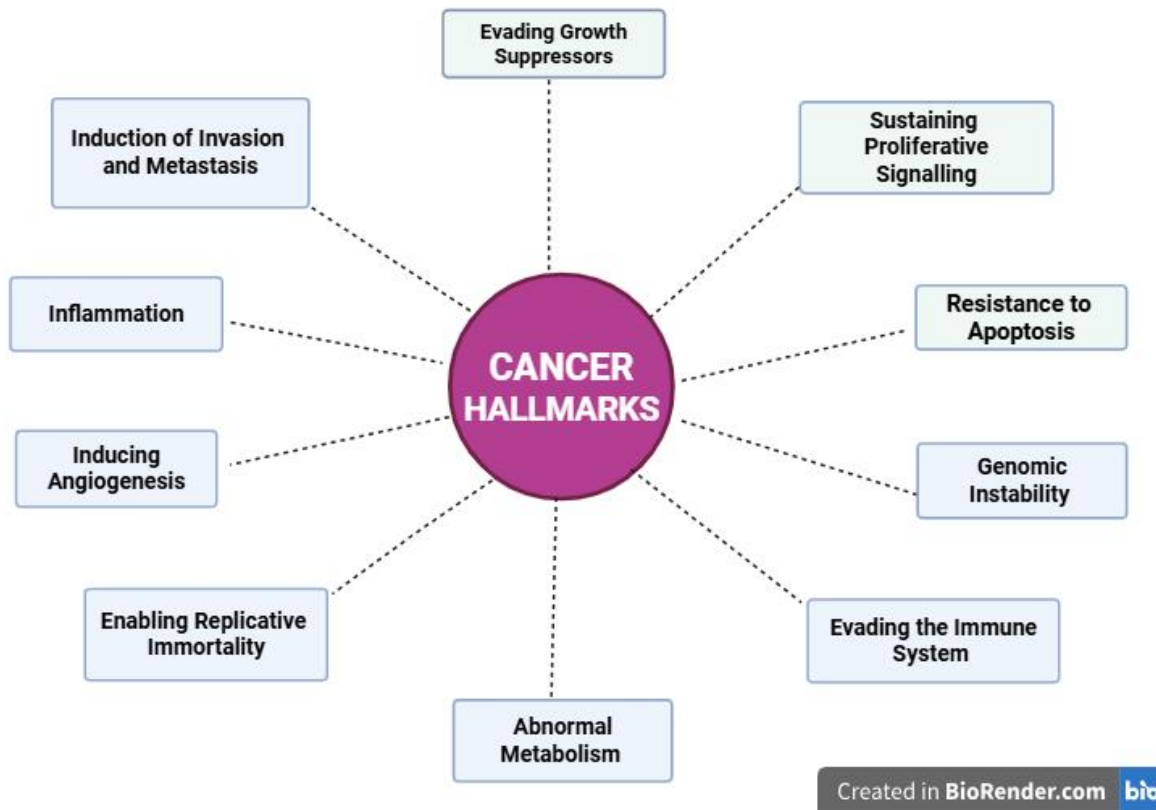


Figure 1. 2 Signs/Hallmarks of cancer cells.

Six cancer hallmarks include evading growth suppressors, induction of invasion and metastasis, inducing angiogenesis, enabling replicative immortality, resistance to apoptosis, and sustaining proliferative signalling. Four additional hallmarks involve abnormal metabolism, evading the immune system, inflammation, and genomic instability. Figure adapted from (Weinberg and Hanahan, 2000, 2011) using BioRender.

1.3 Signalling Pathways in Cancer

As indicated above, aberration of a number of key signalling pathways have been involved in multiple cancer stages (Sever & Brugge, 2015). As detailed below, two main pathways have been recognised to play a critical role in cancer development, the MAP kinase and the PI3kinase /AKT pathway. An additional pathway that has been implicated in linking inflammation/immune function to cancer progression is the Nuclear Factor Kappa B (NFκB) pathway and is the focus of this thesis.

Other pathways, such as Hippo, Wnt/ β -catenin, Hedgehog, and Notch, are not reviewed here – the reader is referred to a number of relevant reviews (Li et al., 2012; Sever & Brugge, 2015).

1.3.1 The Ras/Raf/ MAPK Signalling Pathway

The Ras/Raf/MAPK pathway plays a role in several cellular processes, including differentiation, cell growth, and survival; a defect in this pathway is a hallmark of a number of cancers (Chang et al., 2003; Kolch, 2000). The original focus of the pathway was with respect to growth factors such as PDGF, EGF, and the activation of growth factor receptors, that is, receptor tyrosine kinases (RTKs). Following receptor stimulation, a number of protein/protein interactions result in the activation of the small molecular weight G-protein RAS via GTP/GDP exchange. This initiates a kinase cascade through activation of Raf, MEK and subsequent activation of ERK, which promotes cell cycle progression and controls various cellular processes, including cell differentiation and survival (Kolch, 2000; Ritt et al., 2016). It has been found that mutation of the Ras protein, particularly the K-Ras, which is the common mutated oncogene, promotes cancer development in multiple human cancers, such as lung, hepatocellular, and pancreatic cancers (Dergham et al., 1997; Mascaux et al., 2005; Yang & Liu, 2017). Additionally, a BRAF mutation, especially the V600E mutation within the kinase binding domain of the protein, caused constitutive activation of the pathway via sustained phosphorylation of the activation site, as examined in melanoma and other cancers (Holderfield et al., 2014; Steelman et al., 2011). Other mutations which are oncogenic, not examined here in detail, include overexpression and mutation of growth factor receptors such as FGFR and HER2 (Bahar et al., 2023; Santarpia et al., 2012). More recently, MAP kinase pathways, including JNK, p38, and ERK5, have been identified, and the potential for disruptions in these pathways have been explored (Bahar et al., 2023). These cellular cascades drive cancer proliferation and metastasis in various cancer cells (Chen et al., 2015; Ritt et al., 2016).

1.3.2 The PI3K/AKT Signalling Pathway

Many studies have shown that phosphoinositide 3-kinase and protein kinase B (PI3K/AKT) signalling pathway is essential in regulating cell growth, motility, and survival (Larue & Bellacosa, 2005). Studies have detailed PI3K activation through the binding of growth factors to receptor tyrosine kinases (RTKs) (Vara et al., 2004), which then promotes the phosphorylation of PIP₂ to PIP₃. This key molecule

was found to recruit AKT to the cell membrane, causing its phosphorylation and activation (Alessi et al., 1997). Activation of this pathway promotes many cellular processes (Kennedy et al., 1997; Vara et al., 2004). For example, cell survival is promoted by Akt through phosphorylation and inactivation of proapoptotic proteins such as caspase-9, which enhances cellular proliferation through mTOR-dependent regulatory cascades (Vara et al., 2004).

As with the ERK/MAP kinase pathway, uncontrolled activation of this pathway is related to alterations in major components, for example, AKT or mTOR, leading to cancer development and progression, as examined in lung and prostate cancer (Fumarola et al., 2014; Morgan et al., 2009). Oncogenic mutations in either the PIK3CA gene encoding the p110 α subunit of PI3K or the mutation/deletion of PTEN that functions to dephosphorylate PIP₃ resulted in sustained PI3K/AKT pathway activation, promoting cancer growth (Carnero et al., 2008; Luo et al., 2003; Sever & Brugge, 2015). Furthermore, Hollander and co-workers found that PTEN essentially functioned as a tumour suppressor gene, and its deletion in mice increased the activity of this pathway, resulting in breast and thyroid cancer development (Hollander et al., 2011).

1.3.3 NF- κ B Signalling Pathway

The Nuclear Factor Kappa B (NF- κ B) pathway is a key transcription factor pathway implicated in immune responses, inflammation, and cell survival. Its dysregulation is involved in the oncogenesis of many tumours, such as colorectal (Li & Hong, 2016), breast (Khongthong et al., 2019), lung (Asgarova et al., 2018), and bone metastasis (Santini et al., 2011). Initially discovered in 1986 by Sen and Baltimore using electrophoretic mobility shift assays, NF- κ B was demonstrated as a nuclear factor that bound an 11 base-pair motif (GGGACTTCC) in the immunoglobulin kappa light-chain enhancer in B cells (Sen & Baltimore, 1986). Originally considered to be B-cell-specific, it was subsequently found to be expressed in various cell types and activated by factors such as TNF- α and pathogens (Lenardo & Baltimore, 1989).

To date, five members of the NF- κ B family have been identified and functionally characterised, along with several inhibitory-kappa B (I κ B) proteins that regulate NF- κ B function. As transcription factors, they were found to contain domains responsible for DNA binding and dimerisation, and were cloned using recombinant DNA techniques in HEK293 cells (Ghosh et al., 1998). More recently, an

experimental study has shown that subunit-specific functions could be separated through X-ray crystallography, with RelA being absolutely required for embryonic survival (Alcamo et al., 2002). Almost all NF- κ B subunits are fully activated upon C-terminal activation; both C- and N-terminal activation are required for complete nuclear translocation, and activation of RelB (Dobrzanski et al., 1993).

1.3.3.1 Structure of NF- κ B Family Members

The NF- κ B family of transcription factors comprises five members (RelA (p65), RelB, c-Rel, NF- κ B2 (p100, processed to p52), and NF- κ B1 (p105, processed to p50)) as shown in Figure 1.3 A, each containing a 300-amino-acid region of homology called the Rel Homology Domain (RHD). The RHD mediates DNA binding to the κ B sites (5'-GGRN(Y)YYCC-3'), dimerisation and nuclear translocation, as demonstrated by crystallographic studies of p50- or p65-containing heterodimers (Chen et al., 1998; Mulero et al., 2019). Class II members (RelA, RelB, c-Rel) possess C-terminal transactivation domains (TADs), which are present as a pair in RelA and c-Rel and promote strong transcriptional activation as demonstrated using luciferase assays in HEK293 cells. Class I members (NF- κ B1, NF- κ B2) are processed by ubiquitination-proteasome at the glycine-rich regions to produce p50 (433 amino acids) and p52 (223 amino acids), these subunits lack TADs and act as repressors as homodimers or as cofactors with RelA/RelB. The precursors of p105 and p100 contain ankyrin repeat domains (ARD) that mediate the inhibition of nuclear function until the precursors are proteolysed (Napetschnig & Wu, 2013). Related Non-canonical subunits, for example, ribosomal protein S3 (RPS3), can increase NF- κ B activity, as demonstrated by co-immunoprecipitation in A549 cells (Wan et al., 2007).

1.3.3.2 Structure of Inhibitory-kappa B (IkB) Family Members

The IkB family, including IkB α , IkB β , IkB ϵ , Bcl-3 (Ferreiro & Komives, 2010), IkBzeta (Muta, 2006), and the precursor proteins p100 (NF- κ B2) and p105 (NF- κ B1) (Hayden & Ghosh, 2012) as shown in Figure 1.3 B, contains 5 to 7 ankyrin repeats (ANK) that directly associate with NF- κ B dimers, hiding their Nuclear Localisation Signal (NLS) and thereby sequestering them in the cytoplasm. These family members possess a transactivation region in the C-terminal RHD, which is rich in acidic, hydrophobic amino acids, and serine amino acids for phosphorylation. A change in any of these amino acid sequences results in reduced transcriptional activity and the impairment of NF- κ B transcription itself,

which is mediated by these genes as reported in the dominant-negative I κ B α mutant (Chen et al., 1996). In addition, these subunits share an N-terminal leucine zipper (LZ) domain that permits the NF- κ B subunits to interact with each other.

In a large number of studies, illustrated by TNF- α stimulation in MEFs (Hayden & Ghosh, 2008), the most studied, I κ B member I κ B α (317 residues) has been shown to be phosphorylated at Ser32/Ser36 residues by the IKK complex (IKK α , IKK β , and NEMO), resulting in the ubiquitination and proteasomal degradation, and as indicated below, allowing p65 to translocate to the nucleus. Both I κ B β and I κ B ϵ share this inhibitory effect; however, they differ in their sensitivity to stimuli; I κ B β is involved only in the response to long-lived stimuli such as LPS-treated macrophages. The I κ B, Bcl-3, serves as a nuclear coactivator for p50/p52 homodimers, mainly in B-cell lymphomas, and mediates transcription stimulation through association with histone acetyltransferases, as shown by ChIP assay (Liou & Hsia, 2003). The ANK repeats mediate specific regulation of NF- κ B.

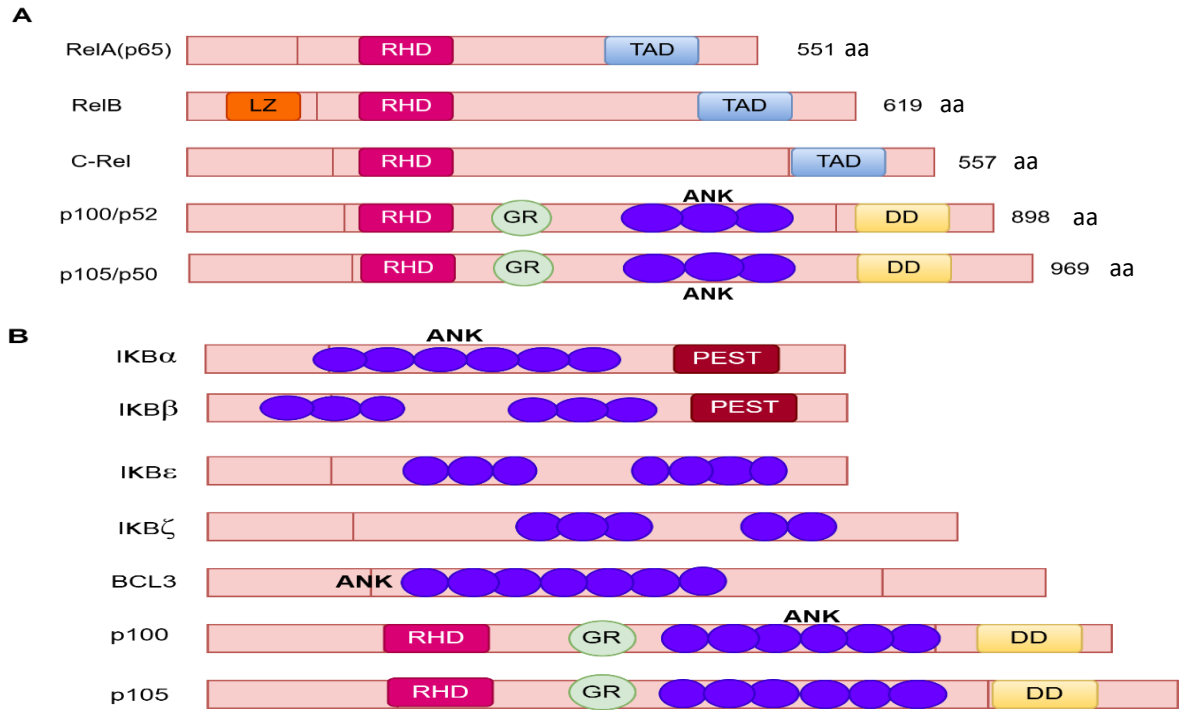


Figure 1. 3 The structure of NF-κB and IκB family protein members.

Panel (A) represents the five family proteins of NF-κB. The RHD in Rel-related proteins (RelA, RelB, c-Rel, p100/p52, p105/p50) controls their dimerisation and binding to DNA. C-terminal TAD is only found in Rel members (Rel A, Rel B and c-Rel). Ankyrin repeats (ANK) are found on p105/p50 and p100/p52 and mediate the sequestering of NF-κB dimers in the cytoplasm through binding to them. The proteolytic process of the C-terminal region for p100 and p105, which is ubiquitin-dependent cleavage, produces p52 and p50 NF-κB subunits. The amino acid count is shown on the right-hand side, next to each NF-κB member. RHD: Rel homology domain; LZ: leucine zipper; TAD: transactivation domain; Panel (B) IκB family members and their expressed proteins with functional domains are shown. PEST region refers to a polypeptide sequence enriched in proline (P), glutamic acid (E), threonine (T), and serine (S); GR indicates the glycine-rich region; and DD denotes the death domain. Figure Adapted from (Zinatizadeh et al., 2021).

1.3.3.3 Structure and Function of the Inhibitory Kappa B Kinases (IKKs)

A major discovery with respect to the regulation of both canonical and non-canonical NF κ B signalling was the IKK complex, which integrates signals from activation of a wide range of activated receptors to NF- κ B activation itself. It is composed of two catalytic subunits, IKK α (85 kDa, 745 residues) and IKK β (87 kDa, 756 residues), and a regulatory subunit, which is termed (NEMO), NF- κ B Essential Modulator (48 kDa, 419 residues) (Ghosh et al., 1998). Each of the catalytic subunits contains an N-terminal kinase domain, ubiquitin-like domain (ULD), leucine zipper (LZ), helix-loop-helix (HLH) domain, and a C-terminal NEMO binding domain (NBD). At least in the case of IKK α the leucine zipper domain in its C-terminal region facilitates dimerisation, a feature of non-canonical NF- κ B pathway. IKK α also contains a nuclear localisation sequence (NLS) as part of the kinase domain (Hacker & Karin, 2006). Figure 1.4, as indicated by X-ray crystallography (Oeckinghaus & Ghosh, 2009). NEMO is a cytoplasmic protein without catalytic activity that is composed of an amino-terminal kinase-binding domain, two coiled-coil (CC1 and CC2) domains, a leucine zipper, and a carboxy-terminal zinc finger domain. It interacts with upstream signals (such as Receptor-interacting protein1(RIP1) and TRAF6) and K63-linked/linear polyubiquitin chains, as demonstrated by co-immunoprecipitation in TNF- α -treated HEK293 cells. The extended structure of NEMO, demonstrating the binding interface that NEMO forms with IKK α /IKK β , allowing for an allosteric kinase activation (Israël, 2000).

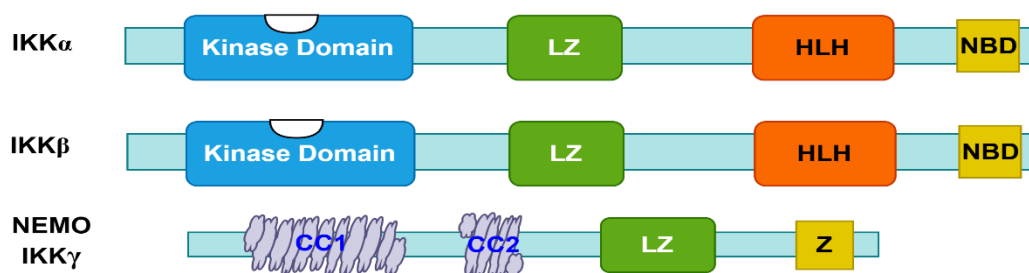


Figure 1. 4 Structure of IKKs, IKK α , IKK β and IKK γ (NEMO).

LZ: leucine zipper motif; HLH: helix-loop-helix domain; NBD: NEMO-binding domain; CC: coiled coil region. Figure Adapted from (Oeckinghaus & Ghosh, 2009).

1.3.3.4 Activation of NF- κ B p100/p52

The key component in the non-canonical NF- κ B pathway is p100 (900 amino acids) (Kim et al., 2000). It is the NF- κ B2 subunit, precursor of p52, which is a central participant involved in the regulation of lymphoid organogenesis, B-cell maturation, as well as oncogenesis. Like the I κ B proteins, the C-terminal ARD of p100 retains RelB within the cytoplasmic p100/RelB complexes (Sun, 2017). Alternative pathway activation is stimulated by NIK and IKK α , which are induced by TNFR ligand (BAFF, CD40L, RANKL) (Shih et al., 2011; Sun, 2017). IKK α phosphorylates p100 at Ser866/Ser870 (C-terminus) and Ser99/Ser108 (N-terminus), and then ubiquitination and partial proteasomal processing to p52, as confirmed by Western blotting in B-cell lines (Sun, 2017). This pathway, controlled by the inhibition of TRAF3 degradation and NIK stabilisation, permits p52/RelB dimers to undergo nuclear translocation and activation of genes such as CXCL13, BAFF, and CCL19, as demonstrated in NIK-deficient mice (Sun, 2017).

Aberrant activation of p100/p52 is oncogenic in cancers. In diffuse large B-cell lymphoma, constitutive activation of p52/RelB was linked to p100 phosphorylation and activation, which facilitates the transcriptional regulation of anti-apoptotic genes such as cIAP. This effect was quantified using RT-qPCR (Collares, 2019). Similarly, in breast cancer, MMP-9 is upregulated by p52/RelB dimers in MDA-MB-231 cells. This factor appears to be one of the key drivers facilitating metastasis, as confirmed by zymography (Zinatizadeh et al., 2021). Experimental studies showed that NIK knockout in lymphoma cells decreased p52 levels (Cildir et al., 2016), and TRAF3 mutations in myeloma enhanced non-canonical NF- κ B signalling (Nishikori, 2005), resulting in enhanced tumour growth.

1.3.3.5 The Molecular Activation of I κ B α in the Canonical NF- κ B Pathway

As indicated above, a key feature of canonical NF- κ B activation involves I κ B α (317 amino acids), the most direct and canonical inhibitor of NF- κ B. This was achieved through cytoplasmic sequestration and degradation in a stimulus-dependent manner. Six ankyrin repeats sequester the dimers of NF- κ B (such as p65/p50) by hiding their nuclear localisation signals (NLS), as indicated by HEK293 cell co-immunoprecipitation data (Hayden & Ghosh, 2008). Stimuli such as TNF- α , LPS, or IL-1 β have been observed to stimulate the IKK complex through IL-1R1 and MyD88-TRAF6; the latter phosphorylates I κ B α at Ser32/Ser36. This caused the beta-Transducin Repeat-Containing Protein β -TrCP (an E3 ubiquitin ligase) mediated Lys48-linked polyubiquitination and proteasomal degradation, resulting in

the liberation of NF- κ B dimers, which were observed using immunofluorescence in IL-1 β -treated MEFs (Hayden & Ghosh, 2008; Shih et al., 2011). The efficacy of IL-1 β in canonical NF κ B signalling has been well established. In A549 cells, IL-1 β induced greater I κ B α degradation compared to TNF- α , accompanied by sustained TRAF6 signalling, as demonstrated by Western blot analysis (Adli et al., 2010).

The fluctuation in activity of NF- κ B has been shown to be controlled by the stability of I κ B α (Hayden & Ghosh, 2008). For example, in colon cancer, IL-1 β -mediated I κ B α degradation in HCT116 cells activates p65, which promotes the proliferation of cells, playing an essential role in this malignancy (Karin, 2006). In addition, Demchenko and coworkers demonstrated that I κ B α mutations or IKK β hyperactivation, in multiple myeloma patient samples, result in constitutive NF- κ B activation that was sensitive to inhibition by IKK inhibitors such as ML120B (Demchenko & Kuehl, 2010).

1.3.4 Signalling Pathways of NF- κ B

There are two primary signalling pathways that regulate NF- κ B activation in cellular environments in response to stimuli. These pathways include canonical (classical) and non-canonical (alternative) pathways, which are described in detail below.

1.3.4.1 Receptor Coupling to the Canonical NF- κ B Pathway

Significant work has identified additional components that link different types of receptors to the IKK complex within the canonical NF- κ B pathway, which is activated by multiple inflammatory stimuli such as TNF- α , IL-1 β , LPS, reaching its component, the IKK complex, or by receptor-stimulating signals such as T-cell (TCR) and B-cell (BCR) receptors (Hayden & Ghosh, 2008; Taniguchi & Karin, 2018). In the stimulated state, a stimulus like IL-1 β engages IL-1R1, leading to the association of MyD88 and TRAF6. Subsequent signalling (TRAF6-TAB2/3-TAK1) activates the IKK complex, resulting in phosphorylation of IKK β (Figure 1.5) and K63-linked polyubiquitination. Activated IKK β phosphorylates I κ B α , targeting it for β -TrCP-mediated ubiquitination and degradation. This degradation releases NF- κ B dimers, commonly (p65/p50 or c-Rel/p50), which translocate to the nucleus (Hayden & Ghosh, 2008). In a mouse model study, TNF- α -treated macrophages were observed to exhibit oscillatory dynamics of NF- κ B signalling mediated by activation of I κ B α through paracrine signalling that induce gene expression and autoimmune disease, through disruption of this dynamic in

response to cytokines (Adelaja et al., 2021). These data highlighted the essential role of TRAF6, TAB2/3, and TAK1 in IL-1 β -induced NF- κ B activation and have important implications for inflammation-related diseases, inflammatory bowel disease, autoimmune diseases, and cancer.

Furthermore, studies have shown that viruses induce IKK β -dependent NF- κ B activation either directly through specific viral proteins, such as Hepatitis C virus or Influenza A virus, via TRAFs or RIP1 receptors, or indirectly through viral RNA or DNA, which act as pathogen-associated molecular patterns recognised by host pattern recognition receptors (Hiscott et al., 2006; Santoro et al., 2003; Schmitz et al., 2014). GPCRs were also examined to activate the IKK β -dependent NF- κ B pathway through a complex mechanism involving G $_{\alpha q}$ and G $_{\beta \gamma}$ subunits triggered by endogenous mediators, such as bradykinin. This activation is essential for inflammation, but it is moderated and transient compared to stronger innate immune receptors, such as TLRs (Xie et al., 2000; Ye, 2001).

1.3.4.2 The Non-Canonical NF- κ B Pathway

As outlined above, the non-canonical NF- κ B pathway (alternative pathway) is a signalling pathway that was found to be activated in a subset of cell types (B cells and lymphoid stromal cells) and characterised by processing of p100 into p52. However, the pathway has proved to be far more ubiquitous than first realised, and I found it in T-cells, epithelial cells, cancer cells, and others. However, unlike the canonical NF- κ B pathway, it is triggered almost exclusively by a subset of the TNFR superfamily, such as the lymphotoxin β receptor (LT β R) (Sun, 2017), BAFFR (Claudio et al., 2002; Dejardin et al., 2002), CD40 (Coope et al., 2002), and receptor activator of NF- κ B (RANK) (Novack et al., 2003; Sun, 2011). Unlike the rapid activation kinetics and IKK β and NEMO-dependent establishment of the canonical NF- κ B pathway, it has slower activation kinetics (Liao et al., 2004), requires new protein synthesis, and is mediated closely by IKK α homodimers and not to IKK β or NEMO (Liang et al., 2006).

The initial receptor binding and upstream signalling activation via TRAF2/3/cIAPs for the non-canonical NF- κ B pathway remain distinct from those for the canonical NF- κ B pathway activation induced via TRAF6/TAK-1 receptor binding (Kendellen et al., 2014; Sun, 2011, 2017).

The non-canonical NF- κ B pathway is triggered by binding of one of the TNFR superfamily receptors to their specific ligands, resulting in the recruitment of adaptor proteins, specifically, TRAF2/3 (Sun,

2011, 2017). TRAF2/3 binds to cellular inhibitor of apoptosis (cIAP1/2), which ubiquitinates the NF- κ B-inducing kinase (NIK) to target it for proteasome-mediated degradation. In unstimulated cells, NIK is kept at low levels by being in a complex with TRAF3, TRAF2, c-IAP1, and c-IAP2, which facilitates its Lys48-linked polyubiquitination and subsequent proteasomal degradation, as shown by ChIP assay of BAFFR-stimulated B cells (Cildir et al., 2016; Sun, 2011; Vallabhapurapu et al., 2008). Binding of the receptor leads to the degradation of TRAF3 and TRAF2; thereby, NIK can be accumulated and auto-phosphorylated (stabilisation of NIK) (Sun, 2011, 2017; Vallabhapurapu et al., 2008).

Then stabilised NIK phosphorylates IKK α that in turn phosphorylates p100, leading to the association of SCF β -TrCP for generating Lys48-ubiquitin ligase and the partial proteasomal processing for p52, as shown in Figure 1.5 (Razani et al., 2011). The generated p52/RelB dimers migrate to the nucleus and activate gene transcription, such as BAFF, essential for B cell survival and also required for lymphoid development and tumour progression, as evidenced in multiple myeloma cells (Cildir et al., 2016).

The non-canonical NF κ B pathway activation is not fully recognised and understood; both IKK α and NIK are potential targets of this pathway inhibition. Therefore, by a deep understanding of this pathway, we can identify potential therapeutic targets for attenuation or prevention of cancer (Ben-Neriah & Karin, 2011). This pathway is studied in the thesis with respect to cytokine induction.

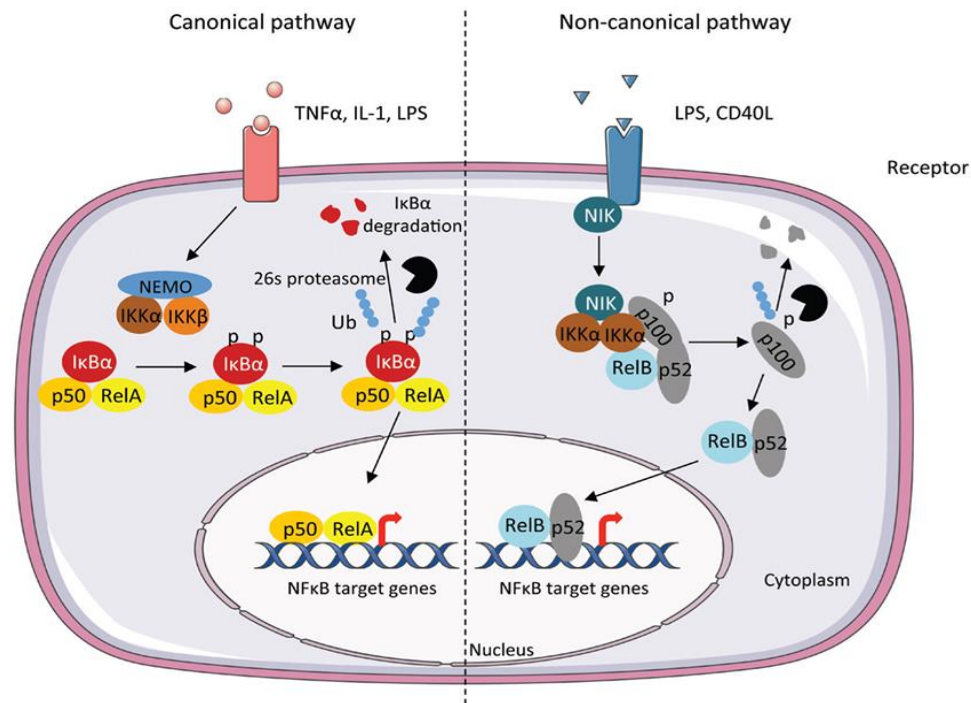


Figure 1. 5 The NF-κB pathways, the Canonical and Non-canonical pathways.

The cytokines activated the canonical pathway, including Interleukin-1 (IL-1), Tumour Necrosis Factor (TNFα), and Lipopolysaccharide (LPS). Activation induces IκBα phosphorylation by the IKK complex, followed by its ubiquitination (Ub) and degradation by the 26S proteasome. Transport the RelA/p50 dimer to the nucleus in its free form to induce target gene transcription. The alternative pathway caused NF-κB-inducing kinase (NIK) upon TNF cytokine-family stimulation, leading to activation of IKKα. NIK-IKKα/p100 recruitment results in phosphorylation of the p100 subunit. This leads to p100 processing and p52 formation in a 26S proteasome-dependent manner, resulting in the activation of p52-RelB that bind to different κB subunits and transcriptional activation of target genes. Figure adapted from (Viennois et al., 2013).

1.3.4.3 The Role of the NF-κB Pathway in Cancer

The NF-κB pathway plays a critical role in cancer hallmarks. Hyperactivation of NF-κB, which is driven by the IKK complex, promotes cancer development. For example, Karin and coworkers demonstrated in colorectal cancer HCT116 cells that the TNF-α-induced IKK activation by promoting IKKβ phosphorylation, allowing IκBα phosphorylation and the subsequent sequestration of p65/p50 dimers (Karin, 2006). NIK-induced phosphorylation of IKKα at serine 176/180 processes p100 to its

active form, p52, in multiple myeloma (MM), and the mutations of TRAF3 exacerbate NIK-IKK α activity that was detected in about 50% of MM tumours (Demchenko et al., 2010). Similarly, NEMO mutations/amplifications, identified in multiple myeloma, abrogate ubiquitin binding and lead to constitutive IKK activation, as confirmed in xenografts model (Annunziata et al., 2007). Recently, in lung cancer, Zinatizadeh's study explained that activation of IKK β increased IL-6 and VEGF, which contributed to tumour growth using A549 cells (Zinatizadeh et al., 2021).

Additionally, IKK β inhibitors such as Aryl cyanide hydroxyphenyl have been tested in lymphoma xenografts and suppressed by about 60% tumour load, indicating therapeutic potency (Cildir et al., 2016). However, the structural plasticity of the IKK complex has popularised it as an attractive therapeutic target, with IKK β inhibitor ML120B being an inhibitor currently under clinical trials.

Greten and coworkers demonstrated the relation between IKK β activation and inflammation-induced tumour development in a mouse model of colitis-associated cancer through upregulating IL-6 levels in MDCs, which was diminished when IKK β was deleted in colorectal cancer (Greten et al., 2004). Suggesting that IL-6 acted as a tumour growth factor.

Notably, a study in breast cancer has shown that LPS and IL-1 β -mediated p65/p50 activity is responsible for the upregulation of Cyclin D1 and cell proliferation, as demonstrated by ChIP-sequencing (Zinatizadeh et al., 2021). Studies in breast cancer models have shown that IKK pathways can also be activated in response to stress, such as reactive oxygen species (ROS), but with a minor effect. Such signals are enhanced by inflammatory cytokine, TNF- α , that induces ROS NF κ B activation through I κ B phosphorylation and degradation, enhancing EMT in breast cancer cells (Dong et al., 2007). Similarly, this response was observed in various cancer cells, depending on cell type-specific, where ROS regulates NF κ B activation through their component phosphorylation (I κ B, IKK), resulting in activation in the cytoplasm or inhibition in the nucleus (Morgan & Liu, 2011). These findings indicate the essential role of the canonical NF- κ B pathway in cancer growth and development.

Another essential pathway in cancer regulation highlighted by researchers worldwide is the non-canonical NF- κ B, which has context-dependent roles and serves as a classic example to understand the contribution of this pathway in a cellular context. For example, in large diffusion B-cell lymphoma, activation of the LT β R by LT α 1 β 2 activates the non-canonical NF- κ B pathway, which translocates

p52/RelB dimer to the nucleus and induces various regulatory genes involved in lymphogenesis using a genomic analysis study in a mouse model (M. Wolf et al., 2010). Furthermore, a study by Santini and coworkers demonstrated that the RANKL-RANK pathway mediates non-canonical NF- κ B activation in breast cancer, enhancing bone metastases as detected in primary breast cancer patients (Santini et al., 2011).

Using genetic studies and preclinical therapeutic inhibition for this pathway was the cornerstone in cancer treatment, particularly for bone cancer (Shi et al., 2025), which has not been clearly examined in previous studies, and this will be discussed in detail.

1.4 The Role of Inflammation in the Tumour Microenvironment

A number of cancer hallmarks come together in the tumour microenvironment (TME). A significant realisation was that the TME comprises an inflammatory environment that supports and shapes tumour development. The basic features of TME components can be subdivided into cellular and non-cellular components, which have unique characteristics and functions. Cellular constituents of the TME consist of cancer cells, immune cells, including cytotoxic T-lymphocytes, B-lymphocytes, tumour-associated macrophages (TAMs), neutrophils, and natural killer cells (Quail & Joyce, 2013; Wang et al., 2017), CAFs (Farhood et al., 2019), endothelial cells (Yang et al., 2021), and adipocytes (Pallegar & Christian, 2020). These cells not only provide support for tumour growth, but are also involved in immune evasion, angiogenesis, and extracellular matrix (ECM) remodelling (Brassart-Pasco et al., 2020).

T cells represent one of the two most abundant immune cells in the TME (Bhandoola & Sambandam, 2006; Y. Chen et al., 2021). T-cells are key players of adaptive immunity, and they include CD8+ cytotoxic T-lymphocyte cells (CTLs), which recognise tumour antigens presented by major histocompatibility complex class I (MHC-I) molecules and directly kill tumour cells in FasL-mediated apoptosis and in granule exocytosis (O'connell et al., 1996; Wiczorek et al., 2017). CD4+helper T cells facilitate the activation of CTLs at least in part by delivering activating signals (CD40-CD40L interaction) and secreting cytokines, such as IL-2, that promote clonal expansion of the CTLs (Bennett et al., 1998; Bourgeois et al., 2002). By contrast, studies demonstrated another kind of T-cells, regulatory T cells (Tregs), which express a transcription factor Foxp3 that act to suppress effector T-cell function via inhibitory cytokines such as TGF- β , promoting immune escape (Wolf et al., 2015).

Furthermore, immune checkpoints strongly affect T-cell function in the TME. For example, inhibitory checkpoints such as PD-1, CTLA-4, and LAG-3, which are highly expressed on exhausted T-cells, allow tumours to avoid immune surveillance by the expression of PD-L1 (Freeman et al., 2000; Leach et al., 1996). Blockade of checkpoints, such as anti-PD-1/PD-L1 antibodies (BMS-936558), reactivates T cells to mediate killing that has shown effectiveness in clinical studies, such as melanoma and non-small cell lung carcinoma (Topalian et al., 2012). However, persistent exposure to the antigen in the TME results in T-cell exhaustion, which is characterised by decreased effector function and diminished proliferative potential (Pauken & Wherry, 2015).

Additionally, interactions of T-cells with other immune cells enhanced anti-tumour immunity. For instance, Dendritic cells (DCs) reconnoiter T-cells via direct antigen presentation to T-cells but are frequently inhibited in their function by TME factors, such as VEGF and PD-1 expression, as examined in ovarian and colorectal cancer (Krempski et al., 2011; Michielsen et al., 2011). Similarly, Myeloid-derived suppressor cells (MDSCs) and TAMs suppress T cells using arginase, nitric oxide, and TGF- β , which create an immunosuppressive environment (Gabrilovich et al., 2012; Mantovani et al., 2017). Moreover, the cells of the innate immune system, such as TAMs and NK cells, are also important. NK cells that are induced by IL-12 and IL-21 can directly kill MHC-I-deficient tumour cells with granzyme B and perforin, which is important for immune surveillance (Smyth et al., 2005). But stromal cells suppress these effector cells, such as TGF- β derived from tumour-associated CAF, which can inhibit NK and CD8⁺ T cell cytotoxicity and proliferation, allowing immune evasion (Flavell et al., 2010).

Another essential element in TME is CAFs, which are a diverse cell population of activated fibroblasts and are abundant in the tumour stroma of a plethora of tumour types. CAFs can exert tremendous effects on TME through multiple mechanisms. By alterations of the ECM, growth factor production, and induction of angiogenesis, they support tumour hallmarks and resistance to therapy (Sarkar et al., 2023). CAFs also secrete a dense ECM of proteins, with collagen being an example, which contributes to tissue stiffness and builds a physical barrier to prevent invading T cells from entering the tumour environment (Stylianou et al., 2019). Factors released by CAFs, such as the chemokine CXCL12, directly stimulate proliferation in lung cancer cells (Wald et al., 2011).

Additionally, CAF-derived factors can diminish T cell migration and recruit immune suppression cells, such as Treg cells and MDSCs. Through this cell interaction, CAFs can induce or inhibit the T cell apoptotic effect, thereby contributing to immunosuppressive TME (Costa et al., 2018).

Strong evidence for these findings comes from experimental studies. For example, Costa and coworkers showed that CAF, notably, the S1 subset, plays a role in immunosuppression, through attracting T lymphocytes and enhancing their differentiation into regulatory T cells in human breast cancer (Costa et al., 2018). CAFs express high PD-L1 and FASL in an *in vivo* study and bind to PD-1 and FAS on T cells, driving antigen-specific CD8⁺ T cell apoptosis. Neutralisation of PD-L2 and FASL caused T cell cytotoxicity induction and anti-cancer activity improvement (Lakins et al., 2018). Furthermore, Ozdemir and coworkers illustrated in pancreatic adenocarcinoma that CAFs depletion decreased the ECM recruitment, increased T cell release and tumour sensitivity to the immune suppressive system (Özdemir et al., 2014). Studies by Salmon and coworkers demonstrated in a murine breast cancer model that CAF-derived CXCL12 creates a peritumoral barrier, and pharmacological targeting of CXCR4 (the CXCL12 receptor) resulted in increased T cell infiltration into tumours and synergy with anti-PD-L1 monoclonal antibody therapy in pancreatic cancer (Feig et al., 2013; Salmon et al., 2012).

CAFs also release cytokines, such as IL-6 and TGF- β , which stimulate tumour development and evade immune surveillance (Kalluri, 2016). For example, IL-6 secreted by CAFs is known to induce STAT3 within cancer cells, promoting their survival and therapeutic resistance in ovarian cancer cells (L. Wang et al., 2018). Endothelial cells are also essential through the chemokines production, such as CXCL8, that recruit and support neutrophils and thereby metastatic spread (Balkwill, 2004).

Additionally, a number of pro-inflammatory mediators are secreted via cells of stromal and immune origin that collectively drive chronic inflammation, which in turn upregulates pro-inflammatory enzymes such as COX-2, thus ultimately inducing DNA damage and genetic instability (Coussens & Werb, 2002). One important mediator is IL-1, a proinflammatory cytokine secreted by macrophages and stromal cells. IL-1 α and IL-1 β can induce the activation of NF- κ B and MAPK signalling pathways in tumour cells, which facilitates cancer development, for example, in breast cancer systems, endothelial adhesion molecules, such as VCAM-1, which promote tumour cell intravasation, are upregulated in response to IL-1 β (Voronov et al., 2003). The CANTOS clinical study (Canakinumab

Anti-inflammatory Thrombosis Outcomes Study) indicated that controlling IL-1 β with canakinumab, a recombinant monoclonal anti-IL-1 β antibody, substantially reduced the incidence and mortality of lung cancer in atherosclerotic patients, which provides further suggestion of IL-1 β 's involvement in inflammation-associated carcinogenesis, although this study was not designed as a cancer prevention study (Ridker et al., 2017).

An essential point needs to be mentioned about the dual effect of cytokines in TME. For example, TGF- β at first inhibits the growth of the tumour epithelial cell but then promotes EMT and Treg recruitment to the metastatic region (Massagué, 2008). Likewise, IFN- γ augments anti-tumour immunity, while paradoxically inducing PD-L1 to permit immune evasion (Taube et al., 2012). Furthermore, it has been found that CCL2 secreted by stromal cells recruits its receptor CCR2+ inflammatory monocytes, facilitating breast tumour metastasis via monocyte-derived VEGF. This effect was inhibited using an anti-CCL2 antibody that neutralises and reduces the interaction with tumour cells (Qian et al., 2011). Evidence reported that PD-1/PD-L1 blockers like pembrolizumab regenerate cytotoxic T cells, but TGF- β inhibitor, galunisertib, block metastasis; however, their action must be balanced to prevent autoimmunity responses (Massagué, 2008; Topalian et al., 2012).

Recent treatment strategies have increasingly targeted these inflammatory networks in the TME. Strategies like inhibiting the CXCL12/CXCR4 pathway through disrupting stromal crosstalk or blocking IL-1 β signalling effectively reduce pro-tumorigenic activity across cancer types. These strategies highlight the importance of targeting inflammation for novel cancer therapies (Feig et al., 2013; Geindreau et al., 2022). Figure 1.6 summarises and presents the link between inflammation and cancer development through the main key components: inflammatory signals, immune cells, pro-tumour effects, and TME changes, which were discussed.

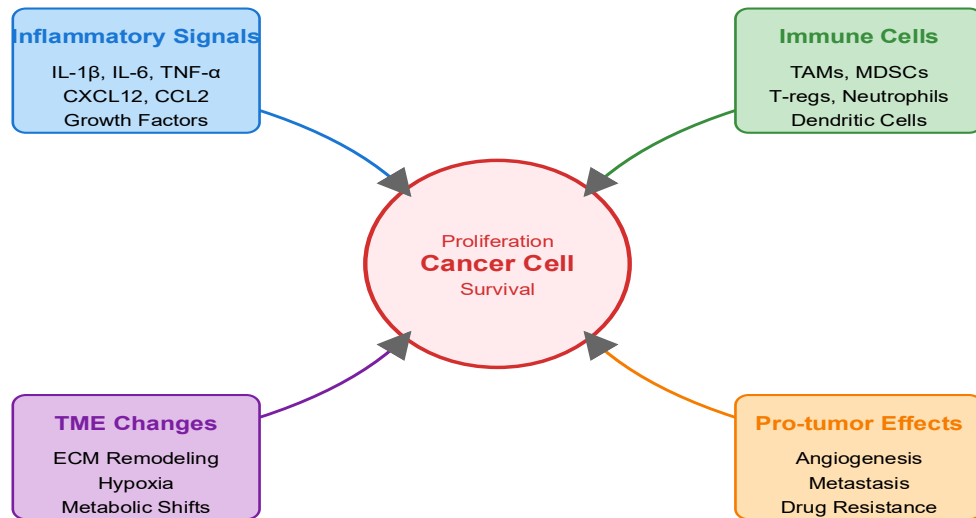


Figure 1. 6 The relationship between inflammation and cancer development.

The blue box (inflammatory signals) includes the central mediators that initiate and sustain inflammation within the tumour microenvironment (TME). The green box (immune cells) refers to tumour-associated macrophages (TAMs), myeloid-derived suppressor cells (MDSCs), dendritic cells, regulatory T cells (T-reg), and neutrophils; these cells infiltrate tumour tissue and exert both pro- and anti-tumour effects, ultimately promoting cancer cell growth and survival. The purple box (TME changes) includes extracellular matrix (ECM) alterations and hypoxia, which drive physical and chemical changes in the TME to support tumour growth and metastasis. The orange box (pro-tumour effects) represents the outcomes of chronic inflammation, such as angiogenesis and metastasis, which enhance tumour progression, survival, and dissemination.

1.5 Osteosarcoma

Osteosarcoma (OS) is the most common type of primary bone cancer, first described by John Abernathy in 1804 (Peltier, 1993). It predominantly affects children and adolescents and accounts for approximately 40% of all primary bone malignancies (Ziyu Ji et al., 2023). The pathogenesis of OS includes many genetic mutations that contribute to the transformation of normal cells into cancerous cells. For example, Czarnecka and colleagues suggested that OS may originate from mesenchymal stem cells (MSCs) or osteoblast precursors. MSCs can differentiate *in vitro* into multiple lineages, including osteogenic, chondrogenic, and adipogenic cell types. This differentiation potential is strongly implicated in the heterogeneity of OS. Furthermore, the activation of TP53 and RB1 in MSCs, along with the development of tumours, supports this association (Czarnecka et al., 2020). The malignant transformation was believed to occur in proliferative precursors, as opposed to post-mitotic, terminally differentiated osteoblasts. Genetic triggers such as TP53, RB1 gene deletion, and activation of oncogenic signalling pathways such as NOTCH, cooperate with microenvironmental pathways such as inflammatory cytokines to drive OS (Walkley et al., 2008).

Furthermore, studies highlight these origins in the bone marrow/bone microenvironment as shown in Figure 1.7, which points to the contribution of MSCs and osteoblasts in the initiation of OS. Studies in osteoblast precursors and MSCs showed that OS is highly vascularised and the WNT and NOTCH signalling are involved in its differentiation, metastasis and drug resistance. The endosteal niche acts as an environment for tumour cells to interfere with bone remodelling, releasing growth factors that support stem and tumorigenic cells. This further underscores the spatial relation between vascular niches and osteoclast-induced resorption in OS, highlighting the potential for therapeutic targeting in the improvement of clinical responses (Abarrategi et al., 2016).

A multi-model analysis study has examined OS phenotypes (osteoblasts, osteocytes, and fibroblast-like cells), MSCs, EPCs, pericytes, and bone cancer cell lines such as U2OS. The study identified various mutation genes such as NOTCH1, BRCA2, APC, PTCH1, and PRKAR1A involved in OS development and metastasis; these mutations are driven by specific markers such as CXCR4 and CD44 (Czarnecka et al., 2020). Overall, the nature of OS etiology is strongly influenced by genetic

microenvironment interaction, which highlights the need for OS to be examined on an individual patient basis.

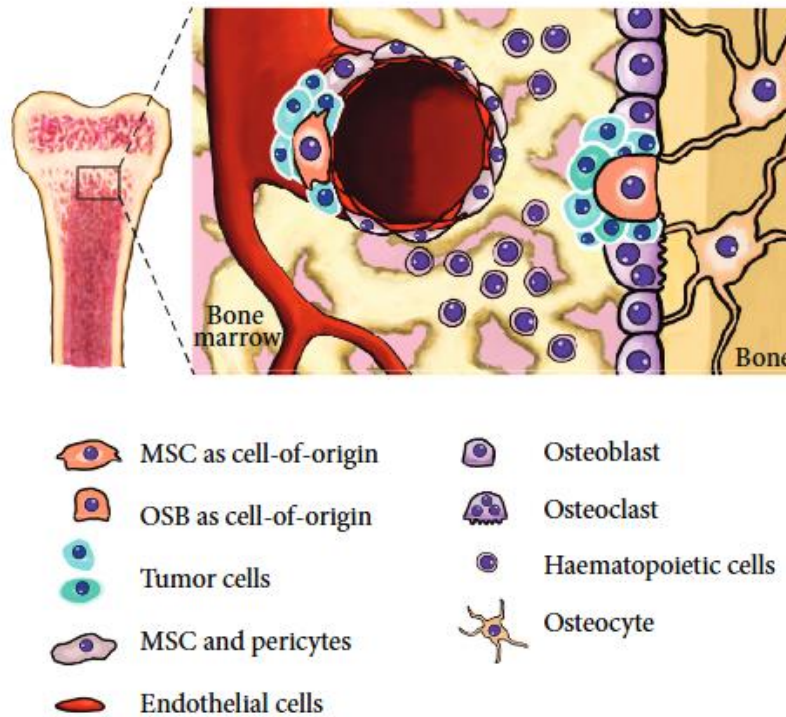


Figure 1. 7 The cells of origin for OS.

Several primary cell types within the bone microenvironment (BME) are essential, particularly mesenchymal stem cells (MSCs) located in a perivascular niche and their osteogenic lineage-committed cells, such as osteoblasts (OSBs). These cells are considered the main candidates for acquiring the initial mutations that promote OS development and trigger tumour formation. Other cell types present in the bone marrow include osteoclasts, osteocytes, endothelial cells, and haematopoietic cells. Figure adapted from (Abarrategi et al., 2016).

1.5.1 Subtypes of Osteosarcoma

1.5.1.1 Classical Osteosarcoma

The conventional type accounts for approximately 80 % of osteosarcoma cases, primarily impacting the metaphyseal areas of long bones. This type is further divided according to the predominant matrix type: osteoblastic, chondroblastic, and fibroblastic variants (Kimura et al., 2017; Picci, 2007).

1.5.1.2 Surface Osteosarcoma

Surface osteosarcomas consist of three different subtypes. The common surface type is the Parosteal type, which includes the posterior region of the distal femur and has a well-known morphology with limited cellular atypia. The second subtype is Periosteal osteosarcoma, primarily chondroblasts, which arises on the bone surface and has a more favourable prognosis than conventional variants. High-grade surface osteosarcoma, the rarest type, exhibits aggressive behaviour identical to conventional high-grade osteosarcoma (Bielack et al., 2002; Nouri et al., 2015).

1.5.1.3 Telangiectatic Osteosarcoma

This uncommon type, accounting for approximately 3-10% of cases, is defined by the presence of blood-filled spaces partitioned by septae that contain highly malignant cells. Although it exhibited an aggressive radiological appearance, certain studies indicated a comparatively improved effect of chemotherapy (Huvos et al., 1982; Liu et al., 2013).

1.5.1.4 Small Cell Osteosarcoma

This variant accounting for around 1-2% of all OS and exhibits similarities to Ewing's sarcoma while producing osteoid matrix. This aggressive variant is characterised by small round cells with little cytoplasm and variable osteoid production (Edeiken et al., 1987; Nakajima et al., 1997).

1.5.2 Signalling Pathways in Osteosarcoma

OS pathogenesis implies complex interactions among many signalling cascades that govern cancer hallmarks, which were previously discussed in Section 1.3. Figure **1.8** illustrates the main signalling cascades activated in osteosarcoma. Two pathways are well documented and described in detail below, while other pathways, JAK/STAT3, PI3K/AKT/mTOR, Hippo, Wnt/ β -catenin, Hh, and Notch, are not discussed in this research, and the provided reviews could guide the interested reader (Z. Ji et al., 2023; Kim et al., 2018; Zhao et al., 2021).

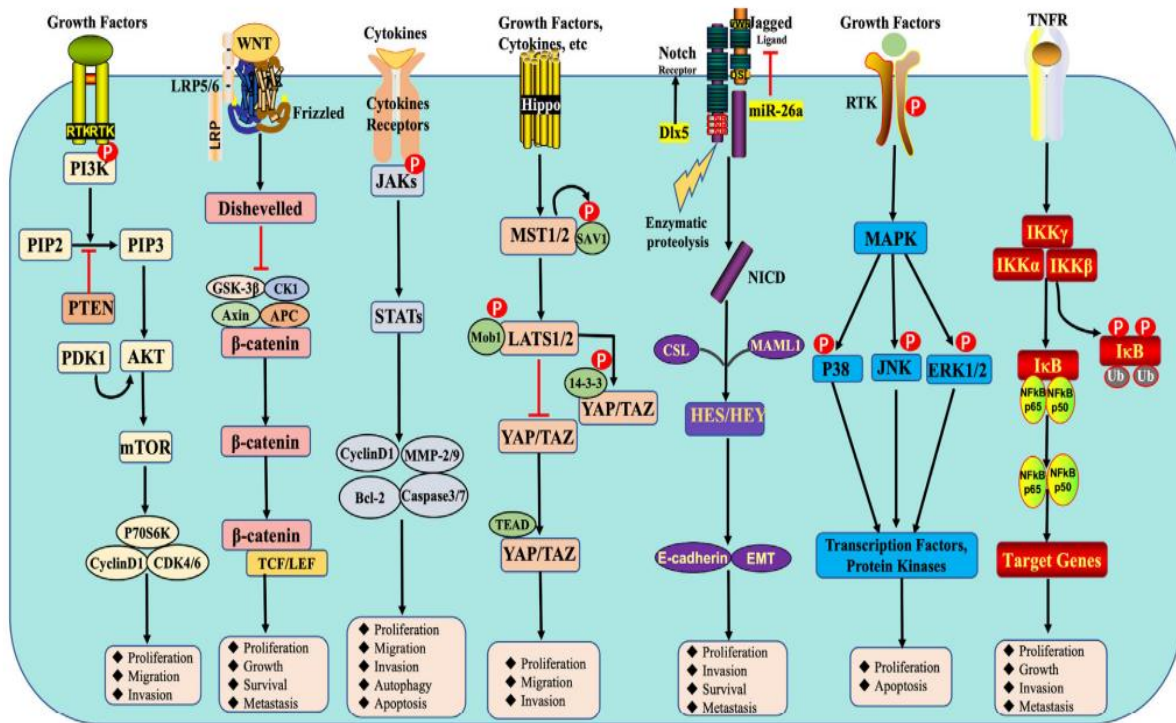


Figure 1. 8 The Main Signalling Pathways in Osteosarcoma and Their Inducing Factors.

Cytokines, GF, TNFR, and other stimuli activate JAK/STAT3, PI3K/AKT/mTOR, Hippo, Wnt/β-catenin, NFκB, and Notch signalling cascades, resulting in the activation of various cellular processes (proliferation, growth, survival, migration, invasion, metastasis, apoptosis, and autophagy). Figure adapted from (Ziyu Ji et al., 2023).

1.5.2.1 The MAPK Signalling Pathways

The MAPK pathway is essential in osteosarcoma hallmarks, particularly the ERK1/2 pathway, which plays a well-documented role in MAPK-mediated pathogenesis and progression through MCL-1 and Ezrin signalling activation (Chandhanayingyong et al., 2012; Pignochino et al., 2009). An experimental study by Pignochino and coworkers demonstrated that the ERK1/2 pathway was associated with tumour proliferation and angiogenesis. The multi-kinase inhibitor Sorafenib inhibited OS by inhibiting ERK1/2 and its downstream mediators, including MCL-1 (anti-apoptotic protein, myeloid cell leukaemia-1) and Ezrin (protein enhancing metastasis), which results in inhibition of tumour growth and vascularisation in pre-clinical models (Pignochino et al., 2009). Similarly, a natural compound showed anticancer activity via inducing apoptosis and autophagy in human OS cells through ROS-modulated ERK1/2 activation (Huang et al., 2018).

In addition, melatonin inhibits OS growth through suppression of ERK1/2 signalling in MG-63 osteosarcoma cells (Liu et al., 2016). Both the JNK and p38 MAPK pathways have two aspects. The protein NOV (a secreted matricellular protein) has also been reported to suppress OS cell growth while activating apoptosis and migration via regulation of p38 MAPK and JNK signals, possibly by crosstalk with AP-1 (Yao et al., 2015). Similarly, these pathways are suppressed by the natural compound Kaempferol, which inhibits bone metastasis in the U2OS cell line (Chen et al., 2013). These results demonstrate how the MAPK pathway might have therapeutic implications for OS.

1.5.2.2 The NF- κ B Signalling Pathway

One of the primary pathways that researchers worldwide are interested in understanding better is the NF- κ B pathway. Therefore, we focused on this pathway in the thesis as a target for potential cancer reduction and therapeutic improvement. This pathway was described earlier in Section 1.3.3.6.2. In osteosarcoma, the NF- κ B pathway is a central driver of bone progression and metastasis, primarily through its canonical (p50/p65-I κ B) signalling, although evidence is now revealing the possibility for crosstalk with alternative (RelB/p52) signalling in bone dynamics (Inoue et al., 2007).

In resting cells, NF- κ B is a cytoplasmic heterodimer complex with an inhibitory protein, I κ B to keep it inactive (Neumann & Naumann, 2007). In bone cancer, dysregulation allows constitutive activation through inflammatory cytokines like TNF- α or IL-1, cellular stress, or TME acidosis, causing signal-mediated enhanced tumour development (Avnet et al., 2017; Gilmore, 2006).

For instance, Li and coworkers have shown that NF- κ B activation in bone cancer cells, including U2OS and MG-63 cells, can increase integrin- β 1, which promotes antiapoptotic signal transduction and bone invasion and metastasis. A pharmacological study using AIIB2 monoclonal antibody, which inhibits integrin- β 1 and NF- κ B inhibitor, JSH-23, decreased murine lung metastasis via inhibiting this pathway, indicating its therapeutic effect (Li et al., 2019).

Studies have shown that NF- κ B induction directly promotes metastatic programs by multiple pathways. For example, in the LM8 OS cell line, VCP (p97) transfected cells, an NF- κ B regulator, promote constant activation of the NF- κ B pathway, increasing the metastatic potential of tumour cells to the lung through expression of MMP-9. Inhibiting VCP-mediated NF- κ B signalling might reduce lung metastasis by regulating the degradation process of phosphorylated I κ B α (Asai et al., 2002). Similarly,

preclinical models showed that Aspirin also inhibited canonical NF- κ B activity in MG-63, U2OS, and 143B cells, accompanied by reduced expression of metastasis-mediated genes such as Bcl2, cIAP1/2, and XIAP, and prevented metastasis in the lung in a dose-dependent manner (D. Liao et al., 2015).

A cancer analysis study highlights the conserved functions of NF- κ B in bone tumour metastasis. In prostate cancer, miR-141-3p (a tumour suppressor miRNA) targeting the TRAF6/NF- κ B axis is downregulated in bone-metastatic prostate cancer cells, promoting metastasis through NF- κ B activation (Huang et al., 2017). Additionally, Santini and coworkers reported in primary breast cancer that expression of RANK is up-regulated and related to skeletal metastasis, indicating a role for NF- κ B signalling in the osteoclast-mediated bone degradation (Santini et al., 2011).

Using genetic studies, the NF- κ B signalling pathway also differentially regulates the resistance to apoptosis. For instance, knocking down lncRNA XIST (X-inactive specific transcript, an oncogene in cancer) in U2OS cells induced canonical NF- κ B activation, which cooperated with p53 to induce expression of the proapoptotic PUMA (p53-upregulated modulator of apoptosis) and induce caspase-3-mediated OS apoptosis (W. Gao et al., 2019). Furthermore, activation of NF- κ B mediated TME acidosis was observed in MSCs, promoting secretion of paracrine factors such as CXCL5, IL-6, IL-8, and MMPs, which influence OS stemness and chemoresistance (Avnet et al., 2017).

Preclinical therapeutic inhibition of the NF- κ B pathway must be target-specific. For example, the herbal drug Asiaticoside suppresses the TRAF6/NF- κ B signalling pathway, reducing OS growth and invasion through inhibition of M2 polarisation of macrophages (Li & Wang, 2022). However, precise and efficient therapeutic strategies are challenging due to the complex arrangement of the pathway and its essential significance in normal cellular activity.

1.5.3 Osteosarcoma Treatment

Based on specific malignancy type and stage, treatment of osteosarcoma involves multiple approaches. Treatment of the localised tumours includes the pre-operative stage, which includes adjuvant chemotherapy for ten weeks to reduce tumour size and remove any micrometastasis (Redondo et al., 2013). The surgical stage and the post-operative stage involve extended chemotherapy for up to one year, with the regimen frequently modified according to the response to pre-operative treatment (Ferguson & Goorin, 2001).

Treatment for metastatic cases remains a significant challenge, as survival rates are considerably decreased in patients diagnosed with metastases. It starts with aggressive chemotherapy, followed by surgery if tumours become resectable, and may incorporate targeted medicines or clinical trials for resistant cases (Italiano et al., 2020). Substantial challenges persist in effective OS management, including managing chemotherapeutic side effects and psychosocial consequences, alongside the challenges in targeting advanced treatments and immunotherapy (Hoang et al., 2004). Furthermore, limited OS clinical trials reduce novel drug development (Mirabello et al., 2009).

Significantly, chemokines and their receptors are now recognised as critical mediators influencing tumour growth and metastasis. Experimental studies evidenced this role through a consistent increase in specific CXC chemokines, which was observed in paediatric OS patients (Li et al., 2011). A dysregulated pattern of chemokine receptor expression was examined in OS tumours, suggesting signalling loops that enhance malignancy (Von Luetichau et al., 2008). CXCR4/CXCL12 axis is a key pathway and functionally involved in OS hallmarks through inducing cell proliferation, survival, and homing (Perissinotto et al., 2005). These findings underscore the importance of chemokines as a pivotal therapeutic target in osteosarcoma. Therefore, we highlight and examine chemokines here in this thesis.

1.6 Chemokines

Chemokines represent a novel and significant category of mediators that connect cancer to inflammation. These are small molecules (8 to 12 kDa) that modulate numerous cellular functions, such as chemotaxis, angiogenesis, haematopoiesis, and immune cell activity, while also facilitating various pathological conditions, including cancer (Griffith et al., 2014; Stockhammer et al., 2000; Taub & Oppenheim, 1994; C. Wang et al., 2018). They have been divided into four classes based on their structural organisation. The largest category comprises CC chemokines, characterised by two adjacent cysteine residues, whereas C chemokines possess only a single N-terminal cysteine residue. Typically, CXC and CX3C chemokines have either one or three extra amino acids (X) introduced between their cysteine residues, as shown in Figure 1.9 (Cuesta-Gomez et al., 2021; Sun et al., 2010; Wang et al., 2006). Other research highlights the novel category of chemokines, identified as chemokine ligands (L) and their corresponding receptors (R) (Zlotnik & Yoshie, 2000). One of the most interesting

chemokines essential in immune responses and pathological conditions is stromal cell-derived factor-1 (SDF-1), also known as CXCL12.

Chemokines can induce their biological effects via binding with their receptors and are classified into four groups (CXCR, CX3CR, CCR, and XCR) based on their targeting chemokine (Burger & Kipps, 2006). Over 20 chemokine receptors and seven receptors present on the cell surface have been identified for binding chemokines (Sun et al., 2010).

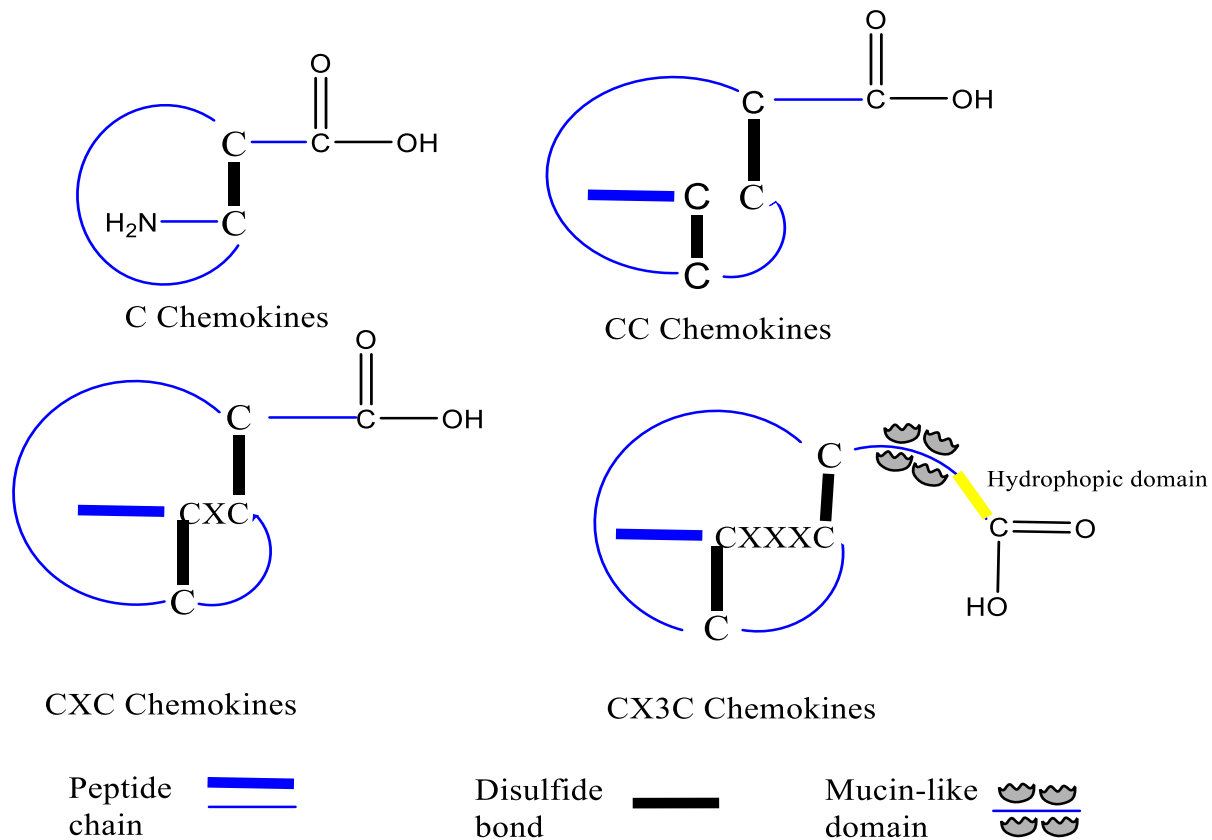


Figure 1. 9 Structure of Chemokine Types. Figure adapted from (Cuesta-Gomez et al., 2021).

1.6.1 Role of Chemokines in Cancer

Chemokines play an important role in cancer biology through diverse and complex functions that regulate migration and targeting of cells between tissues through binding to their G-protein-coupled receptors ($G_{\alpha i}$), as shown in Figure 1.10 (Chow & Luster, 2014). In cancer, the primary function of chemokines is immune cell migration into the TME, affecting the antitumor immunity through immune cells or pro-tumourigenic cells recruitment (Kohli et al., 2022). Diverse chemokines can affect cancer growth by recruiting anti- or pro-tumour immune cells. For example, CXCL9 and CXCL10 significantly correlate with advantageous Th1-biased immune response and cytotoxic T-cell recruitment to malignancies (Vilgelm & Richmond, 2019). Similarly, in a mouse model study, CCL2 can enhance breast cancer metastasis through CCR2 signalling activation, recruiting inflammatory monocytes that differentiate into metastasis-associated macrophages (Kitamura et al., 2015). Furthermore, it has been found that chemokines can affect cancer hallmarks through multiple mechanisms. For instance, the CXCL1, CXCL2, CXCL3, and CCL5 are highly expressed in melanoma cells and implicated in cancer growth and progression (Payne & Cornelius, 2002), while high CXCL12 expression has been examined in breast cancer metastasis (Müller et al., 2001), and OS (Baumhoer et al., 2012).

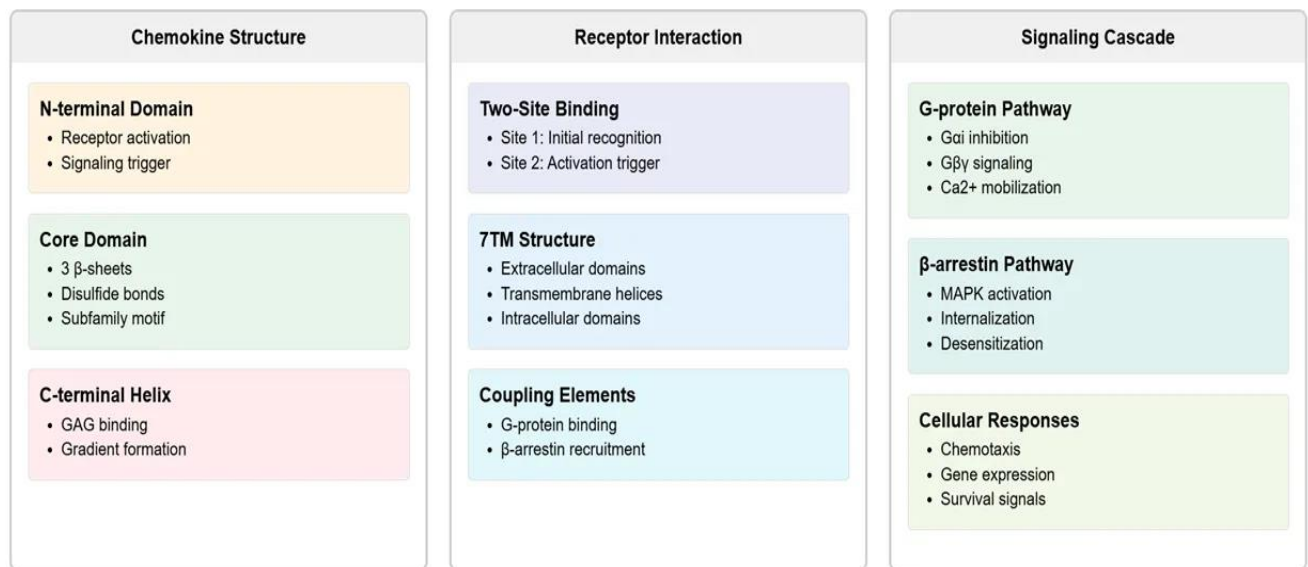


Figure 1. 10 Schematic Representation of Chemokine System Organisation

The scheme shows structural elements, receptor interactions, and signalling pathways that regulate immune cell responses. GAG; GlycosAminoGlycan, 7TM; Seven-TransMembrane, $G_{\alpha i}$; G protein alpha inhibitory subunit, $G\beta\gamma$; G protein beta-gamma subunits, Ca^{2+} ; Calcium ions. Figure adapted from (Chow & Luster, 2014; Griffith et al., 2014; Vilgelm & Richmond, 2019).

1.7 Stromal Cell-derived Factor-1 (SDF-1) CXCL12

An important chemokine member that is involved in immunology and cancer is CXCL12. Initially, CXCL12 was identified as a pre-B cell growth factor. The original name (stromal cell-derived factor-1, or SDF-1) came from its derivation from bone marrow stromal cells (Bleul et al., 1996). CXCL12, which mediates its actions through CXCR4 and CXCR7 receptors, is critical for a number of cellular processes. For example, CXCL12 drives organ-specific arterial distribution during embryogenesis in mice by binding to CXCR4. CXCL12 acts on arterial endothelial cells to upregulate CXCR4, which is essential for arterial development in the gastric system (Ara et al., 2005).

CXCL12 also directs the migration of hematopoietic progenitor cells and mesenchymal stem cells to injury sites, enabling tissue repair and regeneration. Additionally, embryogenesis includes germ cell migration, organ vascularisation, and neural development, which are mediated by CXCL12/CXCR4 signalling. Knockout of CXCL12 or its receptor results in severe developmental defects and embryonic lethality (Cheng et al., 2014). Studies also show that CXCL12 enhances angiogenesis in HUVECs through interaction with CXCR7, activating PI3K/Akt signalling, promoting proliferation and migration, but in mice, CXCL12 also promotes angiogenesis through the CXCR4 signalling pathway, and knockout of CXCR4 induces abnormal vascularisation in mice (Salcedo & Oppenheim, 2003; Zhang et al., 2017). CXCL12 also triggers post-ischemic leukocyte infiltration in murine stroke models through the CXCR4 signalling pathway, and inhibition of this pathway regulates neuroinflammation by reduction of proinflammatory cytokines (Ruscher et al., 2013).

Furthermore, genetic studies have demonstrated the function of CXCL12 in the bone marrow system. For example, mice lacking CXCL12 have been found to have a deficiency in B-cell lymphopoiesis and bone marrow myeloopoiesis. This indicates the essential value of CXCL12 in bone marrow regulation via hematopoietic stem cells (HSCs) during embryonic development (Nagasawa, Hirota, et al., 1996). Similarly, Sugiyama and his group demonstrated the importance of the CXCL12/CXCR4 signalling in adult bone marrow by maintaining the HSC pool interacting with CXCL12-abundant reticular (CAR) cells (Sugiyama et al., 2006).

1.7.1 Structural Features and Components of CXCL12

CXCL12 is classified as one of the fourth class of chemokines CXC, which are composed of two cysteine residues separated by another amino acid (Sun et al., 2010; Wang et al., 2006). Previous studies discovered that CXCL12 has six isoforms in humans (α to ϕ) and three isoforms in animals, with two main isoforms implicated in the regulation of immune responses: α and β (Shirozu et al., 1995; Yu et al., 2006). The functionality of CXCL12 is determined by several critical domains in its molecular structure. The NH₂-terminal region is crucial for receptor activation, with the initial eight amino acids being required, and the first two amino acids (Lysine and Proline) being important (Levoye et al., 2009). This region includes the CXCR4-binding motif with the sequence RFFESH, which improves receptor binding activity (Crump et al., 1997). The central domain contains the BBXB motif (with B indicating basic amino acids and X indicating any other residue), which is essential for glycosaminoglycan (GAG) binding that contains Lysine24, Histidine25, Leucine26, and Lysine27 (Amara et al., 1999).

The variable region between chemokines is the C-terminal region and contributes to receptor binding and activation. In CXCL12, the C-terminus plays a role in G protein-coupled receptor (GPCR) activation (Rik Janssens et al., 2018). All six isoforms of CXCL12 possess identical 67 amino acids but differ in overall length, as illustrated in Figure 1.11. These variants reveal distinct tissue distribution patterns, with CXCL12 α and β mostly present in adult tissues and located in bone marrow, whereas CXCL12 γ is mainly expressed in cardiac tissue, and CXCL12 δ , ϵ , and ϕ show the highest expression in the pancreas (Rik Janssens et al., 2018). Structurally, the heparin-binding domain of CXCL12, and its two splice variants, α and β , which enable dimerisation and gradient formation, are essential for immune cell migration; mutations in the heparin-binding domain reduce GAG and endothelial cell binding, impairing migration of peripheral blood cells and monocyte attraction *in vivo*. GAG binding protects CXCL12 from enzymatic inactivation and facilitates chemokine gradient formation (R. Janssens et al., 2018).

Among these forms, CXCL12 γ displays distinctly unique features. A COOH-terminal extension of 20 amino acids distinguishes it from CXCL12 α . It additionally binds GAGs with tenfold more affinity. Notably, despite its inhibitory effect *in vitro*, CXCL12 elicits the most potent chemotactic response *in vivo* (Rueda et al., 2008). This impact demonstrated the complexity of CXCL12's functions in

biological responses and the importance of its structural variations. The structural characteristics and several splice variants of CXCL12 enable precise regulation of its activity in diverse physiological contexts. Its activity is primarily based on the distribution of its isoforms in tissues, which controls the specialised function. Experiments on mice demonstrated that any chemical alteration in their amino acid constituents inhibited CXCL12 function (Rik Janssens et al., 2018). Moreover, a study involving mice deficient in a GAG binding site demonstrated reduced CXCL12 biological function (Rueda et al., 2012).

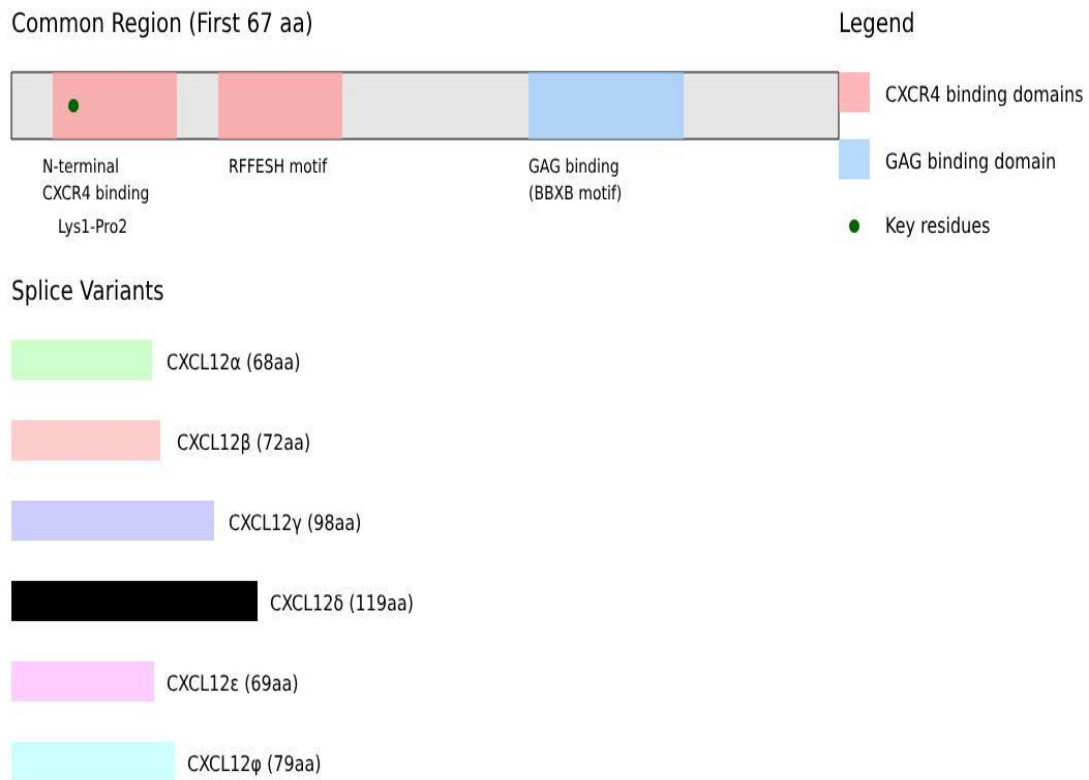


Figure 1. 11 CXCL12 Structure and Splice Isoforms.

CXCL12 contains CXCR4 binding domains with an N-terminal CXCR4 binding site and RFFESH motif, a GAG binding domain with a BBXB motif. Different isoforms of CXCL12 contain various numbers of amino acids. RFFESH: R= Arginine; F= Phenylalanine; E= Glutamic Acid; S= Serine; H= Histidine, GAG: Glycosaminoglycan, aa: amino acids. Figure adapted from (Rik Janssens et al., 2018).

1.7.2 CXCL12 Production

CXCL12 was initially found to be produced from bone marrow stromal cells (Nagasawa, Nakajima, et al., 1996), endothelial cells, but also other cells such as cancer-associated fibroblasts (CAFs) (Orimo et al., 2005; Teng et al., 2016a). The main source of CXCL12 production within the bone marrow is CXCL12-abundant reticular cells (CAR), in comparison to other cell types (Sugiyama et al., 2006). CXCL12 expression is higher during the early stages of bone development, with changes in expression marked in osteoblasts and chondrocyte cells. The CXCL12 production is mechanistically regulated by many factors, such as growth factors, cytokines, and microenvironment effects, with a reverse impact observed in bone marrow spaces in TME. For instance, studies have shown that in osteoblasts, pro-inflammatory cytokines IL-1 β and TNF α both increase CXCL12 expression in a concentration-dependent manner. PTH also induces its expression in *vivo* and in *vitro* studies to promote hematopoietic stem cell (HSC) mobilisation (Jung et al., 2006).

CXCL12 is expressed in TMEs, including in CAFs and hypoxic endothelial cells. Studies have shown that TGF- β and PDGF are involved in CAF by recruitment and function, and CXCL12 produced by CAFs contributes to the recruitment of endothelial precursor cells and immune cells (Östman & Augsten, 2009), CAFs can stimulate CXCL12/CXCR4 signalling to promote tumour progression and motility in gastric cancer cells (Izumi et al., 2016). In contrast, TGF- β downregulates CXCL12 expression in tumour-associated mesenchymal stem cells, which promotes breast cancer metastasis (R. Janssens et al., 2018).

Hypoxia-inducible factor-1 α (HIF-1 α) in hypoxic TMEs promotes the secretion of CXCL12 from endothelial cells and promotes angiogenesis through binding of HIF to the hypoxia response region of CXCR4 promoter, inducing gene transcription and expression (Lopez-Haber et al., 2016; Petit et al., 2007). These complex regulatory factors highlight the potential of CXCL12 in both physiological and pathological processes, depending on specific signals within the tissue microenvironment.

1.7.3 Cellular Mechanisms Activated by CXCL12.

As indicated above, CXCL12 mediated its actions via binding to two GPCRs, predominantly CXCR4 or CXCR7. Upon binding of CXCL12 to CXCR4, a complex network of signalling pathways is activated by the dissociation of heterotrimeric G proteins (G α and G β/γ subunits). This activation

initiates numerous concurrent signalling cascades that control diverse cellular processes, as shown in Figure 1.12 (Yu et al., 2018). The primary pathway includes activating three separate paths by the G_α subunit. NF- κ B activation results in the transcription of pro-inflammatory genes. The other path that promotes VEGF synthesis and angiogenesis is JAK2-STAT3, while the other pathway, such as MAPK or PI3K facilitates cellular hypersensitive responses (Cambier et al., 2023).

Following binding of CXCL12 to CXCR4, the $G_{\beta/\gamma}$ subunit activates two primary signalling pathways. Activation of PI3K triggers a phosphorylation cascade through PDK1 signalling to activate AKT, which is essential for controlling cell survival, migration, and proliferation. For example, studies have shown the importance of CXCL12-mediated PI3K/Akt/mTOR signalling in facial nerve injury repair through enhancing Schwann cell migration (D. Gao et al., 2019). Another pathway involves the conversion of PIP₂ into IP₃ and DAG through the activation of PLC β (Yu et al., 2018). The IP₃ pathway induces calcium release from the endoplasmic reticulum. Then, the calcium signalling with the DAG pathway activates MAPK signalling, activating downstream CXCR4 signalling cascades, including RAS-RAF-MEK-ERK signalling, controlling cell survival and motility (Cambier et al., 2023). Dysregulation of this pathway, inducing pituitary adenoma formation as demonstrated in pituitary cell lines and a mouse xenograft model (Barbieri et al., 2014) In an *in vitro* study, Kim and coworkers illustrated that CXCL12 triggers chemotaxis through $G_{\alpha i}$ -protein-coupled pathways, which are essential in directing hematopoietic progenitor cell migration to the bone marrow (Kim & Broxmeyer, 1998).

Consequently, inhibition strategies for both receptors differ. CXCR4 inhibitor, plerixafor, directly targets the binding site and blocks the $G_{\alpha i}$ -induced signalling and chemotaxis, resulting in physiological homing disruption and pathological spreading (R. Janssens et al., 2018). This was evidenced in bone marrow physiology, a notable example of which Moll and coworkers explain that the CXCL12 in stromal cells is critical for hematopoietic stem cell (HSC) retention. Its functional role has been confirmed in knockout mice of CXCL12 or CXCR4 for HSC mobilisation, and in clinical inhibitory studies, using plerixafor (Moll & Ransohoff, 2010).

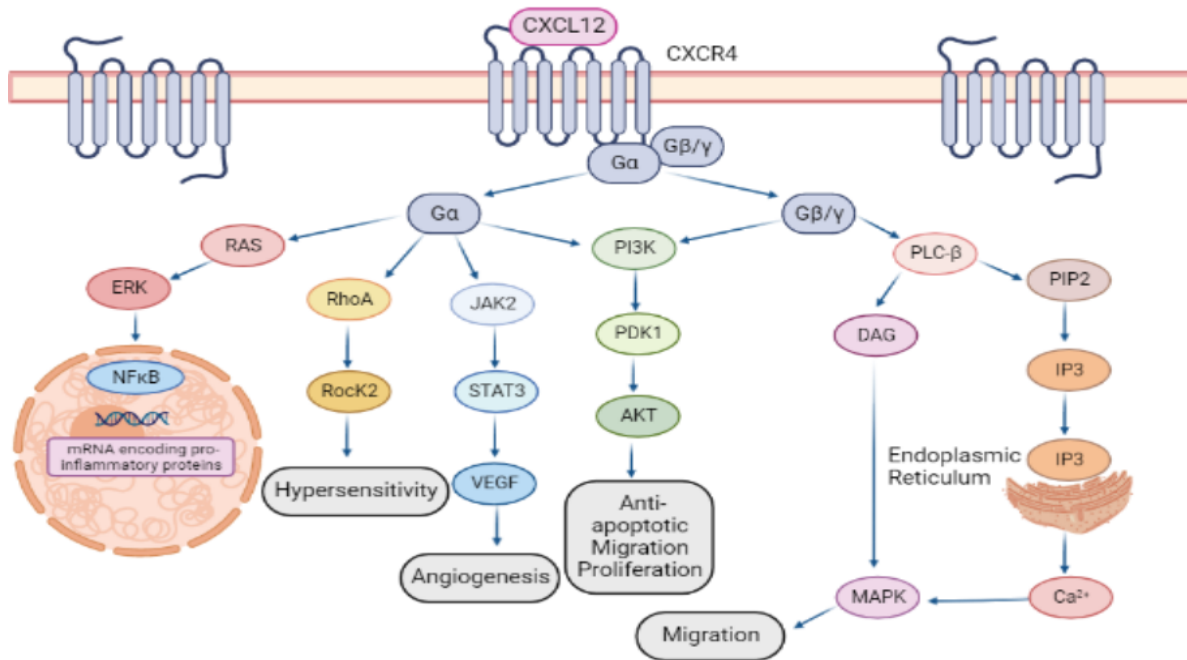


Figure 1. 12 Diagram representation of CXCL12-mediated signalling pathways.

CXCL12 binds to its GPCR, CXCR4, to induce ERK/JAK-STAT/AKT/PLC-β/RhoA pathways and, therefore, allergy, inflammation, and other physiological processes—original Figure made with BioRender.

1.7.4 Signalling Functions of CXCR7

Recent studies have shown that CXCR7 is a typical chemokine receptor that lacks $G_{\alpha i}$ -protein coupling; its activation depends on β -arrestin recruitment upon binding to CXCL12, activating β -arrestin-dependent signalling pathways such as MAPK/ERK. CXCR7 also acts as a scavenger receptor, regulating CXCL12 levels, thereby modulating its availability for CXCR4 signalling, regulating cellular processes such as cell survival and adhesion (R. Janssens et al., 2018). For example, studies have demonstrated the role of CXCR7 activation in atherosclerosis through multiple downstream signalling cascades, such as PI3K/Akt-mediated endothelial repair and reduced endothelial permeability, β -arrestin was mediated desensitisation and internalisation of CXCR7, regulating CXCL12 bioavailability (Murad et al., 2021).

As mentioned above, the inhibition strategy for CXCR7 differs from CXCR4 targeting; using a CXCR7 inhibitor such as CCX771 prevents CXCL12 scavenging and β -arrestin recruitment, resulting in gradient alteration of CXCL12 and downstream signalling pathways modulating CXCR4 activity, which are mediating cellular processes such as angiogenesis (R. Janssens et al., 2018).

1.7.5 Role of CXCL12 in Cancer Development

Although CXCL12 is essential in regulating the immune system responses, this action is important in cancer development, invasion and metastasis. This has been observed through a number of different cellular studies; the use of knockout mice combined with a number of cancer models, and correlative studies using clinical samples. Often, the expression of CXCL12 is linked to CXCR4/expression and defined as the CXCL12/CXCR4 axis.

For example, in ovarian cancer, high expression of CXCL12 is linked to dendritic cell trafficking and adhesion in tumours (Li et al., 2018; Ray et al., 2015; Zou et al., 2001). In ovarian cancer patients, Kryczek and co-workers demonstrated high expression of CXCL12, resulting in tumour development synergistically with VEGF through induced angiogenesis in an *in vivo* assay model (Kryczek et al., 2005). A cellular study on prostate cancer cells revealed that CXCL12 triggers prostate cancer metastasis, which was attenuated through the degradation of CXCL12 by enhancing the activity of CD26/dipeptidyl peptidase IV (DPP4) (Sun et al., 2008). This study was similar to T-cell lymphoma (Sezary syndrome); the migration of CD4⁺ T-cells into blood and skin was found to be linked to the upregulation of CXCL12 and inhibition of DPP4 (Narducci et al., 2006). This was confirmed recently on keloid scars, dysregulation of CXCL12-DPP4 controlled by TGF- β /SMAD signalling enhances CXCR4⁺ inflammatory cells infiltration in the scars (Z. Chen et al., 2021). Additionally, CXCL12 also increased prostate cancer metastasis through the expression and activation of integrin α v β 3 receptors in PC3 and C4-2B cell lines, resulting in enhancement of cell adhesion and invasion, but not in LNCaP cells (Sun et al., 2007).

Furthermore, a study in a mouse xenograft model of breast cancer demonstrated that CXCL12 activation increased breast cancer metastasis to bone marrow and other sites, such as the lung (Ray et al., 2015). A high expression of CXCL12 in human gastric cancer (GC) cells increased tumour growth and invasion by the CAFs mediated integrin β 1 recruitment that activates the CXCL12/CXCR4

signalling pathway (Izumi et al., 2015). Similarly, Avraham's study in mice lacking transcription factors, including ATF3 and the c-Jun dimerisation protein 2 (JDP2), showed that CAFs promote a TME through CXCL12 overexpression, increasing tumour size and cell proliferation relative to the wild-type mice (Avraham et al., 2019).

Experiments by Orimo and his colleagues demonstrated that CAFs extracted from human breast cancer could enhance tumour growth and angiogenesis via increased CXCL12 production more than normal fibroblasts (Orimo et al., 2005). In addition to CAF, growth factors are also essential in cancer-mediated CXCL12 signalling. For example, in lung cancer, CXCL12 activation promotes the overexpression of CTGF by the CXCL12-mediated MEKK1/JNK/ SMAD3 signalling pathway (Lin et al., 2018). Additionally, CXCL12 secreted from bone marrow stromal cells and multiple myeloma cells regulates the migration of monocytes within the TME, and induces anti-apoptotic effects in colon cancer through activation of EGF signalling cascades (Beider et al., 2014; Rigo et al., 2010). In breast cancer models, CXCL12 activates GTPases, including RhoA and Rac1, resulting in enhanced ECM degradation mediated by MMP to maintain metastasis (Mortezaee, 2020), whilst preclinical studies confirmed that Rac1 or RhoA deletion significantly inhibited cancer metastasis and lung colonisation (Mortezaee, 2020; Parri & Chiarugi, 2010).

Multiple studies reported that G protein-coupled receptor kinase (GRK) signalling-mediated arrestin molecule could be activated by the CXCL12/CXCR4 pathway, thus enhancing multiple signalling cascades resulting in cancer hallmarks initiation (Décaillot et al., 2011; Singh et al., 2013; Sun et al., 2010). Research by Liao and coworkers showed the role of CXCL12/CXCR4 signalling in promoting OS survival and lung metastasis through activation of JNK/Akt signalling cascade; this effect was significantly inhibited by CXCR4 antagonist, Plerixafor, in both cellular and mouse models (Y.-X. Liao et al., 2015). Furthermore, miR-494 has shown to inhibit CXCL12/CXCR4 signalling-mediated breast cancer progression by the Wnt/ β -catenin signalling pathway (Song et al., 2015). Similarly, Hall and his colleagues demonstrated that CXCL12/CXCR4 activation induced proliferation in human breast and ovarian cancer cells via the estrogen-ER α signalling pathway, as reported by colorimetric assay (Hall & Korach, 2003). All of these findings support the importance of CXCL12 signalling in cancer regulation.

Whilst not intensively studied, evidence has emerged for CXCR7 in the pro-tumorigenic action of CXCL12. This occurs through stimulation of various signalling cascades, such as MAPK or β -arrestin pathways, or through the CXCR4/CXCR7 heterodimer implicated in cancer development. For example, Decaillot's study showed that the CXCR4/CXCR7 heterodimer enhanced cell migration by the recruitment of β -arrestin and stimulated downstream ERK1/2 and p38 signalling cascades (Décaillot et al., 2011). Similarly, Hernandez and coworkers demonstrated in mouse models, that this heterodimer promotes breast cancer metastasis, with CXCR4 enhancing the dissemination of cancer cells and CXCR7 regulating metastatic action (Hernandez et al., 2011). Further evidence provided by Luker and coworkers illustrated that CXCR7 induced breast cancer cell growth and migration in an *in vivo* study by scavenging CXCL12 from the TME, enhancing tumour progression (Luker et al., 2012).

Likewise, in breast cancer cells, CXCR7 expression induced lung metastasis through enhancing cell survival and proliferation following CXCL12 activation, as reported in an *in vivo* study (Burns et al., 2006). Also, Stacer and co-workers observed that CXCR7 is an important oncogene that possesses tumour suppressor activities related to the metastatic cascade in mice lacking CXCR7, which exhibited a higher recurrent rate of breast cancer following resection (Stacer et al., 2016). However, CXCR7 signalling can also enhance cancer progression through heterodimer pathways. For example, overexpression of CXCR7 binds CXCL12 in nasopharyngeal carcinoma (NPC) cells, enhancing invasion and migration by the CXCR4/CXCR7-CXCL12 axis and downstream G protein signalling pathways (Qiao et al., 2016).

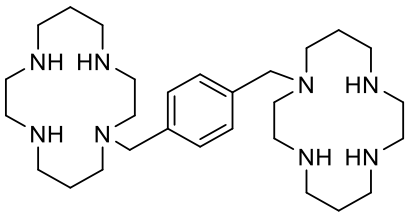
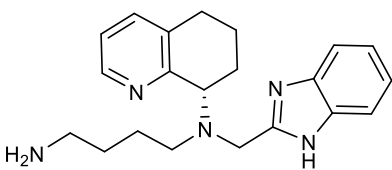
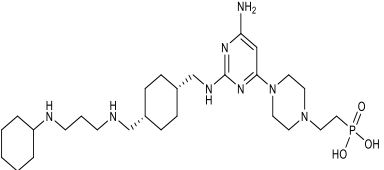
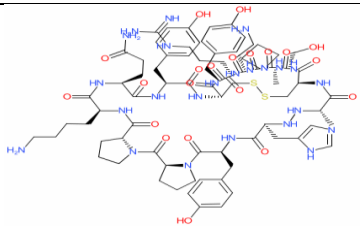
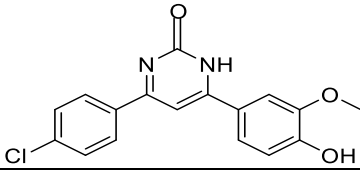
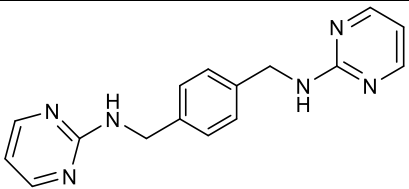
1.7.6 CXCR4 Antagonists

Given the significant role of the CXCL12/CXCR4 axis in aspects of cancer, it has the potential to be a target in cancer treatment. CXCR4 antagonists are classified as small molecules, peptides, and antibodies. Small-molecule antagonists include AMD3100, AMD3465, and Burixafor, which disrupt CXCL12/CXCR4 signalling essential for tumour cell homing to metastatic sites, such as bone marrow and lymph nodes (Bao et al., 2023). Blocking this pathway inhibits metastasis and induces sensitisation to chemotherapy as an adjuvant. For example, in an acute promyelocytic leukemia (APL) mouse model, the cancer cells metastasise to bone marrow with resistance to chemotherapy due to CXCL12. The APL cell mobilisation and chemotherapeutic sensitivity were increased upon administration of the AMD3100 as adjuvant therapy (Nervi et al., 2009). In fact, AMD3100 was the first FDA-approved in

December 2008, and it was used clinically as monotherapy in stem cell mobilisation in lymphoma and myeloma, through its action on hematopoietic stem cell mobilisation into the circulation (Vose et al., 2009). This antagonist showed more inhibitory effects on gastric cancer cell invasion than other compounds, attenuating the CXCL12-mediated integrin $\beta 1$ signalling pathway (Izumi et al., 2015). As adjuvant therapy, Giordano and co-workers demonstrated that radiation therapy exposure in combination with the CXCL12 inhibitor NOX-A12 or AMD3100 could prevent revascularisation and immunosuppression in glioblastoma by inhibition of TAMs and myeloid suppressor cells mobilisation (Giordano et al., 2019).

Another CXCR4 antagonist with potential anti-tumour effects is the peptide analogue CTCE-9908, which reduced metastasis in OS and melanoma in a mouse model, through inhibiting tumour colonisation (Su Young Kim et al., 2008). Furthermore, a potent monoclonal antibody (anti-CXCR4), MDX-1338/Ulocuplumab, was found to inhibit tumour growth in multiple hematologic malignancies by blocking the CXCL12 binding to its receptor CXCR4, thereby preventing cell migration through a direct apoptotic effect, or synergising with drug-induced cytotoxicity (Kuhne et al., 2013). Many CXCR4 antagonists have been reported to have significant *in vitro* inhibitory effects and reduced cancer growth and metastasis. These antagonists are being evaluated in ongoing clinical trials, as shown in Table 1.1 (Bao et al., 2023).

Table 1. 1 The Main CXCR4 Antagonists Used in Cancer Treatment

Drug name	structure	indications	Status completed	Clinical trials.gov
Plerixafor (AMD3100, Mozobil)		MM, NHL, *r/r AML, CLL, pancreatic, ovarian, colorectal cancers, brain tumours	FDA approved. Phase1/2 (completed)	NCT0010366, NCT0073382, NCT0051225, NCT0099005, NCT0090396, NCT0069459,
Mavoxifafor (AMD11070)		Advanced Renal Cell Carcinoma (RCC) Melanoma	Phase1/2 (completed) Phase1 (completed)	NCT02667886 NCT02823405
Burixafor (TG-0054)		MM, NHL	Phase2 (completed)	NCT01458288
Balixafortide (POL6326)		Hematologic malignancies (HM), MM, metastatic Breast cancer	Phase1 (completed)	NCT01413568 NCT01837095 NCT01105403
CTCE-9908		HCC Late-stage solid tumours (Breast, ovarian cancers)	Phase1/2 (completed) Phase1/2 (uncompleted)	NCT03812874
MSX-122		Solid tumours, refractory metastatic or advanced tumours	Phase1 (completed)	NCT00591682

*r/r AML; refractory/relapsed Acute Myeloid Leukemia. All clinical trials were searched from clinicaltrials.gov in January 2025. <https://clinicaltrials.gov/expert-search> on January 19, 2025

1.7.7 Challenges in Developing CXCL12/CXCR4 Inhibitors

Several studies have reported that CXCR4 antagonists have multiple limitations in cancer treatment. These limitations include undesirable toxicity resulting from the disruption of the physiological CXCL12/CXCR4 signalling, adaptive resistance through other pathways, and limited effects in solid tumours, as well as challenges when used in combination with other drugs or with a CXCR7 antagonist (Bao et al., 2023; Giordano et al., 2019; S. Y. Kim et al., 2008). Clinical studies reported CNS-related side effects in pediatric patients, such as visual hallucinations and nightmares, following administration of Plerixafor (AMD3100), these effects necessitate continuous monitoring (Sevilla et al., 2012; Son et al., 2013).

Compensatory pathway activation and tumour resistance can influence the efficiency of CXCR4 antagonists and other medications, complicating the development of effective treatment procedures (R. Janssens et al., 2018; C.-F. Liu et al., 2014; Zhao et al., 2014). For example, studies in immune and endothelial cells have demonstrated that truncation of CXCL12 by CD26 impairs the CXCL12/CXCR4 signalling functionality, resulting in reduced activity. CD26 is necessary for N-terminal cleavage to enhance receptor binding and activation. Both nitration and citrullination represent post-translational modifications that could damage the structural integrity of CXCL12. This damage reduced CXCR4 signalling activity and potency through impaired ability of CXCL12 to bind effectively to and enhance CXCR4 activation (Janssens et al., 2016; R. Janssens et al., 2018). Furthermore, Bieder and co-workers demonstrated that excessive levels of CXCL12 reduced the effectiveness of CXCR4 antagonists in leukemia and multiple myeloma models through competitive receptor saturation, thus confirming that dysregulation of the CXCR4 axis reduces the signalling activity (Beider et al., 2011).

An experimental study by Luker and coworkers demonstrated that CXCR4-dependent cancer cells remained responsive to CXCL12, enabling metastasis from the primary tumour to other CXCL12-expressing organs (Luker et al., 2012). However, CXCR4 antagonists, such as MSX-122, which showed promising efficacy and a safety profile in preclinical studies against specific cancers, still have limited clinical success in supporting the efficacy and safety of human patients during clinical trials (Ghasemi & Ghasemi, 2022).

As outlined previously, CXCR7 can play a role in cancer development by binding CXCL12, providing competition with CXCR4 signalling, thereby disrupting CXCR4 action. For instance, an experimental study showed that CXCR7 regulates chemotaxis through CXCL12 binding, with conformational alteration of CXCR4-mediated G protein activation through receptor heterodimer formation. Interference of CXCR7 with CXCR4 G protein-dependent signalling caused a reduction in calcium responses and CXCR4 activation in transfected HEK-293T cells (Levoye et al., 2009). Similarly, Shi and his colleagues have shown that the interaction of CXCR7 with CXCR4 in various signalling pathways mediated cancer hallmarks, making the selectivity for receptor more challenging to target CXCR4 effectively without undesirable effects (Shi et al., 2020a).

Additionally, *in vivo* and *in vitro* experimental studies revealed that CXCR7 antagonists can control cancer-mediated CXCL12 signalling. For example, CCX771 and CCX754 inhibited the CXCL12-mediated pro-tumour signalling activity, reducing metastatic progression in cancers such as lung cancer (Guillemot et al., 2012), and human renal cancer through mTOR signalling. Also, these antagonists affect glioblastoma through negative regulation of ERK1/2 signalling, as shown by nuclear staining, and via caspase-3/7 activity assays (Hattermann et al., 2010). More recently, CCX662 and CCX771 antagonists have demonstrated efficacy in preclinical studies (Lounsbury, 2020; Shimizu et al., 2011). However, translating these findings into clinical practice remains challenging, with the main limitations of clinical trials evaluating these CXCR7 antagonists.

1.7.8 Cellular factors that regulate CXCL12 expression

Whilst it has been assumed that in some cell types, CXCL12 production is constitutive, a number of extracellular stimuli have been shown to regulate CXCL12 expression via different signalling pathways. CXCL12 has been shown to be produced *in vivo* and *in vitro* by osteoblasts in response to different cytokines, including parathyroid hormone (PTH), IL-1 β , and TNF- α . (Jung et al., 2006; Taichman & Emerson, 1996; Xiao et al., 1997). For example, Calonge and coworkers showed that IL-1 β induced CXCL12 expression in human glioblastoma astrocytoma U373 and U87 cells by binding transcription factor CCAAT/enhancer binding protein β (c/EBP β) to a specific response region at the CXCL12 promoter (Calonge et al., 2010). A similar study showed that six putative binding motifs are located on 1010 base pairs upstream from the transcriptional start site within the region containing Sp1 binding sites. These motifs were shown to be responsible for inducing CXCL12 expression upon

stimulation with IL-1 β in U373 cells but not in other types of cells, as tested in luciferase reporter activity (García-Moruja et al., 2005). This study indicated the specific activity of IL-1 β for the induction of cells depending on their type. A recent study demonstrated that IL-1 α induced expression of CXCL12 by fibroblasts in colorectal cancer cells (HT-29), which enhanced tumour growth and liver metastasis through CXCL12 signalling. This response was attenuated by using an IL-1 α antagonist that inhibits these signalling cascades, confirming the role of the cytokine in CXCL12 regulation (Ma et al., 2021).

In addition, experimental studies have shown that hypoxia induces high expression of CXCL12 in endothelial cells, non-endothelial vascular and perivascular cells, and skeletal myocytes. This response was mediated via HIF-1 and linked to progenitor cell attraction in ischemic tissue (Ceradini et al., 2004; De Falco et al., 2004). However, regulating CXCL12 by hypoxia is important in different types of cancer. For example, Liu and co-workers showed that the HIF1/CXCL12/CXCR4 axis regulates pancreatic cancer progression through activating CXCR4 signalling (Liu et al., 2020). Similarly, Kryczek and his colleagues showed that this axis contributes to ovarian cancer angiogenesis, synergising with VEGF (Kryczek et al., 2005). In breast cancer, hypoxia-mediated HIF signalling induced CXCL12 expression and CXCR4 receptor activation, thereby promoting tumour growth and metastasis (Devignes et al., 2018). Calonge and coworkers have provided more evidence of HIF-1 α -induced CXCL12 expression in U373 and U87 glioma cells (Calonge et al., 2010).

There are factors which can negatively regulate CXCL12, the most studied on is TGF beta, TGF- β is one of the main immunosuppressive cytokines produced by TAMs and mediates macrophage activity through different cascades, such as integrin $\alpha\beta$ 8 /MMP14 signalling (Kelly et al., 2018). A study in murine breast cancer models by Yu and co-workers reported that TGF- β could downregulate CXCL12 expression in MSCs via Smad 3 signalling cascade, which promotes lung metastasis of breast cancer cells (Yu et al., 2017). However, in contrast, in murine breast cancer models, Arwert and coworkers demonstrated that TGF- β secreted from cancer cells can regulate CXCL12/CXCR4 signalling by promoting CXCL12 release on tumour-infiltrating monocytes that are attracted to the tumour site, resulting in upregulation of CXCR4 level and signalling, with enhanced TAM migration and metastasis (Arwert et al., 2018). These findings demonstrate many cellular factors involved in CXCL12 induction; the focus in this thesis is IL-1 β .

1.7.9 Pharmacological and Molecular Inhibition of CXCL12 Production

To date, no published studies have demonstrated the receptor-independent inhibition of CXCL12 induced by cellular factors as a strategy to overcome the limitations of the CXCR4 antagonist. One recent study by Geng and coworkers in a breast cancer mouse model demonstrated the indirect targeting of CXCL12 induction via a vaccine. It explained that a novel DNA vaccine targeting Fibroblast Activation Protein alpha (FAP α), a marker of CAFs in the TME, enhanced anti-tumour effects through reducing the number and activity of FAP α ⁺ CAFs. This led to decreased CXCL12 expression, resulting in a reduction in the myeloid-derived suppressor cells in TME (Geng et al., 2019). This effect was enhanced in the CXCR4-independent pathway.

Due to a lack of evidence, this targeting approach remains therapeutically challenging; therefore, in this thesis, we highlight the potential to inhibit signalling-mediated CXCL12 induction for the first time, demonstrating promising therapeutic activity against various cancer cells.

1.8 Aims of the Study

Previous studies highlighted the challenges in the efficacy and safety profiles of CXCR4 antagonists. Consequently, targeting CXCL12 to attenuate its induction and inhibit associated oncogenic signalling represents an essential therapeutic strategy across various tumours, including bone cancer. Meanwhile, novel CXCL12 inhibitors can now be synthesised, targeting CXCL12 induction rather than the CXCR4 receptor, thereby maximising the activity and reducing the off-target effect. Recently, a commercial chemical library of approximately 5000 compounds was screened against the CXCL12 reporter activity induced by IL-1 β . It identified novel compounds with inhibitory activity (IC₅₀) against IL-1 β -induced CXCL12 promoter activity using the U2OS cell line, with no cytotoxic effect, and a high probability of oral drug formulation (Drug-likeness) as shown in Figure 1.13. A preliminary follow-up study in the Plevin laboratory demonstrated that some of these compounds (KMs) significantly reduced IL-1 β -induced CXCL12 activity (Figure 1.14), highlighting their potential to disrupt cancer-associated signalling. Dependent on these findings, our strategy in this project aims to:

- 1-Synthesising newly reported active compounds in the Jamieson Laboratory (Figure 1.14), targeting CXCL12 production, and assessing their stability using (HPLC, NMR, LC-MS, and HRMS) and cytotoxicity using MTT assay.
- 2-Examine the function of NF κ B and its subunits IKK α and IKK β , TAK1 and MEKK3, as well as other pathways and their involvement in the regulation of CXCL12 expression in U2OS cells
- 3-Evaluate the pharmacological effects of novel CXCL12 inhibitors at the cellular level in terms of their potency against CXCL12 production induced by cytokine IL-1 β .

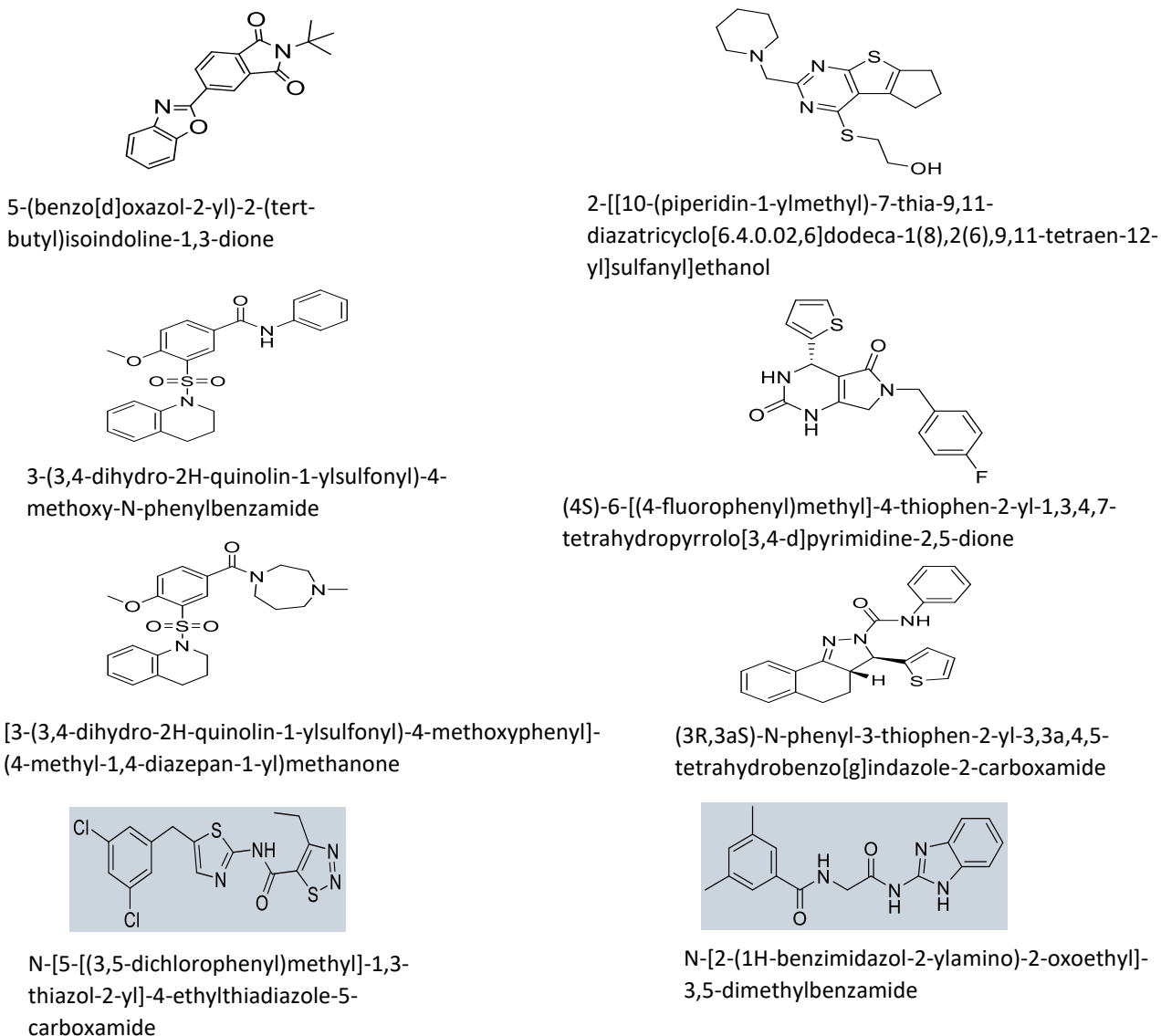
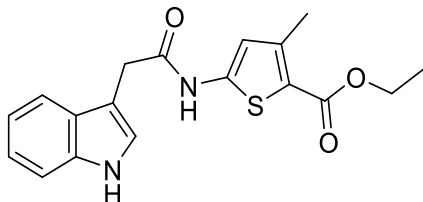
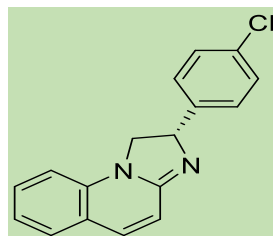


Figure 1. 13 Chemical Structures and Names of Selected CXCL12 Inhibitors.

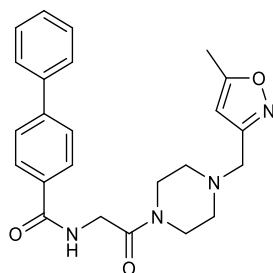
Some of the commercial compounds reported by the University of Dundee demonstrated an inhibitory effect against IL-1 β -induced CXCL12 promoter expression, exhibiting high drug-likeness and no cytotoxic effect on cell viability in U2OS and HEPG2 cells. The compounds in the blue colour showed a cytotoxic effect with less drug-likeness and an inhibitory effect on CXCL12 activity.



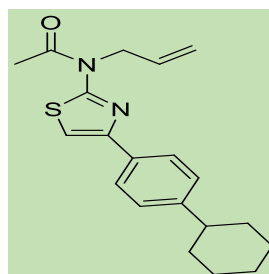
Ethyl 5-[[2-(1H-indol-3-yl)acetyl]amino]-3-methylthiophene-2-carboxylate (**KM6**)



(2S)-2-(4-chlorophenyl)-1,2-dihydroimidazo[1,2-a]quinoline (**KM8**)



N-(2-(4-((5-methylisoxazol-3-yl)methyl)piperazin-1-yl)-2-oxoethyl)-[1,1'-biphenyl]-4-carboxamide (**KM10**)



N-[4-(4-cyclohexylphenyl)-1,3-thiazol-2-yl]-N-prop-2-enylacetamide (**KM11**)

Figure 1. 14 Chemical Structures and Names of Targeted CXCL12 Inhibitors (KM).

The synthesised KM compounds were selected based on their physicochemical properties and investigated in the Plevin laboratory—the compounds KM8 and KM11 (green colour) showed significant inhibitory effects (IC_{50}) against the CXCL12 luciferase reporter assay using the U2OS cell line induced by IL-1 β , with high drug-likeness and no cytotoxic effect on cell viability at normal concentrations (10-20 μ M).

Chapter Two

Materials and Methods

2.1 General Reagents for Biological Assay

Unless otherwise indicated, Sigma-Aldrich Chemical Company Ltd. (Pool, Dorest, UK) or other valuable companies provided all of the materials and reagents used.

Thermo Fisher Scientific UK Ltd (Leicestershire, UK)

Bovine Serum Albumin (BSA, Fraction V)

L–Glutamine Gibco™

Penicillin-Streptomycin (Antibiotics)

Trypsin

Gibco™ Fetal Bovine Serum

McCoy's 5A medium

Dithiothreitol (DTT)

Triton X-100

Adenosine triphosphate (ATP)

Sigma Aldrich, Co., USA

Trisphosphate

Tetramethyl-ethylethylene diamine (TEMED)

Thiazolyl Blue Tetrazolium Bromide (MTT reagent)

Glycerol

MgCl₂

Promega Corporation, Madison, WI, USA

Luciferin

Bio-Rad Laboratories (Hertfordshire, UK)

Bio-Rad DC™ Protein Assay Dye Reagent Concentrate

Pre-stained SDS-PAGE molecular weight markers.

Carl Roth GmbH + CO. KG (Karlsruhe, Germany)

Rotiphorese® Gel 30 (37.5:1) acrylamide

Corning B.V. (Buckinghamshire, UK)

All tissue culture flasks, graduated pipettes, and multi-well plates.

GE Healthcare (Buckinghamshire, UK)

Amersham Hybond ECL Nitrocellulose Membrane

Whatmann (Kent, UK)

Nitrocellulose Membrane, 3MM blotting paper.

Sarsrtedt AG & Co., Ltd. (Leicester, UK)

Serological pipettes 5, 10, 25 mL

2.1.1 Anti-bodies

Cell Signalling Technology (UK)

Anti-p-NF kappa B2 p65 (Rabbit polyclonal, 3031S), (S536)

Anti-p- NF-kappa B2 p100 (Rabbit polyclonal, 4810S), (S866/870)

Anti-p-JNK (Rabbit polyclonal, 9251S), (Y185/T183)

Anti-p-c-Jun (Rabbit polyclonal, 91952), (Ser 63)

Anti-pc/EBP β (Rabbit polyclonal, 3084S), (T235)

Anti-p-p38 (Rabbit polyclonal, D3F9,4522S), (T180/Tyr182)

Anti-p38 (Rabbit polyclonal, 9212S)

Anti-GAPDH (Rabbit monoclonal, 14C10)

Anti-p- IKK α/β (Rabbit polyclonal, 2697S), (Ser 176/180)

Anti-I κ B α (Rabbit polyclonal, 9242S)

Anti-MEKK3(Rabbit polyclonal, 5727S)

Anti- TAK-1 (Rabbit polyclonal, 5206S)

Millipore Limited (UK)

Anti-NFκB p100/p52 (Mouse monoclonal, 32538)

Anti-IKKα (Mouse monoclonal, 14A231)

Santa Cruz Biotechnology (USA)

Anti-NFκB p65 (Mouse monoclonal, Sc 8008)

Anti-JNK (Rabbit polyclonal, Sc 571)

Anti-pERK1/2 (Mouse monoclonal, Sc 7383)

Anti-pERK1/2 (Rabbit polyclonal, Sc 94)

Proteintech (China)

Anti-IκBα (Rabbit polyclonal, 10268- 1- AP)

Anti-IKKβ (Rabbit polyclonal, 15649-1-AP)

2.1.2 Pharmacological Agonists

Insight Biotechnology Limited (UK)

Interleukin-1 beta (IL-1β)

2.1.3 Target Compounds

AMG548 (synthesised in-house, combined NLK/MAPK p38 inhibitor)

IKK2 X1(synthesised in-house IKK beta inhibitor by Prof. Craig Jameison)

KM 6,10 and 11 (synthesised in-house CXCL12 inhibitors)

KM8 (Molport, Latvia)

PD98059 (MEK1 inhibitor, Millipore, USA)

Ponatinib (multi-kinase, MEKK3 inhibitor, Biorbyt, UK)

SB203580 (MAPK p38 inhibitor, Tocris, UK)

SP600125 (JNK inhibitor, Tocris, UK)

SU1261(Strathclyde University IKK alpha inhibitors), (Ki IKK α vs IKK β : are 10 vs. 680 nM)

Takinib (TAK1 inhibitor, Tocris, UK)

5Z-7-Oxozeaenol (TAK1 inhibitor, Millipore, USA)

2.2 Chemical Synthesis

The target compounds were synthesised following procedures in the experimental sections (3.3.3) to (3.3.12).

2.3 Cell Culture

All cells were cultured in T75 cm² flasks, and all cell culture work was performed using aseptic techniques in a Class II Safety Flow Hood.

Human Osteosarcoma (U2OS) cell line

A human U2OS cell line was derived from the bone tissue of a 15-year-old female diagnosed with osteosarcoma. The cells were taken from a differentiated sarcoma of the tibia in 1964 (Bayani et al., 2003), and the origin of the U2OS cell line is the American Type Culture Collection.

2.3.1 Culture of Human Osteosarcoma (U2OS) Cells

The McCoy's 5A medium was the standard medium for these cell lines supplemented with 10% (v/v) foetal bovine serum, 1% (v/v) penicillin/streptomycin, and 1% (v/v) L-glutamine. Cells were cultured in T-75 cm² flasks and incubated at 37°C in a mixture of 95% air and 5% CO₂.

2.3.2 Trypsinisation and Subculture

Cells were sub-cultured once they reached approximately 80-90% confluency. Firstly, the media was aspirated, and the cells were washed once with 1.5 mL of a sterile solution of 0.5% (v/v) trypsin. After trypsin was removed, 2.5 mL of a sterile trypsin solution was put into the flask and placed in the incubator at 37°C, at 5% (v/v) CO₂, for 3 min. Once the cells displayed a round morphology, flasks were given a gentle tap to ensure the cells were fully detached. The flask was then washed with 10 mL of McCoy's 5A media to resuspend the recovered cells, which were used for seeding into fresh flasks 75 cm² or multi-well culture plates (12-well or 6-well) as required. The cells were maintained in 5% CO₂ and 95% air at 37 °C, and the cells were re-fed every two to three days to maintain health.

2.4 Western Blotting

2.4.1 Quiescing Cells

Cells were placed in the incubator at 37 °C and grown until they reached approximately 90% confluency in appropriate cell culture plates. Cells were then serum-starved in FBS-free McCoy's 5A medium for approximately 24 hours prior to stimulation.

2.4.2 Preparation of Whole-Cell Extracts

Cells cultured on 12-well plates were exposed to appropriate concentrations of agonists (IL-1 β) for specific durations or variable concentrations, after which the plates were placed on ice to stop the reaction, and then the media was subsequently aspirated. Cells were washed twice with 750 μ L cold PBS, followed by the addition of 200 μ L of DTT sample buffer (63mM Tris-HCl, (pH 6.8), 2mM Na₄P₂O₇, 5mM EDTA, 10% (v/v) glycerol, 2% (w/v) SDS, 50mM DTT, 0.007% (w/v) bromophenol

blue). Cells were scraped and dispersed using a 21-gauge needle, resulting in repeated shearing of the chromosomal DNA. Extracted cells were placed into Eppendorf tubes with the lid pierced, then boiled for three minutes and stored at -20 °C until use.

2.4.3 SDS-Polyacrylamide Gel Electrophoresis (SDS-PAGE)

SDS-PAGE separated the prepared protein samples. Gel plates were rinsed with 70% (v/v) ethanol before assembly. Distilled water was introduced to the completed plates for approximately one hour to verify that the glass plates were not leaking or flushing. The resolving gels were formulated by combining an appropriate volume (8.5-12% (v/v) of acrylamide (30% acrylamide: 0.8% N, N'-methylenebis-acrylamide (37.5:1)), 0.375M Tris base (pH 8.8), 0.1% (w/v) SDS, 10% (w/v) ammonium persulfate (APS), and TEMED to start the polymerisation process. The solution was poured between the two glass plates arranged in a vertical slab arrangement according to the manufacturer's instructions (Bio-Rad), and 200 µL of 0.1% (w/v) SDS was applied on top of the gel solution. Upon polymerisation of the gels, the SDS layer was eliminated; concurrently, stacking gels were made and directly applied on top of the resolving gel, with the comb quickly put into the stacking gel solution. Following the polymerisation of the gel, the comb was thoroughly extracted, and the gel was positioned in a Bio-Rad Mini-PROTEAN IITM electrophoresis tank containing electrophoresis buffer (0.1% (w/v) SDS, 25 mM Tris, 129 mM glycine). Samples in 20-30 µL aliquots were next introduced into the wells using a microsyringe. A pre-stained SDS-PAGE molecular weight marker with established molecular weights was run simultaneously to determine the molecular weights of a target protein. Samples were subjected to electrophoresis at a constant voltage of 125 V until the bromophenol dye migrated to the bottom of the gel.

2.4.4 Electrophoretic Transfer of Proteins onto Nitrocellulose Membrane

According to Towbin and coworkers' method, gels were transferred to a nitrocellulose membrane (Towbin et al., 1979). The gels were securely affixed to a nitrocellulose membrane and arranged within a transfer cassette, interleaved with two sheets of Whatman 3MM paper and two sponges. The cassette was immersed in transblot buffer (19 mM glycine, 25 mM Tris, and 20% (v/v) methanol) within a Bio-Rad mini-Trans-Blot™ tank, and a steady current of 300 mA was administered for 150 min. During this period, the tank was cooled by incorporating an ice reservoir.

The addition of SDS in the resolving gel provides a negative charge to the proteins, forcing the orientation of the cassette towards the anode alongside the nitrocellulose as shown in Figure 2.1.

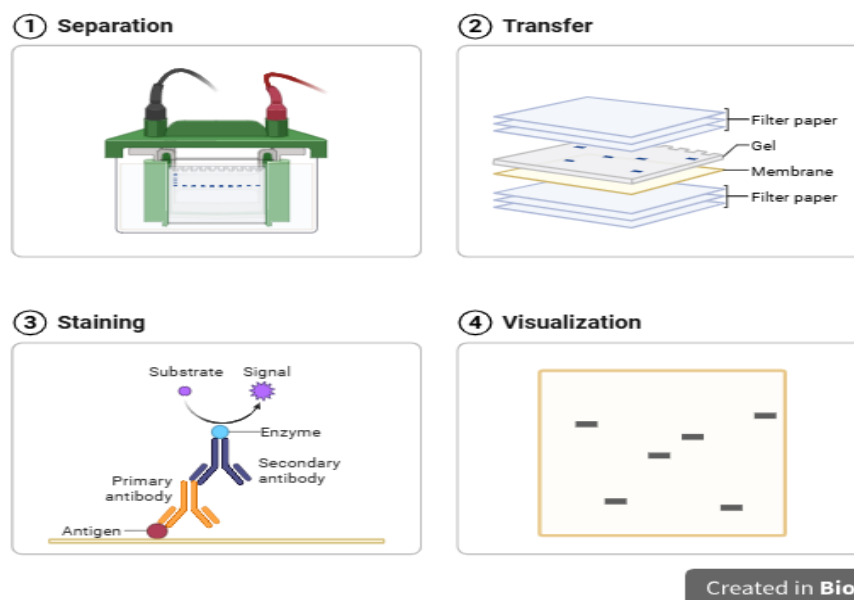


Figure 2. 1 A diagrammatic representation of the SDS-PAGE and Western blotting workflow.

Initially, lysed samples are run on gels to separate proteins by molecular weight (1). Transfer of proteins from the gel to a nitrocellulose membrane is carried out (2). The nitrocellulose membrane is then exposed to blocking in 1% BSA for 2 h and then probed with primary antibody overnight at 4 °C, washed three times for 25 min each and then probed with secondary antibody for 1.5 h (3). Following another three 25 min washes, ECL was utilised for 2 min (4). Proteins were visualised in a dark room using developing film—figure created in BioRender.

2.4.5 Immunological Detection of Proteins

Proteins were transferred to nitrocellulose membranes, which were then removed. The proteins were then blocked by soaking them for 2 h at room temperature on a rotating shaker in a solution of 1% (w/v) BSA in NaTT buffer (20 mM Tris, 150 mM NaCl (pH 7.4), and 0.2% (v/v) Tween-20). The blocking buffer was eliminated, and the membranes were incubated overnight with a particular antibody for the target protein in 0.2% (w/v) BSA in NaTT. Table 2.1 presents the optimal conditions for each antibody. The membranes were rinsed three times with NaTT every 25 min on the subsequent day, with gentle shaking. Subsequently, the membranes were treated for 90 min with

secondary horseradish peroxidase-conjugated IgG (HRP) specific to the primary immunoglobulin, diluted to an appropriate concentration in NaTT buffer containing 0.2% (w/v) BSA. The membrane was washed three times in NaTT at 25-min intervals and the bands of immune-reactive protein were identified by incubation in 6 mL of enhanced chemiluminescence (ECL) reagents (reagent 1 comprises Luminol, Coumaric Acid, 1M Tris-HCl pH 8.5, and distilled H₂O; reagent 2 consists of hydrogen peroxide, 1M Tris-HCl pH 8.5, and distilled H₂O) for 2 min with mild shaking. Following the placement of the membranes in a photographic cassette and their coverage with cling film, they were exposed to X-ray film in a darkroom environment for a duration of 1 to 4 min and developed with a JPI AUTOMATIC X-RAY FILM PROCESSOR MODEL JP-33 as shown in Figure 2.1.

Table 2. 1 Antibodies Used in Western Blots and Their Optimal Conditions

Protein of Interest	Antibody Source	Species	Blocking Conditions	Antibody Conditions
p-p100 (S866/870)	Cell Signalling 4810S	Rabbit	2% BSA in NaTT	1/3000 (4°C)
p100/52	Millipore 32538	Mouse	2% BSA in NaTT	1/6000 (4°C)
p-p65 (S536)	Cell Signalling 3031S	Rabbit	2% BSA in NaTT	1/3000 (4°C)
p65	Santa Cruz Sc 8008	Mouse	2% BSA in NaTT	1/3000 (4°C)
p-p38 (T180/Tyr182)	Cell Signalling 4522S	Rabbit	2% BSA in NaTT	1/2000 (4°C)
p38	Cell Signalling 9212S	Rabbit	2% BSA in NaTT	1/3000 (4°C)
IκB-α	Cell Signalling 9242S	Rabbit	2% BSA in NaTT	1/3000 (4°C)
p-JNK (Y185/T183)	Cell Signalling 9251S	Rabbit	2% BSA in NaTT	1/3000 (4°C)

Protein of Interest	Antibody Source	Species	Blocking Conditions	Antibody Conditions
JNK	Santa Cruz Sc 571	Rabbit	2% BSA in NaTT	1/3000 (4°C)
p-c-Jun (S63)	Cell Signalling 91952S	Rabbit	2% BSA in NaTT	1/3000 (4°C)
TAK-1 (D94D7)	Cell Signalling 5206S	Rabbit	2% BSA in NaTT	1/3000 (4°C)
p- IKK α / β S176/180	Cell Signalling 2697S	Rabbit	2% BSA in NaTT	1/2000 (4°C)
IKK α	Millipore 14A231	Mouse	2% BSA in NaTT	1/1500 (4°C)
IKK β	Proteintech 15649-1-AP	Rabbit	2% BSA in NaTT	1/2000 (4°C)
MEKK3 (D36G5)	Cell Signalling 5727S	Rabbit	2% BSA in NaTT	1/1500 (4°C)
pERK1/2 Tyr 204	Santa Cruz Sc 7383	Mouse	2% BSA in NaTT	1/5000 (4°C)
ERK1/2	Santa Cruz Sc 94	Rabbit	2% BSA in NaTT	1/6000 (4°C)
pc/EBP β (T235)	Cell Signalling 3084S	Rabbit	2% BSA in NaTT	1/6000 (4°C)
GAPDH	Cell Signalling 14C10	Rabbit	2% BSA in NaTT	1/6000 (4°C)

2.4.6 Re-probing and Stripping of Nitrocellulose Membrane

The nitrocellulose membrane was re-probed for additional proteins by stripping it. The nitrocellulose was incubated in a mixture of 15 mL of stripping buffer (0.05M Tris-HCl, 2% (v/v) SDS, and 0.1M of β -mercaptoethanol) at 60 °C for 50 min with mild shaking. After discarding the

stripping buffer, the membrane was rinsed three times in NATT every 5 min to get rid of the stripping buffer residue. The membrane was incubated with a primary antibody overnight at 4 °C in NATT solution with 0.2% (w/v) BSA, followed by a final wash. This step was ready for the immunological detection protocol as described previously.

2.4.7 Scanning Densitometry and Analysis of Expression Levels

Western blots were scanned in an HP Scanjet G2710 Scanner using Adobe Photoshop 5.0.2 software. Images were then captured, normalised with control, and quantified using Scion Image software (Scion Corp., MD, USA). A fold increase in protein was calculated against control or agonist-stimulated control using one-way analysis of variance (ANOVA) via GraphPad Prism software, version 8.0 (GraphPad Software, California, USA).

2.5 Promoter-Linked Reporter Assay

Reporter assay is an approach used to report the spatial-temporal dynamics of gene expression. It is important to investigate the promoter of the gene of interest and whether it is active. Detection of the target gene is done by using different methods based on reporters such as fluorescence reporter, enzyme-based reporter, or luciferase assay reporter (Carter & Shieh, 2010).

2.5.1 CXCL12 Gene Promoter-Linked Luciferase Reporter Activity Assay

In our laboratory, a U2OS-CXCL12 reporter cell line was established using a CXCL12 promoter construct as outlined previously for other cell types (García-Morúa et al., 2005). In 12 well plates, cells were grown to confluency before being starved for 36-40 h by removing the medium and replacing it with serum-free media. Before completing the reporter assay, cells were either pre-treated with hit compounds for an hour or subjected to multiple agonists at specific time points in duplicate for each measured parameter. After stimulation, the reaction was terminated by placing the plate on ice, washing the cells twice with ice-cold PBS, and then adding 200 µL of lysis buffer (25 mM Tris phosphate pH 7.8, 8 mM MgCl₂, 1 mM DTT, 1% Triton X-100, 15% Glycerol) to each well. Cells were scraped from the plate, samples transferred to labelled 1.5 mL Eppendorf tubes, and centrifuged at max RPM at 4°C for 3 min. A 100 µL aliquot of cell supernatant and 100 µL of luciferase buffer (10 mL Lysis buffer, 1mM ATP, 1% BSA, 1mM DTT, 0.25 mM luciferin) were

added and mixed well in a cuvet, then the relative light unit (RLU) was read for each sample in the luminometer over 60 seconds (Berthold, Germany). In some experiments to confirm that the compounds inhibit the gene expression (CXCL12) and not the luciferase enzyme itself, stimulated cell extract/luciferase mixture was incubated with the compounds for 7 min prior to reading on the luminometer.

2.6 MTT Toxicity Assay

Cell viability was assessed through the reduction of 3-(4,5-dimethylthiazol-2-yl)-2,5-diphenyltetrazolium bromide (MTT, Sigma Aldrich) to purple formazan by mitochondrial NAD(P)H-dependent oxidoreductase enzymes. Cells were cultured in 96-well microplates at 50-60% confluence. On the subsequent day, cells were subjected to treatment in triplicate and thereafter incubated at 37 °C in an atmosphere of 5% CO₂ and 95% air for a duration of 7 h. Following incubation, the media was aspirated and substituted with fresh media. MTT 100 µL (1 mg/mL) was administered to each well, and the microplates were incubated at 37°C with 5% CO₂ and 95% air for 2 h, covered in aluminium foil. The medium was subsequently eliminated, and the produced formazan crystals were solubilised by the addition of DMSO. The microplates were incubated for 5 min., after which absorbance readings were recorded at a wavelength of 570 nm using a POLARstar Omega microtiter plate reader (BMG LABTECH, Germany).

2.7 Enzyme-Linked Immunosorbent Assay (ELISA)

2.7.1 Preparation and Treatment of U2OS Cells

The U2OS cells were cultured in a 6-well plate with 1.5 mL of media containing 10% FCS. After reaching 50-60% confluency, the cells were transfected with 50 nM of siRNA IKK α , IKK β , MEKK3, or TAK-1 for the indicated incubation time between 72-96 h, followed by stimulating the cells with IL-1 β (10 ng/mL) for 6 and 24 h, or after two days of culturing the cells, the media was changed, and the cells were pretreated with KM compounds (10-20 µM) for one hour, followed by 6- or 24-h stimulation with IL-1 β . The supernatant of the conditioned cells was collected and centrifuged for 15 min at 4 °C or room temperature at 106 g and processed for assessment of protein expression by ELISA immediately or collected and stored the samples at -20 °C for next-day assessment.

2.7.2 Measurement of Human CXCL12/SDF1-alpha

The concentration of human CXCL12 (Assay Genie, HUF102841, Dublin, Ireland) induced by IL-1 β was quantitatively measured by using a sandwich ELISA system following the supplier's instructions:

Assay procedure:

Following preparation of the antibody working solutions, and kept at 37 °C for at least 30 min before adding to the wells, 100 μ L of assay diluent, standard, control, or samples were added to each well of a microplate in duplicate. Then, the plate was sealed with the provided adhesive strip and incubated for 90 min at 37 °C in 5% CO₂ and 95% air. The plate was washed three times to remove unbound proteins using a washing buffer and was dried well by inverting the plate and hitting clean tissues. Next, 100 μ L of Biotin-labelled antibody was added to each well, then the plate was covered and incubated for 60 min at 37 °C in 5% CO₂, 95% air. After three times of washing, 100 μ L of SABC (HRP-Streptavidin Conjugate) was added to each well. Again, the plate was covered with a new adhesive strip and incubated later for 30 min. Then, the plate was washed five times with washing buffer, and 90 μ L of Tetramethylbenzidine (TMB) was added to each well and incubated at 37 °C for 20 min in the dark by wrapping the plate with tin foil. The reaction was terminated with 50 μ L of 1M H₂SO₄ stop solution (the colour in the wells changed immediately from blue to yellow). At a wavelength of 450 nm, a colour change was detected spectrophotometrically using the POLARstar Omega microtiter plate reader (BMG LABTECH, Germany), and the sample concentrations were compared to the standard curve.

2.7.3 Measurement of Human IL-8 (CXCL8)

The concentration of human IL-8 (Invitrogen, 88-8086, USA) induced by IL-1 β was quantitatively examined by using a sandwich ELISA system according to the instructions of the supplier:

Assay procedure:

The antibody specific for human IL-8 was pre-coated onto a 96-well microplate overnight with shaking in the cold room before starting the experiment. The plate was washed three times with washing buffer (400 μ L), and the wells were dried by inverting the plate and wiping with clean

tissues to remove excess capture antibodies. Then, 150 μ L of ELISA diluent was added to each well to block the wells and incubated at room temperature on a shaker for one hour. The provided adhesive strip was used to cover the plate. Next, the plate was washed three times using a washing buffer, and the same technique was applied as previously. Then, 100 μ L of assay diluent, standard, control, or samples were added to each well, and the plate was covered with an adhesive strip and incubated on a shaker for 2 h at room temperature. The plate was washed three times, and 100 μ L of first and second detection antibodies were applied as previously. After five washes of the plate, 100 μ L of TMB substrate was added to each well and incubated without shaking in the dark by wrapping the plate with tin foil for 15 min. The reaction was terminated with 100 μ L of stop solution (the colour in the wells changed immediately from blue to yellow). At a wavelength of 450 nm, a colour change was detected spectrophotometrically using the POLARstar Omega microtiter plate reader (BMG LABTECH, Germany), and the sample concentrations were compared to the standard curve.

2.8 Treatment of Bone Cancer Cell Line

2.8.1 Testing Compounds

In-house compounds (KM6, KM10, KM11, and AMG548) were developed at the University of Strathclyde, Glasgow, UK. The TAK1 inhibitors Takinib, 5Z-7-oxozeaenol, Ponatinib, and other compounds were purchased from Merck and Millipore. Based on these compounds' weight and molecular weight (M.W.), a 20 mM stock solution was prepared by dissolving the chemicals in a calculated volume of DMSO. The prepared solutions were stored at -20 °C. U2OS cells were treated with diverse concentrations for a pharmacological study.

2.8.2 siRNA-mediated Silencing of Target Genes (TAK1, IKK α , IKK β , and MEKK3) in Cells

Small interfering RNA (siRNA) was used to investigate the roles and activities of various proteins in cellular processes. It is a sequence of double-stranded RNA (20–25 base pairs) that prevents the expression of specific genes with complementary nucleotide sequences by degrading the targeted mRNA, which stops protein synthesis and translation (Elbashir et al., 2001).

In order to observe the effect of the loss of TAK1, IKK α , IKK β , and MEKK3 on the cells, cells were transfected with siRNA against the target protein in comparison to non-target siRNA (NT) supplied from Thermo FisherScientific® (Thermo Fisher Scientific, Surrey, UK). Target sequences are shown in Table 2.2. The newly purchased siRNA was resuspended in an RNase-free 1x siRNA buffer (Dharmacon, Buckinghamshire, UK). To prepare a 20 μ M stock, 500 μ L of 1X siRNA buffer was added to 10 nmol of siRNA and then mixed by pipetting. The diluted solution was then placed on an orbital mixer for 30 min at room temperature before being aliquoted and stored at -20 °C. U2OS cells were seeded into 12-well plates and cultured until they reached approximately 60-70% confluence on the day of transfection. For each well, two labelled Ependorfs were prepared, tube 1 containing the siRNA mixture and tube 2 containing the Lipofectamine® mixture. Tube 1 was made up to 100 μ L with OptiMEM® medium (Life Technologies, Paisley, UK) as follows: 50 nM (2.5 μ L siRNA + 97.5 μ L Opti-MEM®), and 100 nM (5 μ L siRNA + 95 μ L Opti-MEM®). In the second tube, 2-2.5 μ L Lipofectamine RNAiMAX® (Invitrogen®, Paisley, UK) was diluted into 100 μ L OptiMEM®. Lipofectamine RNAiMAX® was the transfection reagent to deliver the siRNA to the cells. Both tubes were then mixed together at a 1:1 ratio and left to incubate at room temperature for 20 min. to allow the formation of complexes. Cells were normally washed with 1 mL Opti-MEM to get rid of excess medium, then replaced with 800 μ L Opti-MEM®. After 20 min, the transfection mixture (Final volume 200 μ L) was added to the appropriate wells dropwise. Plates were incubated for 16 h in 5% CO₂ and 95% air at 37 °C. After this period, the transfection mixture was aspirated and replaced with media containing 10% FCS. The cells were then incubated for 72-96 h at 37 °C, 95% air, and 5% CO₂. Then the cells were treated with an agonist for 30 min. Whole sample extracts were then collected and stored at -20 °C for analysis of target protein expression levels by Western blot analysis (Section 2.4) or ELISA assay (Section 2.7).

Table 2. 2 siRNA Transfection Target Gene, siRNA Target Sequences, and Origin

Target Gene	Target Sequence	On-Target plus SiRNA
IKK α (CHUK)	GCGUGAAACUGGAAUAAU	Human CHUK Cat.no: J-003473-09
IKK β (IKBKB)	GAGCUGUACAGGAGAUAA	Human IKBKB Cat.no: J-003503-13
Non-target (NT)	UGGUUUACAUGUCGACUAA	Non-target Cat.no: D-001810-01-20
MEKK3	GAACCGACGUCACCGGAUG	Human Dharmacon Cat.no: L-003301-00-20
Non-target (NT)	UGGUUUACAUGUCGACUAA	Non-target Cat.no: D-001810-01-20
TAK-1	GAGUGAAUCUGGACGUUUA	Human Dharmacon Cat.no: L-003790-00-20
Non-target (NT)	UGGCUUAUCUUACACUGGA	Non-target Cat.no: D-001810- 10-05

2.9 Data Analysis

All data presented were representative of a minimum of three independent experiments unless otherwise indicated. Data were normalised to fold expression and expressed as One-way ANOVA performed mean \pm S.E.M. Statistical analysis was performed using GraphPad Prism version 8.0 (GraphPad Software, California, USA) with both Dunnett's and Tukey's Post-comparison test (*P < 0.05, **P < 0.01, ***P < 0.001, ****P < 0.0001). GraphPad Prism was also used to calculate the IC₅₀ for KM and purchased compounds. Nonlinear regression analysis was used to determine the concentration response curve and calculate the IC₅₀.

Chapter Three

Chemical Synthesis and Analysis of Novel Inhibitors for CXCL12 Production in Cancer

3.1 Introduction

Bone cancer remains a clinical issue due to its metastatic potential, aggressive nature, and limited treatment strategy (Borges et al., 2022). The cancer hallmarks and CXCL12 role were extensively discussed in Chapter One, Section 1.7. It is one of the molecular targets associated with the progression of bone cancer and has attracted attention (Teicher & Fricker, 2010). A malignant tumour originating from bone tissues, bone cancer damages healthy bone tissues in its pathological role. The quality of life is greatly diminished for patients with bone cancer because they often experience severe chronic pain, dysfunction, and other related symptoms (Colvin & Fallon, 2008).

Regarding bone cancer, the risk of developing this condition is rising rapidly each year. It has been shown that less than 20% of patients with bone cancer survive for a year. Despite surgery, which is only effective in the early stages, standard therapies such as chemotherapy, radiotherapy, and others have proven to be effective but come with challenges, as explained in Sections 1.5.3. Therefore, developing appropriate medications to prevent the onset of bone cancer has far-reaching implications. As mentioned previously, the exacerbation of tumour hallmarks, along with diagnosis and treatment, has been significantly regulated by the chemokine network. Thus, studies on CXCL12 and its inhibition concerning bone progression could lead to a positive and broad impact on medicine in the future.

As described in Sections 1.7.3-1.7.5, CXCL12 primarily exerts its effect through binding to its receptor, CXCR4. For example, upregulation of CXCL12 within the bone microenvironment plays a vital role in tumour growth and resistance to therapy and must be targeted. The CXCL12/CXCR4 signalling plays a crucial role in the tumorigenic environment. This effect not only facilitates the metastatic process but also contributes to tumour survival through activating downstream signalling pathways, which regulate resistance to apoptosis and proliferation. These signalling pathways include PI3K/AKT, MAPK, and NF- κ B, which are described in Section 1.7.5. In a recent study using an *in vivo* model, it has been shown that inhibition of CXCL12 signalling in prostate cancer may abolish metastatic bone development and enhance the therapeutic efficacy of testing drugs such as Plerixafor (Conley-LaComb et al., 2016).

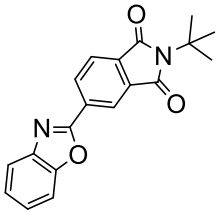
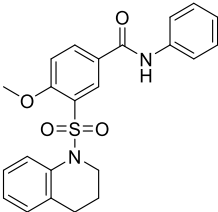
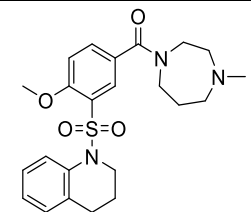
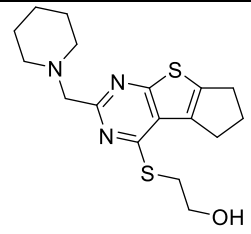
Previous research has shown that therapeutic approaches such as small-molecule antagonists, monoclonal antibodies, and peptide inhibitors target the CXCL12/CXCR4 signalling axis. However, direct inhibition of CXCL12 expression presents several challenges as discussed previously, including chemokine signalling crosstalk, compensatory pathways, and potential off-target effects (Bao et al., 2023; Lin et al., 2019; Shi et al., 2020b).

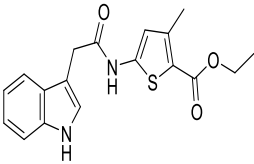
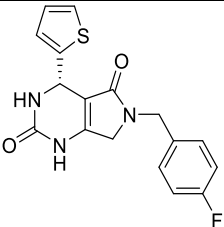
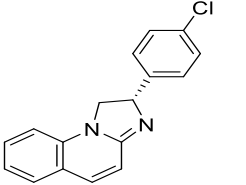
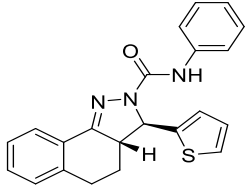
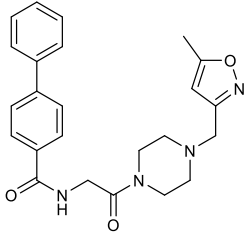
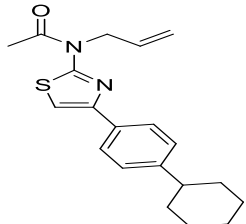
Furthermore, Burger and coworkers demonstrated the importance of combination treatment approaches, integrating CXCL12 inhibitors with known chemotherapeutic drugs to reduce resistance and improve treatment outcomes (Burger & Peled, 2009). Crystallographic and computational studies using structural insights have enabled rational drug design models for improving inhibitor specificity and pharmacokinetics (Kumar et al., 2018). Use of computational chemistry techniques, such as molecular docking, has provided detailed data for the inhibitor binding mode (Prieto-Martínez et al., 2019). The 3D structure of CXCL12 has been recently examined (R. Janssens et al., 2018). Thus, the potential of CXCL12 in the drug design field was shown to be viable.

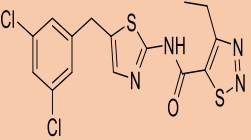
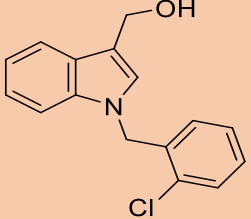
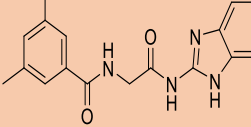
In addition, novel CXCL12 inhibitors have been synthesised, which can target CXCL12 induction rather than the CXCR4 receptor, thereby maximising the activity and reducing the off-target effect. Recently, the University of Dundee reported that a number of compounds were of interest, having been identified through screening of a commercial library of approximately 5000 compounds against CXCL12 gene expression induced by IL-1 β . Based on the screening data, some compounds showed preferable chemical and biological criteria, such as drug-like properties, an inhibitory effect against stimuli-induced CXCL12 gene expression, and a cell cytotoxic effect on U2OS cells as shown in Table 3.1. Three compounds were unfavourable targets for synthesis and testing due to their toxic effects and low drug likeness; they were presented for comparisons with the hit compounds. All of these properties make the compounds presented as hit compounds. The inhibitory potency of each compound was assessed by measuring the IC₅₀ against CXCL12 promoter expression. To determine the potential off-target cytotoxic effects, a cell viability assay was applied. The data were reported as a percentage effect observed at a 10 μ M concentration, which was used as the standard concentration; a high positive value indicates toxicity. Lastly, the quantitative estimate of drug-likeness (QED) was calculated to prioritise compounds with physicochemical properties aligned with those of successful oral drugs.

The preliminary results in U2OS cells stably transfected with a CXCL12 luciferase promoter construct showed a significant reduction in gene expression by some of the reported compounds (Table 3.1), using a luciferase reporter assay technique. Therefore, our goal in this study was to identify chemical structures that can effectively inhibit CXCL12 signalling by abolishing its expression. Some of the reported compounds (KM) were synthesised in the Jamieson lab. Using the chemicals and techniques mentioned in Section 3.3, the KM compounds were successfully prepared, and their chemical stability was also examined using HPLC.

Table 3. 1 Screened chemical compounds and in-house KM compounds with *in vitro* inhibitory potency IC₅₀, Cytotoxicity, and calculated Drug-likeness

Name of Compound	Chemical Structure	IC ₅₀ vs CXCL12 - promoter induction (μM)	pIC ₅₀	CXCL12 % Effect (10 μM)	Cell Viability % Inhibitory Effect (10 μM)	QED	Cytotoxicity Screen
5(benzo[d]oxazol-2-yl)-2-(tert-butyl)isoindoline-1,3-dione		0.2	6.7	102.2	-0.9	0.71	Not cytotoxic
3-(3,4 dihydro-2H-quinolin-1-ylsulfonyl)-4-methoxy-N-phenylbenzamide		7.9	5.1	52.7	0.3	0.67	Not cytotoxic
[3-(3,4-dihydro-2H-quinolin-1-ylsulfonyl)-4-methoxyphenyl]-(4-methyl-1,4-diazepan-1-yl)methanone		4.8	5.3	77.6	3.2	0.72	Not cytotoxic
2-[[10-(piperidin-1-ylmethyl)-7-thia-9,11-diazatricyclo[6.4.0.02,6]dodeca-1(8),2(6),9,11-tetraen-12-yl]sulfany]ethanol		2.1	5.7	97.7	-4.9	0.65	Not cytotoxic

Name of Compound	Chemical Structure	IC ₅₀ vs CXCL12 - promoter induction (μM)	pIC ₅₀	CXCL12 % Effect (10 μM)	Cell Viability % Inhibitory Effect (10 μM)	QED	Cytotoxicity Screen
ethyl 5-[[2-(1H-indol-3-yl)acetyl]amino]-3-methylthiophene-2-carboxylate (KM6)		1.4	5.8	100.3	-9.8	0.66	Not cytotoxic
(4S)-6-[(4-fluorophenyl)methyl]-4-thiophen-2-yl-1,3,4,7-tetrahydropyrrolo[3,4-d]pyrimidine-2,5-dione		1.4	5.8	109.7	8.1	0.88	Not cytotoxic
(2S)-2-(4-chlorophenyl)-1,2-dihydroimidazo[1,2-a]quinoline (KM8)		2.9	5.5	103.2	2.6	0.78	Not cytotoxic
(3R,3aS)-N-phenyl-3-thiophen-2-yl-3,3a,4,5-tetrahydrobenzo[g]indazole-2-carboxamide		1.2	5.9	95.3	2.3	0.70	Not cytotoxic
N-(2-(4-((5-methylisoxazol-3-yl)methyl)piperazin-1-yl)-2-oxoethyl)-[1,1'-biphenyl]-4-carboxamide (KM10)		4.3	5.4	74.4	0.2	0.66	Not cytotoxic
N-[4-(4-cyclohexylphenyl)-1,3-thiazol-2-yl]-N-prop-2-enylacetamide (KM11)		0.2	6.7	124.4	4.0	0.72	Not cytotoxic

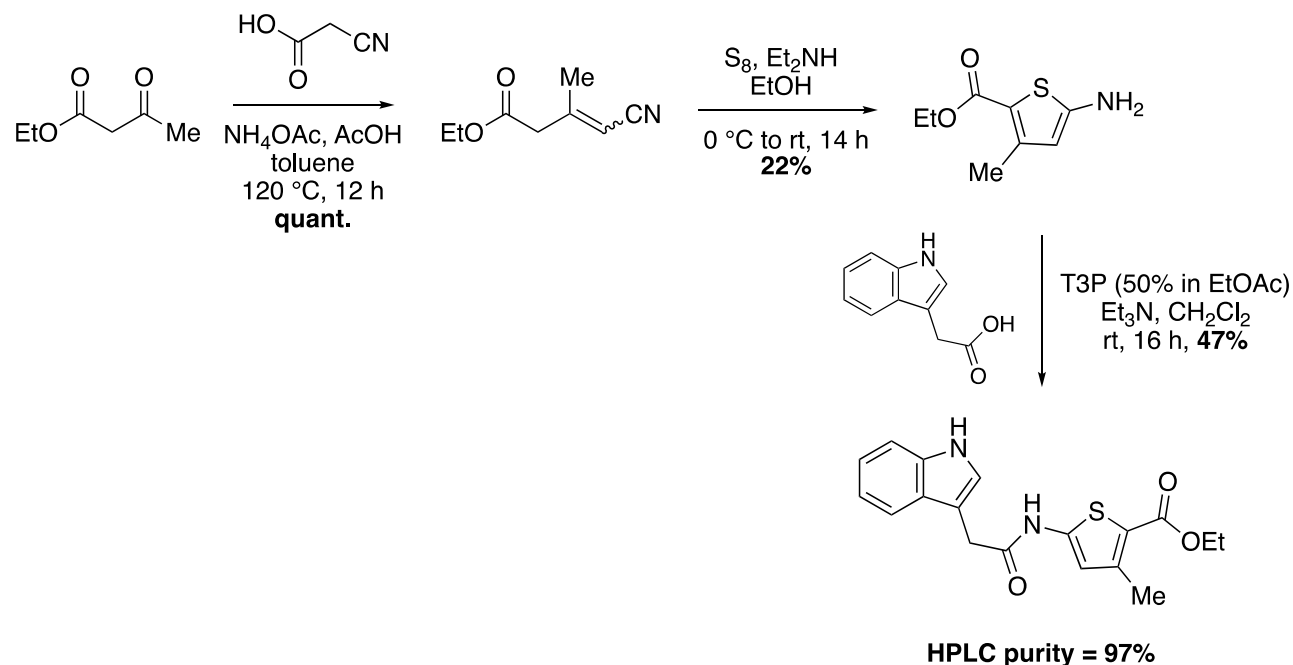
Name of Compound	Chemical Structure	IC ₅₀ vs CXCL12 - promoter induction (μM)	pIC ₅₀	CXCL12 % Effect (10 μM)	Cell Viability % Inhibitory Effect (10 μM)	QED	Cytotoxicity Screen
N-[5-[(3,5-dichlorophenyl)methyl]-1,3-thiazol-2-yl]-4-ethylthiadiazole-5-carboxamide		5.6	5.2	70.2	98.3	0.67	Toxic compound
[1-[(2-chlorophenyl)methyl]indol-3-yl]methanol		0.9	6.1	61.4	104.8	0.76	Toxic compound
N-[2-(1H-benzimidazol-2-ylamino)-2-oxoethyl]-3,5-dimethylbenzamide		1.6	5.8	101.2	101.1	0.68	Toxic compound

IC₅₀, Inhibitory concentration vs CXCL12 promoter induction; QED, Quantitative Estimate of Drug-likeness.

3.2 Results and Discussion

3.2.1 Synthesis of ethyl 5-(2-(1*H*-indol-3-yl)acetamido)-3-methylthiophene-2-carboxylate (KM6)

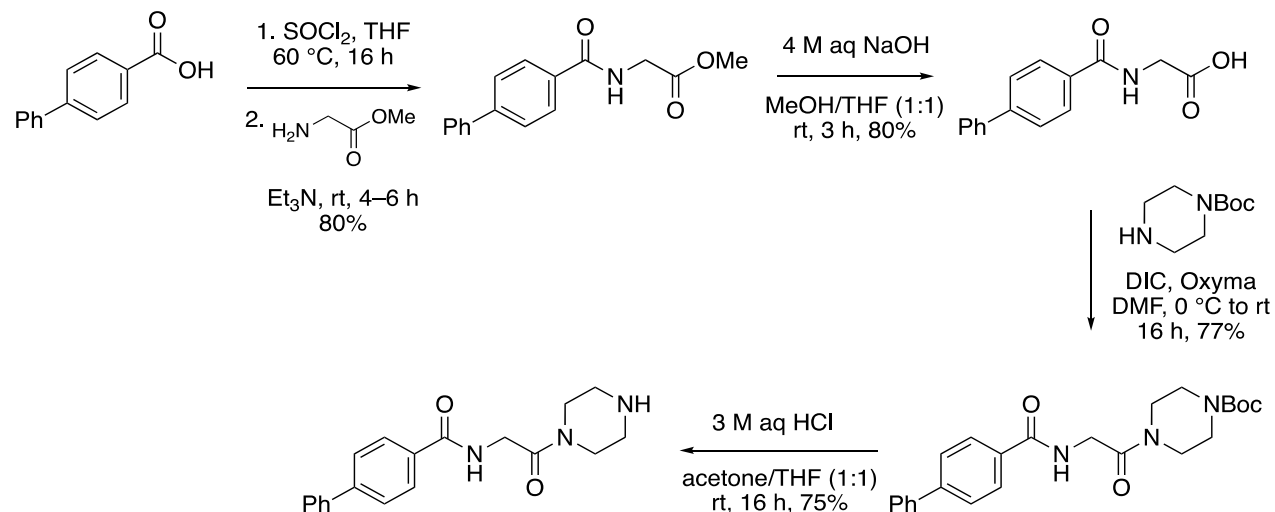
A Knoevenagel condensation reaction with cyanoacetic acid and ethyl acetoacetate provided the acrylonitrile compound in a quantitative yield of stereoisomeric mixture in a ratio of 60:40. A Gewald reaction in the presence of elemental sulfur was used to give the 2-aminothiophene fragment in a yield of 22%. Finally, amide coupling with the 2-aminothiazole fragment and indole-3-acetic acid in the presence of T3P (Propyl phosphonic anhydride) gave KM6 with 47% yield, as shown in **Scheme 3.1**.



Scheme 3.1: Synthesis of KM6

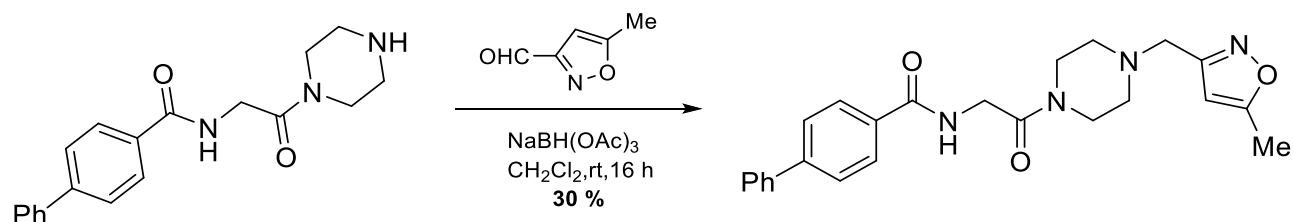
3.2.2 Synthesis of *N*-(2-(4-((5-methyl isoxazole 3yl) methyl) piperazine-1-yl)-2-oxoethyl)-[1,1'-biphenyl]-4-carboxamide (KM10)

The synthesis of NH-piperazine derivative *N*-(2-oxo-2-(piperazine-1-yl) ethyl)-[1,1'-biphenyl]-4-carboxamide is shown in **Scheme 3.2**. The synthesis commenced with the amide coupling of 4-phenylbenzoic acid and glycine methyl ester, through in situ-generated acid chloride. The *n*-acylated glycine methyl ester was hydrolysed under basic conditions to afford acid [1,1'-biphenyl]-4-carbonyl) glycine in a yield of 80%. [1,1'-Biphenyl]-4-carbonyl) glycine and *N*-Boc piperazine were coupled together using DIC and Oxyma as the coupling reagents which gave amide *tert*-butyl 4-(([1,1'-biphenyl]-4-carbonyl) glycy) piperazine-1-carboxylate in a yield of 77%. The Boc protecting group was removed under acidic conditions, affording piperazine derivative *N*-(2-oxo-2-(piperazine-1-yl) ethyl)-[1,1'-biphenyl]-4-carboxamide in a yield of 75%.



Scheme 3.2 Schematic Synthesis of N-(2-oxo-2-(piperazin-1-yl) ethyl)-[1,1'-biphenyl]-4-carboxamide

Next, piperazine derivative N-(2-oxo-2-(piperazine-1-yl) ethyl)-[1,1'-Biphenyl]-4-carboxamide, was subjected to a reductive amination reaction with the appropriate oxazole carbaldehyde analogue, such as 5-methyl isoxazole carbaldehyde, in the presence of sodium triacetoxyborohydride (**Scheme 3.3**). This afforded final compound N-(2-(4-((5-methyl isoxazole 3yl) methyl) piperazine-1-yl)-2-oxoethyl)-[1,1'-Biphenyl]-4-carboxamide after purification by reverse-phase HPLC, in a yield of 30% and 92.4 % purity.

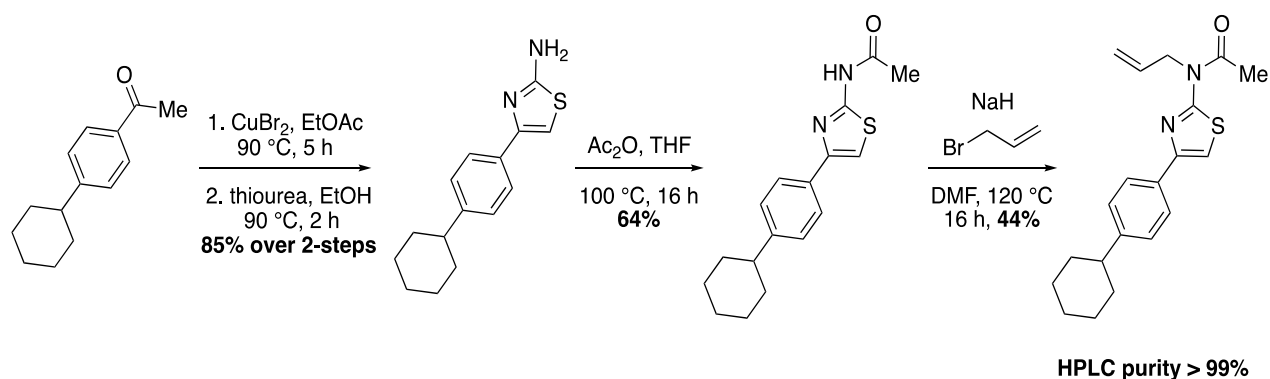


HPLC purity= 92.4%

Scheme 3.3 Schematic Synthesis of KM10

3.2.3 Synthesis of *N*-allyl-*N*-(4-(4-cyclohexylphenyl)thiazol-2-yl)acetamide (KM11)

The synthetic methods of KM11 are detailed in **Scheme 3.4**. Alpha bromination of 1-(4-cyclohexylphenyl)ethan-1-one mediated by copper (II) bromide was followed by the Hantzsch thiazole synthesis using thiourea, which over two steps provided the 2-amino thiazole in a yield of 85%. The amino functional group was subjected to acetylation with acetic anhydride, giving the corresponding acetamide in 64% yield. The amide nitrogen allylation in the presence of sodium hydride gave KM11 in a yield of 44%.

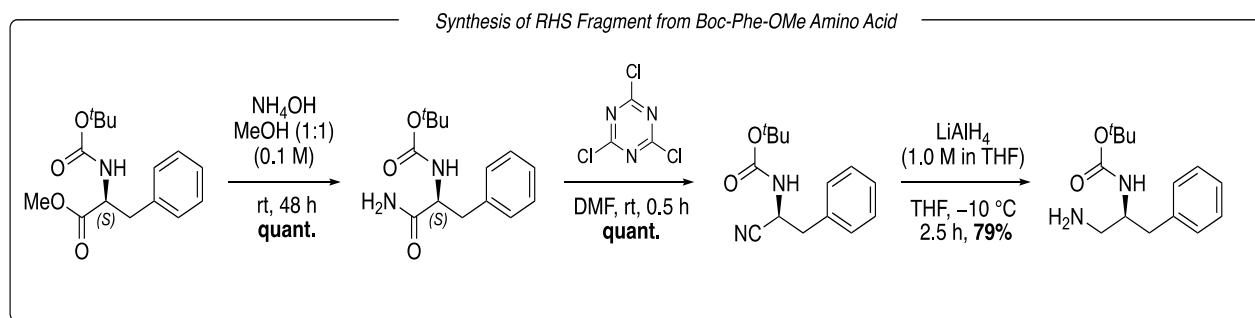


Scheme 3.4: Schematic Synthesis of KM11

In addition, giving our findings during biological experiments, a compound AMG-548 (p38/NLK) inhibitor was synthesised to explore its effect on IL-1 β -induced CXCL12 activity. The chemical synthesis is detailed in the following Sections.

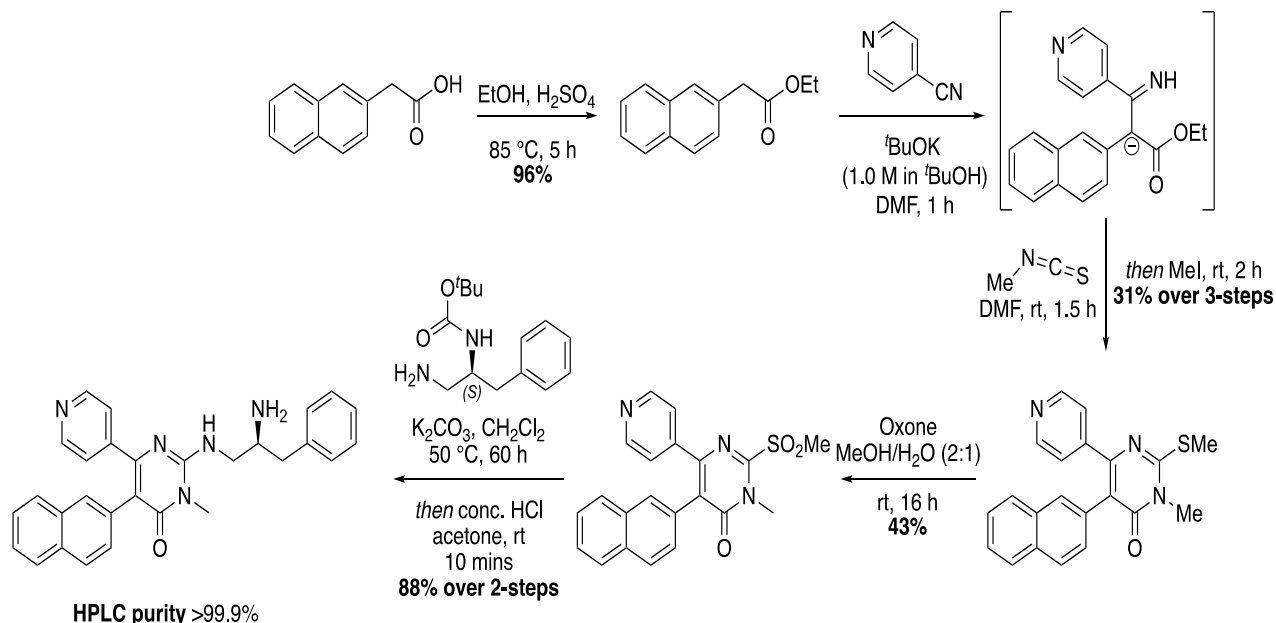
3.2.4 Synthesis of AMG-548 (NLK/p38 inhibitor)

The nucleophilic fragment on the right-hand side was synthesised from Boc-protected phenylalanine methyl ester via aminolysis, followed by dehydration of the primary carboxamide, facilitated by cyanuric chloride, as illustrated in **Scheme 3.5**. Using lithium aluminium hydride for the reduction of the resulting nitrile afforded the required Boc-protected amine in a yield of 79%.



Scheme 3.5: Synthesis of Boc-protected amine

The fragment on the left-hand side was synthesised according to the synthetic method below (**Scheme 3.6**). The substituted pyrimidinone core was constructed using a one-pot procedure as reported by Lu and coworkers (Lu et al., 2006). This included the coupling of naphthaleneacetic acid and 4-cyanopyridine via an enolate/nitrile nucleophilic condensation, followed by cyclisation with methyl isothiocyanate and then S-methylation of the exocyclic thiolate anion. The corresponding sulfone was obtained via the pendant thioether's oxidation with Oxone, an appropriate electrophilic functional group to facilitate a nucleophilic aromatic substitution ($\text{S}_{\text{N}}\text{Ar}$). An $\text{S}_{\text{N}}\text{Ar}$ reaction between the Boc-protected phenylalanine amine and the sulfone, followed by acid-mediated removal of the Boc-protecting group, afforded AMG-548 in 88% yield over two steps.



Scheme 3.6: Synthesis of AMG-548

3.3 Experimental data for KM compounds

3.3.1 General Experimental

All starting materials and reagents were obtained from commercial sources and used without further purification, unless otherwise stated. Acetone, *N,N*-dimethylformamide, ethanol, ethyl acetate, methanol, dichloromethane, 1,4-dioxane, diethyl ether, and petroleum ether 40–60 °C were used as obtained from suppliers without. All dry solvents were purified using a PureSolv SPS-400-5 Solvent Purification System.

Round-bottom flasks or microwave vials of appropriate volume were used for all performed reactions. Reactions were carried out at elevated temperatures using a temperature regulated hotplate/stirrer and DrySyn block with a contact thermometer. Room temperature generally refers to about 20 °C. Reactions requiring a reduced temperature were performed using an ice bath (0

°C) with a temperature probe unless otherwise stated. Brine denotes a saturated aqueous solution of sodium chloride.

Reactions were monitored by TLC using Merck silica gel 60 covered aluminium backed plated F254. TLC plates were visualised under UV light and staining using potassium permanganate solution, vanillin or ninhydrin. Flash column chromatography was performed with Fluorochem silica gel 60 (40–63 μm).

Reverse phase HPLC purification was performed at room temperature on a Gilson preparative HPLC system, which included 322 pumps coupled to a 151 UV/Vis 163 spectrometer, 234 Autoinjector, and a GX-271 liquid handler, equipped with an Agilent Zorbax SB-C18 column (21.2 x 150 mm, 5 μm packing diameter). Purification was done using gradient elution 5–95% acetonitrile in water over 30 min at a 15 mL/min flow rate with 0.1% TFA modifier and UV detection at 254 nm. Analysis was performed by Gilson Trilution v2.0 software. Reverse phase HPLC data were obtained on an Agilent 1200 series HPLC using a Machery-Nagel Nucleodur C18 column using a gradient method 5–95 % acetonitrile (containing 0.1% TFA) in water (containing 0.1% TFA) over 18 minutes at a flow rate of 2 mL/min and UV monitoring at 250 nm.

^1H and ^{13}C NMR spectra were recorded on a Bruker AV3 400 NMR spectrometer at 400 and 101 MHz, respectively or on a Bruker DRX 500 NMR spectrometer at 500 and 126 MHz using the deuterated solvent as the internal deuterium lock. Chemical shifts (δ) are reported in ppm relative to the residual protic solvent where $\delta (\text{CDCl}_3) = 7.26 \text{ ppm}$ (^1H) and $\delta (\text{CDCl}_3) = 77.16 \text{ ppm}$ (^{13}C); $\delta (\text{DMSO}-d_6) = 2.50 \text{ ppm}$ (^1H) and $\delta (\text{DMSO}-d_6) = 39.5 \text{ ppm}$ (^{13}C); ^1H signals are described as singlets (s), doublets (d), triplets (t), quartets (q), multiplets (m), broad (br), app (apparent) or a combination of these and coupling constants are measured in Hz.

The Infrared (IR) spectra were recorded on a Shimadzu FTIR-84005 spectrometer, and the products' frequencies (wavenumbers) are in cm^{-1} . Low-resolution mass spectra were collected utilising an Agilent Technologies 1200 series apparatus equipped with a 6130 single quadrupole LC/MS and a Poroshell EC-C18 column. Analysis was conducted using a gradient approach, eluting with 5–95% acetonitrile (incorporating 5 nM ammonium acetate) and water (containing 5 nM ammonium acetate) over 18 min. at a 1 mL/min flow rate, with UV detection at 254 or 214

nm. HR-MS were collected using a Thermo Scientific Exactive Plus equipped with a Vanquish LC.

HPLC stability analysis was performed using an LC2030 Prominence-I Shimadzu (Kyoto, Japan) with a UV detector. The separation was carried out on a Phenomenex Gemini C18 column (150 mm×4.6 mm×5 µm particle size). The mobile phase used was water with methanol isocratic elution with different compositions depending on the compound (Table 3.2) and a flow rate of 1 mL/min at room temperature with a 254 and 285 nm wavelength— injection volume of 10 µL for all samples. The data was analysed using Lab Solution software by measuring the detected peak area in triplicate with Mean ± R.S.D.

Table 3. 2 Details of the Mobile phase used in HPLC Analysis

Compound	Run Time (min.)	% MP-B ¹	UV Detection λ (nm)	Temperature (°C)	Flow Rate mL/min.
KM6	5	75	254, 285	30	1.0
KM10	5	75	254, 285	30	1.0
KM11	8	90	254, 285	40	1.0

MP-B¹, Mobile phase B (Methanol).

3.3.2 Stability Analysis Study using High-Performance Liquid Chromatography (HPLC)

HPLC is an advanced separation and identification technology applied extensively to analyze and quantify compounds in mixtures, particularly in pharmaceuticals (Steiner et al., 2019). Chromatography operates by passing a liquid sample in the mobile phase through a stationary phase. The stationary phase is a solid support made from silica bonded to different phases packed in a column; the mobile phase is a liquid solvent (such as water, methanol, and acetonitrile) passing through the system under high pressure.

When the sample is loaded, compounds will be distributed between the phases according to their affinity: compounds with high affinity (such as hydrophobic molecules in reverse-phase) will stick to the stationary phase for a longer time, passing more slowly. In comparison, components with low affinity will have faster elution times. This difference in migration provides a distinct separation of the composites as the mobile phase carries them down the column. The eluted compounds are

monitored with a UV-Visible detector, and a chromatogram is developed with peaks corresponding to each compound. Such separation power is affected by parameters including column chemistry and solvent composition (such as gradient elution) and flow rate, which may enable specific, sensitive analyses in fields such as pharmaceutical and biochemistry (Khan, 2017; Moldoveanu & David, 2022).

The stability of pharmaceutical products is crucial for ensuring that drugs maintain their intended effects throughout their shelf lives and comply with safety and efficacy standards set by regulatory bodies. The quality of these products directly influences patient health outcomes, necessitating rigorous testing and validation of stability-indicating methods. Drug stability encompasses the evaluation of how drugs degrade and interact with various formulations and environmental conditions during transportation, storage, and usage (Patil et al., 2023). Therefore, the effect of temperature on the series of KM compounds stability was assessed using HPLC, considering the primary assay procedures prior to starting the experiment, including preparation of stock and standard solutions and method development and validation, as explained in detail below.

3.3.2.1 Preparation of Stock and Standard Solutions for KM Compounds

A 1000 µg/mL stock solution was prepared by dissolving 10 mg of the synthesised KM compounds in 10 mL of methanol, stirring in an ultrasonic bath for 30 min. This stock solution prepared a 7.812 µg/mL solution for all standards used in the stability study by diluting an aliquot with methanol.

Stability:

Stability samples were stored in temperature-controlled rooms at 25°C, 37°C, and 50°C for 7 days. Quantitative analysis was carried out using HPLC, with measurements taken in triplicate at each time point.

3.3.2.2 Method Development and Partial Validation

The method was developed using isocratic elution and mobile phase, and the main details used in the development and validation technique are explained in Table 3.2. The method validation was based on the International Conference on Harmonisation (ICH) guidelines Q2(R1), for validation

of analytical procedures (Guideline, 2005). The parameters required to assay compounds were linearity, range, quantification limit, accuracy, and precision.

Linearity and Range:

The linearity response was assessed in the 1.95–125 µg/mL range. Appropriate amounts of the stock solution were diluted with mobile phase, yielding concentrations of 1.95, 3.90, 7.81, 15.62, 31.25, 62.5, and 125 µg/mL. Triplicate injections of each standard concentration were carried out. The peak area of standard compounds was plotted against the concentrations of standards. The linearity was assessed by calculating the slope, y-intercept, and correlation coefficient (r^2) using least squares regression. Limit of detection (LOD) and limit of quantification (LOQ), LOQ was defined as the lowest concentration of analyte that was reproducibly quantified above baseline following triplicate injection with acceptable intra-assay precision and accuracy. LOD was the smallest concentration detectable by the UV-VIS detector.

These parameters were calculated based on the standard deviation (SD) of the y-intercept and the slope (s) as shown in the following equations (Amanolahi et al., 2017).

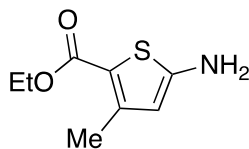
$$\text{LOQ} = 10 \frac{SD}{s} \qquad \text{LOD} = 3.3 \frac{SD}{s}$$

Precision and Accuracy

The repeatability of the analytical method was evaluated by preparing and running the calibration curves of KM compounds (1.95-125 µg/mL) in triplicate, during the same day, under the same experimental conditions. Peak areas were determined and compared. Precision was expressed as a percentage relative standard deviation (R.S.D), and accuracy was expressed by the percentage of recovery using the following formulation:

$$\text{Recovery (\%)} = \frac{\text{Detected concentration}}{\text{Actual concentration}} \times 100$$

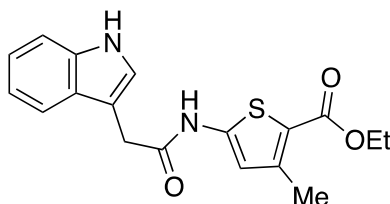
3.3.3 Synthesis of Ethyl 5-amino-3-methylthiophene-2-carboxylate



To a stirred solution of ethyl acetoacetate (4.86 mL, 38.4 mmol) and cyanoacetic acid (3.43 g, 40.3 mmol) in toluene (50 mL) was added ammonium acetate (0.740 g, 9.60 mmol) and acetic acid (1.10 mL, 19.20 mmol) and the resulting reaction mixture was stirred under reflux for 12 h. The mixture was cooled to room temperature and concentrated *in vacuo*. A saturated aqueous solution of ammonium chloride (50 mL) was added, and the mixture was extracted with ethyl acetate (3 × 100 mL). The combined organic extracts were washed with brine (200 mL), dried (MgSO₄), filtered, and concentrated in *vacuo*. This afforded ethyl 4-cyano-3-methylbut-3-enoate as a 60:40 mixture of *E*- and *Z*-isomers, which was used immediately in the next step without purification. The residue was dissolved in ethanol (100 mL) and cooled to 0 °C. Elemental sulfur (9.85 g, 38.40 mmol) was added in one portion, followed by the dropwise addition of diethylamine (4.0 mL, 38.40 mmol), and the suspension was stirred at room temperature for 14 h. The reaction mixture was poured into a saturated aqueous ammonium chloride solution (100 mL) and extracted with ethyl acetate (3 × 200 mL). The combined organic extracts were dried (MgSO₄), filtered, and concentrated in *vacuo*. Purification by flash column chromatography, eluting with 10% ethanol in dichloromethane, afforded ethyl 5-amino-3-methylthiophene-2-carboxylate (1.60 g, 22% yield over two steps) as an orange solid. ¹H NMR (400 MHz, CDCl₃) δ 5.94 (s, 1H), 4.24 (q, *J* = 7.1 Hz, 2H), 2.40 (s, 3H), 1.32 (t, *J* = 7.1 Hz, 3H); ¹³C NMR (101 MHz, CDCl₃) δ 163.3, 156.1, 148.1, 112.1, 111.8, 60.2, 16.4, 14.6; LC-MS *m/z* [M+H]⁺ 186.2, *t_R* = 6.73 min.

Spectroscopic data were aligned with the literature: (Dales, 2008).

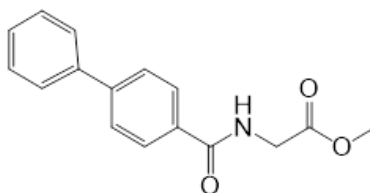
3.3.4 Synthesis of Ethyl 5-(2-(1*H*-indol-3-yl)acetamido)-3-methylthiophene-2-carboxylate (KM6)



An oven-dried flask was charged with 2-(1*H*-indol-3-yl) acetic acid (0.100 g, 0.571 mmol) and ethyl 5-amino-3-methylthiophene-2-carboxylate synthesised in Section 3.3.3 (0.127 g, 0.685 mmol), then dichloromethane (CH₂Cl₂, 10 mL). Triethylamine (0.239 mL, 1.71 mmol) was added, and the mixture was cooled to 0 °C. Propanephosphonic acid anhydride, T3P (0.545 mL, 0.857 mmol; 50% in ethyl acetate) was added dropwise, then the reaction mixture was warmed to room temperature and stirred for 16 h. The reaction mixture was concentrated in *vacuo*, and the residue was purified by flash column chromatography, eluting with 10–30% ethyl acetate in petroleum ether. This afforded ethyl 5-(2-(1*H*-indol-3-yl)acetamido)-3-methylthiophene-2-carboxylate (0.0923 g, 47% yield) as a beige solid. HPLC purity = 97%; **FT-IR** (neat) 3277, 2926, 2603, 2496, 1668, 1595, 1531, 1503, 1474, 1445, 1342, 1260, 1173, 1092, 1036, 980, 833, 754 cm⁻¹; **¹H NMR** (400 MHz, CDCl₃) δ 8.43 (br s, 1H), 8.21 (br s, 1H), 7.55 (dd, J = 7.9, 0.7 Hz, 1H), 7.47–7.42 (m, 1H), 7.30–7.24 (m, 1H), 7.22 (d, J = 2.4 Hz, 1H), 7.17 (ddd, J = 8.0, 7.1, 1.0 Hz, 1H), 6.18 (s, 1H), 4.27 (q, J = 7.1 Hz, 2H), 3.93 (s, 2H), 2.39 (s, 3H), 1.33 (t, J = 7.1 Hz, 3H); **¹³C NMR** (126 MHz, CDCl₃) δ 168.4, 163.5, 144.3, 142.6, 136.6, 126.9, 124.3, 123.3, 120.8, 118.6, 118.2, 115.9, 111.8, 107.9, 60.4, 33.4, 16.0, 14.6; **LC-MS** m/z [M+H]⁺ 343.2, t_R = 8.05 min; **HRMS** (ESI) calcd for C₁₈H₁₉N₂O₃S (M+H)⁺ 343.1105, found 343.1097. NMR and IR figures are illustrated in Appendix 7.

Following Section 3.3.9, KM10 was synthesised in five linear reaction steps, starting from biphenyl-4-carboxylic acid through a strategy highlighted in the functionalisation of the piperazine core in the last step. The method, as shown in Schemes 3.2 and 3.3, was designed to proceed through four isolable and characterised intermediates (**1A-1D**), as detailed below, providing the final **KM10** compound in pure form after purification using reverse-phase HPLC.

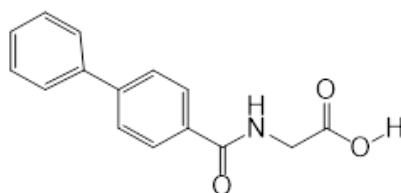
3.3.5 Synthesis of methyl ([1,1'-biphenyl]-4-carbonyl) glycinate (1A)



To a stirred solution of biphenyl-4-carboxylic acid (2.00 g, 10.10 mmol) in dichloromethane (20 mL), thionyl chloride, SOCl_2 (5.85 mL, 80.70 mmol) was added dropwise at room temperature, and the reaction mixture was stirred at 60 °C for 16 h. The reaction mixture was cooled to room temperature and concentrated *in vacuo*. The residue was dissolved in dichloromethane (20 mL), and glycine methyl ester (1.27 g, 10.90 mmol), and triethylamine (2.81 mL, 20.20 mmol) was added at 0 °C. The resulting mixture was warmed to room temperature and stirred until TLC monitoring indicated the consumption of the amine (4–6 h). The reaction mixture was washed with 1 M aqueous hydrochloric acid (3×20 mL) and saturated aqueous sodium bicarbonate (3 ×30 mL). The organic layer was dried (MgSO_4), filtered, and concentrated *in vacuo*. The crude product was purified by flash column chromatography on silica gel (gradient elution with 20–80% ethyl acetate in petroleum ether) to afford methyl ([1,1'-biphenyl]-4-carbonyl) glycinate (2.401 g, 80% yield) as a yellow solid. R_f = 0.45 (70:30 petroleum ether/ethyl acetate).

^1H NMR (500 MHz, CDCl_3) δ 7.92 (d, J = 8.4 Hz, 2H), 7.71 (d, J = 8.3 Hz, 2H), 7.66–7.63 (d, J = 7.9 Hz, 2H), 7.50 (t, J = 7.6 Hz, 2H), 7.42 (t, J = 7.4 Hz, 1H), 6.70 (s, 1H), 4.31 (d, J = 5.0 Hz, 2H), 3.85 (s, 3H); **LCMS** (ESI) m/z 270.2 $[\text{M}+\text{H}]^+$, t_R = 7.52 min.

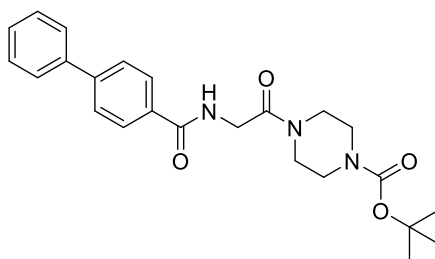
3.3.6 Synthesis of [1,1'-biphenyl]-4-carbonyl) glycine (1B)



To a stirred solution of methyl ([1,1'-biphenyl]-4-carbonyl) glycinate (0.100 g, 3.717 mmol) (**1A**) in (1:1 ratio) tetrahydrofuran and methanol (5 mL:5 mL), 4N NaOH (4 mL) was added, and the mixture was stirred at room temperature for 3 h. After that, the reaction mixture was concentrated, and the residue was dissolved in water. The mixture was acidified with 4 M HCl to pH 2, then extracted with ethyl acetate (3 x 30 mL), dried MgSO₄, and concentrated *in vacuo* which afforded [1,1'-biphenyl]-4-carbonyl) glycine (0.206 g, 80% yield) as a white solid. R_f = 0.371 (90:10 Dichloromethane: Methanol).

¹H NMR (500 MHz, DMSO-*d*₆) δ 8.89 (t, J = 8.9 Hz, 1H), 7.98 (d, J = 8.4 Hz, 2H), 7.81 (d, J = 7.9 Hz, 2H), 7.75 (d, J = 7.9 Hz, 2H), 7.51 (t, J = 7.6 Hz, 2H), 7.42 (t, J = 7.8 Hz, 1H), 3.96 (d, J = 4.0 Hz, 2H). **LCMS** (ESI) m/z 255.1[M+H]⁺, t_R = 5.71 min.

3.3.7 Synthesis of *tert*-butyl 4-([1,1'-biphenyl]-4carbonyl) glycy) piperazine-1-carboxylate (**1C**)

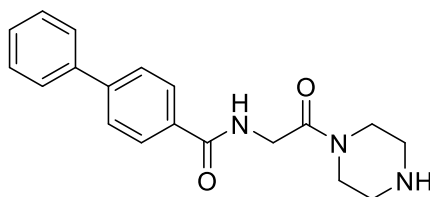


To a stirred solution of [1,1'-biphenyl]-4-carbonyl, glycine (1.00 g, 3.92 mmol) (**1B**) in *N,N*-dimethylformamide (10 mL) at 0 °C, diisopropylcarbodiimide (0.7 mL, 3.92 mmol) was added and stirred for 30 minutes. Oxyma Pure (0.55 g, 3.92 mmol) was added and stirred for 30 min at 0 °C. Then, *N*-boc-piperazine (0.73 g, 3.92 mmol) was added, and the resulting mixture was stirred for 18

hr at room temperature. The reaction mixture was quenched with water and extracted with ethyl acetate (3×30mL). The combined organic extracts were washed with sodium bicarbonate (5×30mL), water (2×30mL), 5% LiCl (5×30mL), saturated brine (2×30mL), and water (2×20mL). Dried over anhydrous MgSO₄, filtered, and concentrated *in vacuo*, which afforded *tert*-butyl 4-((1,1'-biphenyl)-4-carbonyl) glycyl) piperazine-1-carboxylate (1.24 g, 75% yield) as a yellow solid. *R*_f = 0.388 (80:20 ethyl acetate: petroleum ether).

¹H NMR (500 MHz, CDCl₃) δ 7.91 (t, *J* = 8.2 Hz, 2H), 7.67 (d, *J* = 8.1 Hz, 2H), 7.62 (d, *J* = 7.8 Hz, 2H), 7.46 (t, *J* = 7.4 Hz, 2H), 7.38 (t, *J* = 7.4 Hz, 1H), 7.34 (s, 1H), 4.30 (t, *J* = 4.4 Hz, 2H), 3.66 (d, *J* = 3.7 Hz, 2H), 3.48 (t, *J* = 3.5 Hz, 6H), 1.48 (s, 9H). **LCMS** (ESI) *m/z* 424. [M+H]⁺, *t*_R = 8.14 min.

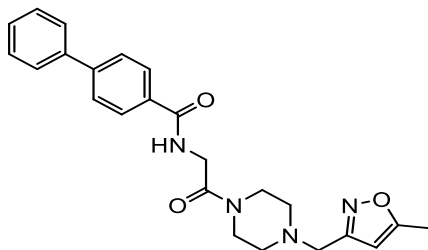
3.3.8 Synthesis of *N*-(2-oxo-2-(piperazin-1-yl) ethyl)-[1,1'-biphenyl]-4-carboxamide (1D)



To a stirred solution of *tert*-butyl 4-((1,1'-biphenyl)-4-carbonyl) glycyl) piperazine-1-carboxylate (**1C**) in acetone/tetrahydrofuran (8 mL, 1:1 v/v ratio) was added 3 M aqueous hydrochloric acid. The resulting solution was stirred overnight at room temperature. After TLC monitoring indicated the completion of the reaction, the mixture was adjusted to pH 9 by dropwise addition of 4 M aqueous sodium hydroxide. The mixture was diluted with water and extracted with dichloromethane (3 × 30 mL). The combined organic extracts were dried (MgSO₄), filtered, and concentrated *in vacuo*. The residue was filtered through a Biotage[®] SCX-II cartridge, eluting with 10% ammonia and methanol, which afforded *N*-(2-oxo-2-(piperazin-1-yl) ethyl)-[1,1'-biphenyl]-4-carboxamide (0.05 g, 30% yield) as a yellow solid.

¹H NMR (500 MHz, DMSO-*d*₆) δ 7.96 (d, *J* = 8.3 Hz, 2H), 7.79 (d, *J* = 7.8 Hz, 2H), 7.74 (d, *J* = 6.7 Hz, 2H), 7.50 (t, *J* = 5.5 Hz, 2H), 7.42 (t, *J* = 7.2 Hz, 1H), 5.48 (s, 1H), 5.46 (br.s, 1H), 4.13 (d, *J* = 4.0 Hz, 2H), 3.63 (dt, *J* = 3.6 Hz, 4H), 3.40 (s, 4H). **LCMS** (ESI) *m/z* 324.3 [M+H]⁺, *t_R* = 6.11 min.

3.3.9 Synthesis of *N*-(2-(4-((5-methylisoxazol 3yl) methyl) piperazin-1-yl)-2-oxoethyl)-[1,1'-biphenyl]-4-carboxamide (KM10)



A mixture of *N*-(2-oxo-2-(piperazin-1-yl) ethyl)-[1,1'-biphenyl]-4-carboxamide (0.038 g, 0.117 mmol) (**1D**), and 5-methyl-1,2oxazole-3-carbaldehyde (0.039 g, 0.351 mmol), were dissolved in dichloromethane (0.7 mL) and the mixture was stirred for 15 min at room temperature. Sodium triacetoxyborohydride (0.104 g, 0.491 mmol) was added and the reaction mixture was stirred at room temperature for 16 h. The reaction mixture was quenched by the addition of a saturated aqueous solution of sodium bicarbonate, then extracted with dichloromethane (3 × 20 ml). The combined organic extracts were dried (MgSO₄), filtered, and concentrated *in vacuo*. Purification of the residue by reversed-phase HPLC on an SB-C18 column using a gradient system (water (0.1% TFA)/acetonitrile (0.1% TFA); 5–95%) followed by lyophilisation afforded *N*-(2-(4-((5-methyl isoxazol 3yl) methyl) piperazine-1-yl)-2-oxoethyl)-[1,1'-biphenyl]-4-carboxamide (0.0223 g, 30% yield) as off white solid.

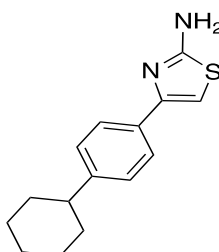
HPLC purity = 92%; *R_f* = 0.60 (9:1 dichloromethane:methanol); **FT-IR** (neat) 3329 cm⁻¹NH, 1676 cm⁻¹, 1649 cm⁻¹ C=O.

¹H NMR (400 MHz, CDCl₃) δ 7.89 (d, *J* = 8.4 Hz, 2H), 7.68 (d, *J* = 8.3 Hz, 2H), 7.62 (dd, *J* = 5.2, 3.3 Hz, 2H), 7.49 – 7.45 (m, 2H), 7.42 – 7.39 (m, 1H), 7.24 (d, *J* = 4.3 Hz, 1H), 6.23 (s, 1H), 4.30 (d, *J* = 4.2 Hz, 2H), 4.24 (s, 2H), 4.01 (s, 2H), 3.89 (s, 2H), 3.28 (br s, 2H), 3.24 (br s, 2H), 2.48 (s, 3H).

^{13}C NMR (101 MHz, CDCl_3) δ 171.8, 166.8, 166.5, 153.5, 131.3, 128.4, 127.6, 127.1, 126.7, 102.2, 76.8, 76.5, 76.1, 50.9, 50.6, 41.0, 38.5, 11.8; **HRMS** (ESI) m/z $[\text{M}+\text{H}]^+$ calc. for $\text{C}_{24}\text{H}_{26}\text{N}_4\text{O}_3$ 419.2078, found 419.2063. NMR, IR, and HPLC Figures are illustrated in Appendix 7.

Following Section 3.3.12, KM11 was synthesised in three reaction steps as shown in Scheme 3.4, starting from 1-(4-Cyclohexylphenyl)ethan-1-one. The reaction process was designed to proceed through two isolable and characterised intermediates (Sections 3.3.10-3.3.11), as detailed below, providing the final **KM11** compound in pure form after purification using reverse-phase HPLC.

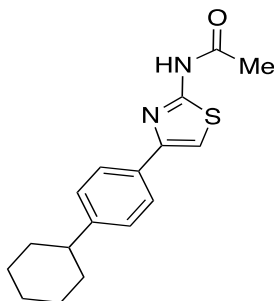
3.3.10 Synthesis of 4-(4-cyclohexylphenyl)thiazol-2-amine



1-(4-Cyclohexylphenyl)ethan-1-one (0.50 g, 2.47 mmol) and copper(II) bromide (1.40 g, 4.94 mmol) were suspended in ethyl acetate (5 mL) and stirred at 90 °C in a sealed tube for 5 h. After cooling to room temperature, EDTA (2.00 g) was added, and the mixture was stirred for 0.5 h. The reaction mixture was filtered through a short pad of Celite, washing with ethyl acetate, and the solvent was removed *in vacuo*. This afforded 2-bromo-1-(4-cyclohexylphenyl)ethan-1-one (0.72 g, quant.), which was used in the next step without further purification. The residue was dissolved in ethanol (5 mL), and thiourea (0.20 mg, 2.70 mmol) was added. The resulting reaction mixture was stirred at 90 °C in a sealed tube for 2 h. The reaction mixture was cooled to room temperature, and the resulting precipitate was collected and dried to afford 4-(4-cyclohexylphenyl)thiazol-2-amine (0.561 g, 85% yield over two steps) as a white solid. **^1H NMR** (400 MHz, $\text{DMSO}-d_6$) δ 8.77 (br s, 2H), 7.63 (d, $J = 7.7$ Hz, 2H), 7.34 (d, $J = 7.7$ Hz, 2H), 7.16 (s, 1H), 1.91–1.64 (m, 5H), 1.54–1.15 (m, 5H), 1H coincident with residual DMSO resonance; **^{13}C NMR** (101 MHz, $\text{DMSO}-d_6$) δ 170.1, 149.0, 139.9, 127.3 (2 \times CH), 126.8, 125.9 (2 \times CH), 101.9, 43.5, 33.7 (2 \times CH_2), 26.2 (2 \times CH_2), 25.5; **LC-MS** m/z $[\text{M}+\text{H}]^+$ 259.2, $t_R = 9.32$ min.

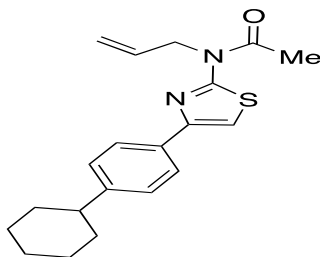
Spectroscopic data were aligned with the literature (Paruch, 2019).

3.3.11 Synthesis of *N*-(4-(4-Cyclohexylphenyl)thiazol-2-yl)acetamide



4-(4-Cyclohexylphenyl)thiazol-2-amine (0.100 g, 0.387 mmol) was suspended in anhydrous tetrahydrofuran (2 mL), and the acetic anhydride (0.5 mL) was added. The reaction vessel was sealed, and the mixture was stirred at 100 °C for 16 h. The reaction mixture was cooled to room temperature and diluted with ethyl acetate (20 mL), washed with saturated aqueous sodium bicarbonate (2 × 20 mL), then brine (20 mL). The organic layer was dried (MgSO₄), filtered, and concentrated *in vacuo* to afford *N*-(4-(4-cyclohexylphenyl)thiazol-2-yl)acetamide (0.074 g, 64% yield) as a white solid. ¹H NMR (400 MHz, CDCl₃) δ 10.9 (s, 1H), 7.72 (d, *J* = 8.1 Hz, 2H), 7.26 (d, *J* = 8.1 Hz, 2H), 2.60–2.48 (m, 1H), 1.94–1.86 (m, 3H), 1.84 (s, 3H), 1.80–1.68 (m, 2H), 1.52–1.20 (m, 5H); ¹³C NMR (101 MHz, CDCl₃) δ 168.4, 159.2, 149.9, 148.6, 132.1, 127.5 (2 × CH), 126.4 (2 × CH), 44.5, 34.5 (2 × CH₂), 27.0 (2 × CH₂), 26.3, 22.9; LC-MS *m/z* [M+H]⁺ 301.4, *t_R* = 9.51 min.

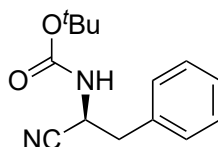
3.3.12 Synthesis of *N*-Allyl-*N*-(4-(4-cyclohexylphenyl)thiazol-2-yl)acetamide (KM11)



N-(4-(4-Cyclohexylphenyl)thiazol-2-yl)acetamide (0.050 g, 0.166 mmol) was added to an oven-dried microwave vial under nitrogen and anhydrous *N,N*-dimethylformamide (2 mL) was added. The mixture was cooled to 0 °C and sodium hydride (0.013 g, 0.333 mmol; 60% in mineral oil) was added slowly. The resulting suspension was warmed to room temperature and stirred for 0.5 h. Allyl bromide (0.022 mL, 0.249 mmol) was added, the microwave vial was sealed and stirred at 120 °C for 16 h. The reaction mixture was cooled to room temperature, diluted with diethyl ether (30 mL), and washed with water (5 × 30 mL) and brine (30 mL). The organic layer was dried (MgSO₄), filtered, and concentrated *in vacuo*. Purification by flash column chromatography, eluting with 10% diethyl ether in petroleum ether, afforded *N*-allyl-*N*-(4-(4-cyclohexylphenyl)thiazol-2-yl)acetamide (0.0251 g, 44% yield) as a beige solid. HPLC purity > 99%; **FT-IR** (neat) 3264, 2920, 2604, 1665, 1595, 1531, 1491, 1474, 1389, 1323, 1267, 1231, 833; **¹H NMR** (400 MHz, CDCl₃) δ 7.79 (d, *J* = 8.2 Hz, 2H), 7.24 (d, *J* = 8.2 Hz, 2H), 7.12 (s, 1H), 6.03 (ddt, *J* = 22.2, 10.2, 5.2 Hz, 1H), 5.26 (apt. dd, *J* = 3.3, 1.1 Hz, 1H), 5.22 (apt. dd, *J* = 10.2, 1.1 Hz, 1H), 4.94 (br s, 2H), 2.58–2.46 (m, 1H), 2.41 (s, 3H), 1.94–1.80 (m, 4H), 1.79–1.72 (m, 1H), 1.50–1.35 (m, 5H); **¹³C NMR** (101 MHz, CDCl₃) δ 170.2, 158.7, 158.2, 148.0, 132.5, 127.2 (2 × CH), 126.1 (2 × CH), 117.3, 108.4, 50.7, 44.5, 34.6 (2 × CH₂), 29.9, 27.0 (2 × CH₂), 26.3, 22.9; **LC-MS** *m/z* [M+H]⁺ 341.3, *t_R* = 10.8 min; **HRMS** (ESI) calcd for C₂₀H₂₅N₂OS (M+H)⁺ 341.1682, found 341.1673. NMR and IR Figures are illustrated in Appendix 7.

As mentioned earlier, compound AMG-548 (p38/NLK) inhibitor was synthesised in Section 3.3.17 in five reaction steps starting from Boc-protected phenylalanine methyl ester and substituted pyrimidinone cores. The method as shown in Schemes 3.5 and 3.6 was designed to proceed through four isolable and characterised intermediates, as detailed below (Sections 3.3.13-3.3.16), providing the final **AMG-548** compound in pure form after purification using reverse phase HPLC. The effect of this compound was explored on IL-1 β -induced CXCL12 activity.

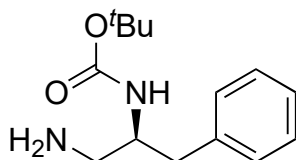
3.3.13 Synthesis of *tert*-Butyl (*S*)-(1-cyano-2-phenylethyl)carbamate



Boc-Phe-OMe (0.500 g, 1.790 mmol) was suspended in a 1:1 mixture of ammonium hydroxide and methanol (20 mL, 0.1 M) and stirred at room temperature for 24 h. The mixture was concentrated in *vacuo* to afford *tert*-butyl (*S*)-(1-amino-1-oxo-3-phenylpropan-2-yl)carbamate (0.473 g, quant.), which was used without further purification. *tert*-Butyl (*S*)-(1-amino-1-oxo-3-phenylpropan-2-yl)carbamate (0.362 g, 1.37 mmol) was dissolved in *N,N*-dimethylformamide (1 mL), and cyanuric chloride (0.126 g, 0.680 mmol) was added in one portion. The reaction mixture was stirred at room temperature for 0.5 h and then diluted with water (50 mL). The precipitate was filtered and washed with 5% aqueous sodium bicarbonate, then water, and dried under vacuum. This afforded *tert*-butyl (*S*)-(1-cyano-2-phenylethyl)carbamate (0.358 g, quant.) as a white solid. $[\alpha]_D^{20} -25.0$ (*c* 0.25, CHCl₃); ¹H NMR (500 MHz, CDCl₃) δ 7.42–7.25 (m, 5H), 4.82 (br s, 2H), 3.15–3.00 (m, 2H), 1.44 (s, 9H); ¹³C NMR (126 MHz, CDCl₃) δ 134.1, 129.6 (2 \times CH), 129.1 (2 \times CH), 128.1, 118.5, 81.5, 43.5, 39.3, 28.3 (3 \times CH₃); LC-MS *m/z* [M–H]⁺ 245.2, *t*_R = 8.25 min.

Spectroscopic data were aligned with the literature (An & Yu, 2015).

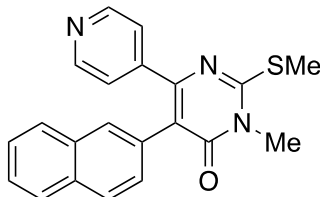
3.3.14 Synthesis of *tert*-Butyl (*S*)-(1-amino-3-phenylpropan-2-yl)carbamate



tert-Butyl (*S*)-(1-cyano-2-phenylethyl)carbamate (0.358 g, 1.450 mmol) was suspended in anhydrous tetrahydrofuran (20 mL) and cooled to -10°C . Lithium aluminum hydride (3.64 mL, 3.640 mmol; 1.0 M in tetrahydrofuran) was added dropwise, and the mixture was stirred at -10°C for 2 h. The reaction mixture was quenched by the addition of water (0.5 mL), followed by 15% aqueous sodium hydroxide (0.5 mL) and then a further portion of water (1.5 mL). The reaction mixture was stirred at room temperature for 0.5 h, then magnesium sulfate was added. The suspension was filtered through a celite plug, washing with ethyl acetate, and concentrated *in vacuo*. This afforded *tert*-butyl (*S*)-(1-amino-3-phenylpropan-2-yl)carbamate (0.288 g, 79% yield) as a colourless oil. $[\alpha]_{\text{D}}^{20} -7.6$ (c 1.0, CHCl_3); $^1\text{H NMR}$ (500 MHz, CDCl_3) δ 7.40–7.15 (m, 5H), 4.75 (br s, 1H), 3.90–3.74 (m, 1H), 2.90–2.73 (m, 3H), 2.62 (dd, $J = 13.1, 6.7$ Hz, 1H), 1.42 (s, 9H); $^{13}\text{C NMR}$ (126 MHz, CDCl_3) δ 155.9, 138.2, 129.4 ($2 \times \text{CH}$), 128.5 ($2 \times \text{CH}$), 126.5, 79.3, 54.1, 44.7, 38.9, 28.5 ($3 \times \text{CH}_3$); **LC-MS** m/z $[\text{M}+\text{H}]^+$ 251.3, $t_{\text{R}} = 5.94$ min.

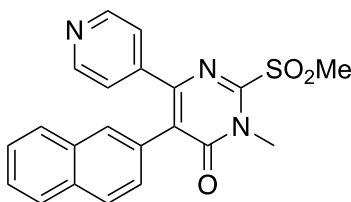
Spectroscopic data were aligned with the literature (Kondoh et al., 2020).

3.3.15 Synthesis of 3-Methyl-2-(methylthio)-5-(naphthalen-2-yl)-6-(pyridin-4-yl)pyrimidin-4(3H)-one



To a stirred solution of ethyl 2-(naphthalen-2-yl)acetate (1.000 g, 4.670 mmol) and 4-cyanopyridine (0.486 g, 4.670 mmol) in anhydrous *N,N*-dimethylformamide (10 mL) was added potassium *tert*-butoxide (4.67 mL, 4.670 mmol; 1.0 M in *tert*-butanol) dropwise. The deep red solution was stirred at room temperature for 1.5 h. Methyl isothiocyanate (0.376 mg, 5.140 mmol) in anhydrous *N,N*-dimethylformamide (2 mL) was added in one portion, and the mixture was stirred at room temperature for 1.5 h. Methyl iodide (0.320 mL, 5.140 mmol) was added dropwise, and the resulting mixture was stirred at room temperature for 2 h. Water (100 mL) was added dropwise and the mixture was stirred for 16 h. The mixture was extracted with ethyl acetate (3 × 100 mL), and the combined organic extracts were dried (MgSO₄), filtered, and concentrated *in vacuo*. Purification by flash column chromatography, eluting with 20–50% ethyl acetate in petroleum ether, afforded 3-methyl-2-(methylthio)-5-(naphthalen-2-yl)-6-(pyridin-4-yl)pyrimidin-4(3H)-one (0.522 g, 31% yield) as a light yellow solid. ¹H NMR (500 MHz, CDCl₃) δ 8.43 (d, *J* = 4.7 Hz, 2H), 7.86–7.70 (m, 4H), 7.52–7.41 (m, 2H), 7.31–7.23 (m, 3H), 3.65 (s, 3H), 2.68 (s, 3H); ¹³C NMR (126 MHz, CDCl₃) δ 162.4, 161.5, 154.5, 149.6 (2 × CH), 146.0, 133.2, 132.8, 130.8, 130.3, 128.4, 128.2, 127.9, 127.7, 126.4, 126.1, 124.0 (2 × CH), 120.5, 31.0, 15.1; LC-MS *m/z* [M+H]⁺ 360.2, *t_R* = 8.31 min.

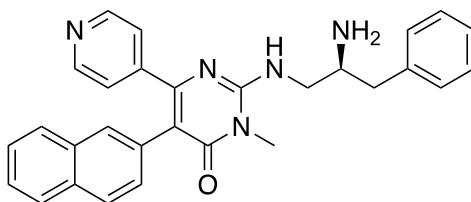
3.3.16 Synthesis of 3-Methyl-2-(methylsulfonyl)-5-(naphthalen-2-yl)-6-(pyridin-4-yl)pyrimidin-4(3H)-one



3-Methyl-2-(methylthio)-5-(naphthalen-2-yl)-6-(pyridin-4-yl)pyrimidin-4(3H)-one (0.100 g, 0.278 mmol) was suspended in methanol (20 mL) and water (8 mL), then Oxone[®] (0.513 g, 0.834 mmol) was added in one portion. The resulting reaction mixture was stirred at room temperature for 16 h. The solvent volume was reduced *in vacuo*, and the mixture was extracted with dichloromethane (3 × 30 mL). The combined organic extracts were dried (MgSO₄), filtered and concentrated *in vacuo*. Purification by flash column chromatography, eluting with 100% ethyl acetate, afforded 3-methyl-2-(methylsulfonyl)-5-(naphthalen-2-yl)-6-(pyridin-4-yl)pyrimidin-4(3H)-one (0.047 g, 43% yield) as a yellow solid. ¹H NMR (500 MHz, CDCl₃) δ 8.46 (d, *J* = 4.9 Hz, 2H), 7.86–7.72 (m, 4H), 7.56–7.44 (m, 2H), 7.23 (dd, *J* = 8.5, 1.7 Hz, 1H), 7.18 (d, *J* = 6.0 Hz, 2H), 3.97 (s, 3H), 3.53 (s, 3H); ¹³C NMR (126 MHz, CDCl₃) δ 161.5, 154.4, 153.2, 150.0 (2 × CH), 144.4, 133.4, 133.2, 130.4, 129.2, 128.5, 128.5, 128.3, 127.9, 127.5, 127.2, 126.6, 123.7 (2 × CH), 40.9, 31.1; LC-MS *m/z* [M+H]⁺ 392.2, *t_R* = 7.79 min.

LC-MS analysis of the reaction mixture showed the desired product, sulfoxide, and pyridine N-oxide by-products. Adding further portions of Oxone resulted in increased formation of the pyridine N-oxide with deleterious effects on the yield of the desired sulfone.

3.3.17 Synthesis of (S)-2-((2-Amino-3-phenylpropyl)amino)-3-methyl-5-(naphthalen-2-yl)-6-(pyridin-4-yl)pyrimidin-4(3H)-one (AMG-548)



3-Methyl-2-(methylsulfonyl)-5-(naphthalen-2-yl)-6-(pyridin-4-yl)pyrimidin-4(3H)-one (0.104 g, 0.266 mmol) and *tert*-butyl (S)-(1-amino-3-phenylpropan-2-yl)carbamate (0.100 g, 0.399 mmol) were dissolved in dichloromethane (2 mL) and potassium carbonate (0.092 g, 0.665 mmol) was added. The mixture was stirred at 50 °C in a sealed vial for 60 h. The reaction mixture was cooled, diluted with dichloromethane (20 mL) and washed with saturated aqueous sodium bicarbonate (20 mL), dried (MgSO₄), filtered and concentrated *in vacuo*. The crude residue was dissolved in acetone (10 mL) and concentrated hydrochloric acid (0.5 mL) was added dropwise. The mixture was stirred at room temperature for 10 min, then concentrated *in vacuo*. The residue was dissolved in methanol and filtered through a Biotage[®] SCX-II cartridge, eluting with methanol and then 7 M ammonia in methanol. Purification by flash column chromatography, eluting with 10–25% methanol in ethyl acetate, afforded (S)-2-((2-amino-3-phenylpropyl)amino)-3-methyl-5-(naphthalen-2-yl)-6-(pyridin-4-yl)pyrimidin-4(3H)-one (0.108 g, 88% yield over 2-steps) as a yellow solid. HPLC purity >99.9%; [α]_D²⁰ +20.7 (*c* 0.5, CHCl₃); **FT-IR** (neat) 3308, 3022, 2922, 1641, 1535, 1466, 1437, 820, 745, 700 cm⁻¹; **¹H NMR** (500 MHz, CDCl₃) δ 8.37 (d, *J* = 6.0 Hz, 2H), 7.77 (d, *J* = 7.8 Hz, 1H), 7.74–7.63 (m, 3H), 7.46–7.37 (m, 2H), 7.34 (t, *J* = 7.3 Hz, 2H), 7.30–7.26 (m, 1H), 7.24–7.16 (m, 5H), 5.81 (br s, 1H), 3.85–3.77 (m, 1H), 3.48 (s, 3H), 3.36–3.26 (m, 2H), 2.90 (dd, *J* = 13.4, 4.8 Hz, 1H), 2.64 (dd, *J* = 13.5, 7.7 Hz, 1H), 1.68 (br s, 2H); **¹³C NMR** (101 MHz, CDCl₃) δ 163.0, 156.8, 152.7, 149.5 (2 \times CH), 147.1, 138.2, 133.4, 132.6, 132.3, 130.4, 129.3 (2 \times CH), 128.9 (2 \times CH), 128.1, 127.71, 127.68, 126.9, 126.0, 125.9, 124.2 (2 \times CH), 114.6, 52.2, 47.3, 43.2, 27.6, one carbon resonance not evident; **LC-MS** *m/z* [M+H]⁺ 462.3, *t*_R = 6.66 min; **HRMS** (ESI) calcd for C₂₉H₂₈ON₅ (M+H)⁺ 462.2288, found 462.2284. NMR and IR Figures are illustrated in Appendix 7.

3.4 Analysis of Compound Stability Intended for Pharmacological Testing

A stability assessment of the synthesised compounds was conducted to assess the efficiency and main mechanisms involved in their effect on target gene (CXCL12) expression in biological studies. This work aimed to evaluate the effect of temperature variations on the stability of these compounds.

It is known that most biological experiments performed on cancer cells use a culture medium and biological environments between 25 °C and 37 °C in mammalian cells. Such a temperature range reflects physiological conditions and optimal cell survival and activity during the experiments (Freshney, 2015). An initial stability analysis is crucial to guarantee the stability of downstream biological experiments. Characterising the behaviour of KM compounds under such experimental conditions, particularly their temperature stabilities, helps explain the results found in cancer cell biology studies and allows for a more accurate assessment of their mechanism of action towards CXCL12 gene expression. However, the effect of temperature on KM compounds' stability was assessed using HPLC.

3.4.1 Results and Discussion

3.4.1.1 Quantitative HPLC Analysis and Calibration Curve of KM10

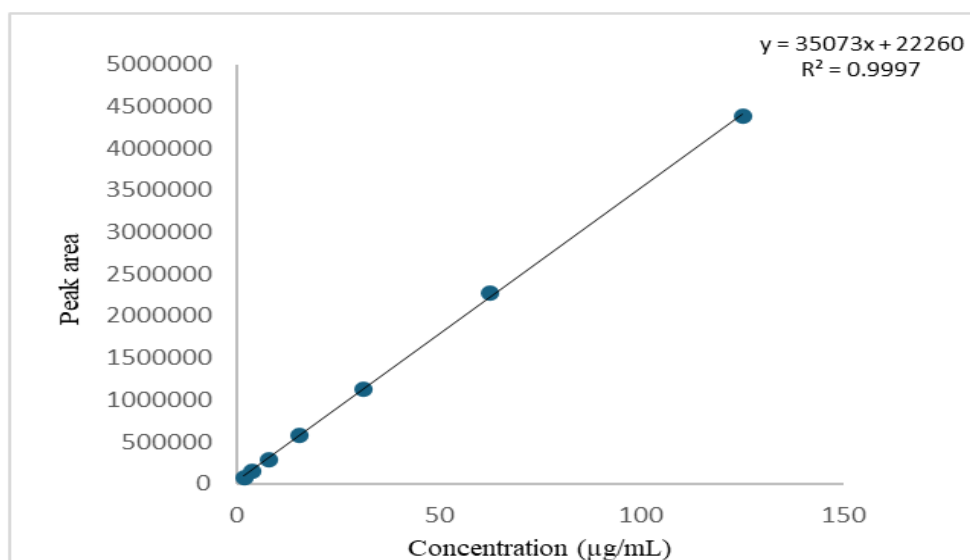
A calibration curve for KM10 was established using seven concentration levels ranging from 1.9 to 125 µg/mL. Each concentration was analysed in triplicate using HPLC, and the resulting peak areas were recorded. The mean, standard deviation (SD), and relative standard deviation (RSD) for each level were calculated to assess the precision of the analytical method as described in Section 3.3.2.2.

Linearity and Precision

The calibration data demonstrated excellent linearity over the tested range, with RSD values consistently below 0.004 for all concentration levels, indicating high precision of the HPLC method as described in Section 3.3.2.2. The LOD of KM10 was determined as 0.0136 µg/mL and the LOQ as 0.0411 µg/mL. The summary of the calibration data is shown in Table 3.3:

Table 3. 3 Calibration data of KM10

Conc. (µg/mL)	Mean Area	SD	RSD
1.9	73849.667	144.050	0.195
3.9	144731.67	271.883	0.188
7.8	284678	643.345	0.226
15.62	570101.67	883.462	0.155
31.25	1132582.3	361.713	0.032
62.5	2271110	2606.342	0.115
125	4375726.7	6829.652	0.156

**Figure 3. 1 Calibration curve of KM10 by HPLC**

The data support a high degree of reproducibility within the tested range, and the resulting curve can be reliably used to quantify KM10 in stability samples.

Sample Stability Analysis (Day 0)

A freshly prepared KM10 sample was analysed under the same conditions. The measured peak areas were: 309291, 308982, and 309521. This yielded a mean of 309264.66, SD = 270.46, and RSD = 0.087 indicates excellent repeatability. Using the calibration curve, the calculated concentration of KM10 in this sample was determined to be 8.05 µg/mL, which increased slightly from the expected

nominal value (7.80 µg/mL), further confirming the method's accuracy. Figure 3.2 illustrates the calibration curve of KM10, confirming linearity across the studied range (Snyder, 2011).

In Figure 3.3, the compound KM10 was subjected to a short-term study. The chromatograms were analysed, and the concentrations were determined using the peak area.

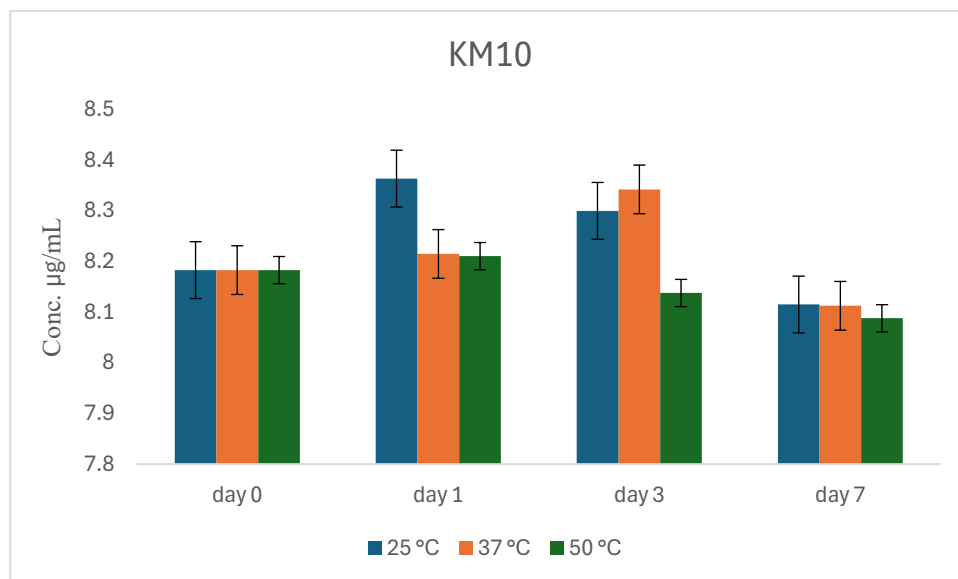


Figure 3. 2 Short-term thermal stability study for 7 days at 25 °C, 37 °C, and 50 °C for KM10

Stability Under Ambient and Physiological Conditions

From the analytical data, KM10 exhibited excellent stability under ambient (25°C) and physiological (37 °C) temperature conditions. The percentage of the original concentration retained at each time point remained consistently above 100%, indicating negligible degradation. Specifically, concentrations at 25°C were 102.21%, 101.43%, and 100.39% on Days 1, 3, and 7, respectively. At 37 °C, the values were similarly stable at 100.39%, 101.95%, and 102.81%. Low relative standard deviation (RSD < 0.6%) demonstrated high analytical precision in all cases (Figure 3.6). These findings suggest that KM10 is chemically stable in environments relevant to pharmaceutical storage and *in vivo* conditions, supporting its suitability for further preclinical development (Waterman, 2005).

Similarly, KM10 stability was observed under accelerated thermal conditions (50 °C). Although the compound retained approximately 100.34% of its initial concentration on Day 1, the value slightly declined to 99.45% by Day 3, with no significant drop in the concentration observed at Day 7 (98.84%) as shown in Figure 3.3, indicating stability of the active compound with consistent analytical precision ($RSD < 0.25\%$). However, the compound contains an amide bond, which is potentially susceptible to hydrolysis under elevated temperatures and moisture, as reported in studies for amide linkage compounds (Gonçalves et al., 2007). Building up the established understanding of degradation pathways in pharmaceutical stability testing (Baertschi, 2016), this investigation evaluates the potential stability of KM10 at elevated temperatures.

3.4.1.2 Quantitative HPLC Analysis and Calibration Curve of KM11

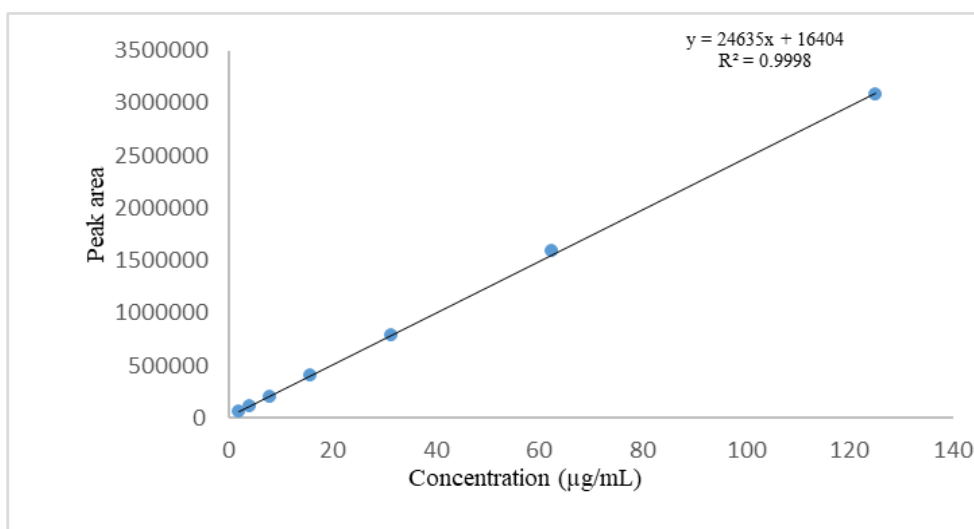
A quantitative HPLC method was developed and applied to the compound KM11 to determine its linearity, precision, and suitability for concentration determination in pharmaceutical matrices as described in Section 3.3.2.2.

Calibration Curve and Linearity

The calibration curve was constructed using seven concentration points ranging from 1.9 to 125 $\mu\text{g/mL}$. Each concentration level was injected in triplicate, and the mean peak area was calculated. The method demonstrated excellent linearity with a consistent increase in peak area with concentration and minimal deviation, as observed in the low relative standard deviation (RSD) values, as shown in Table 3.4. This confirms the robustness and repeatability of the analytical method. The LOD of KM11 was determined as 0.0256 $\mu\text{g/mL}$ and the LOQ as 0.0773 $\mu\text{g/mL}$.

Table 3. 4 Calibration data of KM11

Conc. (µg/mL)	Mean Area	SD	RSD
1.9	54464.33	190.505	0.0035
3.9	107188	137.390	0.0013
7.8	203393.3	410.215	0.0020
15.62	408634	313.597	0.0008
31.25	780907	3077.066	0.0039
62.5	1588272	2269.764	0.0014
125	3080725	7320.465	0.0024

**Figure 3. 3 Calibration curve of KM11 by HPLC**

Sample Stability Analysis (Day 0)

A freshly prepared KM11 sample was analyzed at Day 0, with recorded peak areas of 209773, 209363, and 210189. The calculated mean area was 209775 with a relative standard deviation of 0.0020. Referencing the calibration curve, the sample concentration was approximately 7.85 µg/mL, confirming the method's applicability and precision for absolute sample quantification. Figure 3.4 illustrates the calibration curve of KM11, confirming linearity across the studied range.

Stability Under Ambient and Physiological Conditions

The stability of KM11 was studied by monitoring its concentration after storage at three different temperatures (25 °C, 37 °C, and 50 °C) for several days (1, 3, and 7 days). The concentration was calculated based on area readings from the HPLC instrument, and the standard deviation (SD) and R.S.D % were calculated to evaluate the variability of the results in Table 3.4 according to the equation described in Section 3.3.2.2.

At 25 °C, the analysis results showed that the compound concentration remained stable throughout the storage period. The concentration on the first day was 8.00 µg/mL, increasing slightly to 8.01 µg/mL on the seventh day, as shown in Figure 3.5. The RSD value remained less than 0.25%, indicating high accuracy and stability. The percentage change did not exceed 3%, indicating the stability of the compound at this temperature.

At 37 °C, the results also showed good stability at this temperature. There was no significant decrease in the compound concentration over the three days of storage, but rather a slight increase from 7.81 to 8.03 µg/mL (Figure 3.5). The RSD values also remained very low (less than 0.21%), indicating the stability of the compound's chemical composition.

At 50 °C, despite the elevated temperature, the compound continued to demonstrate acceptable stability, with the concentration not decreasing significantly, reaching 7.83 µg/mL on day 7, compared to 7.97 µg/mL on day 1 (Figure 3.5). However, the RSD values less than or equal to 0.25% were observed, and the percentage change did not exceed 3%, indicating the stability of the compound at this temperature.

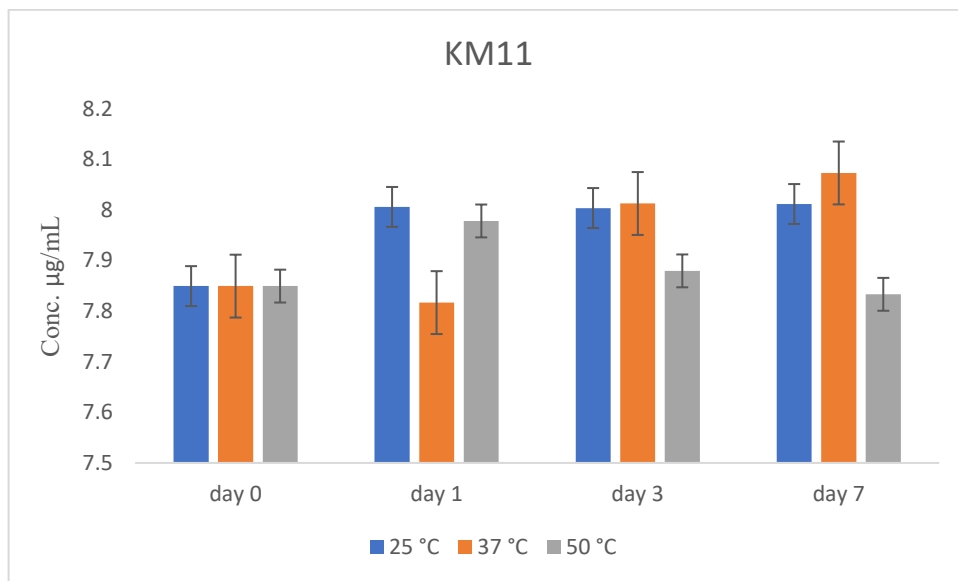


Figure 3. 4 Short-term thermal stability study for 7 days at 25 °C, 37 °C, and 50 °C for KM11

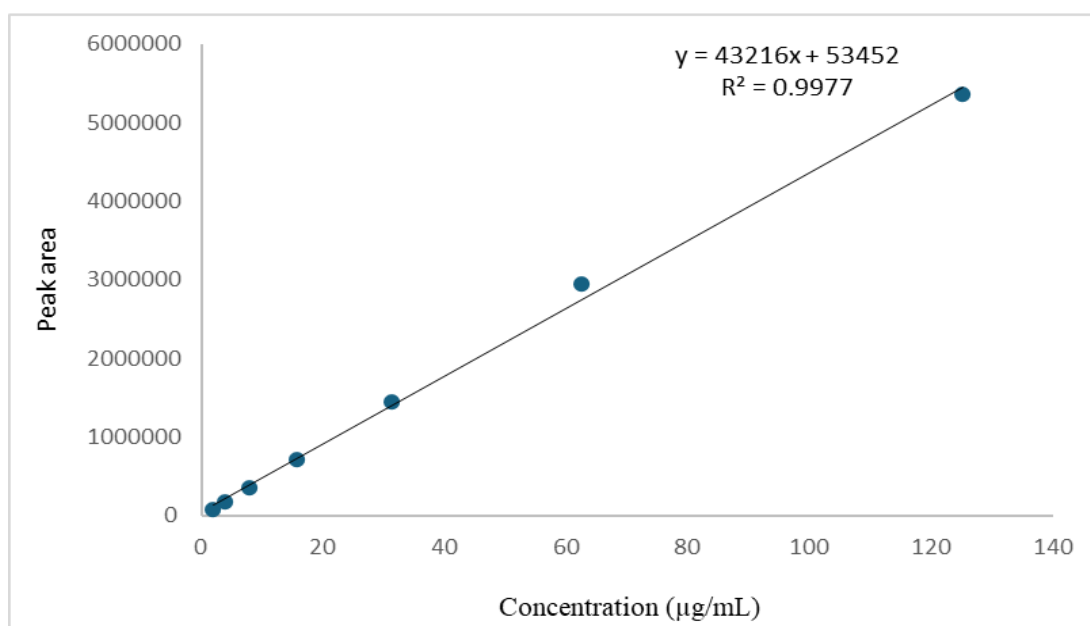
3.4.1.3 Quantitative HPLC Analysis and Calibration Curve of KM6

This study employed a quantitative HPLC method to determine compound KM6 across standard concentrations and in an unknown test sample. The obtained results were evaluated in terms of linearity, precision, reproducibility, and accuracy, all of which are fundamental parameters for validation as described in Section 3.3.2.2. This demonstrates the system's capacity to respond proportionally across the entire concentration range, a critical feature indicating linearity. Such linearity is essential to ensure reliable quantification of unknown samples and is typically confirmed through calibration curve fitting, often yielding a correlation coefficient (R^2) close to 1.0, as shown in Figure 3.6.

The LOD of KM6 was determined as 0.0213 µg/mL and the LOQ as 0.0646 µg/mL. The standard deviation (SD) and R.S.D % of KM6 were calculated to evaluate the variability of the results in Table 3.5.

Table 3. 5 Calibration data of KM6

Conc. (µg/mL)	Mean Area	SD	RSD
1.9	86093.5	279.307	0.324
3.9	180361	104.652	0.058
7.8	362022.5	847.821	0.234
15.62	711577	2247.185	0.316
31.25	1454432	2816.406	0.194
62.5	2939918	111.723	0.004
125	5356064	25465.037	0.475

**Figure 3. 5 Calibration curve of KM6 by HPLC**

Precision was assessed by calculating the standard deviation (SD) and relative standard deviation (RSD%) for each concentration as described in Section 3.3.2.2. The RSD values across the dataset ranged between 0.003% to 0.47%. This trend is common in chromatographic analysis, where signal fluctuations and noise have more pronounced effects at higher signal intensities (Khan, 2017). The unknown test sample was analyzed in triplicate, resulting in a mean area of 341,260.67 and an RSD of 0.37%, demonstrating good intra-sample consistency. When interpolated using the established

calibration curve, the corresponding concentration of the unknown sample was estimated to be 7.72 µg/mL. This value is consistent with the trend observed for the standard solutions and falls within the linear range of the method.

The accuracy between the calculated concentration and the actual standard concentration (7.8 µg/mL) is 98.82%, which supports the accuracy of the quantification and the robustness of the calibration.

To assess the chemical stability of KM6 under the tested conditions, replicate analyses were conducted, and the resulting peak areas were used to calculate the percentage of retained concentration relative to the reference (100% expected). The observed concentrations ranged between 6.42 µg/mL and 6.76 µg/mL, corresponding to 84.0% to 87.5% of the nominal concentration (assumed to be ~7.72 µg/mL based on previous calibration).

At 25 °C, the analysis results showed that the compound concentration remained stable throughout the storage period. The concentration on the first day was 6.57 µg/mL, decreasing slightly to 6.44 µg/mL on the seventh day, as shown in Figure 3.7. The RSD value is less than 0.6%, indicating accuracy and stability within the accepted range. The percentage change did not exceed 18%, indicating a stability issue of the compound at this temperature, although the compound degradation was less than 20%.

Similarly, the results at 37 °C and 50 °C showed a stability issue. The compound concentration significantly decreased over the three days of storage from 7.72 to 6.48 and 6.57 µg/mL, respectively (Figure 3.7). The RSD values were less than 0.6 %, indicating a stability issue with the compound's chemical composition.

These results indicate a modest reduction in assayable KM6 content, ranging from 17% to 14%, depending on the sample set. The relative standard deviation (RSD%) across all measurements remained within acceptable analytical limits (typically <1%), suggesting that the observed decrease in concentration is not due to analytical variability, but rather reflects true chemical degradation or reduced stability of KM6 under the applied conditions. Notably, the reduction in concentration was primarily observed between Day 0 and Day 1, which may indicate either early instability of the compound or potential issues with the analytical procedure.

This degree of degradation could be attributed to environmental factors such as light, heat, or humidity, intrinsic chemical instability, possibly due to labile functional groups in KM6 (amide linkages), Matrix effects in solution that accelerate hydrolysis or oxidation. Such a 14–17% reduction in stability does not align with early-phase pharmaceutical stability profiles, where initial degradation of $\leq 15\%$ is considered manageable (Waterman, 2005). However, further investigation or repetition of the analysis is warranted to draw definitive conclusions regarding the stability of KM6.

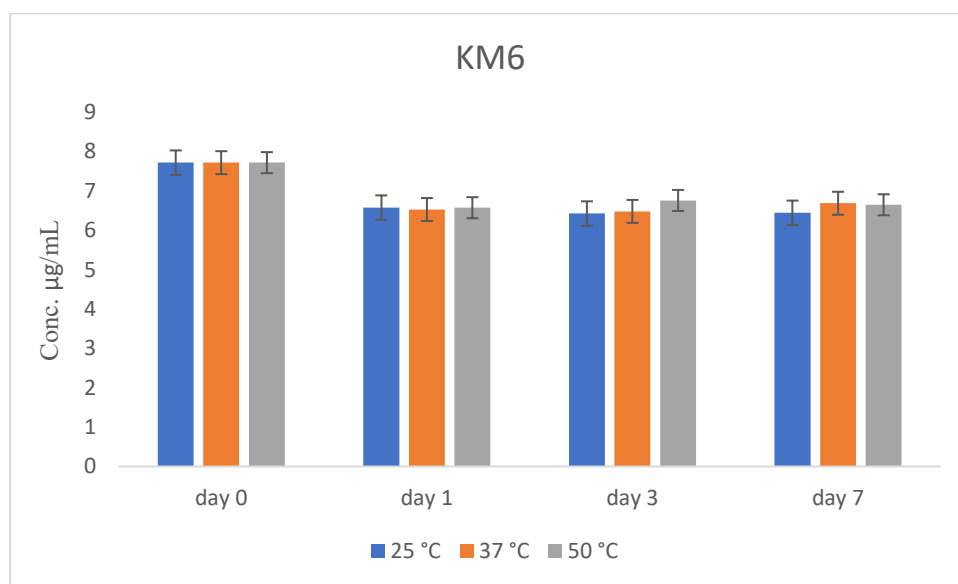


Figure 3. 6 Short-term thermal stability study for 7 days at 25 °C, 37 °C, and 50 °C for KM6

However, for long-term storage or formulation, this highlights the necessity for protective packaging, pH-controlled media, or incorporation of stabilizers. Implications of degradation studies (e.g., under acidic, basic, oxidative, and thermal conditions) are recommended to elucidate the precise degradation pathways of KM6. Moreover, investigating the nature of the degradation products via LC-MS or NMR would provide insights into structural vulnerabilities and assist in designing more stable analogues if needed (Baertschi, 2016; Connors, 1986).

3.5 Conclusion

The targeted compounds KM6, KM10, and KM11 were synthesised successfully using various chemical techniques, and the calibration results confirm that the HPLC method used for quantifying KM compounds is precise, accurate, and linear over a wide range of concentrations. Based on the above results, it can be concluded that KM10 and KM11 compounds showed good chemical stability under various storage conditions for up to 7 days, particularly at 25 °C and 37 °C.

At 50 °C, slight changes in the readings were observed, indicating that solubility is often a function of temperature (Mota et al., 2009), which might explain the variances observed in some way. However, they remained within acceptable limits, indicating their relative tolerance to high temperatures in the short term.

In contrast, the KM6 compound exhibited reduced stability with mild degradation in its chemical composition. An analytical evaluation suggests that further experimental replication and investigation using LC-MS or NMR are required.

Chapter Four

IL-1 β -dependent Signalling

Pathways involved in CXCL12

induction in U2OS Cells

4.1 Introduction

As mentioned before, the chemokines, including CXCL12, play essential roles in cancer progression and development through the recruitment of cells within the TME, thus enhancing many signalling cascades, inducing cancer hallmarks. Huang and co-workers reported that the CXCL12/CXCR4 inhibitor, AMD3100 and siRNA targeting CXCR4 inhibited human OS metastasis induced by CXCL12 expression (Huang et al., 2009). Many studies reported CXCL12 upregulation in various human cancers, including osteosarcoma (Dai et al., 2023; Li et al., 2018; Teng et al., 2016b). Previously, Garcia-Moruja reported IL-1 β -induced CXCL12 gene expression in a U373-cell line (García-Moruja et al., 2005) Using that construct, we generated a U2OS-CXCL12 cell line and examined signalling pathways regulating CXCL12 induction.

4.1.1 The effect of IL-1 β on CXCL12 expression in U2OS cells

Initially, a time course (0-8 hours) for IL-1 β -induced CXCL12 activity was generated in the U2OS cell line. The results, as shown in Figure 4.1 (A), revealed that after a delay of 2 hours, there was an increase in reporter activity reaching a peak between 6 and 8 hours at approximately 4-fold of basal levels (Fold stim at 6 hours = 4.02 ± 1.37 , $P < 0.001$).

Next, a concentration-response curve was established for IL-1 β as shown in Figure 4.1 (B). IL-1 β caused a concentration-dependent increase over the low ng/mL range, which reached a significant level between 3 and 10 ng/mL (Fold stim- 3.34 ± 0.44 , 3.46 ± 0.43 , respectively). From these experiments, a stimulation time of 6 hours was chosen for subsequent reporter experiments (see Section 2.5.1), and 10 ng/mL of IL-1 β was used as an optimal concentration. These findings indicate the role of IL-1 β in CXCL12 induction in U2OS cells, which are compatible with previous experimental studies for cell stimulation (Calonge et al., 2010), and the starting point for the subsequent experiments.

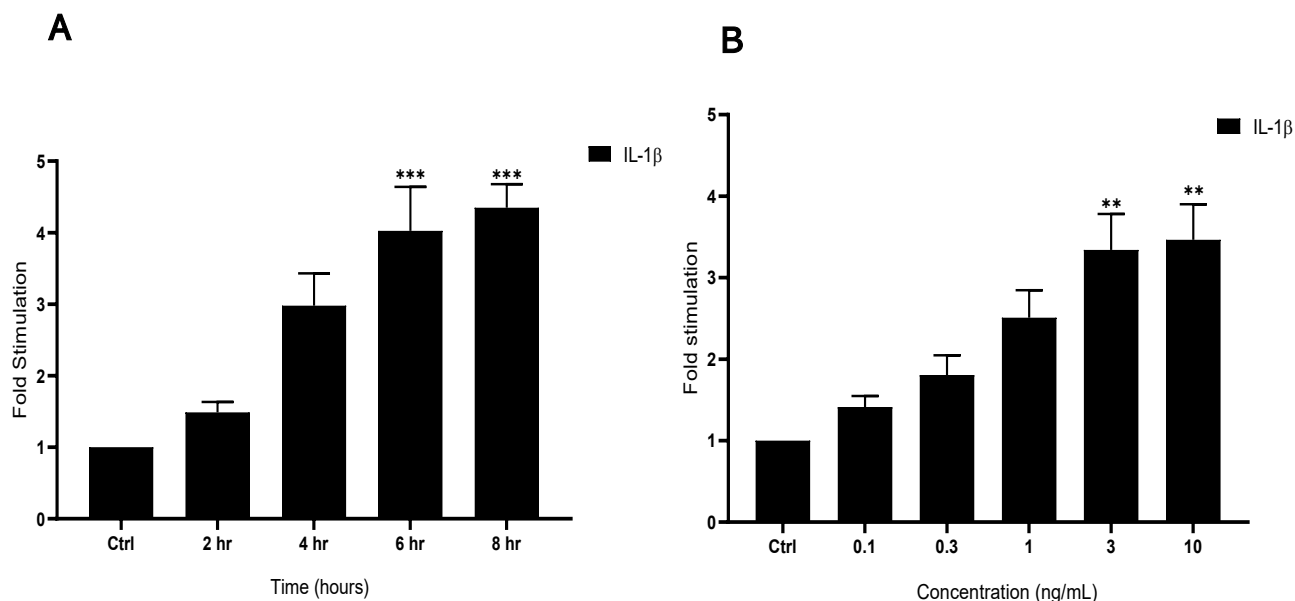


Figure 4. 1 Effect of IL-1 β on CXCL12 expression in U2OS cells.

U2OS cells were grown in 12-well plates and treated with 10 ng/mL IL-1 β for the indicated times (A). Cells were treated with increasing concentrations of IL-1 β for 8 hours (B). Whole-cell lysates were prepared, and CXCL12 expression was measured using reporter assay, as previously described in Section 2.5.1. *** $P < 0.001$, ** $P < 0.01$, vs control (n=5).

4.2 IL-1 β Induces MAP Kinase Signalling Pathways in U2OS Cells

Previous studies found that IL-1 β was able to stimulate a number of signalling pathways (Pyrillou et al., 2020; Weber et al., 2010; Zhang et al., 2020). Thus, we started to explore the signalling cassettes that may regulate the induction of CXCL12. This includes the MAP kinases; extracellular regulated (ERK), c-Jun-N-terminal (JNK), and p38 MAP kinase. In particular, ERK, which is known to regulate c/EBP β phosphorylation (Park et al., 2004; Raymond et al., 2006), resulting in activation of CXCL12 in various cell lines as demonstrated by Calonge and co-workers in U373 cancer cells (Calonge et al., 2010).

4.2.1 The effect of IL-1 β on Phosphorylated ERK in U2OS Cells

The effect of IL-1 β on ERK 1/2 activation was then examined. As shown in Figure 4.2, the U2OS cells were treated with IL-1 β over a time course of (0-120 min). For the phosphorylation of ERK1/2, there was no difference in the stimulation of ERK1/2 signalling compared to non-stimulated cells at early time points. Only at 30 min was there a slight increase, which was insignificant compared to non-stimulated cells. Furthermore, the IL-1 β -induced C/EBP β phosphorylation was also examined to confirm the effect of the ERK/c/EBP β pathway on gene transcription. U2OS cells were also treated with IL-1 β over a time course of (0-24 h), for ERK1/2 phosphorylation. There was no C/EBP β phosphorylation at time points up to 6 hours compared to non-stimulated cells. Following 16 h of stimulation, the phosphorylation signals increased and stayed elevated up 24 h, as shown in Figure 4.2, panel C. These findings contradict the early stimulation of the reported c/EBP β phosphorylation, indicating no effect of IL-1 β on the ERK1/2 signalling pathway and delayed activation of c/EBP β .

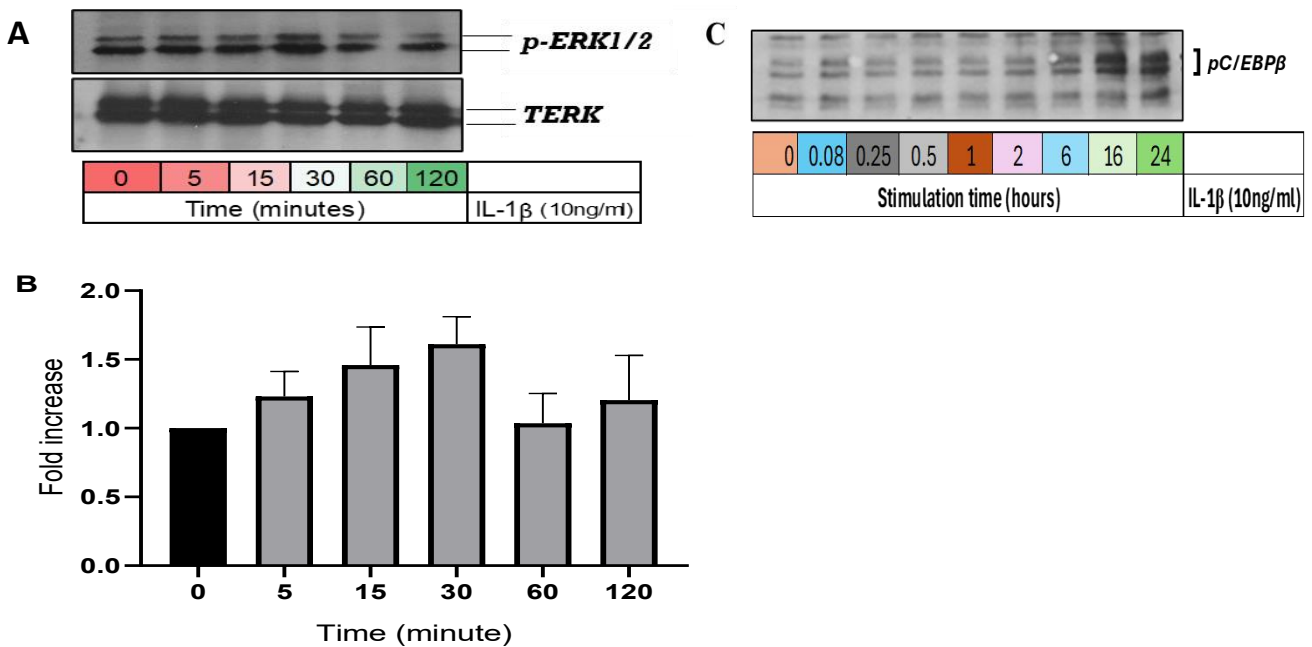


Figure 4. 2 Time course of IL-1β-induced phosphorylation of ERK and c/EBPβ in U2OS cells. U2OS cells were grown in 12-well plates and treated with 10 ng/mL of IL-1β for the times indicated. Whole-cell lysates were prepared for separation using SDS-PAGE and analysed by Western Blotting using pERK1/2 antibody and pc/EBPβ. (A) Western Blots represent the phosphorylation of ERK1/2 (42,44 kDa) and total ERK (42,44 kDa), which was used as a loading control. In panel (B), blots were semi-quantified by scanning densitometry and results expressed as fold stimulation relative to control for pERK1/2. Panel (C) represents the phosphorylation of pC/EBPβ (35,38 kDa). Each value represents the mean ± SEM of three independent experiments. Data were analysed using a one-way ANOVA test.

4.2.2 The effect of IL-1β on Phosphorylated JNK in U2OS Cells

As IL-1β-induced ERK signalling was not observed in U2OS cells, the effect of IL-1β on JNK activation was examined. As shown in Figure 4.3, the U2OS cells were treated with IL-1β over a time course of (0-120 min). Phosphorylation of JNK was observed as early as 15 min and reached a higher stimulation at 30 min (Fold stim- 8.17 ± 2.46 , $P < 0.01$). Then, this response started to decrease gradually over time, returning to near basal values by 120 minutes.

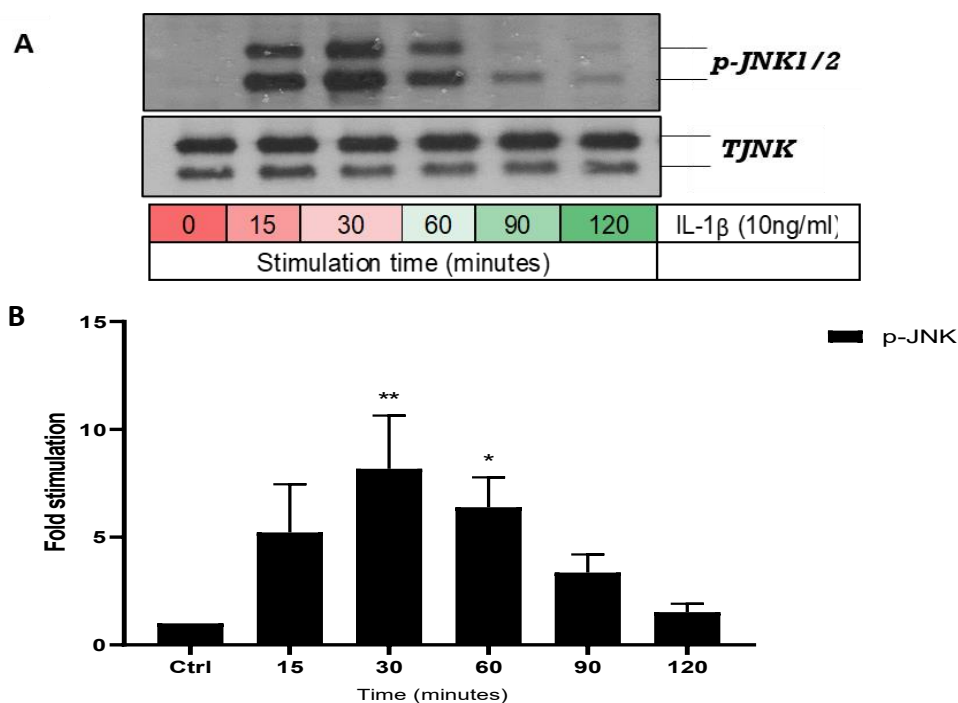


Figure 4. 3 Time course of IL-1 β -induced phosphorylation of pJNK in U2OS cells.

U2OS cells were treated with 10 ng/mL of IL-1 β for the times indicated. Whole-cell lysates were separated using SDS-PAGE and analysed by Western Blotting with ppJNK antibodies. (A) Western Blots represent the phosphorylation of JNK (46,54 kDa) and total JNK, which was used as a loading control. Blots were semi-quantified by scanning densitometry and results expressed as fold stimulation relative to control for pJNK (B). Each value represents the mean \pm SEM of three independent experiments. Data were analysed using a one-way ANOVA test, ** $P < 0.01$, * $P < 0.05$ vs control.

4.2.3 The effect of IL-1 β on Phosphorylated p38 in U2OS Cells

Next, the effect of IL-1 β on p38 MAPK activation was examined. As shown in Figure 4.4, the U2OS cells were treated with IL-1 β over a time course of 0-120 min. Phosphorylation of p38 MAPK was observed as early as 15 min and reached a higher stimulation at 30 min (Fold stims- 2.68 ± 0.07 , $P < 0.001$). Then, this response started to decrease gradually over time, returning to near basal values by 120 minutes.

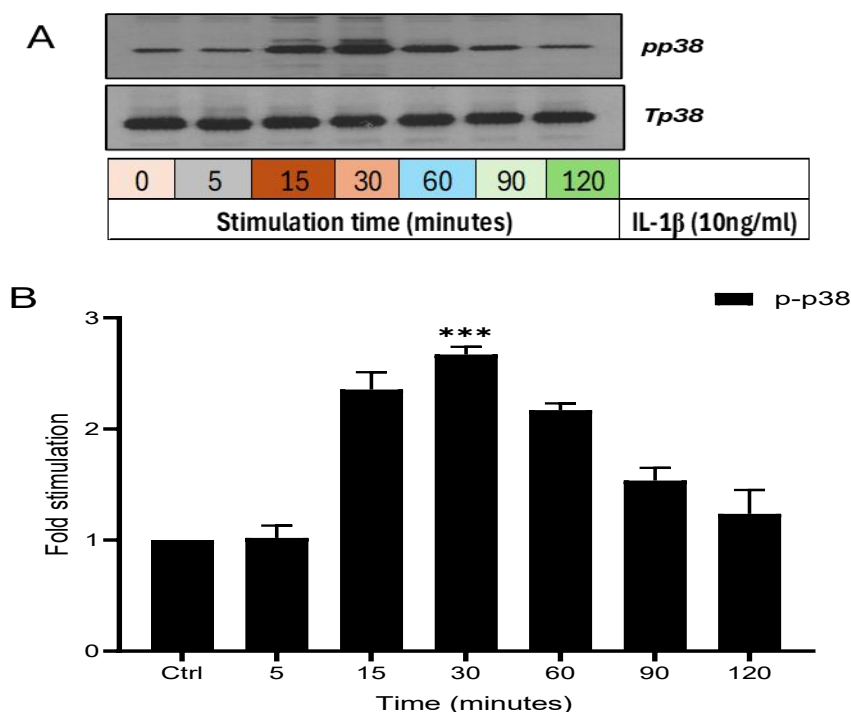


Figure 4. 4 Time course of IL-1 β -induced phosphorylation of p38 in U2OS cells.

U2OS cells were treated with 10 ng/mL of IL-1 β for the times indicated. Whole-cell lysates were separated using SDS-PAGE and analysed by Western Blotting with pp38 antibodies. (A) Western Blots represent the phosphorylation of p38 (38 kDa) and total p38 (38 kDa), which was used as a loading control. Blots were semi-quantified by scanning densitometry and results expressed as fold stimulation relative to control for pp38 (B). Each value represents the mean \pm SEM of three independent experiments. Data were analysed using a one-way ANOVA test, *** P < 0.001 vs control.

4.3 IL-1 β -mediated activation of canonical NF- κ B signalling in U2OS cells

4.3.1 The effect of IL-1 β on Cellular I κ B- α and p65 Phosphorylation in U2OS Cells

It has been found that IL-1 β activates I κ B- α degradation, and phosphorylates the p65 subunit, leading to nuclear translocation and gene transcription through heterodimer interaction with RelA, enhancing cellular responses in tumour cells (Alkalay et al., 1995; Verstrepen et al., 2008). For this reason, the effect of IL-1 β on canonical NF- κ B components was tested over a time course of (0-120 min). Figure 4.5 shows that I κ B α breakdown was noticed early after IL-1 β stimulation, with a substantial drop in cellular levels between 15 and 60 min (P < 0.001). The extent of I κ B α degradation peaked at 30 min (3.0% of basal I κ B α expression), after which, I κ B α expression gradually increased and returned to

baseline levels by 120 min. IL-1 β also caused a rise in the phosphorylation of p65 NF- κ B after 15 min, which reached a maximum at 60 min (Fold stim - 14.67 ± 0.62 , $P < 0.01$) before progressively reverting to baseline levels by 120 min. These results indicate the rapid stimulation of canonical NF- κ B components via IL-1 β in U2OS cells.

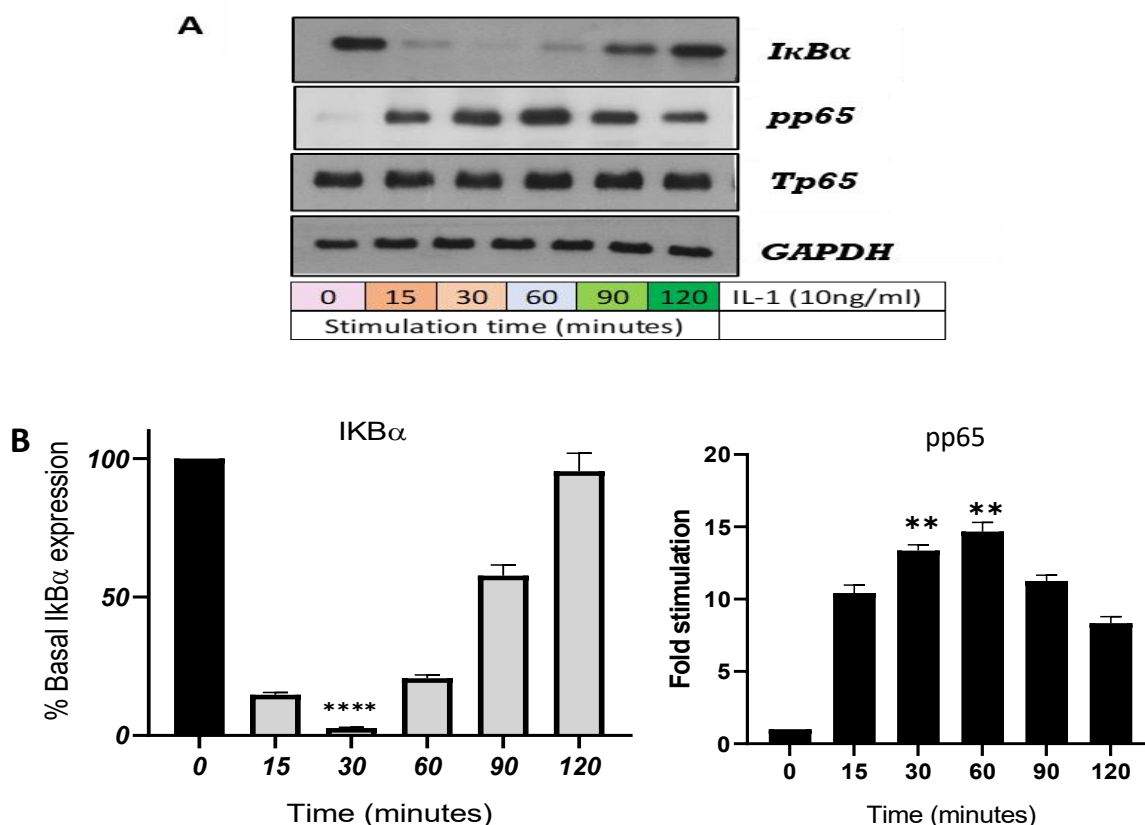


Figure 4. 5 Time course of IL-1 β -induced I κ B α degradation and p65 phosphorylation in U2OS cells.

U2OS cells were grown in 12-well plates and treated with 10 ng/mL of IL-1 β (0-120 min). Whole-cell lysates were separated using SDS-PAGE and analysed by Western Blotting for (A) I κ B α degradation (39 kDa), p65 phosphorylation (65 kDa), total p65 and GAPDH (37 kDa) as a loading control. In panel (B), blots were semi-quantified by scanning densitometry, and the results expressed as fold stimulation relative to the control. Each value represents the mean \pm SEM of three independent experiments. Data was analysed using a one-way ANOVA test, **** $P < 0.0001$, ** $P < 0.01$ vs. control.

4.4 IL-1 β Induces Non-Canonical NF- κ B Signalling in U2OS Cells

4.4.1 The effect of IL-1 β on p100 phosphorylation and p52 Formation in U2OS Cells

Having established that IL-1 β is able to strongly activate the canonical NF κ B pathway, the effect upon elements of the non-canonical pathway was assessed. As in previous experiments, the effect of IL-1 β on the phosphorylation and degradation of p100 NF- κ B2 was studied over a time course of (0-120 min) (McIntosh et al., 2023). Figure 4.6 showed IL-1 β -induced phosphorylation of p100 after 15 min, which reached a maximum between 30 and 60 min (30 minutes, fold stim = 35.50 ± 2.30 , $P < 0.01$), after which levels then returned toward basal values. In contrast, the levels of p100 and p52 remained unchanged with time. Taken together, these results indicate that IL-1 β activates a component of the non-canonical NF- κ B pathway in U2OS cells through phosphorylation of a key IKK α target, pp100 at Ser 866/870.

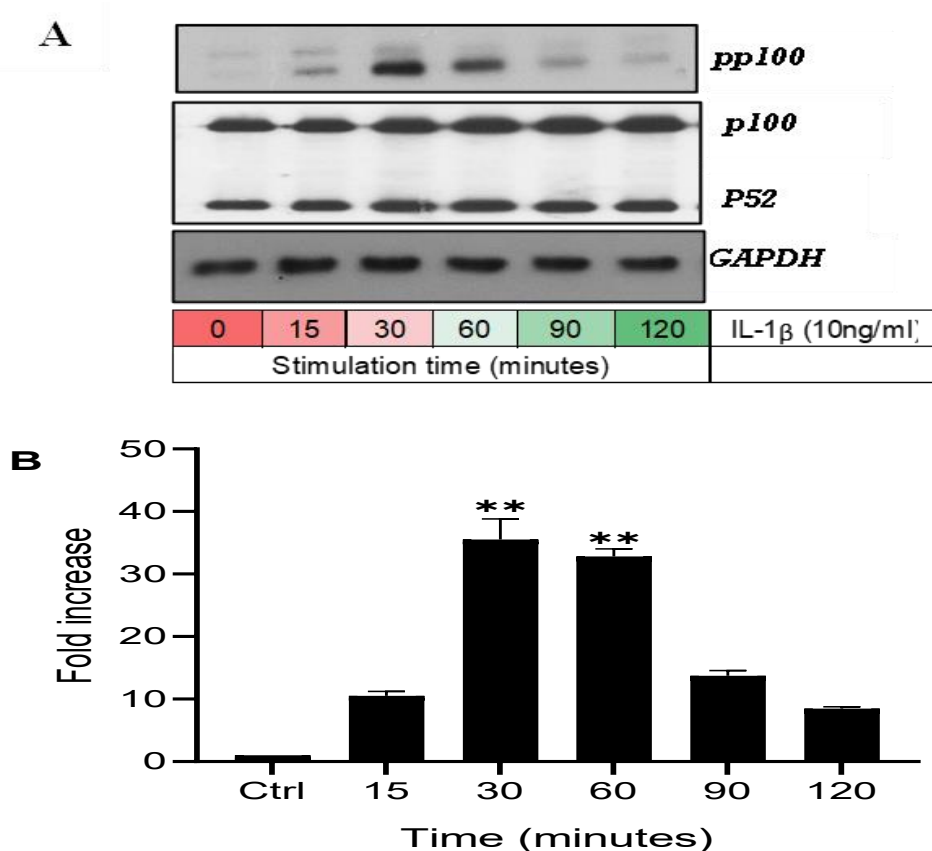


Figure 4. 6 Time course of IL-1 β -induced p100 phosphorylation in U2OS cells.

U2OS cells were grown in 12-well plates and treated with 10 ng/mL of IL-1 β (0-120 minutes). Whole-cell lysates were separated using SDS-PAGE and analysed by Western Blotting for (A) p100 phosphorylation (100 kDa), p52 (52 kDa), and GAPDH (37 kDa) as a loading control. In Panel (B), blots were semi-quantified by scanning densitometry and the result expressed as fold stimulation relative to the control for pp100. Each value represents the mean \pm SEM of three independent experiments. Data was analysed using a one-way ANOVA test, **P < 0.01 vs control.

4.5 Effect of NF- κ B Inhibition upon Cellular Signalling mediated by IL-1 β in U2OS Cells

4.5.1 Effect of IKK- β Inhibition upon Canonical NF- κ B signalling induced by IL-1 β in U2OS Cells

As reported previously, IKK β plays a crucial role in the cellular degradation of I κ B α and phosphorylation of p65 (Hayden & Ghosh, 2008; Liu et al., 2017). Therefore, the role of this pathway in the regulation of the signalling responses was assessed using the IKK β inhibitor, IKK2 X1 (Baxter

et al., 2004), and the results are shown in Figure 4.7. The data indicate that IL-1 β induced significant I κ B α degradation by 94% (% basal I κ B α expression 6%, $P < 0.0001$) compared to non-stimulated cells. Pre-treatment with IKK2 X1 but only at high concentrations (20 and 30 μ M) partially reversed the loss in cellular I κ B α in cells exposed to IL-1 β (% basal I κ B α expression -17 %, 27%, $P < 0.01$, $P < 0.05$ respectively), with no effect on I κ B α loss for the compound alone. The results revealed that IKK β was important in the classical NF- κ B pathway induced by IL-1 β in U2OS cells, but did not fully confirm the effectiveness of the inhibitor.

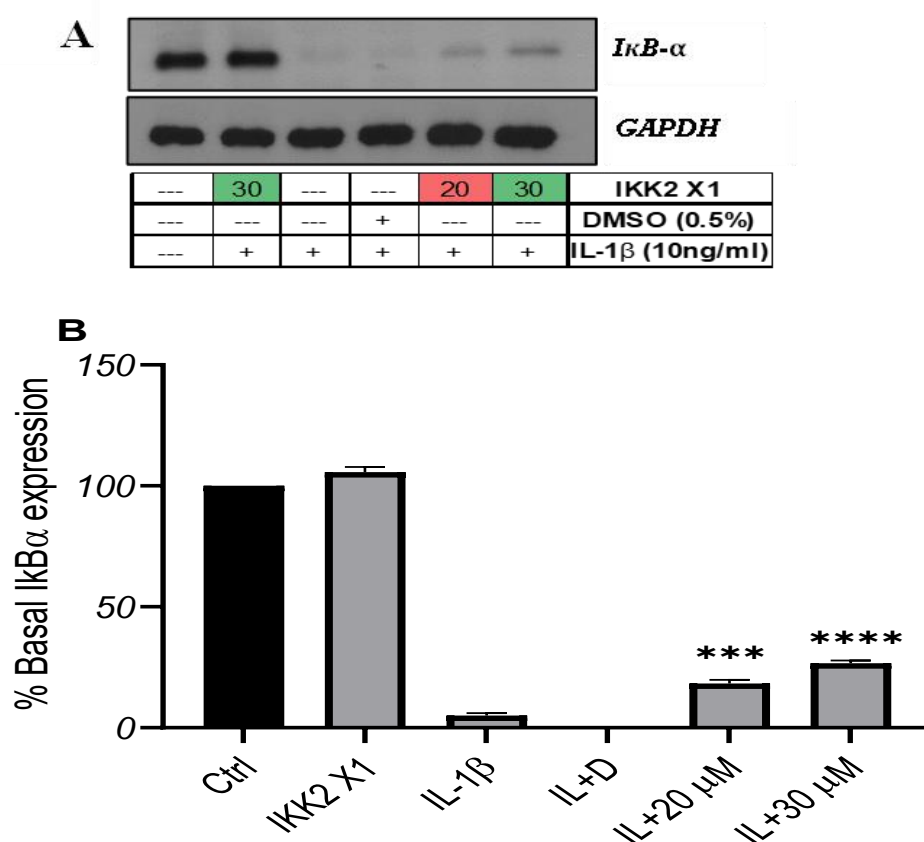


Figure 4. 7 Effect of IKK2 X1 on IL-1 β -induced cellular I κ B α degradation in U2OS cells.

U2OS cells were pre-treated with IKK β inhibitor, IKK2X1 for 1 h before stimulation with IL-1 β (IL, 10 ng/mL) for a further 30 min. Whole-cell extracts were assessed for A) I κ B α degradation (39 kDa), and GAPDH (37 kDa), which was used as a loading control. In panel (B), blots were semi-quantified by scanning densitometry and the results expressed as a percentage of basal expression relative to the control for I κ B α . Each value represents the mean \pm SEM of three independent experiments. Data was analysed using a one-way ANOVA test, **** $P < 0.0001$, *** $P < 0.001$ vs agonist-stimulated control.

4.5.2 Effect IKK α - Inhibition upon Canonical NF- κ B Signalling Induced by IL-1 β in U2OS Cells

Having examined the important role of IKK α in cellular responses through phosphorylation of its main marker, the p100 subunit (Claudio et al., 2002; McIntosh et al., 2023), the regulation of this pathway was assessed using the selective IKK α inhibitor SU1261 (Riley et al., 2024). IL-1 β -induced an approximate 21-fold increase in p100 phosphorylation in U2OS cells compared to non-stimulated cells (Fold stim for IL-1 β – 21.09 ± 2.03 , $P > 0.0001$), as shown in Figure 4.8. Pretreatment of the cells with SU1261 significantly reduced p100 phosphorylation in a low micromolar range (0.3-20 μ M), and at 10 and 20 μ M effectively abolished IL-1 β stimulation compared to agonist stimulated cells (Fold stim for IL-1 β + 10 μ M SU1261- 5.47 ± 0.37 , $P > 0.0001$).

These results revealed that the alternative NF- κ B pathway induced by IL-1 β clearly implicates IKK α in U2OS cells.

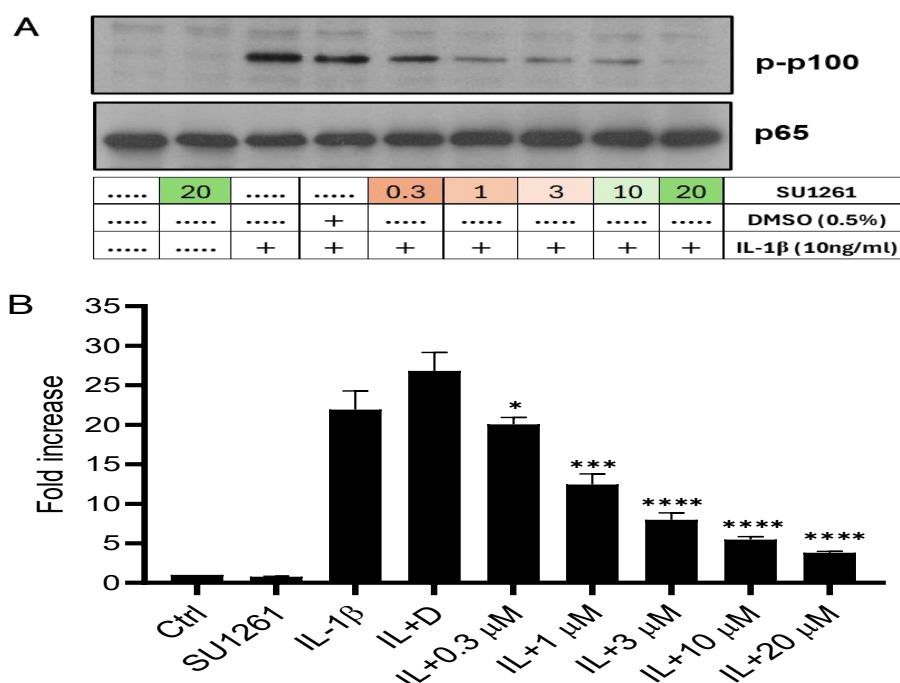


Figure 4. 8 Effect of SU1261 on IL-1 β -induced p100 phosphorylation in U2OS cells.

U2OS cells were pre-treated with IKK α inhibitor SU1261 for 1 h before stimulation with IL-1 β (IL, 10 ng/mL) for a further 30 min. Whole-cell extracts were assessed for A) p100 phosphorylation (100 kDa), and total p65 (65 kDa) as a loading control. In panel (B), blots were semi-quantified by scanning densitometry and the results expressed as a percent basal expression relative to control for pp100. Each value represents the mean \pm SEM of three independent experiments. Data was analysed using a one-way ANOVA test, **** $P < 0.0001$, *** $P < 0.001$, * $P < 0.05$ vs agonist-stimulated control.

4.5.3 Effect of siRNA-mediated silencing of cellular IKK α and IKK β expression on NF- κ B signalling pathways in U2OS Cells

Having used pharmacological inhibition of p100 phosphorylation-mediated IL-1 β stimulation, an alternative strategy utilised siRNA. Deletion of IKK β and IKK α has been used previously in various cancer cells, including U2OS cells (Mahato et al., 2011; McIntosh et al., 2023).

4.5.3.1 Knockdown efficiency of siRNA-mediated silencing of IKK α and IKK β in U2OS Cells

Initially, IKKs were knocked down using siRNA, and it was shown that transfecting U2OS cells with increasing concentrations of IKK α and IKK β siRNA for 72 h induced effective silencing. Figure 4.9 showed no effect of non-targeting siRNA on IKK α expression, whilst the IKK α siRNA effectively reduced the IKK α expression at 50 and 100 nM; the loss in expression was about 85% compared with non-targeting control (50 nM: % basal IKK α expression = 14.00 ± 2.97 ; 100 nM: % basal IKK α expression = 17.00 ± 2.58 , $P < 0.001$). Additionally, IKK α siRNA was not found to exert an off-target effect on IKK β .

The knockdown efficiency of siRNA IKK β in U2OS cells was examined using the same approach. Figure 4.10 illustrates that following transfection of siRNA IKK β (50 and 100 nM) into U2OS cells for 72 h, IKK β knockdown was successfully achieved by more than 90% compared with non-targeting control (50 nM: % basal IKK β expression = 8.33 ± 2.75 ; 100 nM: % basal IKK β expression = 8.00 ± 2.65 , $P < 0.0001$). Non-targeting (NT) siRNA (50 and 100 nM) was again without effect. Moreover, treatment of cells with siRNA IKK β showed no off-target effect on IKK α expression. Therefore, the optimal concentration for siRNA transfection used for further experiments was 50 nM.

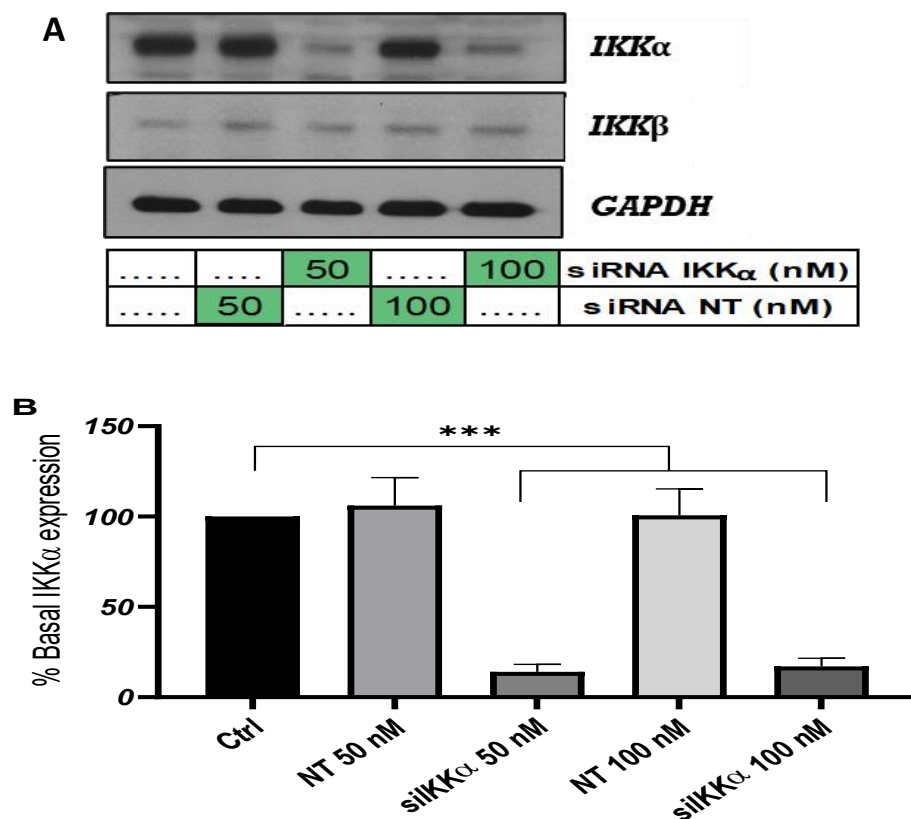


Figure 4. 9 The effect of IKK α siRNA on IKK α expression in U2OS cells.

U2OS cells were transfected with 50 nM and 100 nM siRNA IKK α or non-targeting construct (NT) for 72 h. In panel A, whole-cell extracts were assessed for IKK α (84 kDa), IKK β (86 kDa), and GAPDH (37 kDa), which was used as a loading control. In Panel B, blots were semi-quantified for the percentage of basal IKK α expression by scanning densitometry, and results expressed relative to the untreated control. Each value represents the mean percentage knockdown \pm S.E.M. of three independent experiments. Data was analysed using a one-way ANOVA test, ***P < 0.001 vs control.

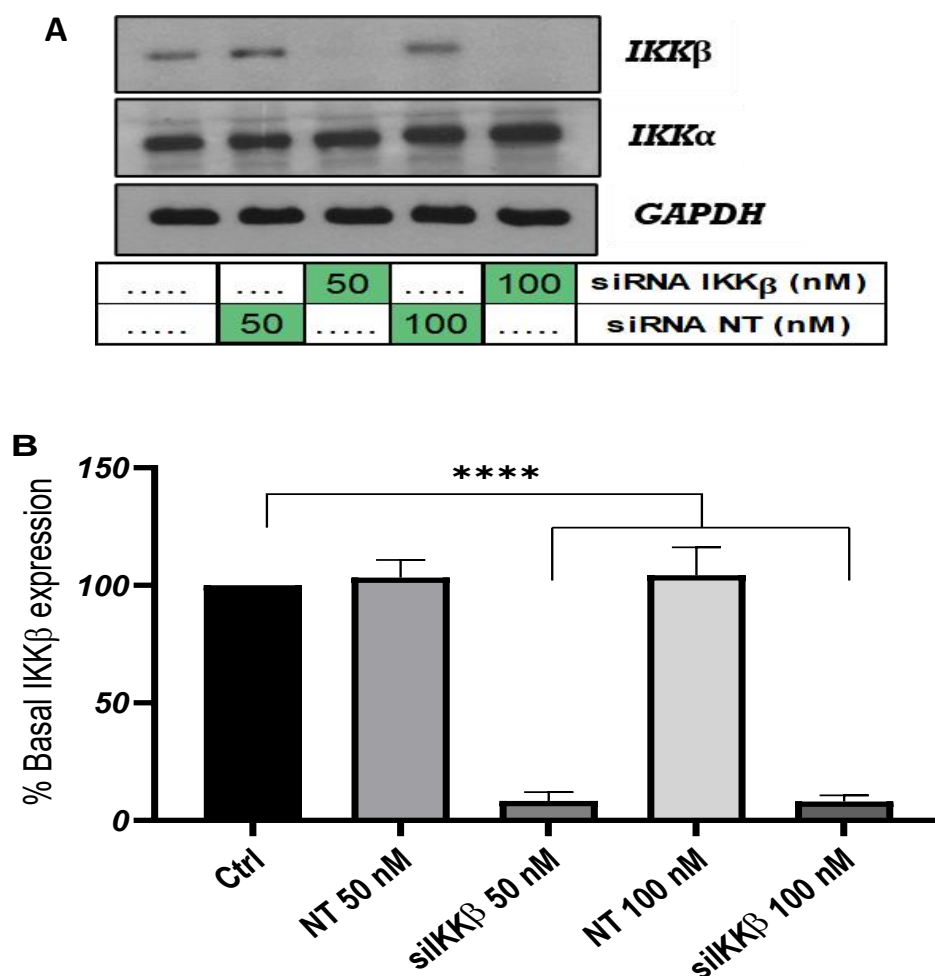


Figure 4. 10 The effect of IKK β siRNA on IKK β expression in U2OS cells.

U2OS cells were transfected with 50 nM and 100 nM siRNA IKK α or non-targeting (NT) for 72 h. In panel A, whole-cell extracts were assessed for IKK β (86 kDa), IKK α (84 kDa), and GAPDH (37 kDa), which was used as a loading control. In Panel B, blots were semi-quantified for the percentage of basal IKK β expression by scanning densitometry, and results expressed relative to the untreated control. Each value represents the mean percentage knockdown \pm S.E.M. of three independent experiments. Data was analysed using a one-way ANOVA test, ****P < 0.0001 vs control.

4.5.3.2 The effect of IKK α siRNA Silencing on IL-1 β -Induced Phosphorylation of p100 in U2OS Cells

Next, it was determined if siRNA IKK α could affect the phosphorylation of p100 and p100 processing in U2OS cells. Figure **4.11** demonstrated that IL-1 β strongly stimulated p100 phosphorylation at 30 minutes (Fold increase = 8.53 ± 0.97 , $P < 0.001$). Following transfection with IKK α siRNA at 50 nM, IL-1 β -induced phosphorylation of p100 was considerably reduced by around 75% in comparison to the non-target (NT) control (IKK α siRNA 50 nM; Fold increase = 2.50 ± 0.12). This was associated with a marked loss in IKK α expression, whilst IKK β expression was unaffected. Additionally, it was noted that there was no difference in the levels of p100 and p52 following siRNA knockdown in control and IL-1 β -stimulated cells.

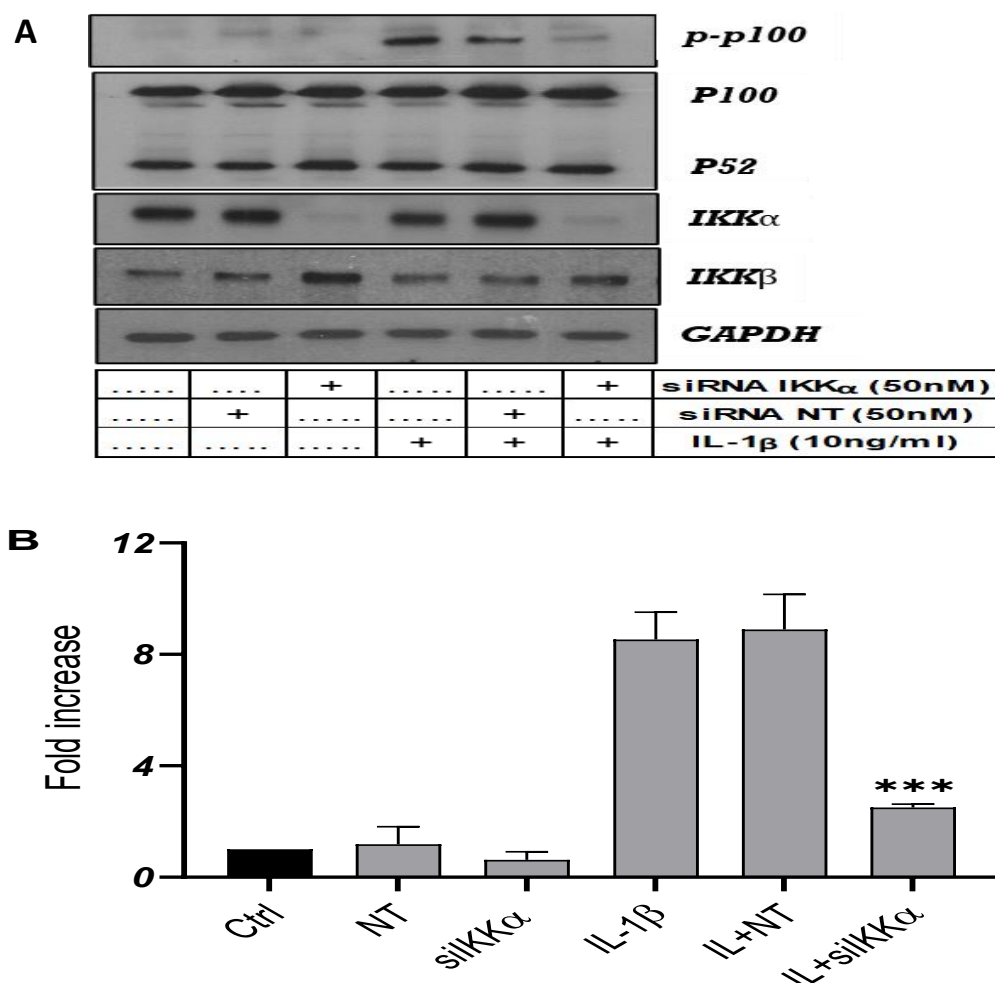


Figure 4. 11 The effect of IKK α siRNA upon IL-1 β -mediated phosphorylation of p100 in U2OS cells.

U2OS cells were transfected with non-targeting (NT) siRNA 50 nM, IKK α siRNA 50 nM for 72 h before stimulation with IL-1 β (IL, 10ng/mL) for 30 min. In panel A, whole-cell extracts were assessed for p-p100 (100 kDa), p52 (52 kDa), IKK α (84 kDa), IKK β (86 kDa), and GAPDH (37 kDa), which was used as a loading control. In panel B, blots were semi-quantified by scanning densitometry and results expressed as fold increases relative to the control for p100 phosphorylation. Each value represents the mean \pm SEM of three independent experiments. Data was analysed using a one-way ANOVA test, ***P < 0.001 vs agonist and nontargeting control.

4.5.3.3 The effect of IKK β siRNA Silencing on IL-1 β -Induced Cellular I κ B α loss in U2OS Cells

The effect of IKK β siRNA on IL-1 β -induced cellular I κ B α loss in U2OS cells was also determined. Figure 4.12 showed that IL-1 β significantly induced cellular I κ B α loss at 30 min compared to control by around 80 % (% basal I κ B α expression 20.61 ± 3.75). Surprisingly, following transfection with IKK β siRNA at 50 nM, there was no I κ B α reversal with a non-significant increase in cellular degradation compared to the non-target (NT) control. This suggests that IKK α may substitute IKK β signalling through contribution to I κ B α phosphorylation and cellular degradation, as reported previously (Adli et al., 2010; Solt et al., 2007).

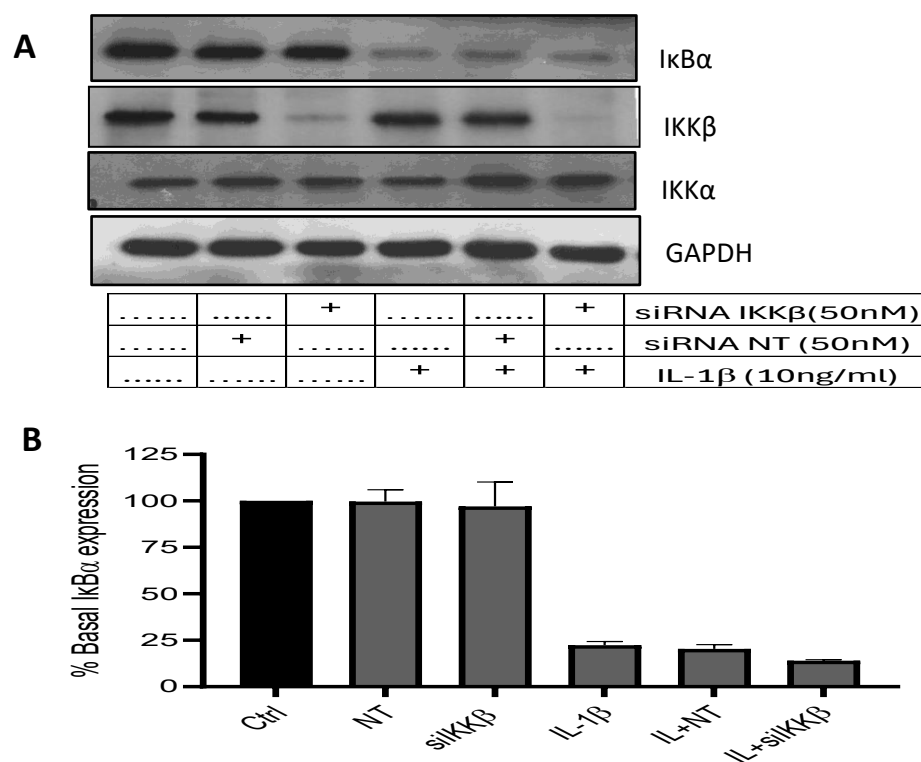


Figure 4. 12 The effect of IKK β siRNA upon IL-1 β -mediated cellular degradation of I κ B α in U2OS cells.

Cells were transfected with non-targeting (NT) siRNA 50 nM, IKK β siRNA for 72 h before stimulation with IL-1 β (IL, 10 ng/mL) for 30 min. In panel A, whole cell extracts were assessed for I κ B α (39 kDa), IKK β (86 kDa), IKK α (84 kDa), and GAPDH (37 kDa), which was used as a loading control. In panel B, blots were semi-quantified by scanning densitometry and results expressed as a fold increase relative to control for cellular I κ B α loss. Each value represents the mean \pm SEM of three independent experiments. Data was analysed using a one-way ANOVA test.

4.5.3.4 The effect of IKK α and IKK β siRNA Double Knockdown on IL-1 β -Induced p100 Phosphorylation in U2OS Cells

Whilst IKK α but not IKK β knockdown reduced IL-1 β -induced phosphorylation of p100, the effect of both together was examined to determine if there was any co-operation between IKK α and IKK β in regulating p100 phosphorylation. Following stimulation, Figure 4.13 showed that IL-1 β alone induced more than a 10-fold increase in p100 phosphorylation at 30 minutes compared to non-stimulated cells (Fold increase = 10.76 ± 0.62 , $P < 0.0001$). Following transfection with siRNA IKK α , there was a 50-60% inhibition of the IL-1 β response (Fold increase = 6.22 ± 0.36 , $P < 0.0001$).

By contrast, there was no effect following siRNA mediated IKK β rundown, which was similar to the levels observed following NT treatment (Fold increase = 10.82 ± 0.58). Following double knockdown of IKK α and IKK β siRNA at 50 nM, which reduced both proteins by more than 75% compared with the non-target (NT) control, IL-1 β -induced phosphorylation of p100 was significantly inhibited. However, the degree of inhibition was similar to that observed for single knockdown siRNA IKK α cells (IKK α and β siRNA double knockdown; Fold increase = 6.16 ± 0.72 , $P < 0.0001$), with no additional effect of IKK β siRNA. Additionally, it was noted that there was no difference in the levels of p100 and p52 in control and IL-1 β -stimulated cells for any of the knockdown strategies. These results confirm that IL-1 β -induced phosphorylation of p100 is dependent on IKK α but, not IKK β . Again, the single or double siRNA knockdown did not significantly reverse I κ B α loss after 95 % of cellular degradation induced by IL-1 β compared to NT control, as shown in Figure 4.13. However, the knockdown had no effect on cell survival as assessed by GAPDH expression. Furthermore, as shown in Figure 4.14, preliminary results demonstrated that combined SU1261, IKK α inhibitor, and IKK β knockdown slightly reversed I κ B α loss compared to non-targeted treated cells. This result was consistent with the effect of both IKK α and IKK β siRNA alone and suggests that IKK α is not substituting for IKK β in the regulation of canonical signalling.

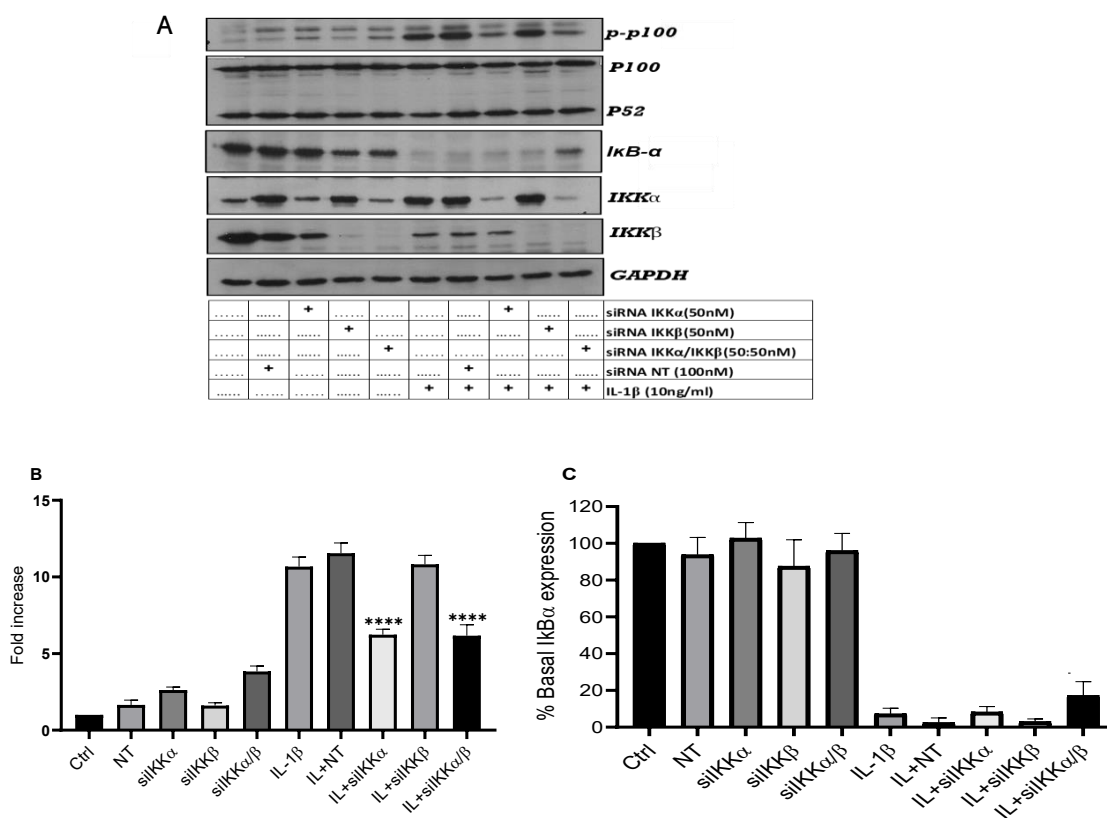


Figure 4. 13 The effect of IKK α and IKK β siRNA double knockdown upon IL-1 β -mediated p100 phosphorylation and cellular I κ B α degradation in U2OS cells.

Cells were transfected with non-targeting (NT) siRNA 100 nM, IKK α and IKK β siRNA (50 nM) for 72 h before stimulation with IL-1 β (IL, 10 ng/mL) for 30 min. In panel A, whole-cell extracts were assessed for p-p100 (100 kDa), p52 (52 kDa), IKK α (84 kDa), IKK β (86 kDa), I κ B α (39 kDa), and GAPDH (37 kDa), which was used as a loading control. In panel B and C, blots were semi-quantified by scanning densitometry and the results expressed as fold increase relative to control for p100 phosphorylation and cellular I κ B α loss. Each value represents the mean \pm SEM of three independent experiments. Data was analysed using a one-way ANOVA test, ****P <0.0001 vs agonist and nontargeting control.

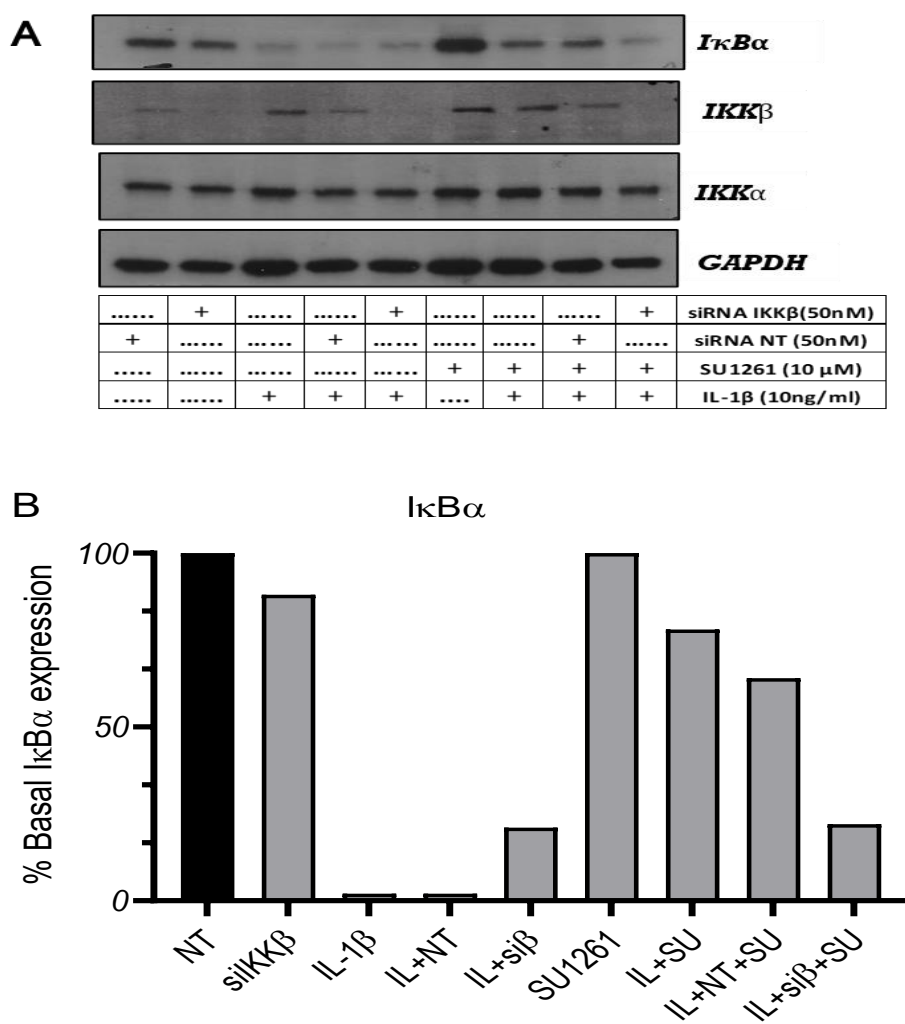


Figure 4. 14 The effect of combined IKKβ siRNA and IKKα inhibition upon IL-1β-mediated cellular IkBα degradation in U2OS cells.

Cells were transfected with non-targeting (NT) siRNA 50 nM, IKKβ siRNA (50 nM) for 72 h, then the cells were pre-treated with IKKα inhibitor SU1261 (10 μM) for 1 h before stimulation with IL-1β (IL, 10 ng/mL) for 30 min. In panel A, whole-cell extracts were assessed for IKKα (84 kDa), IKKβ (86 kDa), IkBα (39 kDa), and GAPDH (37 kDa), which was used as a loading control. In panel B, blots were semi-quantified by scanning densitometry and the results expressed as fold increase relative to control for cellular IkBα loss. Each value represents one experiment.

4.6 Effect of TAK1 Inhibition on IL-1 β -Induced Cellular Signalling in U2OS Cells

4.6.1 Effect of 5Z-7oxozeaenol (5Z-7oxo) on IL-1 β -induced JNK phosphorylation in U2OS cells

A number of studies have demonstrated a role for TAK-1 on cytokine-induced MAP kinase signalling, in particular, JNK and p38 MAPK (Wang et al., 2022; Wei et al., 2016). Therefore, the effect of TAK1 inhibitor, 5Z-7oxozeaenol (abbreviated as 5Z-7oxo) was examined in this study. As shown in Figure 4.15, IL-1 β -stimulated phosphorylation of JNK in U2OS cells more than 10-fold (Fold stim for IL-1 β = 11.35 ± 3.20 , $P > 0.001$). Pre-treatment with 5Z-7oxo significantly decreased JNK phosphorylation in the low micromolar range (Fold stim for IL-1 β + 10 μ M 5Z-7-oxo = 0.81 ± 0.14 , $P > 0.0001$, approximate IC_{50} = 0.86 μ M). These findings confirmed the role of TAK1 in the regulation of MAPK signalling exemplified by inhibition of JNK activation and phosphorylation.

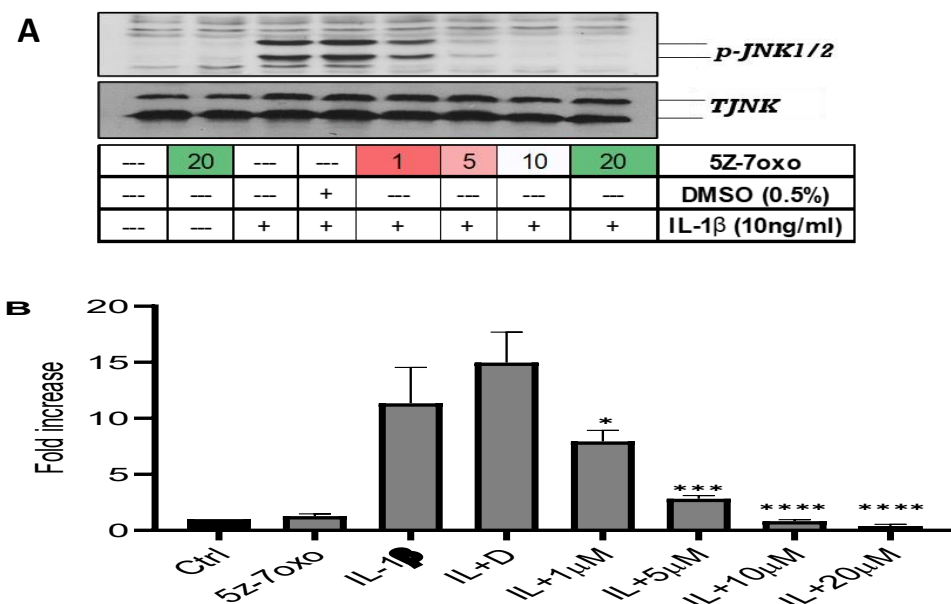


Figure 4. 15 Effect of TAK1 inhibitor 5Z-7oxo on IL-1 β -induced phosphorylation of JNK in U2OS cells.

Cells were pre-treated with increasing concentrations of 5Z-7oxo for 1 h before stimulation with IL-1 β (IL, 10 ng/mL) for a further 30 min. Whole-cell extracts were assessed for A) JNK phosphorylation (46,54 kDa), and total JNK which was used as a loading control. In panel B, blots were semi-quantified by scanning densitometry, and the results expressed as a fold increase relative to the control for pJNK phosphorylation. Each value represents the mean \pm SEM of three independent experiments. Data was analysed using a one-way ANOVA test, **** $P < 0.0001$, *** $P < 0.001$, * $P < 0.05$, vs IL-1 β and DMSO (D) as an agonist-stimulated control.

4.6.2 Effect of 5Z-7oxo on IL-1 β - Induced Cellular I κ B α Degradation and p65 Phosphorylation in U2OS Cells

Next, the effect of the TAK1 inhibitor, 5Z-7oxo on canonical NF- κ B markers, cellular I κ B α loss, and p65 phosphorylation were examined in U2OS cells. The results in Figure 4.16, panel (B) showed significant I κ B α degradation induced by IL-1 β (% basal I κ B α expression- 9.00 ± 0.58 %, $P < 0.0001$). Pre-treatment of the cells with 5Z-7oxo significantly reversed I κ B α loss in a low micromolar range (1-20 μ M), in comparison with non-treated cells. I κ B α expression returned to near basal values at 10 and 20 μ M (% basal I κ B α expression- 86.67 ± 3.71 %, 89.67 ± 3.38 % respectively, $P < 0.0001$, $IC_{50} = 2$ μ M). Furthermore, panel (C) showed that IL-1 β also induced an 8-fold increase in p65 phosphorylation compared with non-stimulated cells (Fold stim for IL-1 β – 8.107 ± 0.319 , $P > 0.0001$). This response was significantly inhibited by 5Z-7oxo over a low micromolar range (Fold stim for IL-1 β +10 μ M- 1.60 ± 0.95 , IL-1 β +20 μ M- 0.54 ± 0.06 , $P > 0.0001$). Collectively, these findings indicate the role of TAK1 in the canonical NF- κ B pathway in U2OS cells.

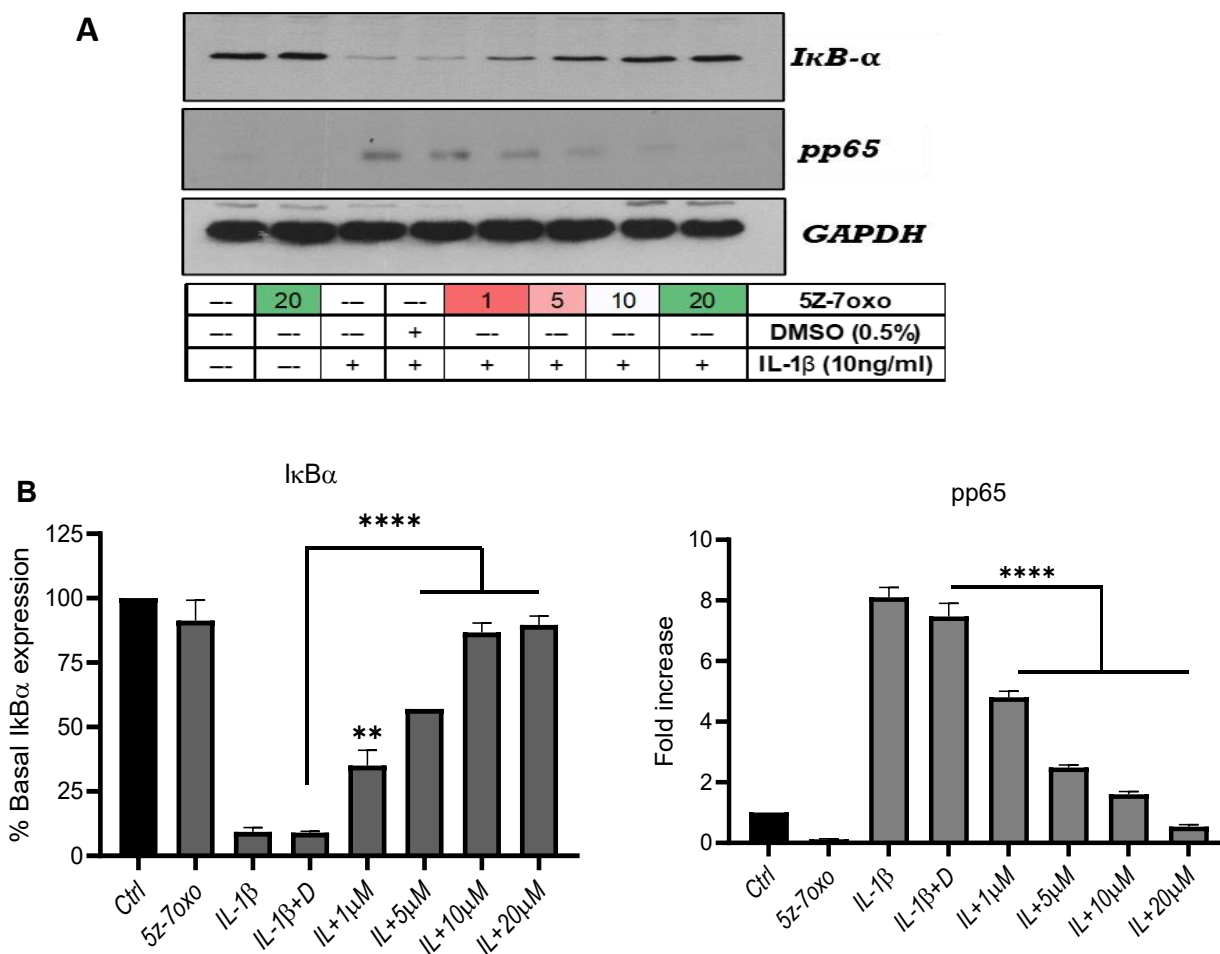


Figure 4. 16 Effect of the TAK1 inhibitor 5Z-7oxo on IL- 1 β -mediated cellular IκBα degradation in U2OS cells.

Cells were pre-treated with 5Z-7oxo for 1 h before stimulation with IL-1 β (IL,10 ng/mL) for a further 30 min. Whole-cell extracts were assessed for A) IκBα (39 kDa), p65 phosphorylation (65 kDa), and GAPDH (37 kDa), which was used as a loading control. Blots were semi-quantified by scanning densitometry and the results expressed as fold increase relative to control for B) IκBα degradation, C) p65 phosphorylation. Each value represents the mean \pm SEM of three independent experiments. Data was analysed using a one-way ANOVA test, ****P <0.0001, **P <0.01 vs IL-1 β and DMSO as an agonist-stimulated control.

4.6.3 Effect of 5Z-7oxo on IL-1 β -Induced p100 Phosphorylation in U2OS Cells

The next set of experiments assessed the effect of 5Z-7oxo on p100 phosphorylation, the non-canonical NF- κ B marker. IL-1 β -induced an approximate 12-fold increase in p100 phosphorylation in U2OS cells (Fold stim for IL-1 β – 12.18 ± 0.70 , $P > 0.001$), as shown in Figure 4.17. Pretreatment of the cells with 5Z-7oxo significantly reduced p100 phosphorylation in a low micromolar range (1-20 μ M), and at 10 and 20 μ M effectively abolished IL-1 β stimulation (Fold stim for IL-1 β + 10 μ M 5Z-7-oxo- 1.70 ± 0.56 , $P > 0.001$). Also, there was no effect on p100 processing and p52 formation in pre-treated cells compared to the control.

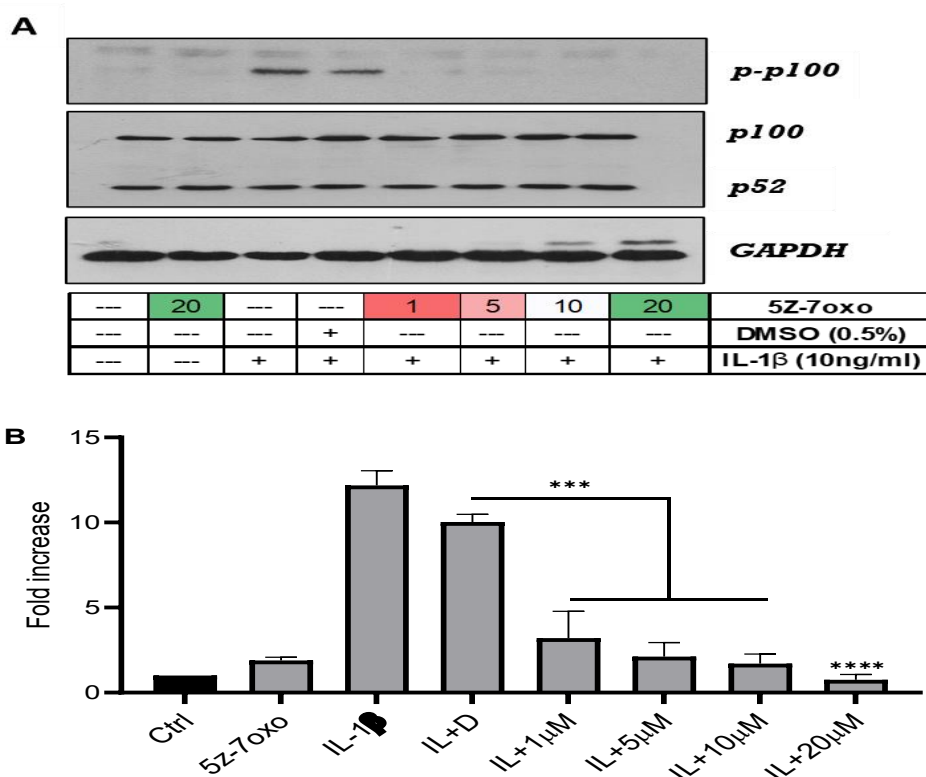


Figure 4. 17 Effect of TAK1 inhibitor 5Z-7-oxo on IL-1 β induced phosphorylation of p100 in U2OS cells.

Cells were pre-treated with 5Z-7-oxo for 1 h before stimulation with IL-1 β (IL,10 ng/mL) for a further 30 min. Whole-cell extracts were assessed for A) p100 phosphorylation (100 kDa), p52 (52 kDa), and GAPDH (37 kDa), which was used as a loading control. Blots were semi-quantified by scanning densitometry, and the results expressed as a fold increase relative to the control for B) pp100. Each value represents the mean \pm SEM of three independent experiments. Data was analysed using a one-way ANOVA test, **** $P < 0.0001$, *** $P < 0.001$ vs IL-1 β and DMSO as an agonist-stimulated control.

4.6.4 Effect of siRNA-mediated silencing of cellular TAK1 on signalling pathways stimulated by IL-1 β in U2OS Cells

4.6.4.1 Knockdown Efficiency of siRNA-mediated Silencing of TAK1 in U2OS Cells

Initially, two concentrations of TAK1 siRNA were transfected into U2OS cells for 72 h, which was identified to be sufficient time for silencing in experiments to optimise the knockdown of TAK1 using siRNA. To rule out any effects that might arise as a result of the transfection procedure, the same concentration of non-targeting (NT) siRNA was also utilised. Figure 4.18 showed that both concentrations of siRNA (50 and 100 nM) successfully reduced endogenous TAK1 expression by almost 90% with no effect on cell survival as assessed by GAPDH expression, whereas the NT construct had no effect on the target protein (50 nM: % basal TAK1 expression = 18 ± 2.34 ; 100 nM: % basal TAK1 expression = 7.5 ± 1.75 , $P < 0.0001$).

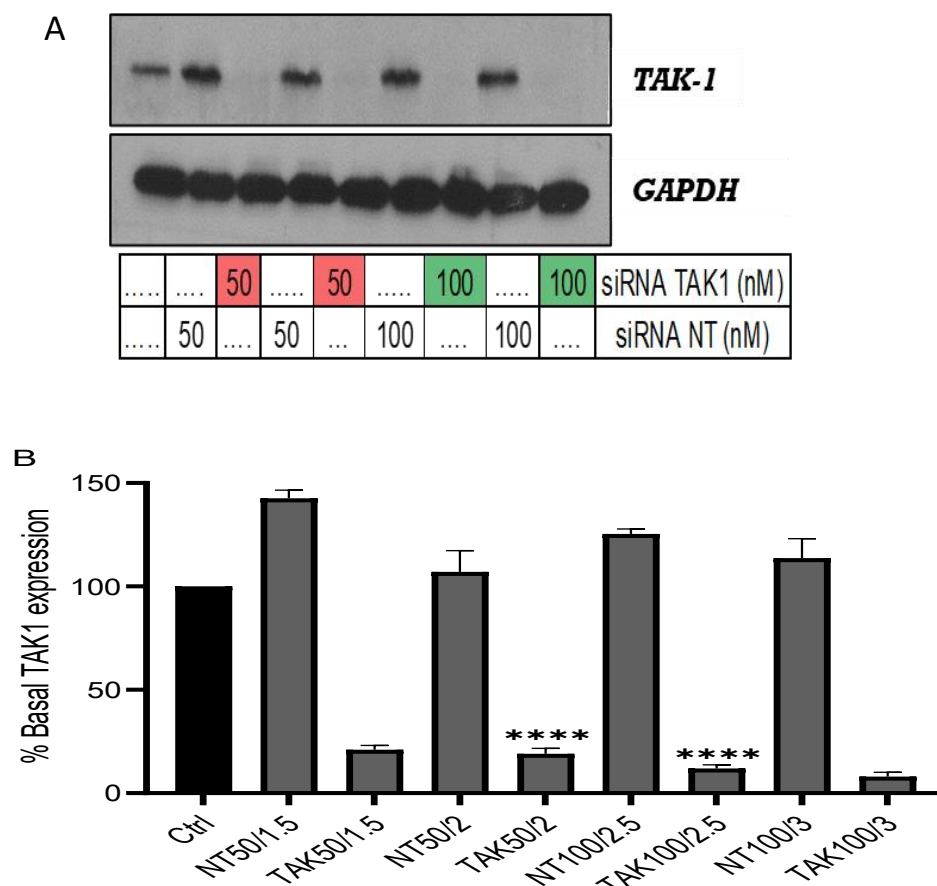


Figure 4. 18 The effect of siRNA TAK1 on TAK1 expression in U2OS cells.

Cells were transfected with siRNA TAK1 or non-targeting (NT) up to a concentration of 100 nM for 72 h. Whole-cell extracts were assessed for A) TAK1 (80 kDa), and GAPDH (37 kDa), which was used as a loading control, as outlined in Section 2.3.2. Blots were semi-quantified for a percentage of basal TAK1 expression by scanning densitometry and results expressed as a relative to untreated control for B) TAK1 expression. Each value represents the percentage knockdown of three independent experiments, ****P < 0.0001 vs non-targeting control.

4.6.4.2 The effect of TAK1 siRNA silencing on IL-1 β -Induced JNK phosphorylation in U2OS Cells

The impact of siRNA TAK1 on IL1 β -induced JNK phosphorylation in U2OS cells was investigated after the knockdown conditions were optimised. Figure 4.19 showed IL1 β -induced an approximately 17-fold increase in JNK phosphorylation at 30 min (Fold stim. = 17.74 ± 2.07 , $P < 0.0001$). This response was significantly reduced by about 80% following siRNA TAK1 rundown compared to control, with no general effect on the cells when assessed with the GAPDH expression (50 nM TAK1 siRNA Fold increase = 4.08 ± 0.12 , $P < 0.0001$). This result confirmed the role of TAK1 in the regulation of the MAP kinase signalling pathway, exemplified by JNK.

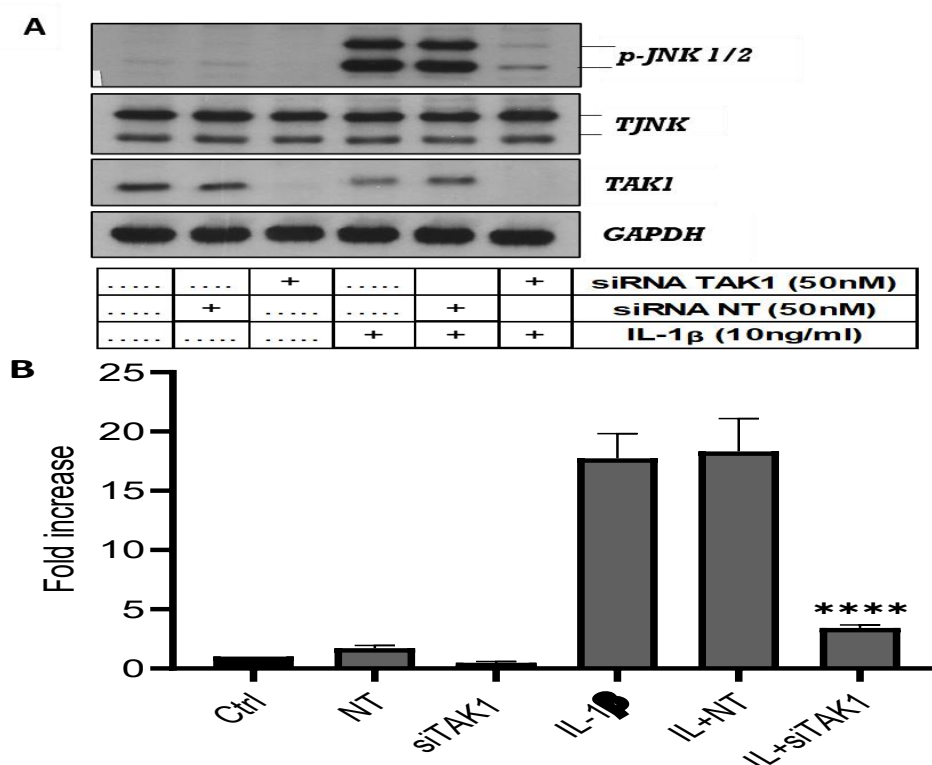


Figure 4. 19 The effect of TAK1 siRNA upon IL-1 β -mediated phosphorylation of JNK in U2OS cells.

Cells were transfected with non-targeting (NT) siRNA 50 nM, TAK1 siRNA for 72 h before stimulation with IL-1 β (IL,10 ng/mL) for 30 min. Whole cell extracts were assessed for A) p-JNK (54,46 kDa), total JNK (54,46 kDa), TAK1 (80 kDa), and GAPDH (37 kDa), which was used as a loading control. Blots were semi-quantified by scanning densitometry, and the results expressed as fold increase relative to the control for B) JNK phosphorylation. Each value represents the mean \pm SEM of three independent experiments. Data was analysed using a one-way ANOVA test, **** $P < 0.0001$ vs non-targeting control.

4.6.4.3 The effect of TAK1 siRNA silencing on IL-1 β -Induced p38 phosphorylation in U2OS Cells

As we identified previously, the effect of siRNA TAK1 on IL1 β -induced JNK phosphorylation in U2OS cells, the effect of TAK1 knockdown on p38 phosphorylation was also investigated. Figure 4.20 also shows that IL1 β -induced more than 13-fold increase in p38 phosphorylation at 30 min (Fold stim = 13.66 ± 1.83 , $P < 0.001$). Following transfection of the cells with siRNA TAK1 which reduced expression by over 90%, IL-1 β stimulation was essentially abolished (50 nM TAK1 siRNA Fold increase = 0.35 ± 0.24 , $P < 0.001$). This result confirmed the role of TAK1 in the regulation of the MAP kinase signalling pathway through its major components, JNK and p38.

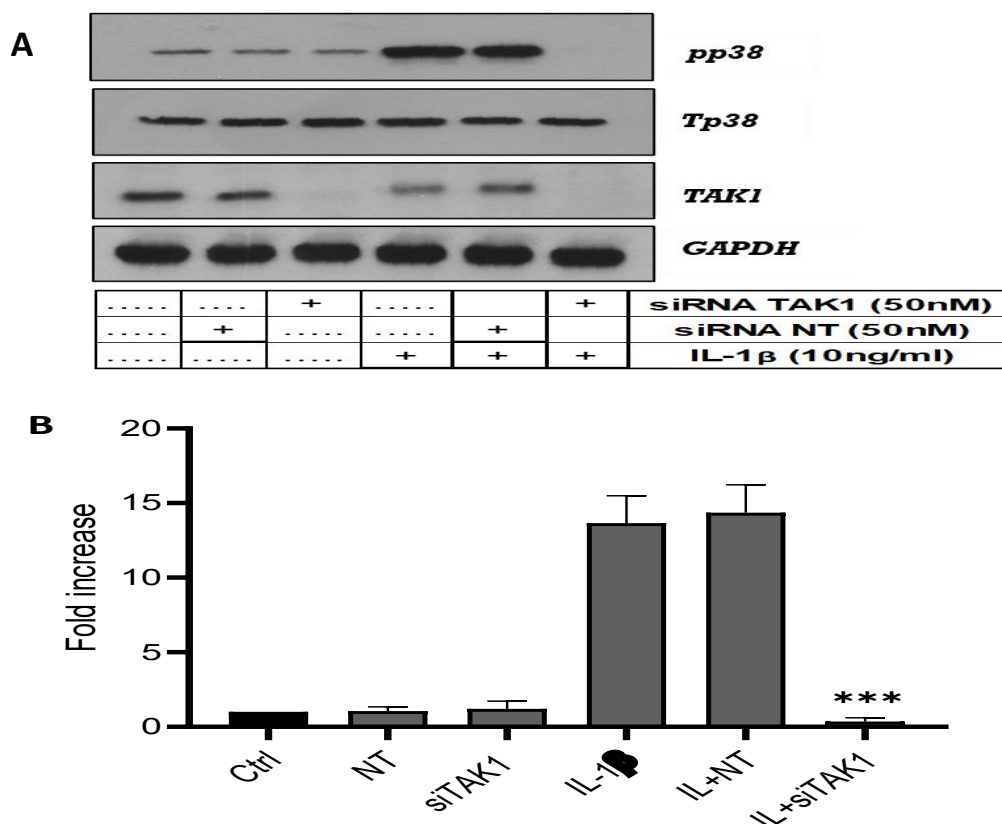


Figure 4. 20 The effect of TAK1 siRNA upon IL-1 β -mediated phosphorylation of p38 in U2OS cells.

Cells were transfected with non-targeting (NT) siRNA 50 nM, TAK1 siRNA for 72 h before stimulation with IL-1 β (IL, 10 ng/mL) for 30 min. Whole cell extracts were assessed for A) pp38 (38 kDa), total p38 (38 kDa), TAK1 (80 kDa), and GAPDH (37 kDa), which was used as a loading control. Blots were semi-quantified by scanning densitometry, and the results expressed as fold increases relative to the control for B) p38 phosphorylation. Each value represents the mean \pm SEM of three independent experiments. Data was analysed using a one-way ANOVA test, *** $P < 0.001$ vs non-targeting control.

4.6.4.4 The effect of TAK1 siRNA Silencing on IL-1 β -Induced cellular I κ B- α Degradation and p65 Phosphorylation in U2OS Cells

The effect of siRNA TAK1 on cellular I κ B- α loss induced by IL-1 β was assessed. Figure **4.21** shows IL1 β -induced complete cellular I κ B- α loss (% basal I κ B α expression- 2.25 ± 1.25 %, $P < 0.0001$) and more than 6-fold increase in p65 phosphorylation at 30 min compared to basal (Fold stim = 6.46 ± 0.89 , $P < 0.001$). Following siRNA TAK1 transfection (50 nM), which significantly deleted TAK-1 compared to GAPDH, cellular I κ B- α degradation was not significantly changed compared to IL-1 β -stimulated cells, although there was a change in the migration of residual I κ B α . Similarly, IL-1 β -stimulated p65 phosphorylation was not significantly affected (50 nM TAK1 siRNA; fold increase = 3.78 ± 0.34). In contrast to effects on MAP kinase signalling, these results do not suggest a role for TAK1 in the regulation of I κ B- α loss and phosphorylation of p65 in U2OS cells, which are the main markers for the canonical NF- κ B signalling pathway.

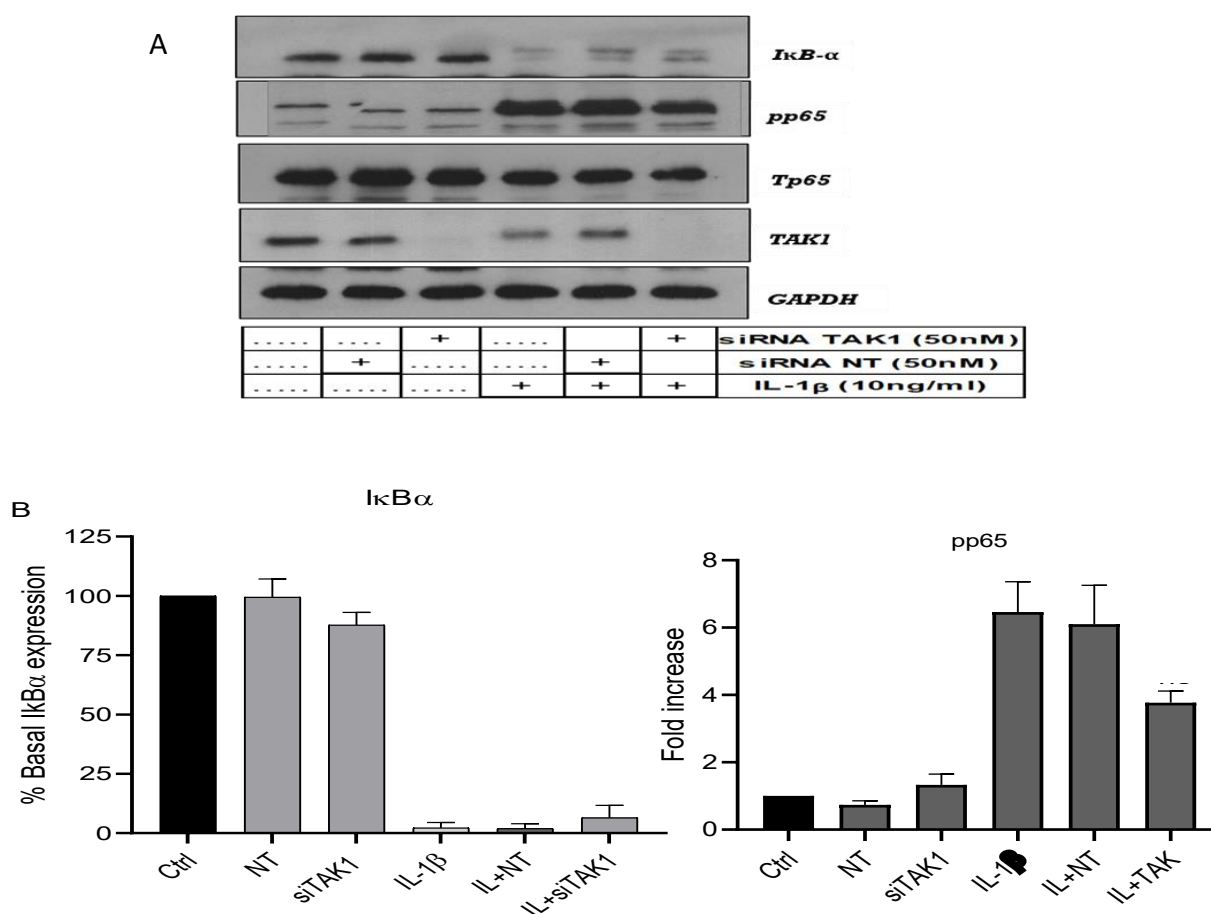


Figure 4. 21 The effect of TAK1 siRNA upon IL-1 β -mediated cellular I κ B- α loss and p65 phosphorylation in U2OS cells.

Cells were transfected with non-targeting (NT) siRNA 50 nM, TAK1 siRNA for 72 h before stimulation with IL-1 β (IL, 10 ng/mL) for 30 min. Whole cell extracts were assessed for A) I κ B- α loss (39 kDa), TAK1 (80 kDa), pp65 (65 kDa), total p65 (65 kDa), and GAPDH (37 kDa), which was used as a loading control. Blots were semi-quantified by scanning densitometry and the results expressed as fold increase relative to the control for B) I κ B- α loss and p65 phosphorylation. Each value represents the mean \pm SEM of three independent experiments, ns non-significant vs IL-1 β and NT as an agonist-stimulated control. Data was analysed using a one-way ANOVA test.

4.6.4.5 The effect of TAK1 siRNA Silencing on IL-1 β -Induced p100 phosphorylation in U2OS cells

As in previous experiments, the effect of siRNA TAK1 on IL1 β -induced p100 phosphorylation in U2OS cells was investigated. Figure 4.22 showed IL-1 β -induced a more than 13-fold increase in p100 phosphorylation at 30 min (Fold stim=13.38 \pm 2.63, P <0.0001). This response was significantly inhibited following siRNA TAK-1, reducing the signal by over 50% (50 nM TAK1 siRNA Fold increase = 5.91 \pm 0.84, P <0.01), with no effect on cell survival when assessed by GAPDH expression. In contrast, the p100 processing to p52 in either control or IL-1 β stimulated cells was not affected by TAK1 siRNA. These results suggest a role of TAK1 in the regulation of p100 mediated by IKK α .

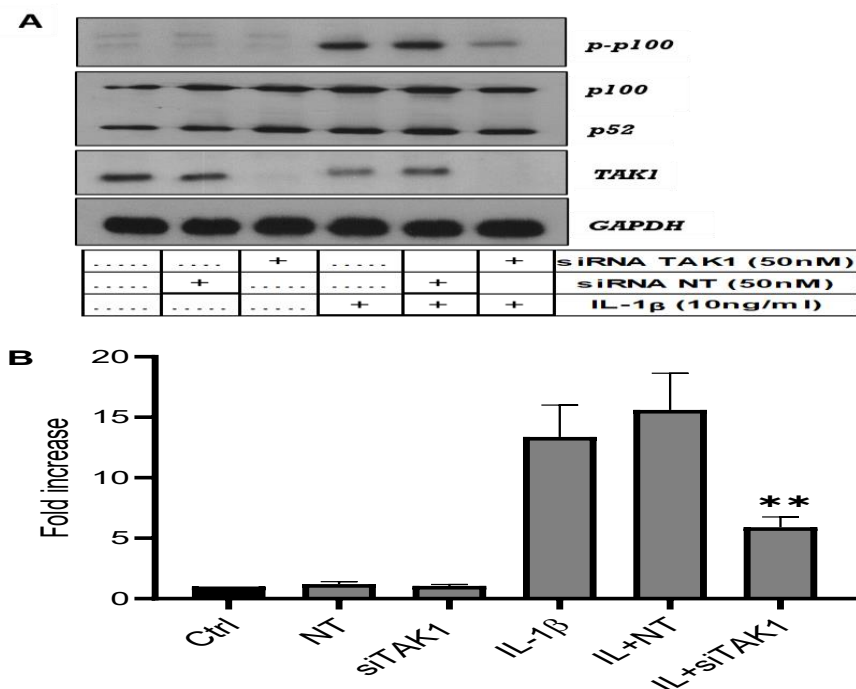


Figure 4. 22 The effect of TAK1 siRNA upon IL1 β -mediated phosphorylation of p100 in U2OS cells.

Cells were transfected with non-targeting (NT) siRNA 50 nM, and TAK1 siRNA (50 nM) for 72 h before stimulation with IL1 β (IL, 10 ng/mL) for 30 min. Whole cell extracts were assessed for A) p-p100 (100 kDa), TAK1 (80 kDa), and GAPDH (37 kDa), which was used as a loading control. Blots were semi-quantified by scanning densitometry, and the results expressed as fold increases relative to the control for B) p100 phosphorylation. Each value represents the mean \pm SEM of three independent experiments. Data was analysed using a one-way ANOVA test, ** P <0.01 vs. non-targeting control.

4.6.4.6 The effect of TAK1 siRNA silencing on IL-1 β -induced phosphorylation of IKK α / β in U2OS cells

The results obtained from previous experiments showed the role of TAK1 on IKK α signalling through inhibition of IL1 β -induced p100 phosphorylation in U2OS cells, with no significant effect on IKK β signalling. However, in order to confirm this effect, the effect of siRNA TAK1 on phosphorylation of the IKK α / β complex stimulated by IL1 β was examined. Figure 4.23 shows that IL1 β induced a 15-fold increase in phosphorylation of the complex at 30 min (Fold stims=15.32 \pm 1.24, $P < 0.0001$). This response was significantly inhibited, both IKK α and IKK β phosphorylation was inhibited following siRNA TAK1 (50 nM TAK1 siRNA Fold increase = 5.10 \pm 1.73, $P < 0.001$). This result was consistent with the previous experiments identifying a role for TAK1 in the regulation of the IKK alpha pathway induced by cytokines.

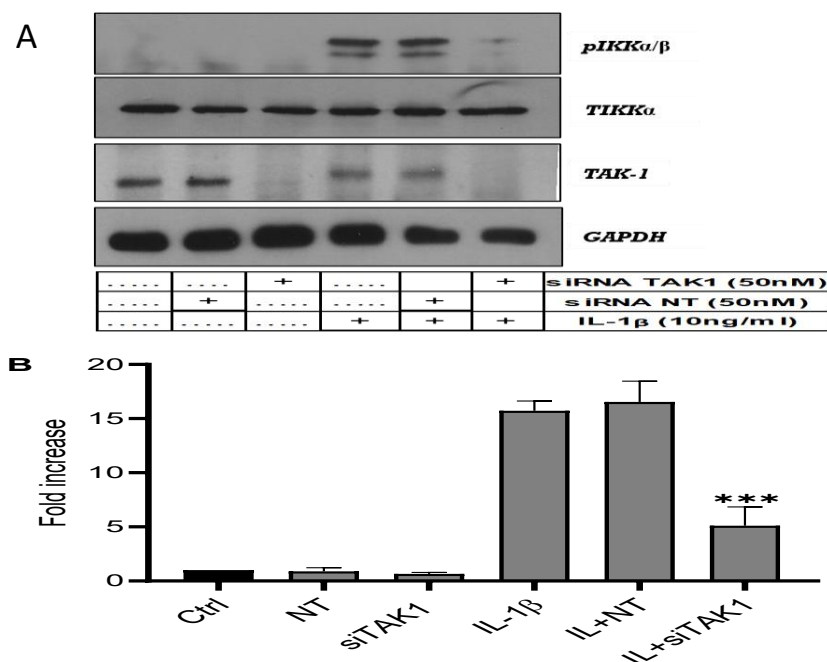


Figure 4. 23 The effect of TAK1 siRNA upon IL-1 β -mediated phosphorylation of IKK α / β in U2OS cells.

Cells were transfected with non-targeting (NT) siRNA 50 nM, and TAK1 siRNA (50 nM) for 72 h before stimulation with IL1 β (IL,10 ng/mL) for 30 min. Whole cell extracts were assessed for A) pIKK α / β phosphorylation (84,86 kDa), TAK1 (80 kDa), total IKK α (84 kDa), and GAPDH (37 kDa), which were used as a loading control. Blots were semi-quantified by scanning densitometry and the results expressed as fold increase relative to control for B) pIKK α / β phosphorylation. Each value represents the mean \pm SEM of three independent experiments. Data was analysed using a one-way ANOVA test, *** $P < 0.001$ vs IL-1 β plus NT as an agonist-stimulated control.

4.7 Effect of Mitogen-Activated Protein Kinase Kinase Kinase 3 (MEKK3) inhibition on IL-1 β -induced cellular signalling in U2OS cells

Studies have shown an interaction between TAK1 and MEKK3 signalling cascades in the activation of NF- κ B downstream signalling in response to cytokines and other factors such as *H-pylori* (Sokolova et al., 2014; Zhang et al., 2019). Therefore, the effect of MEKK3 deletion or inhibition in U2OS cells was examined using both molecular and pharmacological approaches.

4.7.1 Effect of siRNA-mediated silencing of cellular MEKK3 expression on IL-1 β -stimulated signalling Pathways in U2OS cells

4.7.1.1 Knockdown efficiency of siRNA-mediated silencing of MEKK3 in U2OS cells

Using the same approach as for TAK1 siRNA, two concentrations of MEKK3 siRNA were transfected into U2OS cells for 96 h, which was discovered to be the appropriate time for silencing. To exclude any effects that might arise as a result of the transfection procedure, the same concentration of non-targeting (NT) siRNA were also applied. Figure 4.24 showed that concentrations of siRNA (50 and 100 nM) successfully reduced endogenous MEKK3 expression by more than 90% in both stimulated and non-stimulated cells compared to non-transfected cells, whereas the NT construct had no effect (50 nM: % basal MEKK3 expression = 6 ± 2.78 ; 100 nM: % basal MEKK3 expression = 4 ± 2.08 , $P < 0.0001$). Furthermore, knockdown showed no effect on cell survival as assessed by GAPDH expression.

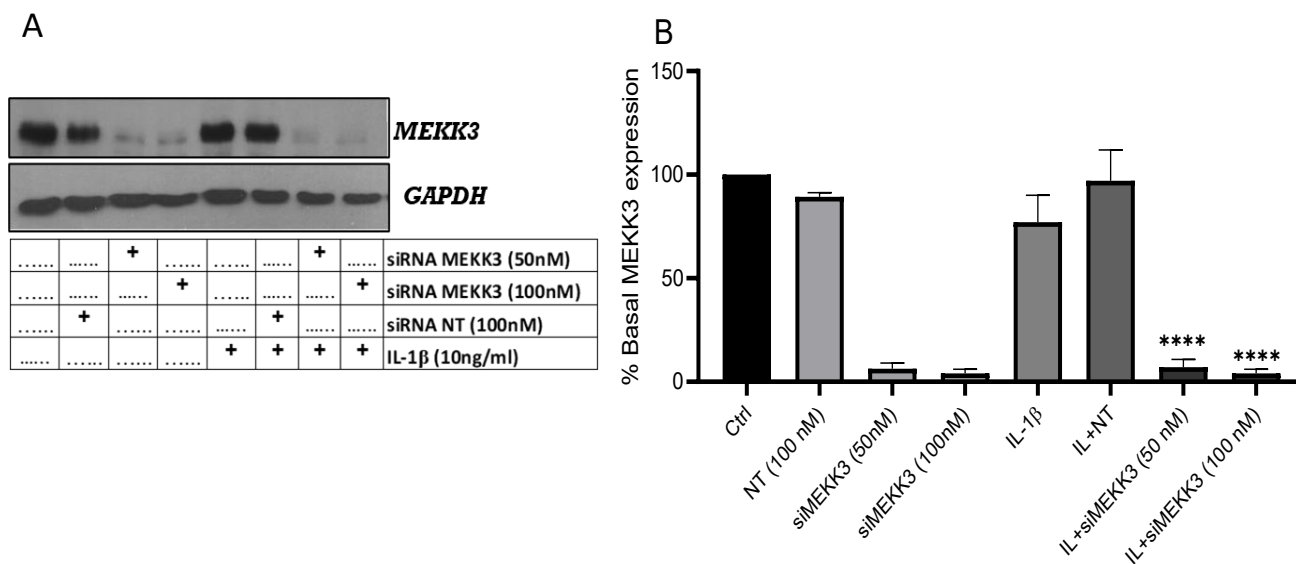


Figure 4. 24 The effect of siRNA MEKK3 on MEKK3 expression in U2OS cells.

Cells were transfected with siRNA MEKK3 or non-targeting (NT) at 50 nM and 100 nM for 96 h. Whole-cell extracts were assessed for A) MEKK3 (78 kDa), and GAPDH (37 kDa), which was used as a loading control, as outlined in Section 2.3.2. Blots were semi-quantified for a percentage of basal MEKK3 expression by scanning densitometry, and the results expressed as a relative to untreated control for B) MEKK3. Each value represents the mean \pm SEM of three independent experiments. Data was analysed using a one-way ANOVA test, **** $P < 0.0001$ vs IL-1 β and NT as an agonist-stimulated control.

4.7.1.2 The effect of MEKK3 siRNA Silencing on IL-1 β -Induced JNK Phosphorylation in U2OS Cells

The impact of siRNA MEKK3 on IL1 β -induced JNK phosphorylation in U2OS cells was investigated after the knockdown conditions were optimised. Figure 4.25 showed IL1 β -induced a more than 13-fold increase in JNK phosphorylation at 30 min (Fold stim=13.55 \pm 1.91, P <0.0001). Interestingly, this response was slightly increased following siRNA MEKK3 (50 and 100 nM) compared to the NT control. This result did not support a role for MEKK3 in the regulation of the JNK signalling cascade.

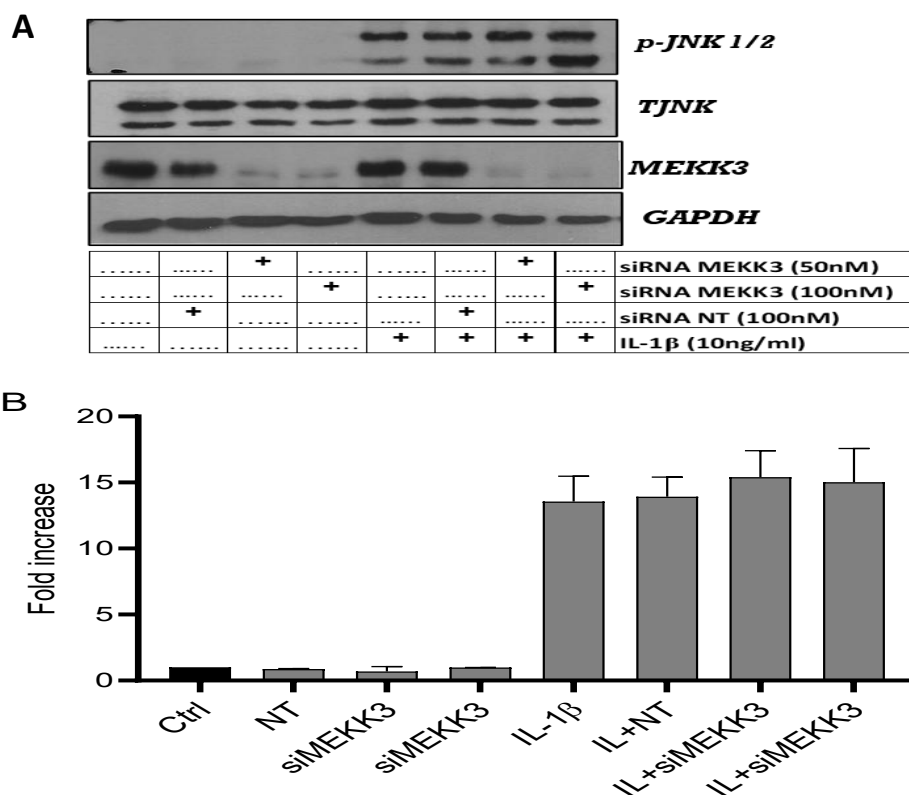


Figure 4. 25 The effect of MEKK3 siRNA upon IL-1 β -mediated phosphorylation of JNK in U2OS cells.

Cells were transfected with non-targeting (NT) siRNA 100 nM, MEKK3 siRNA (50-100 nM) for 96 h before stimulation with IL-1 β for 30 min. Whole cell extracts were assessed for A) pJNK phosphorylation (54,46 kDa), total JNK (54,46 kDa), MEKK3 (78 kDa), and GAPDH (37 kDa), which was used as a loading control. Blots were semi-quantified by scanning densitometry and the results expressed as fold increase relative to control for B) pJNK phosphorylation. Each value represents the mean \pm SEM of three independent experiments. Data was analysed using a one-way ANOVA test, ns non-significant vs IL-1 β and NT as an agonist-stimulated control.

4.7.1.3 The effect of MEKK3 siRNA Silencing on IL-1 β -Induced Phosphorylation of p100 and Cellular I κ B- α Degradation in U2OS Cells

The effect of siRNA MEKK3 on p100 phosphorylation and cellular I κ B- α loss induced by IL-1 β was assessed as markers of both IKK α and IKK β activity. Figure 4.26 showed IL1 β -induced more than 14-fold increase in p100 phosphorylation (Fold stims= 14.50 ± 1.40 , $P < 0.0001$), with complete cellular I κ B- α loss (% basal I κ B α expression- 13.33 ± 6.58 %, $P < 0.0001$) at 30 minutes. Following siRNA MEKK3 (50 and 100 nM), which reduced MEKK3 expression by over 80%, these IL-1 β -induced responses were not significantly altered when compared to IL-1 β plus NT stimulation. Furthermore, there was no effect on the expression of p100/p52. Taken together, these results do not suggest a role for MEKK3 in the regulation of either IKK α - or IKK β -dependent NF- κ B signalling in response to IL-1 β .

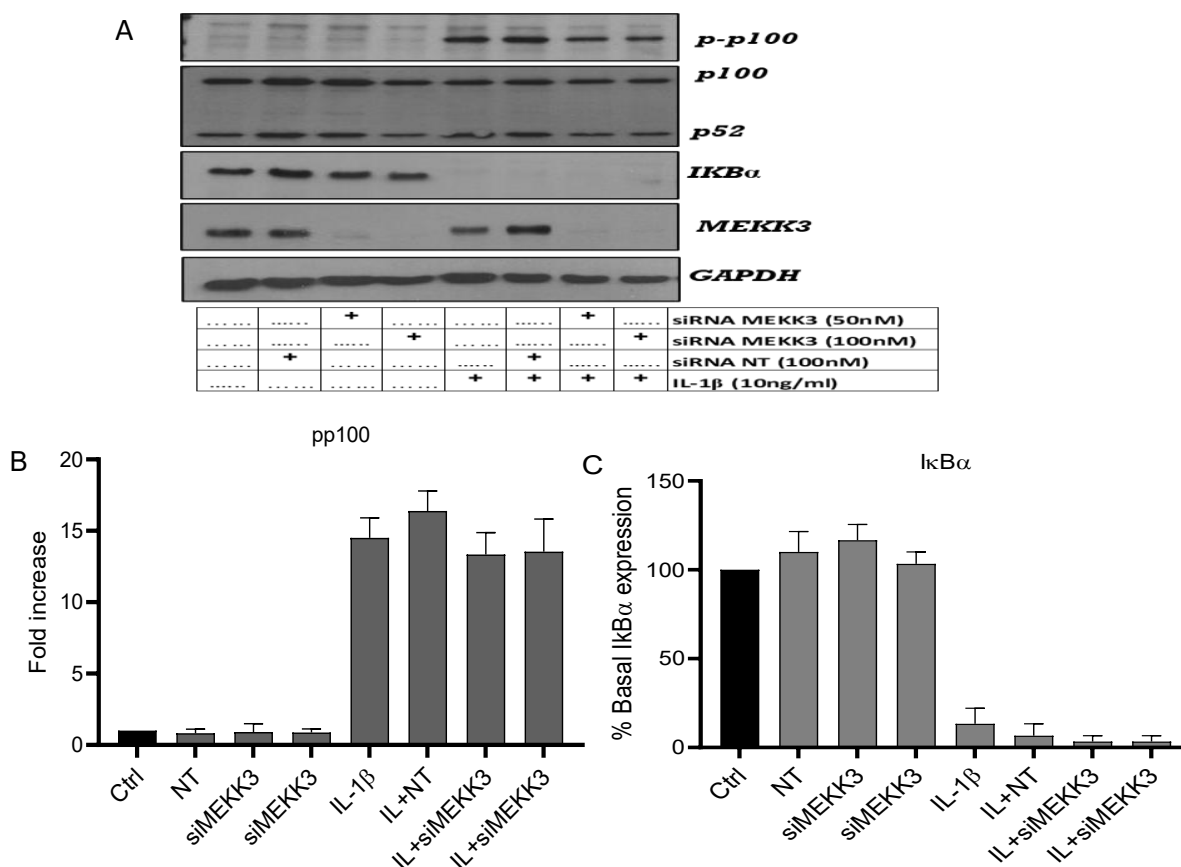


Figure 4. 26 The effect of MEKK3 siRNA upon IL-1β-mediated p100 phosphorylation and cellular IκB-α loss in U2OS cells.

Cells were transfected with non-targeting (NT) siRNA 100 nM, MEKK3 siRNA (50 and 100 nM) for 96 h before stimulation with IL-1β (IL, 10 ng/mL) for 30 min. Whole cell extracts were assessed for A) p-p100 (100 kDa), cellular IκB-α loss (39 kDa), MEKK3 (80 kDa), and GAPDH (37 kDa) which was used as a loading control. Blots were semi-quantified by scanning densitometry and the results expressed as fold increase relative to control for B) pp100 phosphorylation, C) IκB-α degradation. Each value represents the mean \pm SEM of three independent experiments. Data was analysed using a one-way ANOVA test, ns, non-significant vs IL-1β and NT as an agonist-stimulated control.

4.8 Effect of Combined TAK-1/MEKK3 siRNA Silencing upon IL-1 β -Inducing Signalling Pathways in U2OS Cells

As described previously, a synergistic effect between both TAK1 and MEKK3 was reported, particularly with respect to NF- κ B signalling (Sokolova et al., 2014). Therefore, the effect of combined siRNA TAK1 and MEKK3 in this study was examined.

4.8.1 Effect of combined TAK-1 and MEKK3 siRNA silencing on IL-1 β -induced MAPK signalling

Following stimulation of U2OS cells, Figure 4.27 shows that IL1 β -induced more than a 13-fold increase in JNK phosphorylation at 30 min (Fold stims= 13.29 ± 1.27 , $P < 0.0001$). This response was significantly reduced following siRNA TAK-1 by about 70% (50 nM) (Fold stims= 4.62 ± 0.88) whilst total JNK was not affected. Alone, MEKK3 siRNA was without effect on phosphorylation levels. The combined knockdown of siRNA TAK-1 and MEKK3 gave a decrease in JNK, which was essentially the same as siRNA TAK-1 alone (Fold stims= 5.12 ± 1.42 , $P < 0.01$). siRNA MEKK3 treatment did not result in any amplification of the inhibition. These findings do not suggest a synergistic effect of MEKK3 with TAK1 in the regulation of the JNK signalling cascade.

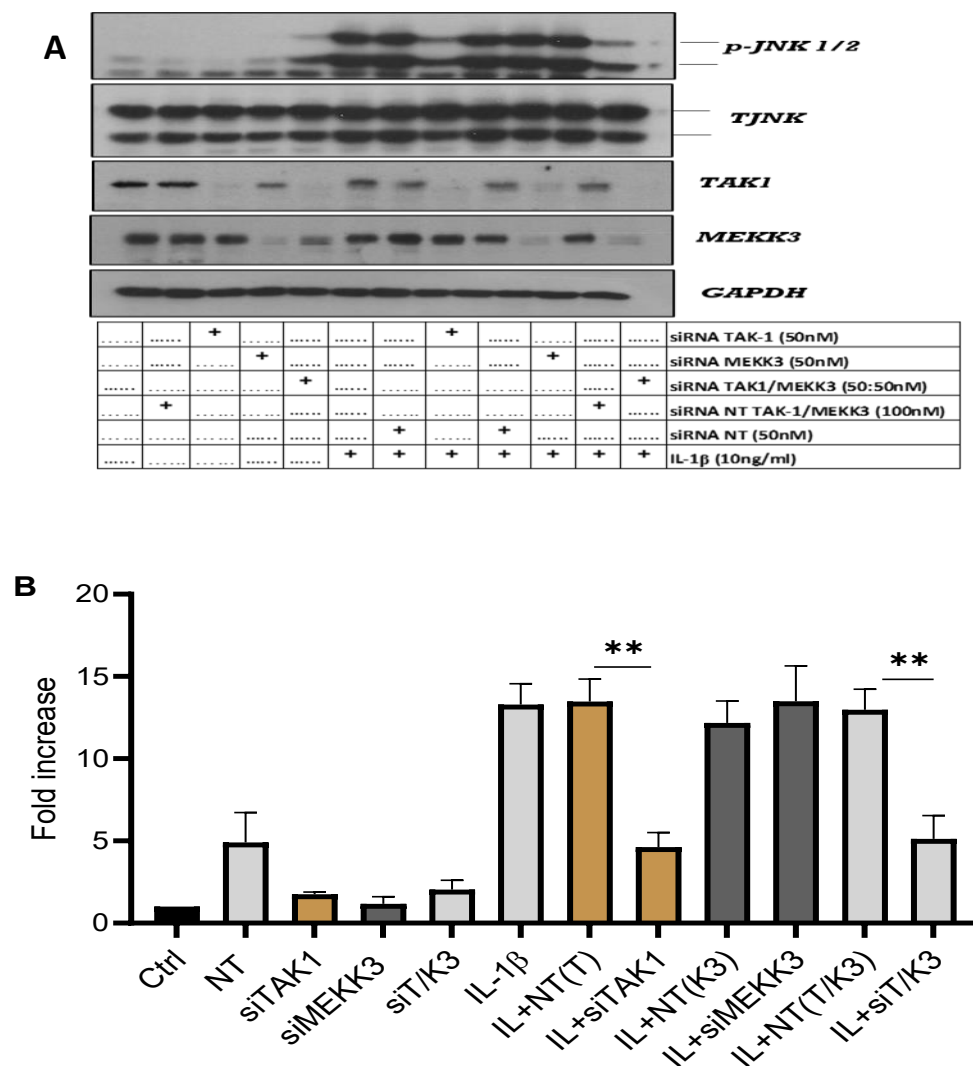


Figure 4. 27 The effect of combined TAK1 and MEKK3 siRNA upon IL-1 β -mediated phosphorylation of JNK in U2OS cells.

Cells were transfected with non-targeting (NT) siRNA 100 nM, TAK-1 siRNA (T), MEKK3 siRNA (K3) (50 nM) for 96 h before stimulation with IL-1 β (IL, 10 ng/mL) for 30 min. Whole cell extracts were assessed for A) pJNK phosphorylation (54,46 kDa), total JNK (54,46 kDa), TAK-1 (80 kDa), MEKK3 (78 kDa), and GAPDH (37 kDa), which was used as a loading control. Blots were semi-quantified by scanning densitometry, and the results expressed as fold increase relative to the control for B) pJNK phosphorylation. Each value represents the mean \pm SEM of three independent experiments. Data was analysed using a one-way ANOVA test, **P < 0.01 vs IL-1 β and NT as an agonist-stimulated control.

4.8.2 The effect of combined TAK1 and MEKK3 siRNA silencing on IL-1 β -induced cellular I κ B- α degradation in U2OS Cells

Within the same experimental setup, the effect of the combined siRNA knockdown on cellular I κ B- α loss induced by IL-1 β was also assessed. Figure **4.28** shows IL-1 β -induced cellular I κ B- α loss by approximately 87% (% basal I κ B- α expression = 13.25 ± 4.15 , $P < 0.0001$) at 30 min. Following single siRNA treatments with TAK-1 or MEKK3 siRNA, there was no reversal of the IL-1 β response, although for TAK-1 siRNA, there was a reversal of the shift in the residual band, indicative of an inhibition of phosphorylation. Furthermore, the combined siRNA TAK-1 and MEKK3 (50 nM), did not show a reversal of the loss in I κ B α mediated by IL-1 β . These results suggest no additional impact of the combined TAK-1 and MEKK3 knockdown in the regulation of the canonical NF- κ B signalling pathway.

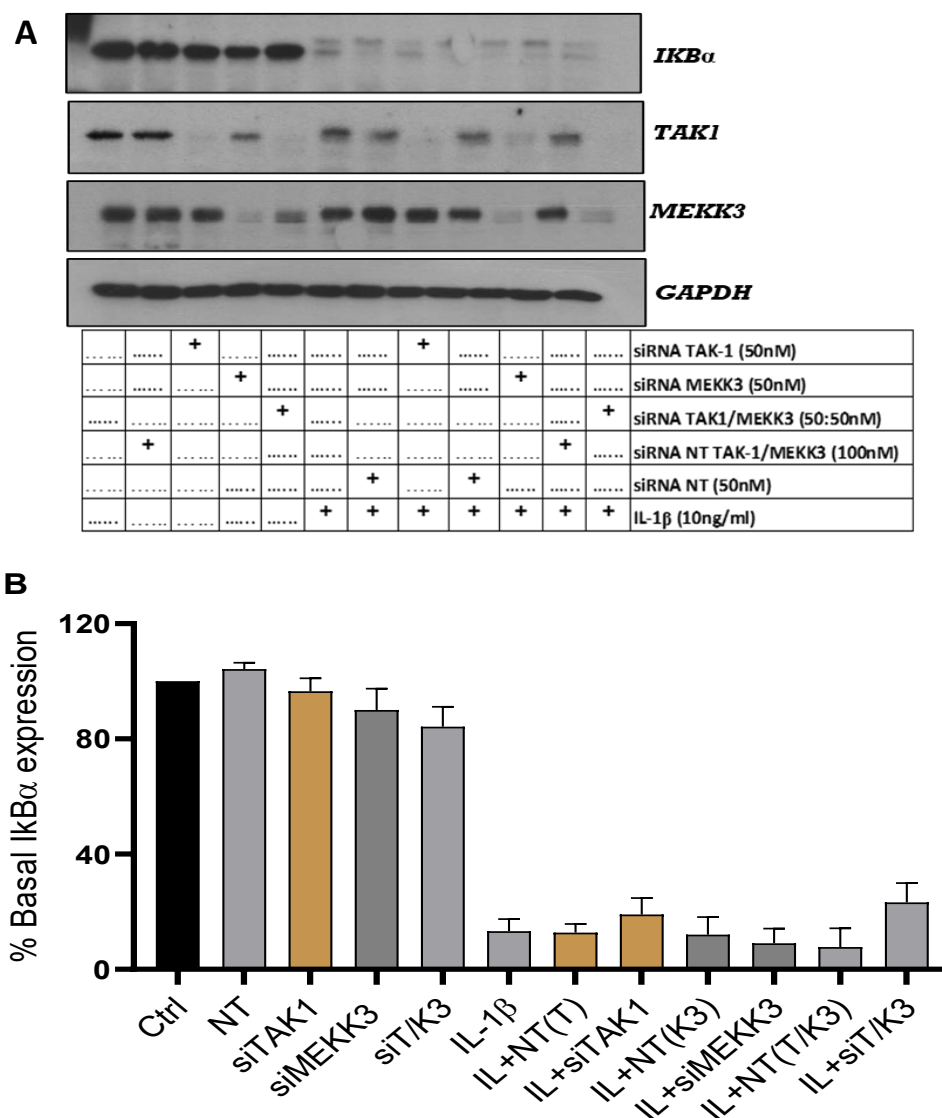


Figure 4. 28 The effect of combined TAK1 and MEKK3 siRNA upon IL-1 β -mediated cellular I κ B α loss in U2OS cells.

Cells were transfected with non-targeting (NT) siRNA 100 nM, TAK-1 siRNA (T, 50 nM), MEKK3 siRNA (K3, 50 nM) for 96 h before stimulation with IL-1 β (IL, 10 ng/mL) for 30 min. Whole cell extracts were assessed for A) cellular I κ B α loss (39 kDa), TAK-1 (80 kDa), MEKK3 (78 kDa), and GAPDH (37 kDa), which was used as a loading control. Blots were semi-quantified by scanning densitometry, and the results expressed as fold increase relative to control for B) I κ B α degradation. Each value represents the mean \pm SEM of three independent experiments. Data was analysed using a one-way ANOVA test.

4.8.3 The effect of combined TAK-1 and MEKK3 SiRNA silencing on IL-1 β -induced p100 and IKK α/β phosphorylation in U2OS cells

As in previous experiments, the effect of both siRNA TAK1 and MEKK3 knockdown on IL1 β -induced p100 phosphorylation in U2OS cells was investigated following individual or combined siRNA TAK1 and MEKK3 knockdown. Figure 4.29 shows that IL1 β -induced a more than 40-fold increase in p100 phosphorylation at 30 min (Fold stim=45.43 \pm 6.92, $P < 0.0001$). Once again, when TAK-1 siRNA was used along, there was a significant inhibition of p100 phosphorylation; however, in response to MEKK3 rundown, there was no effect on the IL-1 β signal.

Whilst the combined knockdown was inhibited this response markedly compared to NT control as shown in panel (B) (Fold increase= 27.39 \pm 6.86, $P < 0.05$) the TAK-1 siRNA alone strongly inhibited p100 phosphorylation (50 nM TAK1 siRNA Fold increase= 19.77 \pm 2.76, $P < 0.01$), while the MEKK3 knockdown did not significantly affect the stimulation. Moreover, the p100 processing to p52 was not affected by TAK1 and MEKK3 knockdown alone or together.

The same experiment was conducted to measure IKK α/β phosphorylation induced by IL1 β . IL1 β stimulated an approximately 8-fold increase in pIKK α/β phosphorylation at 30 min, as shown in Figure 4.29 (Fold stim=7.96 \pm 0.89, $P < 0.0001$), the combined knockdown inhibited this response markedly compared to NT control, as shown in panel (C) (Fold increase=5.10 \pm 0.63, $P < 0.01$). However, the TAK-1 siRNA alone strongly inhibited IKK α/β phosphorylation (50 nM TAK1 siRNA Fold increase= 4.31 \pm 1.71, $P < 0.001$) while the MEKK3 knockdown did not significantly alter the stimulation. These results suggest the involvement of TAK1 in the regulation of the IKK alpha signalling pathway, with no role of MEKK3.

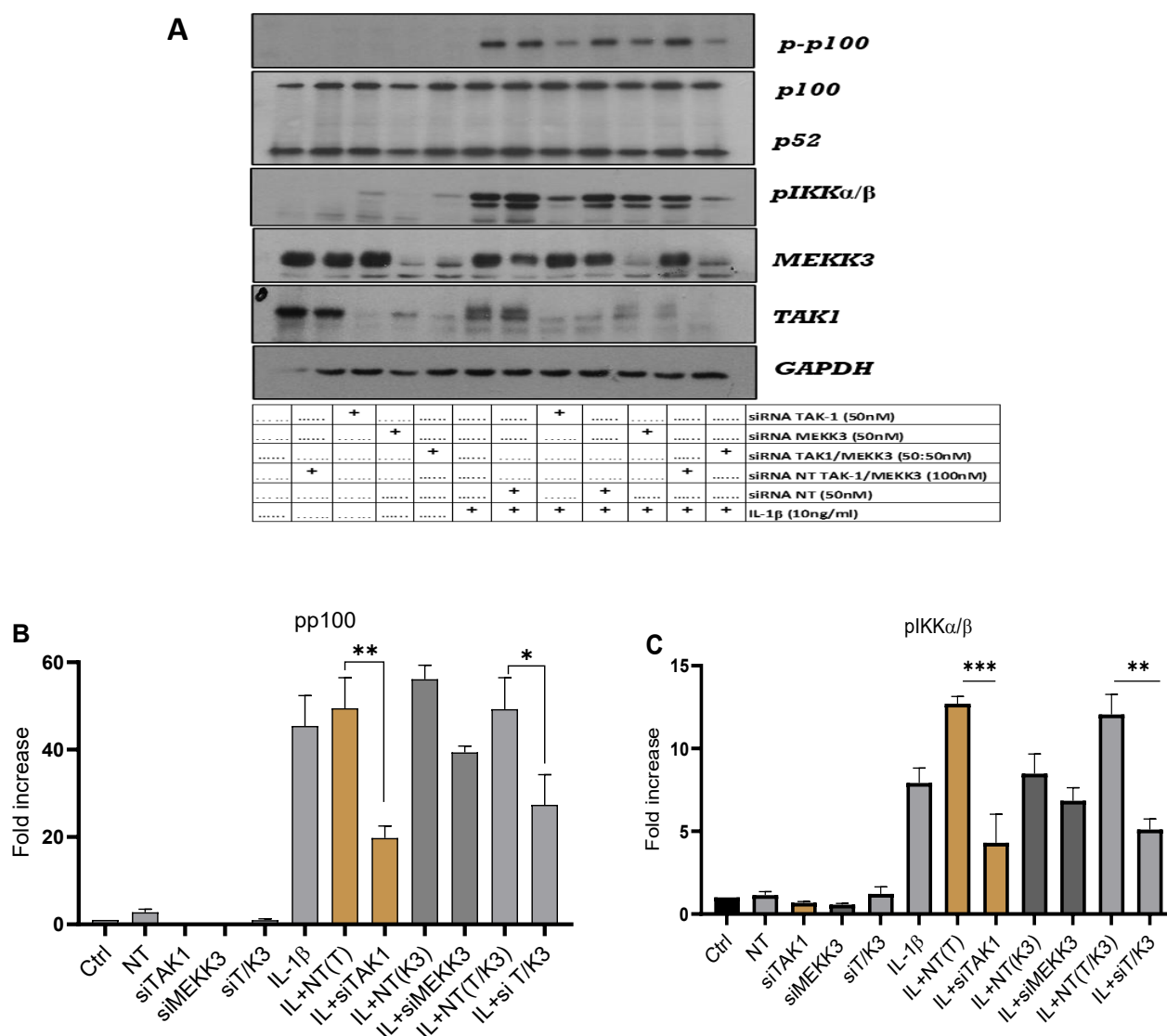


Figure 4. 29 The effect of combined TAK-1 and MEKK3 siRNA upon IL-1 β -mediated phosphorylation of p100 and IKK α/β in U2OS cells.

Cells were transfected with non-targeting (NT) siRNA 100 nM, TAK-1 siRNA (T, 50 nM), MEKK3 siRNA (K3, 50 nM) for 96 h before stimulation with IL-1 β (IL, 10 ng/mL) for 30 min. Whole cell extracts were assessed for A) p-p100 (100 kDa), p52 (52 kDa), p-IKK α/β (84,86 kDa), TAK-1 (80 kDa), MEKK3 (78 kDa), and GAPDH (37 kDa), which was used as a loading control. Blots were semi-quantified by scanning densitometry, and the results expressed as fold increase relative to the control for B) p100 phosphorylation, C) IKK α/β phosphorylation. Each value represents the mean \pm SEM of three independent experiments. Data was analysed using a one-way ANOVA test, *** P < 0.001, ** P < 0.01, * P < 0.05 vs IL-1 β and NT as an agonist-stimulated control.

4.9 Identification of the signalling pathway (s) involved in IL-1 β -induced CXCL12 activity in U2OS-CXCL12 cells

4.9.1 Effect of MAP Kinase Inhibition upon Cellular Signalling Stimulated by IL-1 β in U2OS Cells

4.9.1.1 Effect of JNK inhibition upon ppJNK induced by IL-1 β in U2OS cells

The effect of the JNK inhibitor SP600125 was examined in the following experiment. Figure **4.30** showed that IL-1 β stimulated pJNK phosphorylation significantly compared to unstimulated cells (Fold stims for IL-1 β +DMSO = 46.94 ± 0.86 , $P < 0.001$). In panel **B**, this stimulation was significantly inhibited via SP600125 at 10 and 20 μ M (Fold stims for IL-1 β +SP600125 at 10 μ M = 17.63 ± 1.06 , $P < 0.05$).

The same experiment was repeated for p-cJun as shown in panel **C**, and IL-1 β significantly stimulated the phosphorylation compared to unstimulated cells (Fold stims for IL-1 β +DMSO = 8.64 ± 1.38 , $P < 0.01$). This stimulation was also inhibited significantly via SP600125 at 10 and 20 μ M (Fold stims for IL-1 β +SP600125 at 10 μ M = 4.93 ± 0.89 , $P < 0.05$).

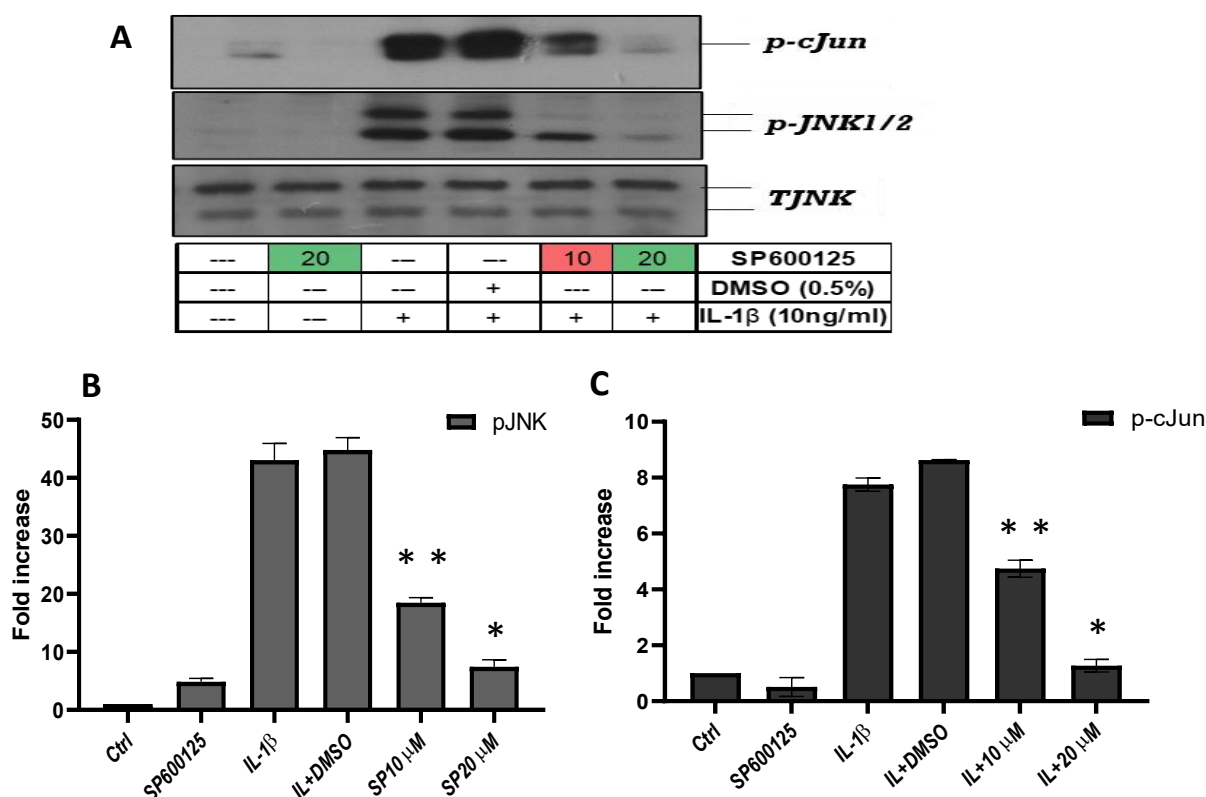


Figure 4. 30 Effect of SP600125 on IL-1 β -induced phosphorylation of JNK in U2OS cells.

U2OS cells were pre-treated with SP600125 for 1 h before stimulation with IL-1 β (IL,10 ng/mL) for 30 min. Whole-cell extracts were assessed for A) JNK phosphorylation (46,54 kDa), pc-Jun phosphorylation (48 kDa), and total JNK (46,54 kDa), which was used as a loading control. Blots were semi-quantified by scanning densitometry and the result expressed as a fold increase relative to control for B) pJNK, and C) pc-Jun. Each value represents the mean \pm SEM of three independent experiments. Data were analysed using a one-way ANOVA test, ** $P < 0.01$, * $P < 0.05$ vs IL-1 β + DMSO.

4.9.1.2 Effect of MAPK inhibitors on IL-1 β -induced CXCL12 luciferase activity in U2OS-CXCL12 Cells

Having established the role of IL-1 β in MAPK signalling regulation, particularly p38 and JNK, as well as the impact of pharmacological inhibition of these pathways, such as JNK inhibitor SP600125, on IL-1 β -induced signalling was also demonstrated in U2OS cells. Therefore, the role of IL-1 β on CXCL12 induction was examined in this chapter.

Initially, the effect of MAP Kinase inhibitors (JNK, p38, and ERK) on IL-1 β -induced CXCL12 activity was tested in U2OS cells. After 1 h treatment with 10 and 20 μ M concentrations of the inhibitors, cells were stimulated with IL-1 β for a further 6 h. As shown in Figure 4.31, IL-1 β significantly induced CXCL12 activity in U2OS cells to levels at approximately 3-4-fold of basal values. Following treatment with JNK inhibitor SP600125 panel (A), there was no significant effect on IL-1 β -induced reporter. In contrast, following treatment with the MEK/ERK inhibitor PD98059 panel (B), IL-1 β reporter activity showed a trend towards an increase, but this was not significant. Finally, the effect of p38 inhibitor SB203580 panel (C), caused a small but significant decrease (20-25%) in CXCL12 activity across a number of experiments.

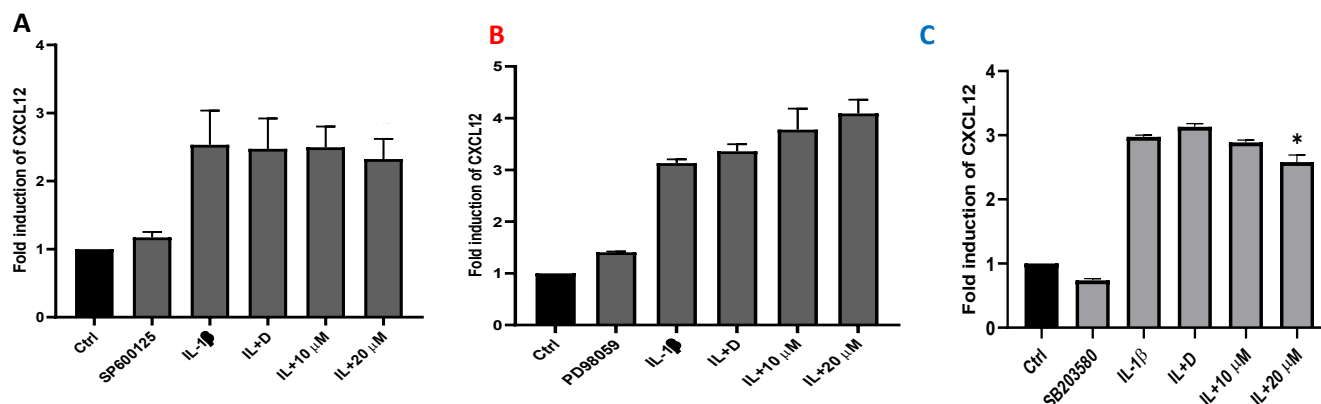


Figure 4. 31 Effect of MAPK inhibitors upon IL-1 β -mediated CXCL12 activity in U2OS cells. U2OS cells were pre-treated with JNK inhibitor (SP600125) (A), MEK/ERK inhibitor (PD98059) (B), and p38 inhibitor (SB 203580) (C) for 1 h before stimulation with IL-1 β (10 ng/mL) for a further 6 h. Cell lysates were assayed for luciferase activity as previously described in Section 2.5.1. The data shown was expressed as fold induction, and each value represents the mean \pm SEM of three independent experiments, ns, non-significant, *P < 0.05 vs IL-1 β + DMSO.

4.9.1.3 Effect of NF- κ B inhibitors on IL-1 β -induced CXCL12 induction in U2OS cells

Having established the relative effects of pharmacological inhibition of both IKK α and IKK β -dependent NF κ B signalling in U2OS cells, the effect upon CXCL12 induction was examined. Therefore, the IKK α inhibitor SU1261 (IKK α Ki = 10 nM, Ki = 680 nM) (Anthony et al., 2017) and the canonical IKK-beta inhibitor, IKK2 X1, were tested in U2OS-CXCL12 cells using the luciferase reporter activity.

As shown in Figure 4.32, the results revealed that IL-1 β induced a normal, 3-fold increase in CXCL12 activity at 10 ng/mL (Fold induction = 2.96 ± 0.29 , $P < 0.001$). This induction was significantly inhibited at low micromolar molar concentration, 3 and 10 μ M of SU1261, as shown in panel A (Fold induction at 10 μ M 1.13 ± 0.07 , $P < 0.001$). In contrast, the IKK2 X1 inhibitor alone caused a significant increase in reporter activity but showed little effect on the IL-1 β response, as shown in panel B.

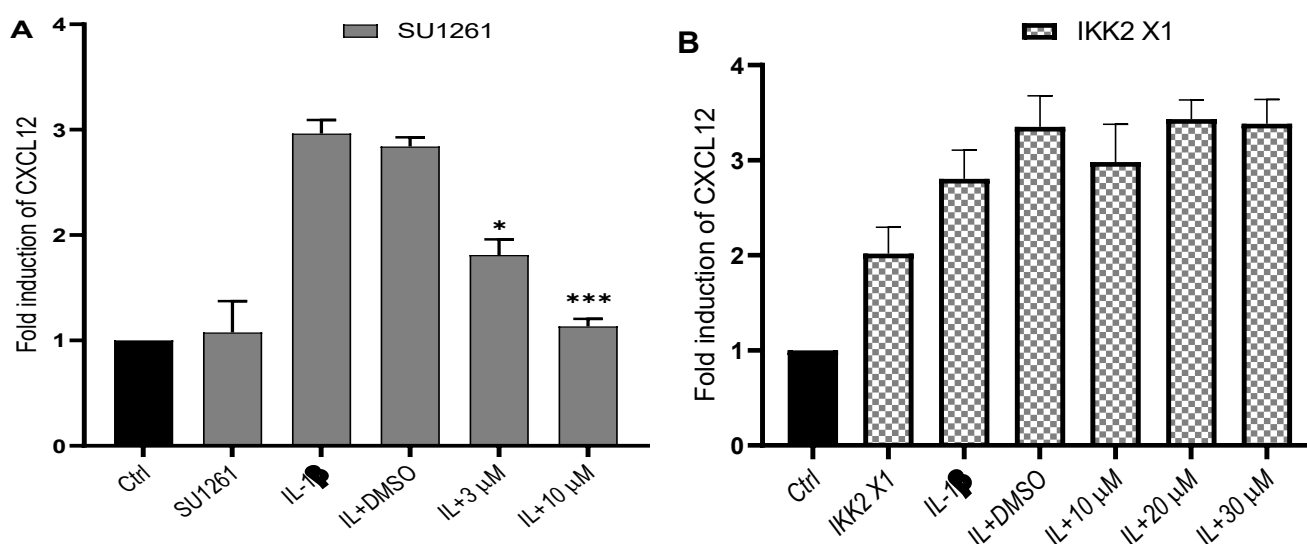


Figure 4. 32 The effect of NF- κ B inhibitors upon IL-1 β -mediated CXCL12 activity in U2OS cells.

U2OS cells were pre-treated with the selective IKK- α inhibitor, SU1261 (panel A), and IKK- β inhibitor, IKK2 X1 (Panel B) for 1 h before stimulation with IL-1 β (IL, 10 ng/mL) for a further 6 h. Cell lysates were then measured for luciferase activity as previously described in Section 2.5.1. Data shown was expressed as fold induction and each value represents the mean \pm SEM of three independent experiments. *** $P < 0.001$ vs agonist stimulated control.

4.9.2 Characterisation of the role of IKK α and IKK β in the regulation of IL-1 β -induced CXCL12 activity in U2OS-CXCL12 cells

Figure 4.33 shows that transfecting cells with 50 nM NT, siRNA IKK α , and IKK β alone led to an increase in CXCL12 compared to the non-transfected cells. Following stimulation with IL-1 β for 6 h, there was a noticeable increase in CXCL12 activity (3-4 fold), this was potentiated by NT siRNA (Fold induction = 6.32 ± 0.30), and also siRNA IKK α and IKK β (Fold induction for IKK α and IKK β = 6.50 ± 1.08 , 7.53 ± 1.02 respectively). This suggests that neither IKK α nor IKK β has a role in IL-1 β -stimulated CXCL12 activity, and the IKK α inhibitor, SU1261, examined in Figure 4.12, has an off-target effect.

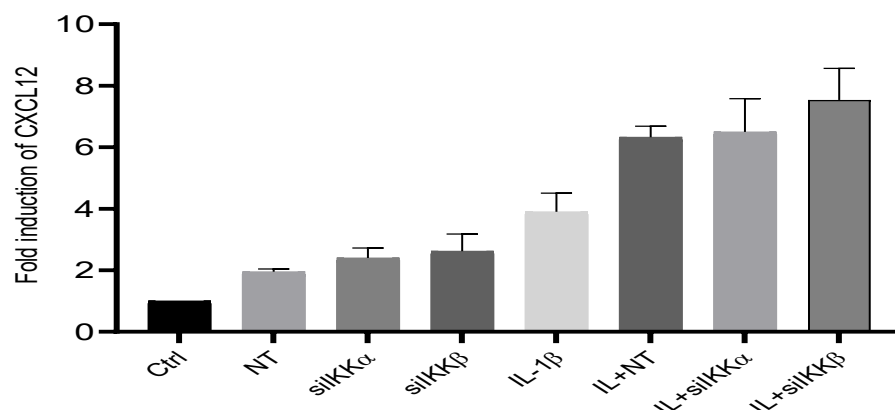


Figure 4. 33 The effect of siRNA IKK α and IKK β on IL-1 β -induced CXCL12 activity in U2OS CXCL12 cells.

Cells were transfected with 50 nM of non-targeting (NT), IKK α siRNA (50 nM), and IKK β siRNA (50 nM), for 72 h before stimulation with IL-1 β (IL, 10 ng/mL) for a further 6 h. Whole-cell extracts were then measured for luciferase activity as previously described in Section 2.5.1. Data shown expressed as fold induction, and each value represents the mean \pm SEM of three independent experiments. Data was analysed using a one-way ANOVA test.

The next experiment tested the effect of combining siRNA IKK α and IKK β on CXCL12 induction. Figure 4.34 showed that the NT and IKK α and IKK β siRNA double knockdown alone induced a marked increase in CXCL12 reporter activity. Whilst IL-1 β -stimulated the usual 4-fold increase in activity, this was increased slightly following NT transfection or siRNA IKK α or IKK β alone (Fold induction for IKK α and IKK β = 6.39 ± 1.05 , 7.42 ± 1.25 , respectively). Double knockdown had no significant effect on IL-1 β stimulation (Fold induction= 6.09 ± 1.07). This again indicates that IKK α and IKK β does not influence CXCL12 induction and no evidence for co-operation between these kinases was indicated.

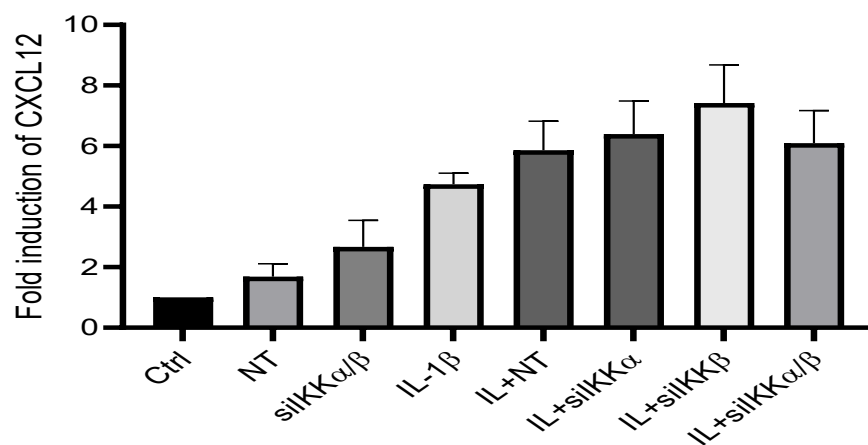


Figure 4. 34 The effect of siRNA IKK α and IKK β double knockdown on IL-1 β -induced CXCL12 activity in U2OS CXCL12 cells.

Cells were transfected with 100 nM of non-targeting (NT), IKK α siRNA, and IKK β siRNA (50 nM), for 72 h before stimulation with IL-1 β (IL, 10 ng/mL) for a further 6 h. Whole-cell extracts were then measured for luciferase activity as previously described in Section 2.5.1. Data shown expressed as fold induction, and each value represents the mean \pm SEM of three independent experiments. Data was analysed using a one-way ANOVA test.

4.9.2.1 The effect of IKK α and IKK β siRNA in combination with SU1261 in the Regulation of IL-1 β -induced CXCL12 induction in U2OS-CXCL12 cells

Having established a lack of effect of IKK α and IKK β siRNA on CXCL12 induction in response to IL-1 β , the effect of combined IKK α inhibitor SU1261 with IKK α /IKK β siRNA in U2OS cells was examined to identify the selectivity of the inhibitor on CXCL12 induction. Figure 4.35 shows that transfecting cells with 50 nM NT, siRNA IKK α and IKK β alone led to an increase in CXCL12 compared to the non-transfected cells. Additionally, the CXCL12 activity was increased by more than 3-fold after stimulation with IL-1 β for 6 h. Again, both siRNA IKK α and IKK β increased the activity compared to NT control (Fold induction for IKK α and IKK β = 3.95 ± 0.41 , 4.32 ± 0.30 , respectively). Moreover, the cells were also treated with 10 μ M IKK α inhibitor, SU1261 and the data showed that the inhibitor significantly inhibited the activity following stimulation with IL-1 β compared with the agonist-stimulated control (Fold induction= 1.06 ± 0.48 , $**P < 0.01$). This response did not change when cells were treated in combination with siRNA IKK β and interestingly, when cells treated with both siRNA IKK α and SU1261 (Fold induction= 1.38 ± 0.41). These findings suggest an off-target effect of SU1261 not related to its inhibition of IKK α .

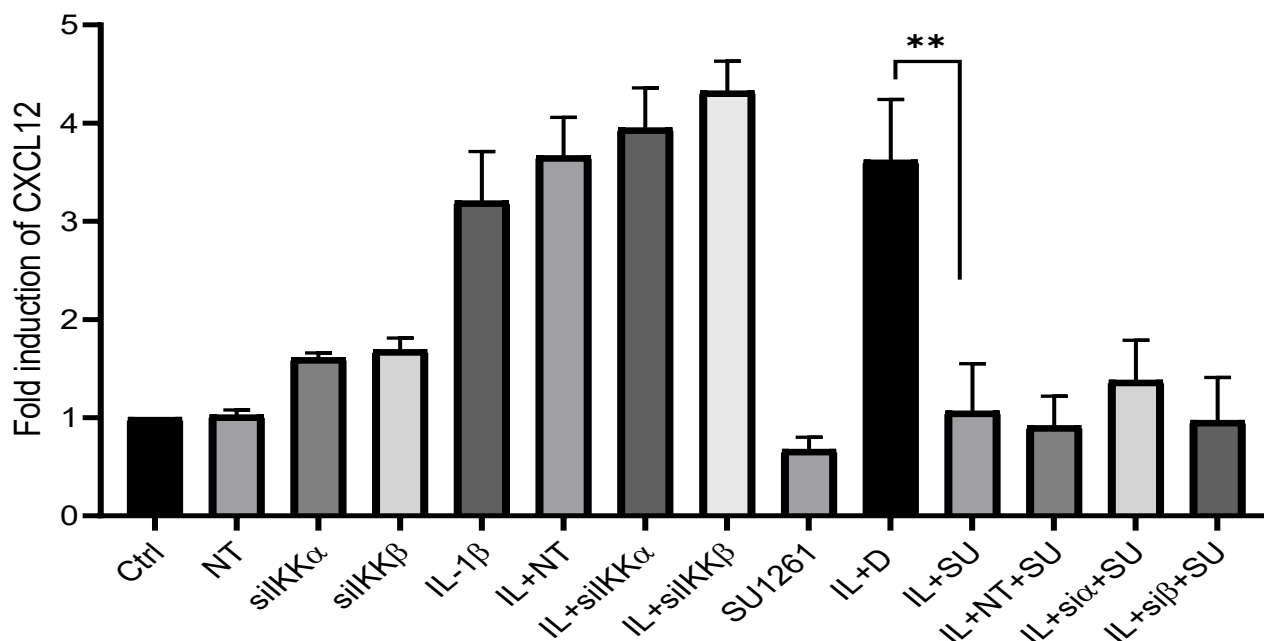


Figure 4. 35 The effect of combined SU1261 with siRNA IKK α and IKK β on IL-1 β -induced CXCL12 activity in U2OS CXCL12 cells.

Cells were transfected with 50 nM of non-targeting (NT), IKK α siRNA (si α , 50 nM) and IKK β siRNA (si β , 50 nM), for 72 h before being treated with 10 μ M SU1261(SU) for 1h and stimulated with IL-1 β (IL, 10 ng/mL) for a further 6 h. Whole-cell extracts were then measured for luciferase activity as previously described in Section 2.5.1. Data shown expressed as fold induction, and each value represents the mean \pm SEM of three independent experiments. Data was analysed using a one-way ANOVA test, **P < 0.01 vs agonist and nontargeting control.

Having established that neither IKK α nor IKK β is likely to regulate CXCL12, other pathways were investigated. Possible regulatory targets include NEMO-like kinase (NLK), TAK-1 and MEKK3, known to be activated in response to IL-1 β (Jurida et al., 2015; Weber et al., 2010; Yao et al., 2007).

4.9.3 The effect of combined p38/NLK inhibition on IL-1 β -induced cellular signalling and CXCL12 induction in U2OS Cells

4.9.3.1 The effect of combined p38/NLK inhibition on IL-1 β -induced cellular I κ B α degradation and p65 phosphorylation in U2OS Cells

The effect of the combined p38/NLK inhibitor, AMG548 on the canonical NF- κ B pathway was examined through assessing the cellular I κ B α loss and p65 phosphorylation. Figure 4.36 showed that IL-1 β significantly induced cellular I κ B α loss at 30 min compared to basal by around 95%. Following the pre-treatment of the cells with p38/NLK inhibitor in the micromolar range, the cellular I κ B- α degradation was not influenced compared to non-stimulated cells and the compound alone. Furthermore, AMG548 showed no significant effect on the phosphorylation of p65 after a 7-fold increase by IL-1 β . Suggesting no inhibitory effect for the canonical NF- κ B pathway by AMG548.

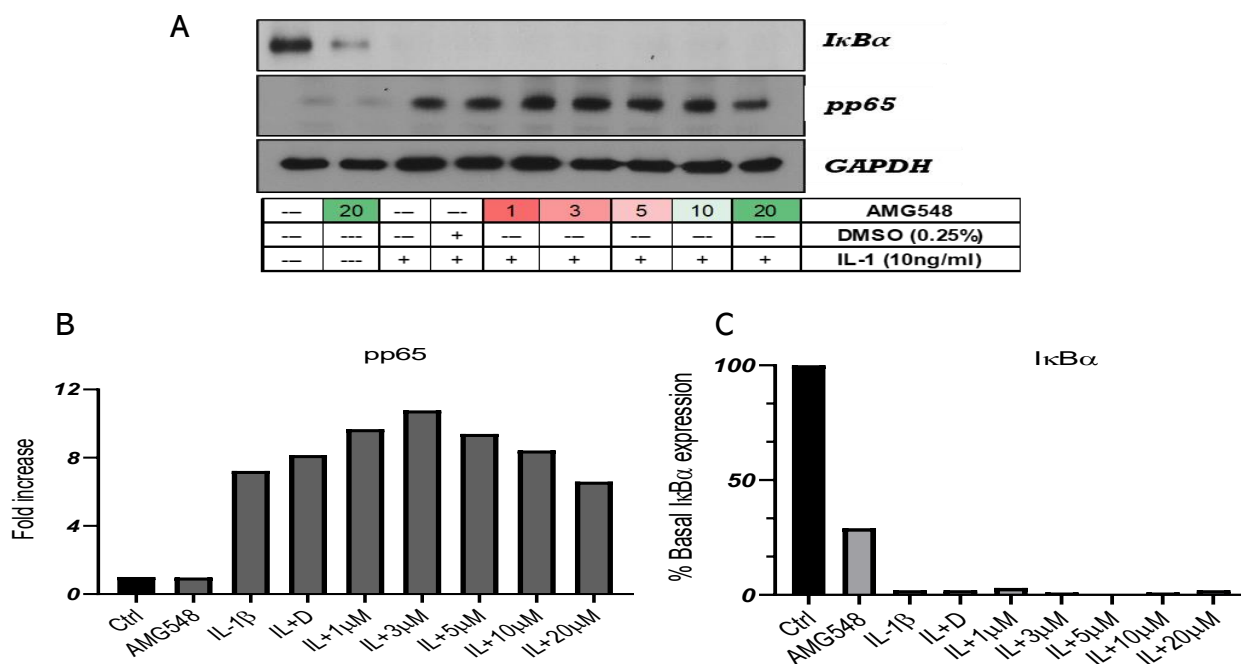


Figure 4. 36 Effect of AMG548 on IL-1 β -induced cellular I κ B α loss and p65 phosphorylation in U2OS cells.

Cells were pre-treated with AMG for 1 h before stimulation with IL-1 β (IL,10 ng/mL) for 30 min. Whole-cell extracts were assessed for A) I κ B α loss (39 kDa), p65 phosphorylation (65 kDa), and GAPDH (37 kDa), which was used as a loading control. Blots were semi-quantified by scanning densitometry and the result expressed as a fold increase relative to control for B) I κ B α and p65 phosphorylation. Each value represents one experiment.

4.9.3.2 The effect of Combined p38/NLK Inhibition on IL-1 β -induced p100 phosphorylation in U2OS Cells

The same experiment was done for the non-canonical NF- κ B pathway to assess the effect of the combined p38/NLK inhibitor, AMG548, on p100 phosphorylation, which is the main component of the pathway. Figure 4.37 showed that IL-1 β induced a more than 5-fold increase in p100 phosphorylation at 30 min compared to non-stimulated cells. Following the pretreatment of the cells with AMG548 in the micromolar range (1-20 μ M), the phosphorylation of p100 was not affected compared to non-stimulated cells and the compound alone. Also, there was no effect on p100 processing and p52 formation in pre-treated cells compared to the compound alone. These results suggest no inhibitory effect of AMG548 on the non-canonical NF- κ B pathway.

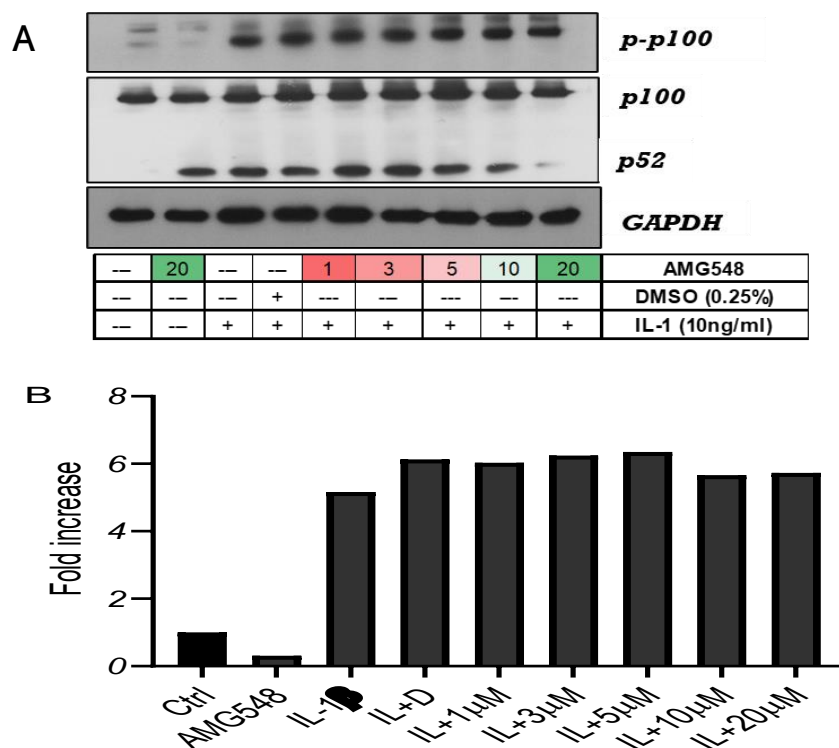


Figure 4.37 Effect of AMG548 on IL-1 β -induced phosphorylation of p100 in U2OS cells.

Cells were pre-treated with AMG for 1 h before stimulation with IL-1 β (IL, 10 ng/mL) for 30 min. Whole-cell extracts were assessed for A) p100 phosphorylation (100 kDa), p52 (52 kDa), and GAPDH (37 kDa), which was used as a loading control. Blots were semi-quantified by scanning densitometry, and the result expressed as a fold increase relative to the control for B) phosphorylation of p100. Each value represents one experiment.

4.9.3.3 The effect of combined p38/NLK inhibition on IL-1 β -induced JNK phosphorylation in U2OS Cells

An additional test examined the effect of AMG548 on IL-1 β -induced JNK phosphorylation in U2OS cells. Following more than a 20-fold increase in IL-1 β -induced JNK phosphorylation, the results in Figure 4.38 showed that pretreatment of the cells with AMG548 did not reduce JNK phosphorylation in a low micromolar range (1-20 μ M), compared to non-stimulated cells and AMG548 alone. This result indicates no role of AMG548 on the IL-1 β -induced JNK pathway.

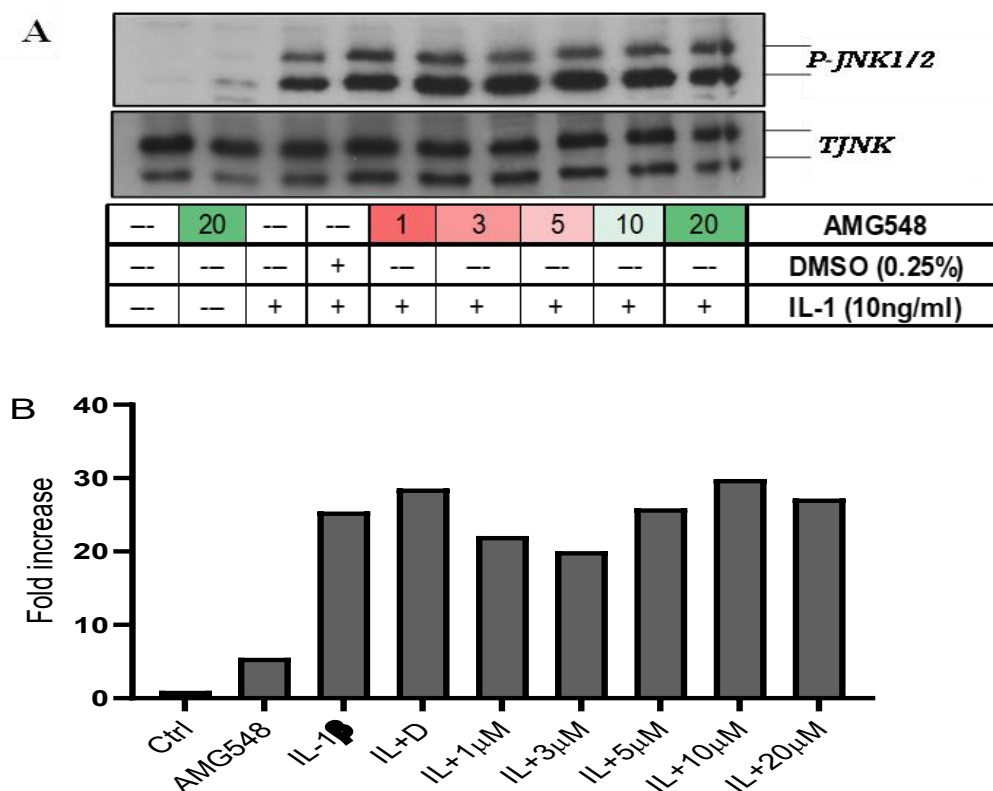


Figure 4. 38 Effect of AMG548 on IL-1 β -induced phosphorylation of pJNK in U2OS cells.

Cells were pre-treated with AMG for 1 h before stimulation with IL-1 β (IL,10 ng/mL) for 30 min. Whole-cell extracts were assessed for A) pJNK (46,52 kDa) and total JNK (46,52 kDa), which was used as a loading control. Blots were semi-quantified by scanning densitometry and the result expressed as a fold increase relative to control for B) pJNK phosphorylation. Each value represents one experiment.

4.9.3.4 Effect of combined MAPK p38/NLK inhibitor on IL-1 β -induced CXCL12 reporter activity in U2OS Cells

The previous results in Figure 4.31 showed a marginal inhibitory effect of SB203580 on IL-1 β -induced CXCL12 reporter activity. Recent findings have suggested that SB203580 can have off-target activity at another MAP kinase, Nemo-like kinase (NLK). Therefore, the dual NLK/p38 inhibitor AMG548 was examined (Verkaar et al., 2011; Wilkes et al., 2020). The results in Figure 4.39A showed that IL-1 β stimulated a 3-fold increase in activity. Pre-treatment with AMG548 caused a concentration-dependent inhibition of the IL-1 β response in the low to mild micromolar range

(Fold stim for IL-1 β +10 μ M AMG548- 1.50 ± 0.06 , $P < 0.0001$). **Figure 4.39 (B)** shows that the concentration of AMG548 at which 50 % of CXCL12 activity was inhibited (IC_{50}) was 4.40 μ M.

During these experiments with AMG548, a compromise of cell integrity was observed; therefore, the MTT assay was carried out as shown in Figure 4.40 (A) and (B). The results showed that AMG548 caused a concentration-dependent decrease in cell viability at both 7 and 24-h incubation periods (cell viability at 20 μ M, at 7 h and 24 h =72 %, and 64 % respectively). This finding did not support a clear role for NLK in CXCL12 induction with the possibility of cell compromise.

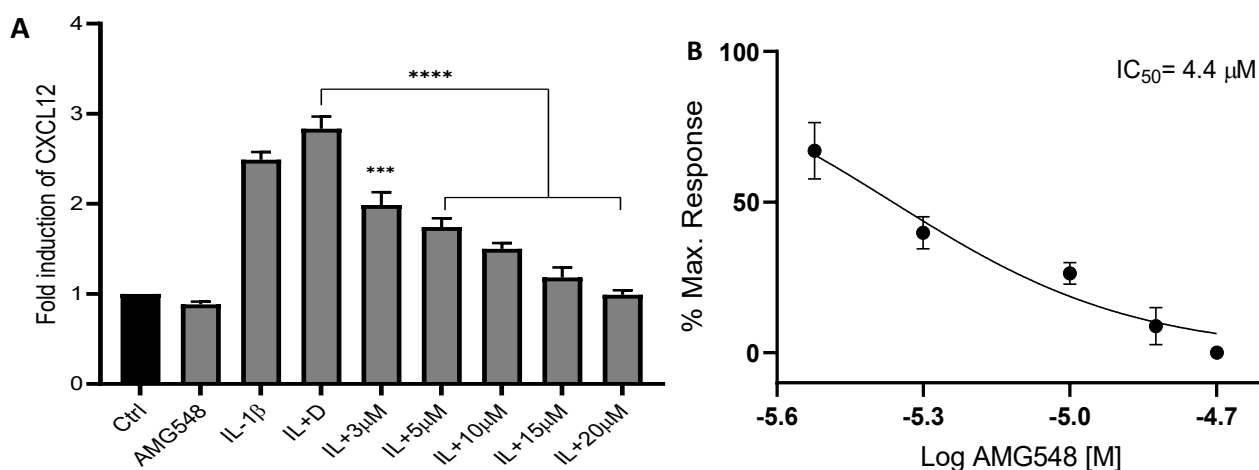


Figure 4. 39 The effect of AMG548 upon IL-1 β stimulated CXCL12 induction in U2OS cells. U2OS cells were pre-treated with increasing concentrations of AMG548 for 1 h before stimulation with IL-1 β (IL,10 ng/mL) for a further 6 h. Cell lysates were then measured for luciferase activity as previously described in Section 2.5.1. The data shown was expressed as fold induction and each value represents the mean \pm SEM of three independent experiments for (A). Each value expressed as a percent of maximum stimulation for (B), **** $P < 0.0001$, *** $P < 0.001$ vs IL-1 β + DMSO.

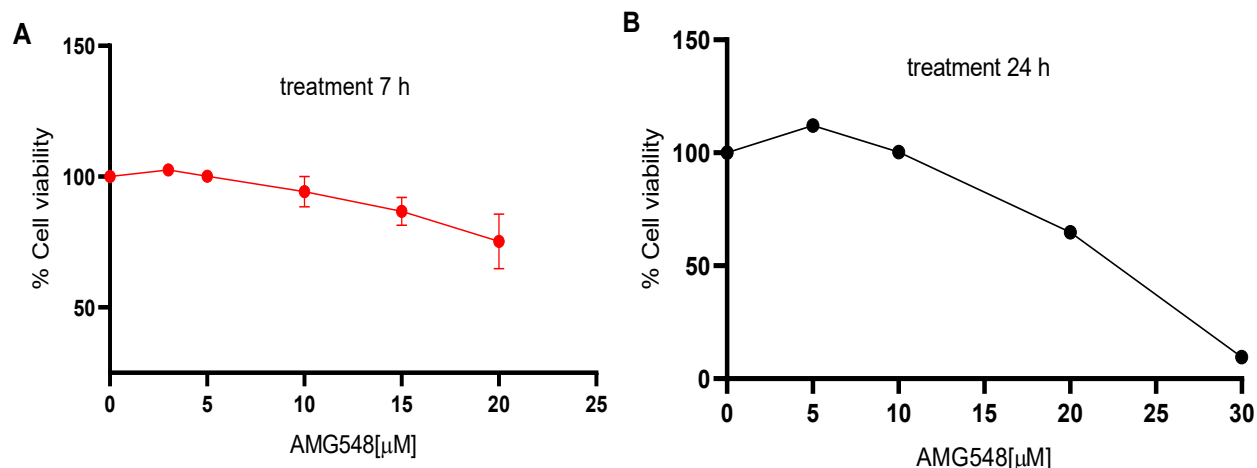


Figure 4.40 Effect of AMG548 on U2OS cell viability using MTT Assay.

U2OS cells were grown in 96-well plates as previously described in Section 2.6 using increasing concentrations of AMG548 for 7 h (A) and 24 h (B). U2OS cells treated with DMSO provided a negative control, and H_2O_2 (400 μM) acted as a positive control. Triplicates were averaged for each experiment. Data shown expressed the viability of U2OS cells in three independent experiments at 7 h, with one for 24 h treatment.

4.9.4 Effect of TAK1 Inhibitors on IL-1 β -induced CXCL12 Activity in U2OS Cells

Having established the effectiveness of pharmacological TAK-1 inhibition on IL-1 β stimulated signalling parameters, the role of TAK1 on CXCL12 luciferase activity was examined, using the TAK1 inhibitor 5Z-7oxozeaenol (abbreviated as 5Z-7-oxo) (Sokolova et al., 2014; Wei et al., 2016) and also Takinib (Totzke et al., 2017). The results shown in Figure 4.41 demonstrate that IL-1 β significantly induced more than a 3-fold increase in CXCL12 activity at 10 ng/mL (Fold stimulation for IL-1 β = 3.63 ± 0.17 , $P > 0.0001$). This induction was significantly inhibited by 5Z-7-oxo over the 10-30 μM concentration range, where IL-1 β stimulation was reduced between 3-10 μM (Fold stim for IL-1 β + 10 μM 5Z-7-oxo = 1.35 ± 0.49 , IC_{50} 5.03 μM , $P > 0.001$). A complete inhibition of the IL-1 β response was achieved at 20 μM (Fold stim for IL-1 β + 20 μM 5Z-7-oxo = 0.53 ± 0.19 , $P > 0.0001$).

5Z-7-oxo has been shown to have negative effects on cell survival and viability (Shi et al., 2021). Therefore, the effect of 5Z-7-oxo was tested on cell viability over a similar concentration range at both 7 h and 24 h using an MTT assay. The results in Figure 4.42 showed a noticeable effect of 5Z-7-oxo on cell survival and viability of around 30% with 7 h treatment, as shown in panel (A), and more than 50% with 24 h treatment, as shown in panel (B) at 10 μ M concentration. The high drop in cell viability with longer treatment was similar to another study that tested the anticancer effect of 5Z-7-oxo for a longer time in the B-NHL cell line (Wu et al., 2013). This longer treatment does not allow the role of TAK1 to be clearly established.

Therefore, the effect of another TAK-1 inhibitor, Takinib on CXCL12 induction was examined, and the results are shown in Figure 4.43. IL-1 β stimulated a 3-fold increase in CXCL12 activity. Takinib caused a concentration-dependent inhibition of the IL-1 β response between 10-30 μ M (Fold stims for IL-1 β +10 μ M- 1.72 ± 0.14 , IC₅₀ 3.35 μ M, P < 0.001). The inhibition was achieved over a larger concentration range than for 7-oxo. However, there are clear issues with Takinib with respect to cell viability.

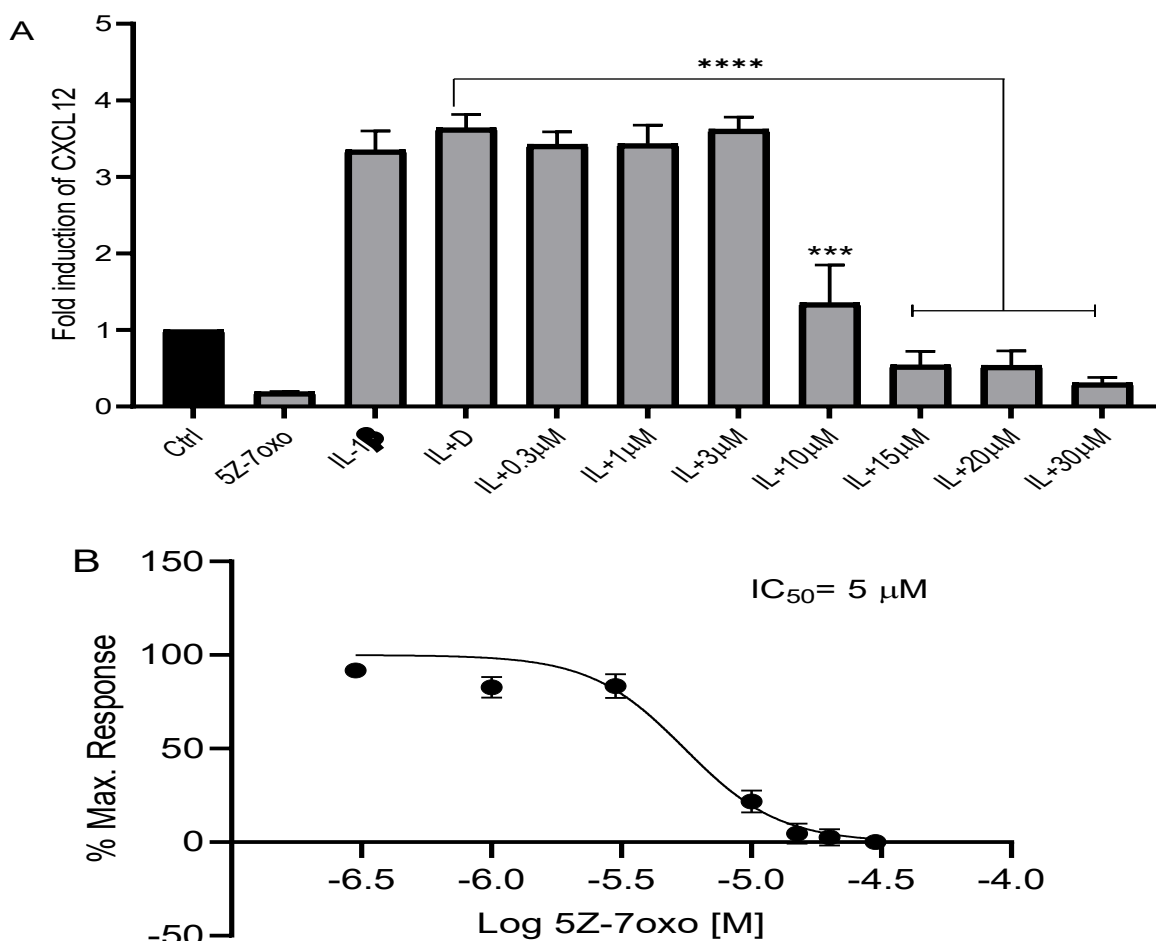


Figure 4. 41 The effect of TAK1 inhibitor, 5Z-7oxo upon IL-1 β -induced CXCL12 activity in U2OS cells.

Cells were pre-treated with increasing concentrations of 5Z-7oxo (A) for 1 h before stimulation with IL-1 β (IL,10 ng/mL) for a further 6 h, and the percentage increase in response of CXCL12 activity (B). Cell lysates were then measured for luciferase activity as previously described in Section 2.5.1. Data shown expressed fold induction and U2OS cell viability. Each value represents the mean \pm SEM of three independent experiments for 5Z-7oxo upon CXCL12 activity. ****P < 0.0001, ***P < 0.001 vs agonist stimulated control.

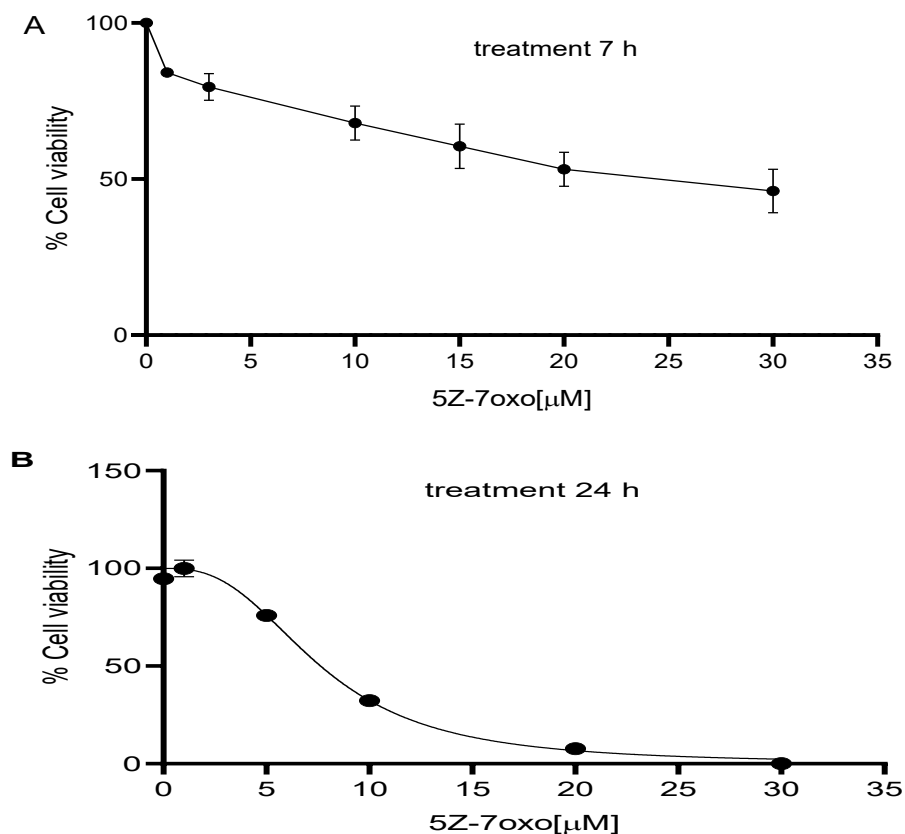


Figure 4. 42 Effect of TAK1 inhibitor, 5Z-7oxo on U2OS cell viability.

Cells were grown in 96-well plates as previously described in Section 2.6 using various concentrations of 5Z-7oxo for 7 h (A) and 24 h (B). U2OS cells treated with DMSO provided a negative control and H_2O_2 (400 μM) acted as a positive control. Triplicates were used for each experiment. Data shown expressed as U2OS cell viability in three independent experiments.

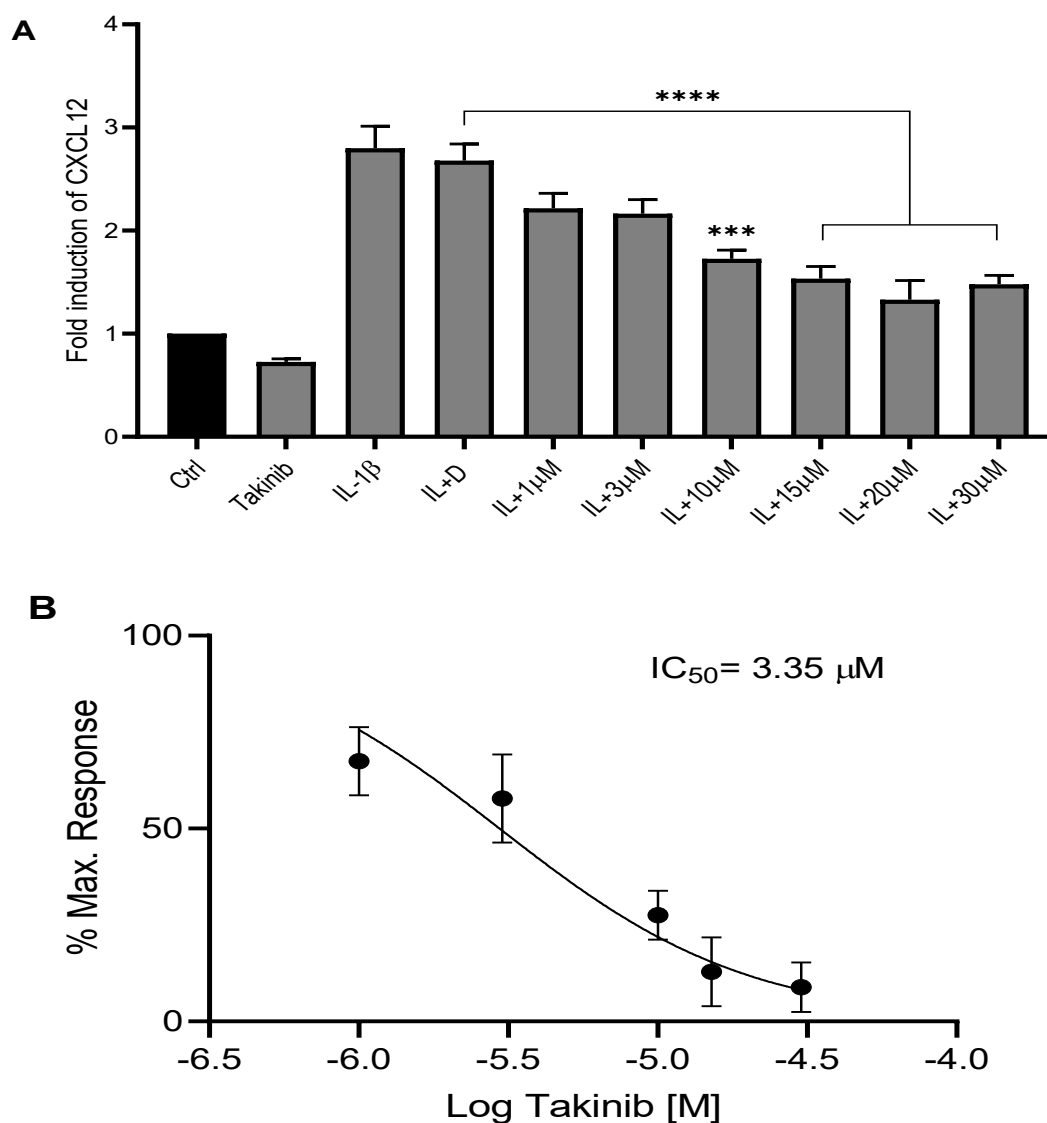


Figure 4. 43 The effect of TAK1 inhibitor, Takinib, upon IL-1 β -induced CXCL12 activity in U2OS cells.

Cells were pre-treated with increasing concentrations of Takinib for 1 h before stimulation with IL-1 β (IL,10 ng/mL) for a further 6 h (A), and the percentage increase in response of CXCL12 activity (B). Cell lysates were then measured for luciferase activity as previously described in Section 2.5.1. Data shown expressed as fold induction and each value represents the mean \pm SEM of three independent experiments for Takinib. **** P < 0.0001, *** P < 0.001, vs agonist stimulated control.

4.9.4.1 The effect of TAK-1 siRNA on IL-1 β - induced CXCL12 activity in U2OS-CXCL12 cells

Having established the effect of TAK-1 siRNA on IL-1 β stimulated MAP kinase and NF-kappa B signalling pathways, the next step was to assess the effect of TAK-1 run down on CXCL12 induction using reporter assay.

Figure 4.44 shows that IL-1 β induced a 3-fold increase in CXCL12 activity compared to control (Fold induction = 3.06 ± 0.16 , $P < 0.0001$). Transfecting cells with siRNA TAK1, which consistently reduced TAK-1 expression by over 80% as shown in panel (A), led to a small significant reduction by about 20 % in IL-1 β -stimulated CXCL12 reporter activity compared to the non-target (NT) control, as shown in panel (A) (TAK1 siRNA 50 nM: Fold induction 2.53 ± 0.04 , $P < 0.01$), with no cell damage as assessed by GAPDH expression. The results suggest that TAK1 plays a minor role in regulating IL-1 β -stimulated CXCL12 activity and that the effect of TAK-1 inhibitors may include an off-target element.

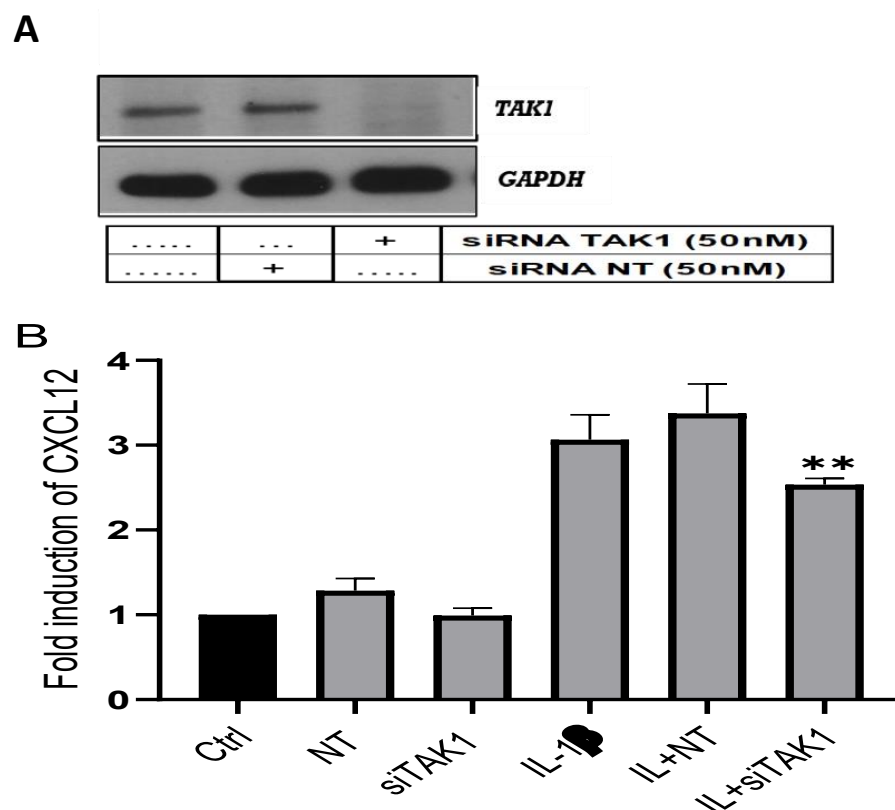


Figure 4. 44 The effect of siRNA TAK1 on IL-1 β -induced CXCL12 activity in U2OS CXCL12 cells.

Cells were transfected with 50 nM of non-targeting (NT), TAK1 siRNA (50 nM), panel (A) for 72 h before stimulation with IL-1 β (IL, 10 ng/mL) for a further 6 h. Whole-cell extracts were then measured for luciferase activity, panel (B) as previously described in Section 2.5.1. Data shown was expressed as fold induction. Each value represents the mean \pm SEM of three independent experiments. Data was analysed using a one-way ANOVA test, **P < 0.01 vs IL-1 β and NT as an agonist-stimulated control.

4.10 Regulation of CXCL12 production by ELISA

Due to the findings obtained from the reporter experiments that showed the role of CXCL12 induction and signalling pathways, including TAK-1 and MEKK3 in U2OS cells stimulated by IL-1 β , additional experiments were performed to confirm those effects using an ELISA assay.

4.10.1 Detection of CXCL12 Protein Expression in U2OS Cells using ELISA Assay

Having examined the effect of TAK-1 on CXCL12 activity induced by IL-1 β , it is essential to determine the effect of TAK1 in the regulation of CXCL12 expression using ELISA. At the beginning, Figure 4.45 shows a time course up to 24 h for IL-1 β (10 ng/mL) for the induction of CXCL12 expression in U2OS cells. IL-1 β stimulation induced the strongest CXCL12 response expression by approximately a 4-fold increase in expression level between 4-8 h in comparison to non-stimulated cells; the maximum level of approximately 6-fold was achieved at 24 h of stimulation. This finding demonstrated that IL-1 β strongly up-regulates CXCL12 expression in U2OS cells, as previously examined by our group, thus confirming the luciferase reporter data.

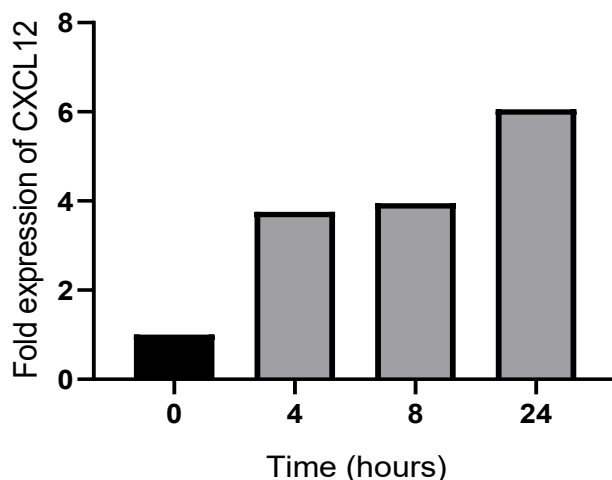


Figure 4. 45 Time course of IL-1 β induction of CXCL12 in U2OS cells.

Cells were seeded in 6-well plates and then stimulated with IL-1 β (10 ng/mL) for the indicated time points. Supernatants were collected, and the CXCL12 protein levels were assessed using an ELISA assay, as described in Section 2.7. The experiment was performed in duplicate.

4.10.1.1 Effect of TAK-1 siRNA on IL-1 β induced CXCL12 Protein Expression using ELISA in U2OS Cells

Next, the role of TAK1 in the regulation of CXCL12 induction was examined using an ELISA assay. As shown in Figure 4.46, IL-1 β produced a marked 9-fold increase in CXCL12 protein expression in comparison to non-stimulated cells (Fold expression = 9.80 ± 1.83 , $P < 0.0001$). Interestingly, TAK1 knockdown had no significant effect on IL-1 β -induced CXCL12 expression compared to a 20% inhibition of CXCL12 reporter activity. This result again suggests no essential role for TAK1 in the regulation of CXCL12 expression induced by IL-1 β .

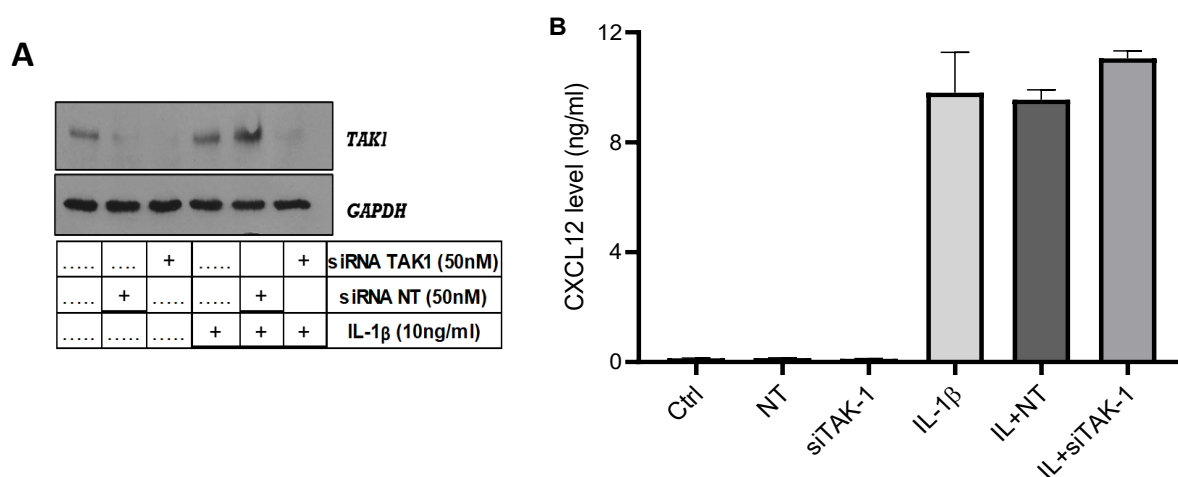


Figure 4. 46 The effect of TAK-1 siRNA upon CXCL12 protein levels in U2OS cells.

Cells were seeded in 6-well plates and transfected with 50 nM of non-targeting (NT), TAK-1 siRNA (50 nM), panel (A) for 72 h before stimulation with IL-1 β (IL,10 ng/mL) for a further 6 h. Supernatants were collected and CXCL12 protein levels were assessed by ELISA assay, panel (B) as outlined in Section 2.7. Three independent experiments were performed in duplicate, and the results expressed as means \pm SEM. Data was analysed using a one-way ANOVA test.

4.10.2 Detection of CXCL8 (IL-8) Protein Expression in U2OS Cells using ELISA Assay

Studies have shown upregulation of not only CXCL12, but also CXCL8 (IL-8) within the tumour microenvironment (TME) (Baker et al., 2019; Han et al., 2021; Michelini et al., 2018). Therefore, the expression of IL-8 was used as a comparator to assess the involvement of specific signalling pathways. Initially, a time course was established for IL-8 production in IL-1 β -stimulated U2OS cells.

Figure 4.47 showed that IL-1 β induced more than a 5-fold increase in IL-8 expression level at 4 h (Fold expression level= 5.56 ± 0.53 , $P < 0.01$), compared to non-stimulated cells, and more than a 4-fold increase at 8 h (Fold expression= 4.87 ± 0.56 , $P < 0.05$). High expression level of IL-8 was observed at 24 h by approximately 9-fold increase compared to non-stimulated cells (Fold expression= 9.67 ± 1.00 , $P < 0.001$). This result demonstrated that IL-1 β upregulates IL-8 expression in U2OS cells.

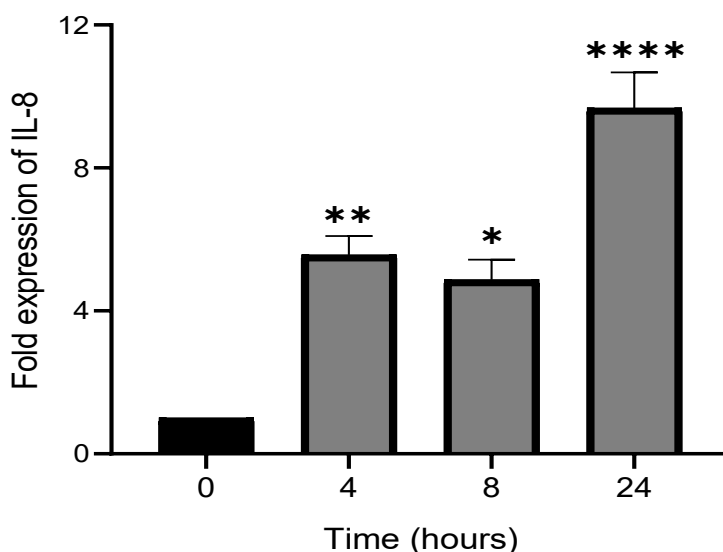


Figure 4. 47 Time course of IL-1 β induction of IL-8 in U2OS cells.

Cells were seeded in 6-well plates and then stimulated with IL-1 β (10 ng/mL) for the indicated time points. Supernatants were collected, and the IL-8 protein levels were assessed using an ELISA assay, as described in Section 2.7. Three independent experiments were performed in duplicate, and the results expressed as means \pm SEM. Data was analysed using a one-way ANOVA test, * $P < 0.05$, ** $P < 0.01$, *** $P < 0.001$ vs non-stimulated control.

4.10.2.1 Effect of TAK-1 siRNA silencing on IL-1 β induced IL-8 protein expression in U2OS-cells

Figure 4.48 showed that IL-1 β induced approximately 17-fold increase in IL8 protein expression in comparison to non-stimulated cells (Fold expression = 16.97 ± 0.46 , $P < 0.0001$). TAK-1 siRNA knockdown significantly reduced IL-8 protein expression compared to NT control by about 50% (Fold expression = 9.34 ± 1.30 , $P < 0.001$). This result confirmed the role of TAK-1 in IL-8 regulation induced by IL-1 β in U2OS cells.

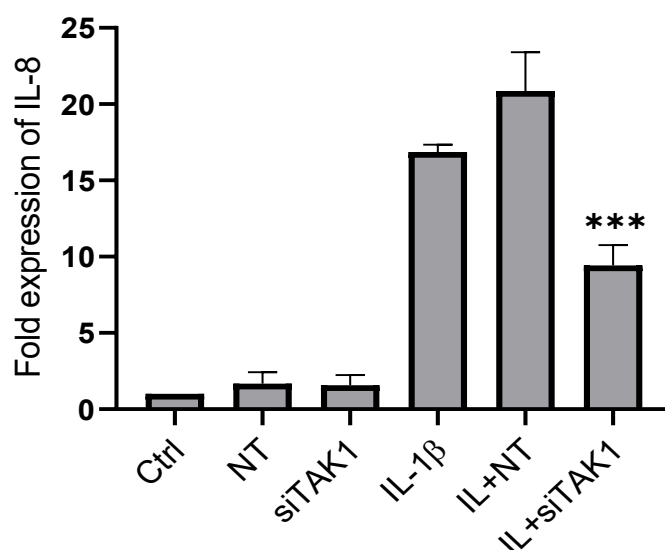


Figure 4. 48 The effect of TAK-1 siRNA upon IL-8 protein levels in U2OS cells.

Cells were seeded in 6-well plates and transfected with 50 nM of non-targeting (NT), TAK-1 siRNA (50 nM) for 72 h before stimulation with IL-1 β (IL, 10 ng/mL) for a further 24 h. Supernatants were collected, and IL-8 protein levels were assessed using an ELISA assay, as outlined in Section 2.7. Three independent experiments were performed in duplicate, and the results expressed as means \pm SEM. Data was analysed using a one-way ANOVA test, *** $P < 0.001$ vs IL-1 β and NT as an agonist-stimulated control.

4.10.3 The role of MEKK3 in the regulation of IL-1 β - stimulated CXCL12 induction in U2OS cells

Although MEKK3 knockdown did not affect IL-1 β -induced NF κ B and MAP kinase signalling the same strategy was employed to assess CXCL12 production. Figure 4.49 showed that IL-1 β -induced an increase in CXCL12 activity approximately 5-fold compared to control (Fold induction - 5.11 ± 0.48 , $P < 0.0001$). Transfecting cells with siRNA MEKK3, as shown in panel (A) led to good run down of the target protein in the relevant cell samples. This resulted in a reduction in basal activity but also a significant reduction by about 70 % in IL-1 β -stimulated CXCL12 activity compared to the non-target (NT) control, as shown in panel (B) (MEKK3 siRNA 50 nM and 100 nM: Fold induction 1.97 ± 0.47 , 2.19 ± 0.4 , $P < 0.0001$ respectively). The results suggest that MEKK3 mediates IL-1 β -stimulated CXCL12 activity. Furthermore, because siRNA MEKK3 showed a reduction in reporter activity compared to basal, the effect of siRNA MEKK3 was tested on cell viability at both concentrations (50 nM and 100 nM) using an MTT assay. The results in Figure 4.49, panel (C), showed that siRNA MEKK3 had no significant impact on cell viability at 50 nM, there was around a 10 % decrease at 100 nM after 96 h incubation.

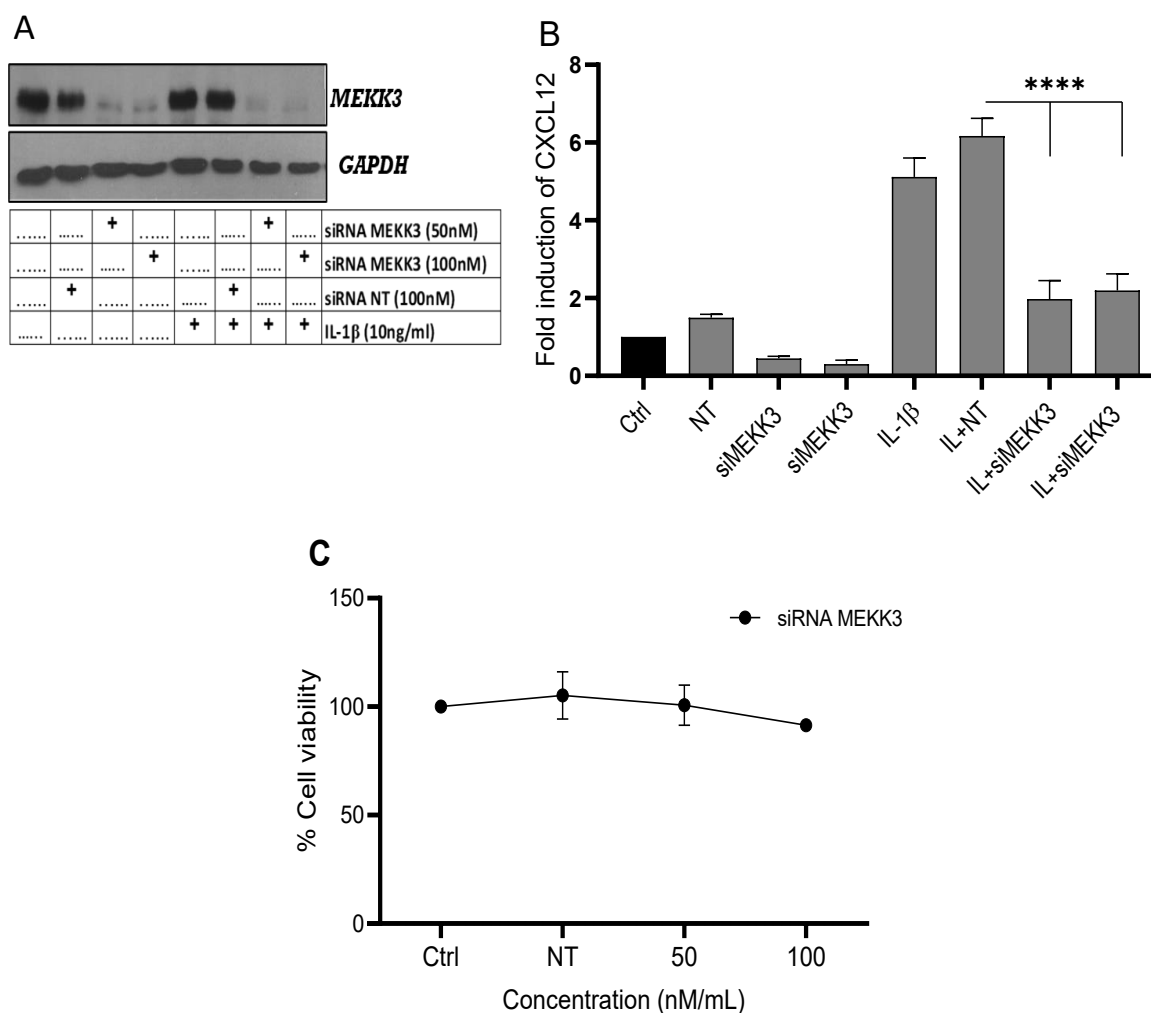


Figure 4. 49 The effect of siRNA MEKK3 on IL-1 β -induced CXCL12 activity in U2OS-CXCL12 cells.

Cells were transfected with 100 nM of non-targeting (NT), MEKK3 siRNA (50,100 nM), panel (A) for 96 h before stimulation with IL-1 β (IL,10 ng/mL) for a further 6 h. Whole-cell extracts were then measured for luciferase activity, panel (B) as previously described in Section 2.5. Effect of siRNA MEKK3 on U2OS cell viability panel (C). Cells were grown in 96-well plates as previously described in Section 2.6 using two concentrations (50 and 100 nM) for 96 h. U2OS cells treated with H₂O₂ (400 μ M) acted as a positive control. Triplicates were used for each in three independent experiments. Data shown was expressed as fold induction, and each value represents the mean \pm SEM of three independent experiments. Data was analysed using a one-way ANOVA test, ****P< 0.0001 vs IL-1 β and NT as an agonist-stimulated control.

Since surprisingly, a role for MEKK3 in CXCL12 induction has been observed, other strategies were employed. It has been reported that Ponatinib, a multi-kinase inhibitor in different cancer types, is able to inhibit MEKK3 signalling *in vivo* and *in vitro* models (Choi et al., 2018; Gozgit et al., 2012; Kaewlert et al., 2024). Therefore, the effect of Ponatinib on IL-1 β -induced CXCL12 activity was examined. Figure 4.50 (A) showed that IL-1 β significantly induced more than a 3-fold increase in CXCL12 activity at 10 ng/mL compared to control (Fold induction= 3.32 ± 0.36 , $P < 0.0001$). This response was slightly reduced at 0.3 μ M of Ponatinib and inhibited significantly over the 1-10 μ M concentration range (Fold stim for IL-1 β + 3 μ M- 1.21 ± 0.12 , IL-1 β + 10 μ M Ponatinib - 0.60 ± 0.04 , $P > 0.001$, $P > 0.0001$ respectively).

Additionally, Ponatinib at high concentrations reduced basal CXCL12 induction. Therefore, the effect of Ponatinib was tested on cell viability between 0.3-10 μ M using the MTT assay. The results in Figure 4.50, panel (B), showed a minor effect of Ponatinib on cell survival and a reduction in viability of around 19 % with 7 h of treatment at 10 μ M concentration.

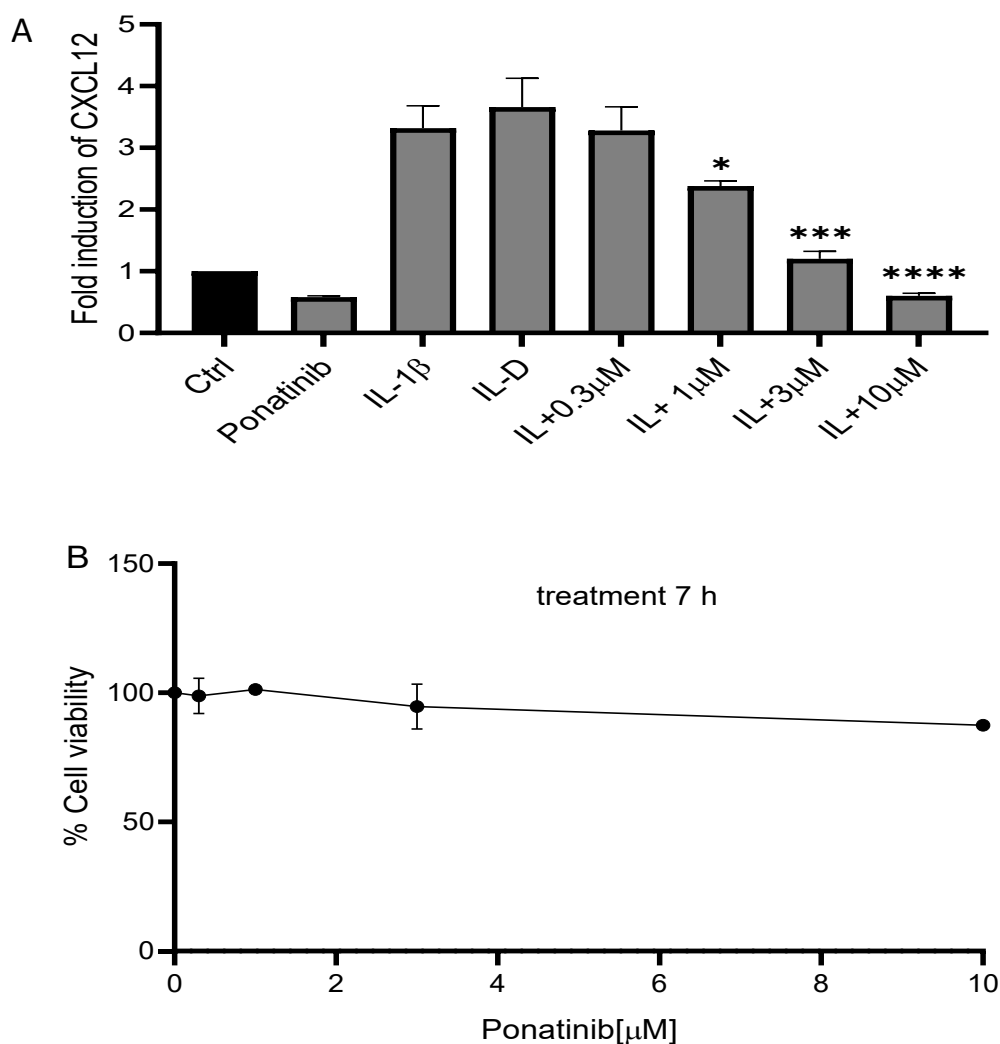


Figure 4. 50 The effect of MEKK3 inhibitor, Ponatinib upon IL-1 β -mediated CXCL12 activity in U2OS cells.

Cells were pre-treated with increasing concentrations of Ponatinib (A) for 1 h before stimulation with IL-1 β (IL,10 ng/mL) for a further 6 h. Cell lysates were then measured for luciferase activity as previously described in Section 2.5.1. Effect of MEKK3 inhibitor, Ponatinib on U2OS cell viability (B). Cells were grown in 96-well plates as previously described in Section 2.6 using various concentrations of Ponatinib for 7 h. U2OS cells treated with DMSO provided a negative control, and H₂O₂ (400 μ M) acted as a positive control. Triplicates were used for each in three independent experiments. Data shown was expressed as fold induction and U2OS cell viability. Each value represents the mean \pm SEM of four independent experiments for Ponatinib upon CXCL12 activity, ****P< 0.0001, ***P< 0.001, *P< 0.05 vs agonist stimulated control.

4.10.4 The role of MEKK3 in the regulation of IL-1 β -induced CXCL12 protein expression using ELISA in U2OS cells

Next, the role of MEKK3 in CXCL12 regulation was examined using an ELISA assay. Figure 4.51 shows that IL-1 β -induced more than a 40-fold increase in CXCL12 protein expression in comparison to non-stimulated cells after 6 h of stimulation (Fold expression = 43.46 ± 4.91 , $P < 0.0001$). MEKK3 siRNA knockdown resulted in significantly reduced CXCL12 protein compared to NT control, levels were reduced by about 70% (Fold expression = 16.13 ± 4.17 , $P < 0.0001$) with no effect on the cells as assessed by GAPDH expression. This result confirmed a role for MEKK3 in CXCL12 induction stimulated by IL-1 β in U2OS cells.

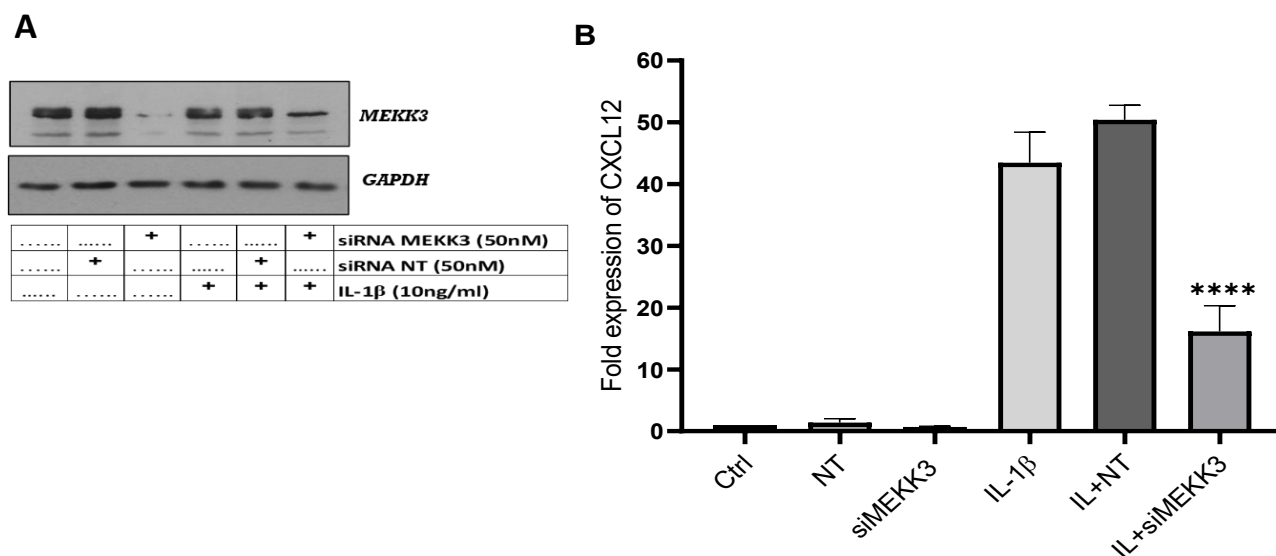


Figure 4. 51 The effect of MEKK3 siRNA upon CXCL12 protein levels in U2OS cells.

Cells were seeded in 6-well plates and transfected with 50 nM of non-targeting (NT), MEKK3 siRNA (50 nM), panel (A) for 96 h before stimulation with IL-1 β (IL,10 ng/mL) for a further 6 h. Supernatants were collected and CXCL12 protein levels were assessed using an ELISA assay, panel (B) as outlined in Section 2.7. Three independent experiments were performed in duplicate, and the results expressed as means \pm SEM. Data was analysed using a one-way ANOVA test, **** $P < 0.0001$ vs IL-1 β and NT as an agonist-stimulated control.

4.10.5 Effect of MEKK3 SiRNA Silencing on IL-1 β induced IL-8 Protein Expression in U2OS-Cells

Having established that MEKK3 was involved in the regulation of CXCL12 production, it was essential to determine if the effect was general for all cytokines or specific for CXCL12. Thus, the impact of MEKK3 siRNA knockdown on IL-1 β -induced IL-8 protein expression was examined using ELISA. Following 24 h stimulation, Figure 4.52 shows that IL-1 β induced an approximate 13-fold increase in IL-8 protein expression in comparison to non-stimulated cells (Fold expression= 12.94 ± 1.41 , $P < 0.0001$). MEKK3 siRNA knockdown had no effect on IL-8 protein expression compared to the NT control. This result confirmed the specific role of MEKK3 in CXCL12 regulation in IL-1 β -stimulated U2OS cells.

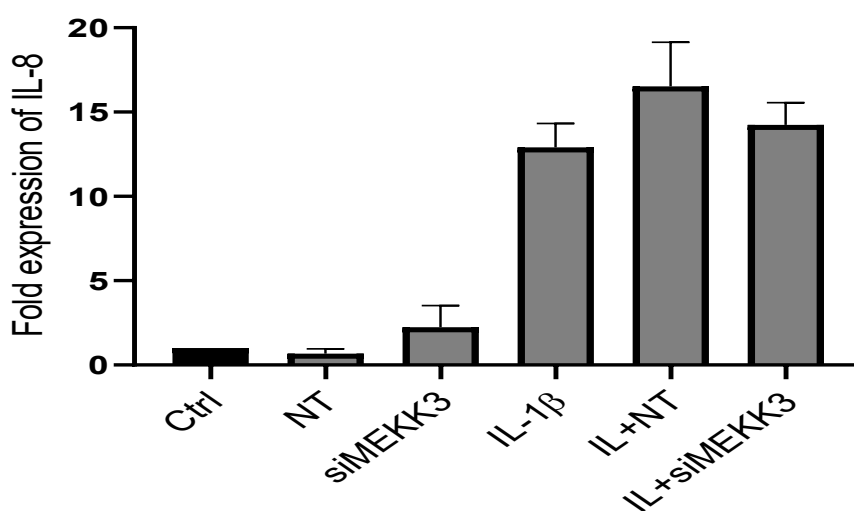


Figure 4. 52 The effect of MEKK3 siRNA upon IL-8 protein levels in U2OS cells.

Cells were seeded in 6-well plates and transfected with 50 nM of non-targeting (NT), MEKK3 siRNA (50 nM) for 96 h before stimulation with IL-1 β (IL, 10 ng/mL) for a further 24 h. Supernatants were collected, and IL-8 protein levels were assessed using an ELISA assay as outlined in Section 2.7. Three independent experiments were performed in duplicate, and the results expressed as means \pm SEM. Data was analysed using a one-way ANOVA test vs IL-1 β and NT as agonist-stimulated control.

4.11 Discussion

This chapter is divided into two parts. The first section deals with characterising signalling pathways in response to IL-1 β in U2OS cells, the second part then provides evidence for the role of each pathway in the regulation of CXCL12 induction.

Previous studies with U373 cells have demonstrated that there are six putative binding motifs that are located on 1010 base pairs upstream from the transcriptional start site within the region containing Sp1 binding sites. It was shown that these motifs are responsible for inducing CXCL12 expression upon stimulation with IL-1 β (García-Moruja et al., 2005). Initial studies showed that IL-1 β treatment resulted in a 4-fold increase of CXCL12 expression at 6-8 h. Therefore, this cell line was ideal for studying cell signalling parameters with respect to CXCL12 induction.

Initial signalling experiments sought to focus on the MAP kinase pathway. The CXCL12 promoter is known to have a c/EBP β site on the promoter region (Calonge et al., 2010). Studies have shown that c/EBP β phosphorylation is essential for activation (Calonge et al., 2010; Kim et al., 2007) and that this is controlled principally by ERK through phosphorylation on threonine 235 or 188 residues (Hungness et al., 2002; Park et al., 2004; Raymond et al., 2006). The initial findings in this chapter did not support the idea of ERK activation as a significant pathway for CXCL12 induction in this cell type; ERK activity was negligible relative to other cell studies where the relationship between ERK and c/EBP β has been studied. Indeed, additional experiments showed some increased phosphorylation of c/EBP β , but that was outwith the time span for CXCL12 induction (Figure 4.2). It is interesting to note that this is different to other studies in osteosarcoma cells, in which IL-1 β was effective in activating ERK (Huang et al., 2009). The results in this chapter do show that IL-1 β , as expected, was able to activate JNK, its downstream target C-Jun and p38 MAP kinase, well-recognised signalling cassettes downstream of IL-1 receptor induction.

Having questioned the role of ERK and c/EBP β in the regulation of CXCL12 by virtue of a lack of ERK activity, an examination of the NF κ B pathway was indicated. Whilst no putative NF κ B sites are featured in the CXCL12 promotion, is it possible that the pathway plays an indirect role as yet uncharacterised. It was found that, as expected, IL-1 β strongly stimulated the canonical NF κ B pathway as assessed by examining the loss of I κ B α and phosphorylation of p65. However, identifying

a role for IKK β remained difficult. Whilst IKK β run down using siRNA was successful, the effect on I κ B α loss was negligible, whilst high concentration of the IKK β inhibitor drug was only partially effective. This contrasts with previous studies that showed the significant inhibition of I κ B α loss (Baxter et al., 2004; Kishore et al., 2003), including some from our laboratory, which showed reversal of I κ B α loss, albeit at high concentrations of inhibitor (McIntosh et al., 2023). Effective reversal of I κ B α loss was found most clearly using DN IKK β adenovirus (Craig et al., 2025).

A number of studies have suggested that IKK α is able to function as a substitute for IKK β in the regulation of the canonical NF κ B pathway in various cells (Adli et al., 2010; Prescott et al., 2022), and it is possible that a similar co-regulatory pathway is a feature of U2OS cells. However, preliminary experiments showed very little reversal of I κ B α loss following siRNA IKK β in combination with SU1261 (Figure 4.14). It is more possible that the inhibitor failed to fully inhibit IKK β , and the degree of amplification requires only a small amount of IKK β to remain active.

Studies have shown that TAK-1 operates as a regulatory kinase upstream of IKK β in the canonical cascade. Indeed, preincubation with the TAK-1 inhibitor, 5Z-7oxo, was able to fully reverse the loss in I κ B α in response to IL-1 β . This agrees with a number of studies in immune and cancer models, which show that many stimuli, such as IL-1 β and TNF, activate and phosphorylate TAK-1, resulting in IKK complex phosphorylation, particularly IKK β (Mukhopadhyay & Lee, 2020; Sakurai, 2012). This effect was abolished using TAK-1 inhibitor, 5Z-7oxo, which completely blocks IL-1 β -induced signalling activation in cervical cancer and glioblastoma cells (Campolo et al., 2020; Guan et al., 2017). However, it should be noted that again, the TAK-1 siRNA run down was unable to cause reversals in IL-1 β -induced I κ B α loss. However, the degree of inhibition of IKK β phosphorylation was limited to 66%. Therefore, it is again possible that residual IKK beta activity is sufficient to cause activation of the canonical pathway.

A second and striking aspect of IL-1 β -induced signalling is related to “non-canonical” signalling. As has been found previously in the laboratory, results in this chapter showed that IL-1 β mediated a strong increase in the phosphorylation of p100 NF κ B2. This was consistent with previous findings in endothelial cells (Craig et al., 2025), and in U2OS and DU145 cell lines (McIntosh et al., 2023); phosphorylation was transient and not associated with the formation of p52, a phenomenon usually associated with non-canonical NF κ B signalling, driven by agonists such as LIGHT, Lymphotoxin

(LT), CD40L and others (Cildir et al., 2016; Sun, 2011, 2017). In a previous study in U2OS cells, CRISPR-induced deletion of IKK α , resulted in significantly reduced p100 phosphorylation (McIntosh et al., 2023). Results from this chapter confirmed these findings, pre-incubation with IKK α siRNA or pre-treatment with SU1261, a selective IKK alpha inhibitor, were also effective in reducing p100 phosphorylation. In contrast, IKK β siRNA was without on IL-1 β -induced p100 phosphorylation effect, suggesting that this mode of phosphorylation is indeed IKK α -dependent.

These findings are significant as they question the accepted model of regulation of p100 phosphorylation. For the non-canonical NF κ B pathway, it has been shown that the upstream MAP3K NIK has a predominant role. Studies show that following activation of NIK by TNF family members (CD40L, BAFF) and others, NIK directly phosphorylates human IKK α at specific residues (Ser176/180) in biochemical experiments, activating its kinase activity as reported in an *in vitro* kinase assay (Ling et al., 1998). Similarly, Xiao and coworkers demonstrated the importance of NIK in non-canonical NF κ B pathway activation through p100 phosphorylation; they showed that wild-type NIK expression in NIK-deficient cells restored the activation of IKK α and p100 phosphorylation with p52 formation (Xiao et al., 2004; Xiao et al., 2001). Other papers from the laboratory showed that whilst pharmacological inhibition of NIK using CW15337 (Haselager et al., 2021) was able to inhibit LT or LIGHT-induced p100 phosphorylation in either U2OS cells or HUVECs, the compound did not affect the IL-1 β response. This suggests that NIK is not required to bring IKK into proximity with p100 as has been suggested by previous studies (Craig et al., 2025; McIntosh et al., 2023).

Activation of the non-canonical NF κ B pathway is dependent on agonist-induced stabilisation of NIK (Sun, 2017); this seems unlikely to have occurred in such a short time frame as identified for IL-1 β stimulation; the lack of p100 degradation provides further evidence for the lack of NIK involvement in the IL-1 β response; NIK is well recognised to be essential for the degradation of p100 and the formation of p52 through binding of p100 to beta-transducin repeats-containing proteins (β -TrCP) E3 ubiquitin ligase (Xiao et al., 2004; Xiao et al., 2001), resulting in nuclear translocation and regulating target genes through p52/RelB dimers (Sun, 2017). Studies have shown that NIK knockout in B cells, fibroblasts, or Human embryonic kidney (HEK293T) cells blocked p100 phosphorylation and p52 generation by preventing IKK α phosphorylation (Sun, 2017; Xiao et al., 2001).

Further experiments in this chapter sought to identify the regulatory mechanisms involved in IL-1 β -induced p100 phosphorylation. Experiments identified TAK-1 as being essential for p100 phosphorylation. Pre-treatment of cells with the TAK-1 inhibitor, 5Z-7oxo (Ninomiya-Tsuji et al., 2003; Wu et al., 2013) causes a concentration-dependent inhibition of p100 phosphorylation, whilst treatment with TAK-1 siRNA caused a significant albeit partial inhibition (Figures 4.22 and 4.23). Additional experiments showed that under these treatment conditions, IL-1 β induction of pIKK α was also reduced by TAK-1 inhibition. Taken together, this would suggest that TAK-1-mediated phosphorylation of p100 in turn mediates the phosphorylation of p100.

A number of studies have identified TAK-1 as upstream in the IL-1 β -induced signalling pathway. TAK-1 has been shown to regulate IL-1 β signalling in innate immune cells and in disease-relevant cells such as human chondrocytes through TRAF6 ubiquitination, which recruits TAB2/3 subunits, resulting in TAK-1 autophosphorylation and activation via TAK-TAB complex; this was enhanced through IL-1R-mediated IRAK, TRAF6, and MyD88 recruitments in response to IL-1 β (Ajibade et al., 2013; Xu & Lei, 2021). TAK-1 inhibition has been shown to regulate MAP kinase signalling, and the canonical NF κ B pathway (Marine et al., 2022; Wang et al., 2022).

Experiments in this thesis showed similar findings, although there was some variation in the relative concentration sensitivity for each pathway, with JNK and p38 phosphorylation being highly sensitive to TAK-1 knockdown (Figures 4.19 and 4.20). However, despite several studies demonstrating multiple functions for TAK-1, there is no evidence to support the idea that TAK-1 may be directly involved in regulating p100, for example, by bringing IKK α into contact with p100 to allow phosphorylation to take place. If time allowed, TAK-1 immunoprecipitation experiments may have revealed binding of TAK-1 to p100, functioning as a substitute for NIK.

Further preliminary experiments were conducted to assess any additional aspects of co-regulation of the pathway. One MAP3 kinase studied was MEKK3. MEKK3 has been shown to work in concert with TAK-1 in regulating NF κ B signalling in response to IL-1 β and infection (Di et al., 2008; Sokolova et al., 2014; Zhang et al., 2019). However, siRNA strategies that significantly reduced MEKK3 protein expression were without effect either alone or in combination with TAK-1 knockdown (Figures 4.26 and 4.29).

MEKK3 has been shown to act as a central signalling site activated by upstream receptors or stressors such as TNF- α . Instead, it acts primarily by phosphorylation and activation of kinases downstream signalling, such as IKKs, triggering various signalling cascades, implicated in inflammation, including NF- κ B pathway (Sokolova et al., 2014; Zhang et al., 2019), cell growth and death through the Hippo/YAP/TAZ pathway, and angiogenesis (Lu et al., 2021). When this kinase is dysregulated, especially over-expressed and driving NF- κ B, it leads to pathologies such as cancer (Zhang et al., 2019).

Having established the signalling that is stimulated in response to IL-1 β in U2OS cells, such as activation of JNK and p38 signalling (Chen et al., 2019) and NF- κ B activation (Craig et al., 2025) (McIntosh et al., 2023; Vertegaal et al., 2000), the role of each cascade was examined. Initial experiments excluded the MAP kinase cascade. Pre-treatment of cells with selective inhibitors at various concentrations were found to be largely ineffective at inhibiting CXCL12 activity. For SP600125 (Bennett et al., 2001), inhibition of JNK phosphorylation was observed using Western blotting (Figure 4.30), confirming that the pre-treatment of the cells with compounds was effective. Whilst the effect of PD98059 and SB203580 on pERK and p38 MAP kinase were not studied in this thesis, there is ample evidence in the literature that these compounds are effective at these concentrations, such as SP600125 (Assi et al., 2006; Bennett et al., 2001), PD98059 and SB203580 (Kohno & Pouyssegur, 2003; Reiners Jr et al., 1998).

The findings in this thesis clearly indicated little involvement of MAP kinase pathways in the regulation of CXCL12 induction. However, there was a caveat, treatment with SB203580 was found to inhibit reporter activity by approximately 30% (Figure 4.31). Recent studies have shown that SB203580 inhibits Nemo-like kinase (NLK) (Ohnishi et al., 2010). Nemo-like kinase is a Serine/threonine MAP kinase (Coulombe & Meloche, 2007). NLK regulates several cellular functions in a cell-context-dependent manner via the Wnt signalling cascade (Ishitani et al., 2003).

More recent studies have expanded NLK's role in regulating migration, proliferation, and apoptosis through downstream signalling cascades including SMADs, AP-1, and T-cell factor/Lymphoid enhancer-binding factor (TCF/LEF) (Daams & Massoumi, 2020; Huang et al., 2015). Previous studies have illustrated crosstalk between NLK with MAPK (Ohnishi et al., 2010) and NF- κ B signalling (Li et al., 2014), a preliminary additional experiment in this thesis using pharmacological

inhibition showed that NLK had no effect on MAPK and NF- κ B signalling induced by IL-1 β . A study by Zhang and coworkers demonstrated the crosstalk of NLK with TAK-1-C/EBP β activation induced via IL-1 β , involving ATF5 (Activated transcription factor-5) stabilisation; however, this finding was not replicated in our study as TAK-1 siRNA did not affect CXCL12 induction (Zhang et al., 2015). If time allowed, studies using NLK siRNA may have been useful to determine if this kinase played a role in CXCL12 induction.

Other experiments focused on the role of IKK α in the regulation of CXCL12 induction. Initially, pharmacological evidence pointed to a role for IKK α in regulating CXCL12 reporter activity, as the IL-1 β response was sensitive to the selective IKK α inhibitor SU1261. SU1261 has been shown to be selective with respect to stimulation of the non-canonical NF κ B pathway (Anthony et al., 2017) and IL-1 β stimulation in HUVECs (Craig et al., 2025). However, no studies have looked at the effect of SU1261 on longer-term functions, and there is the possibility of off-target effects. This idea was supported by the finding that siIKK α was without effect on either reporter activity or protein/synthesis and release as assessed by ELISA. Indeed, a combination of siRNA/SU1261 strongly supported the notion of an off-target effect; SU1261 was effective in IKK α knockdown cells (Figure 4.35).

Certainly, more studies are needed to determine the off-target effects of SU1261 and other related compounds. Studies in drug development have shown caused off-target effects of most drugs examined using in *vivo* and in *vitro* models, which could actually work on both pharmacologically effective or provide side effects (Sadri, 2023). This effect was noted in SB203580, which inhibited phosphoinositide-dependent protein kinase 1 (PDK1) activity in IL-2 stimulated T cells through a p38-independent pathway (Lali et al., 2000), and Imatinib drug (Glevic), which inhibits c-Kit and PDGF receptor tyrosine kinases in addition to AB1 tyrosine kinase selectivity in chronic myeloid leukemia (Cismowski, 2007).

A similar problematic issue was indicated when assessing the role of TAK-1. Initially, there was strong pharmacological evidence in support of a role for TAK-1 in the regulation of CXCL12 induction; however, siRNA did not show any inhibition. One issue is the nature of the inhibition of TAK-1 by 7-oxo. Studies show that there is a kinetic action of 7-oxo; under different times of pre-treatment the potency of the drug is increased. Studies suggest that the concentration of 7-oxo to inhibit CXCL12 reporter activity is too high. Treatment of the B-NHL cell line with various

concentrations of 7-oxo over 2-16 h, resulted in a significant concentration and time-dependent reduction in cell viability. Furthermore, N-RAS mutant cancer cells exhibited concentration-dependent sensitivity to TAK-1 inhibition, showing variable responses across the same range of concentrations (Wu et al., 2013). Given that TAK-1 inhibition induces apoptosis in cells, it complicates the comparison of effects on CXCL12 induction and overall cell viability.

The role of IKK α in the regulation of gene induction has been studied in different models. IKK α regulates proinflammatory genes in a context-dependent manner. It activates TNF- α , IL-6 and CXCL2 in mouse lung epithelial cells (Yang et al., 2008) conversely, in macrophages and LPS-induced activation, IKK α inhibits TNF- α , IL-6, and IL-1 β expression (Lawrence et al., 2005). Additionally, IKK α regulates Bcl2, A1, and chemokines depending on specific cellular contexts (Häcker & Karin, 2006; Karin & Lin, 2002). Furthermore, LT β R activation by LIGHT or LT ligands caused the recruitment of IKK α to specific promoters, where IKK α phosphorylates histone H3 to facilitate NF- κ B-dependent transcription, including the induction of adhesion molecules ICAM-1 and VCAM-1 (Anest et al., 2003; Madge et al., 2008; M. J. Wolf et al., 2010). Studies have shown that IKK α knockdown blocked LIGHT or LT-mediated p52 formation in endothelial cells (Kucharzewska et al., 2019; Madge et al., 2008).

In contrast, TAK-1 regulation of IL-8 through NF- κ B activation has been previously demonstrated (Harada et al., 1994; Russo et al., 2014; Waugh & Wilson, 2008). In addition, IL-8 has AP-1 binding sites on the promoter, so this is likely to be regulated through TAK-1 via JNK and p38 MAP kinase pathways rather than IKK α (Russo et al., 2014; Waugh & Wilson, 2008). If time allowed, IKK α siRNA may have been used to clarify this finding further, but it was unlikely to be involved.

Finally, and intriguingly, experiments showed for the first time the potential for MEKK3 to regulate the induction of CXCL12. Transfection with siRNA inhibited both CXCL12 reporter activity and CXCL12 protein as assessed by ELISA (Figures 4.48 and 4.50). Equivalent studies assessing IL-8 formation showed no effect, suggesting that the effect was not a general effect on all inflammatory genes. This is the first identification of a role for MEKK3 in CXCL12 induction. In addition, the inhibitor Ponatinib (Choi et al., 2018) also showed strong inhibition of CXCL12 at low micromolar concentrations (Figure 4.49). It is of course recognised that there are considerable limitations of using such an inhibitor, which is recognised to be a multi-kinase inhibitor for Abelson tyrosine-

protein kinase 1 (ABL), FGFR, Non-Receptor and Receptor Tyrosine Kinase, PDGFR, VEGFR2, and RET, with significant toxicity as demonstrated *in vitro* and *in vivo* models (Choi et al., 2018; Gozgit et al., 2012).

The role of MEKK3 in the regulation of inflammatory gene induction is challenging to fit it into a model explaining the effect on CXCL12 induction. As we discussed above, MEKK3 significantly inhibited CXCL12 induction. However, a comprehensive examination of NF- κ B and MAPK signalling induced by IL-1 β showed no effect of MEKK3 on both NF- κ B and MAPK (particularly JNK) pathways, alone (Figures 4.25 and 4.26) or in combination with siRNA TAK-1 (Figures 4.27, 4.28, and 4.29). These findings are clear contrast to earlier research that showed MEKK3 involvement in IL-1 β -induced NF- κ B and JNK activation in fibroblasts and cancer cells (Qin et al., 2006; Yao et al., 2007; Zhang et al., 2019). Similarly, a study by Sokolova and coworkers demonstrated a crucial MEKK3 involvement in NF- κ B activation during *H. pylori* infection (Sokolova et al., 2014). Nevertheless, some additional studies are warranted to determine the validity of the observations.

Chapter Five

Characterisation of KM Compounds

on IL-1 β -stimulated CXCL12

induction in U2OS bone Cancer Cells

5.1 Introduction

Building on earlier findings, it can be stated that IL-1 β potently induces CXCL12 expression in U2OS osteosarcoma cells, as evidenced by increased both reporter activity and protein levels expression. These findings investigated the underlying signalling pathways and revealed a complex regulatory network involving multiple kinases and transcription factors. IL-1 β activated several central signalling cascades, including MAP kinases and NF- κ B pathways. However, these pathways did not play a significant role in IL-1 β -induced CXCL12 upregulation in osteosarcoma cells. Surprisingly, MEKK3 was implicated as a specific regulator of CXCL12 expression induced via IL-1 β , activated independently of classical inflammatory pathways.

In this chapter, a number of inhibitors of CXCL12 induction, previously identified, were screened by luciferase reporter assay in U2OS-CXCL12 cells. Several hits were synthesised and identified, as described in Chapter Three. These compounds, abbreviated as KM compounds, have not been extensively explored with respect to CXCL12 expression induced by proinflammatory cytokines. As this research aims to target CXCL12 induction rather than CXCR4/7 receptor activation, this chapter examines the impact of these KM compounds on IL-1 β -induced signalling cascades and CXCL12 expression.

5.2 The effect of novel KM compounds on IL-1 β -induced CXCL12 luciferase activity in U2OS cells

Following the synthesis of KM compounds, a number were tested on IL-1 β -induced CXCL12 expression in the osteosarcoma cell line using a luciferase reporter assay. After 1 h treatment with the KM compounds at a micromolar concentration range, cells were stimulated with IL-1 β for a further 6 h.

As shown in Figure 5.1, IL-1 β significantly induced a more than 3-fold increase in CXCL12 activity in U2OS cells compared to control. Following treatment with selected KM compounds, KM3, KM9, and KM10, there was no effect on IL-1 β -induced reporter activity. Additionally, preliminary results for compounds KM4 and KM7 were tested with high concentrations, and no effect on the reporter activity was observed. Furthermore, as shown in Figure 5.2, other tested compounds, KM2, KM5, and KM6, significantly inhibited CXCL12 activity after stimulation with IL-1 β . However, there was a noticeable effect on cell integrity and viability compared to untreated cells, as shown in Figure 5.3.

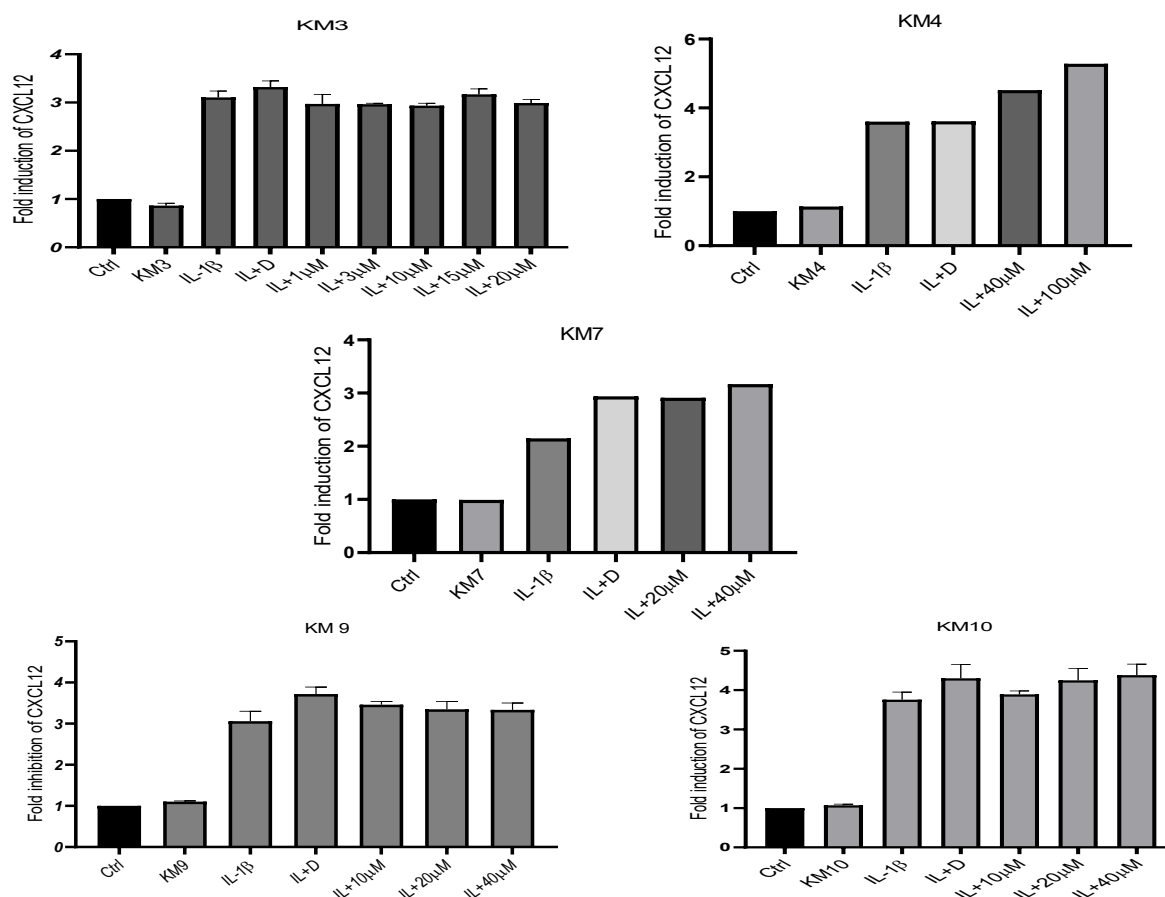


Figure 5.1 The effect of KM compounds upon IL-1 β -induced CXCL12 activity in U2OS-CXCL12 cells.

Cells were pre-treated with increasing concentrations of KM3, KM4, KM7, KM9, and KM10 for 1 h before stimulation with IL-1 β (IL, 10 ng/mL) for a further 6 h. Cell lysates were then measured for luciferase activity, as previously described in Section 2.5.1. Data shown expressed as fold induction, and each value represents the mean \pm SEM of three independent experiments. Data was analysed using a one-way ANOVA test.

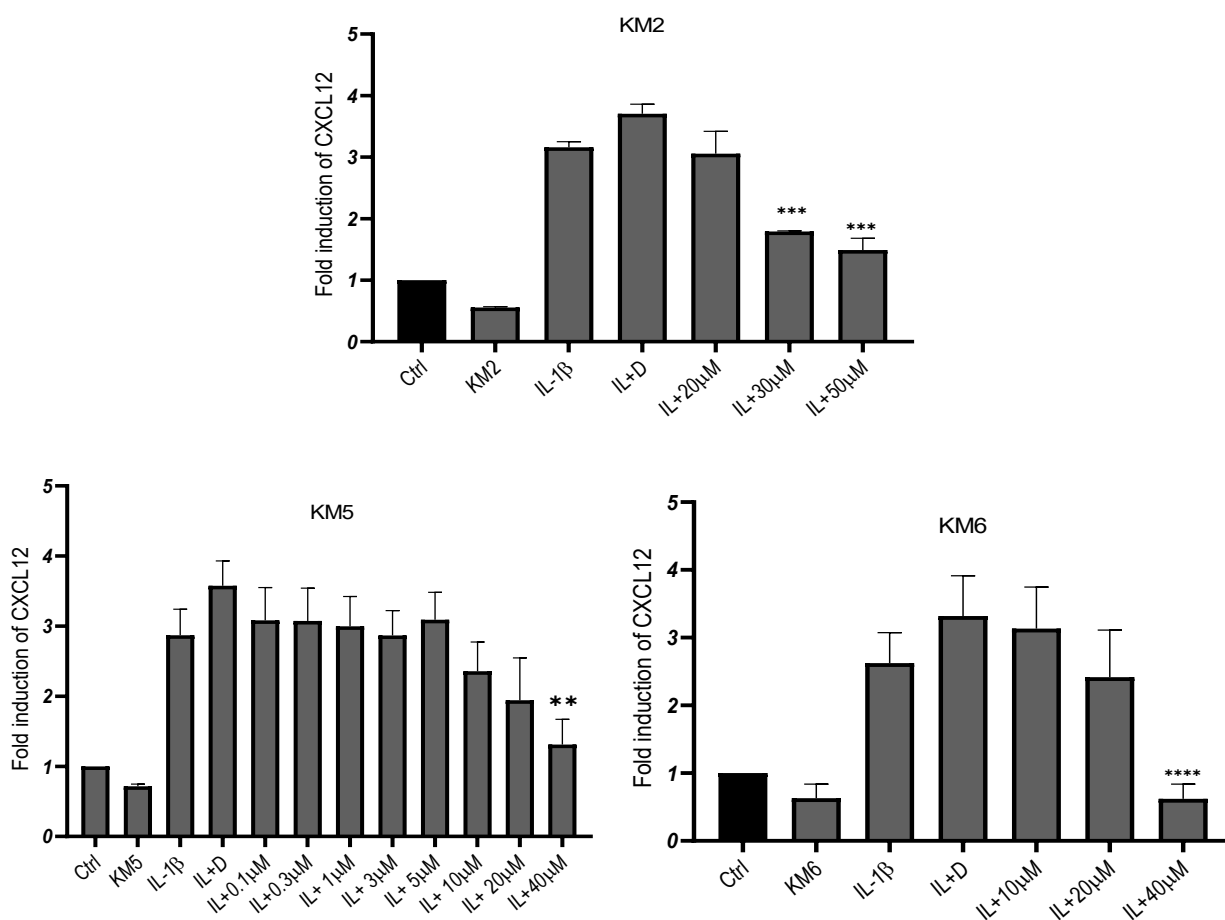


Figure 5. 2 The effect of KM compounds upon IL-1 β -induced CXCL12 activity in U2OS cells. Cells were pre-treated with increasing concentrations of KM2, KM5, and KM6 for 1 h before stimulation with IL-1 β (IL,10 ng/mL) for a further 6 h. Cell lysates were then measured for luciferase activity, as previously described in Section 2.5.1. Data shown expressed as fold induction, and each value represents the mean \pm SEM of three independent experiments. Data was analysed using a one-way ANOVA test, ****P<0.0001, ***P<0.001, **P<0.01 vs IL-1 β and DMSO as an agonist-stimulated control.

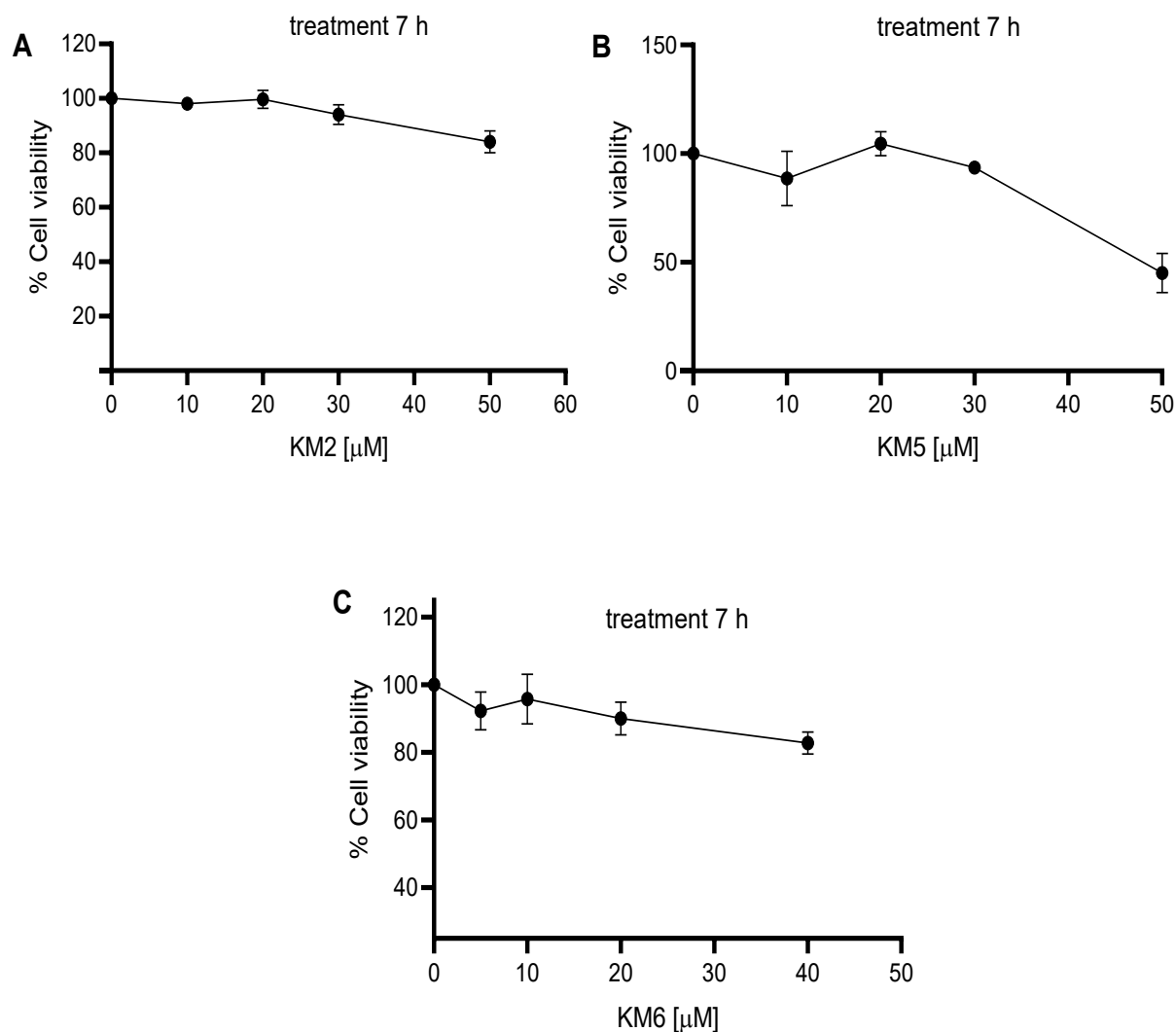


Figure 5. 3 Effect of KM compounds KM2, KM5, and KM6 on U2OS cell viability.

Cells were grown in 96-well plates and examined with MTT assay as previously described in Section 2.6, using various concentrations of KM compounds, KM2 (A), KM5 (B), and KM6 (C) for 7 h. U2OS cells treated with DMSO provided a negative control, and H₂O₂ (400 μ M) acted as a positive control. Triplicates were used for each experiment. Data shown expressed as U2OS cell viability in three independent experiments. The results were normalised to treated control and plotted on a log scale as a percentage of the control relative to absorbance.

In conducting the previous experiments, two promising compounds that showed a significant effect on IL-1 β -induced CXCL12 activity in U2OS cells were KM8 and KM11. Figure 5.4 shows the inhibitory effect of KM8 on IL-1 β -induced CXCL12 activity. IL-1 β significantly increased CXCL12 reporter activity by more than 3-fold (Fold stims= 3.37 ± 0.46 , $P < 0.05$). Following treatment with **KM8** over the 0.3-20 μ M concentration range, there was a significant concentration-dependent reduction in the reporter activity (Fold stim at 10 μ M- 1.39 ± 0.52 , IC_{50} = 5.21 μ M, $P < 0.05$).

Similarly, Figure 5.5 shows IL-1 β -induced more than 3-fold in CXCL12 activity (Fold stims = 3.43 ± 0.48 , $P < 0.01$). However, in cells treated with **KM11** over the same micromolar range, CXCL12 reporter activity was significantly inhibited between 5-20 μ M (Fold stims at 10 μ M- 1.26 ± 0.23 , IC_{50} =2.45 μ M, $P < 0.01$).

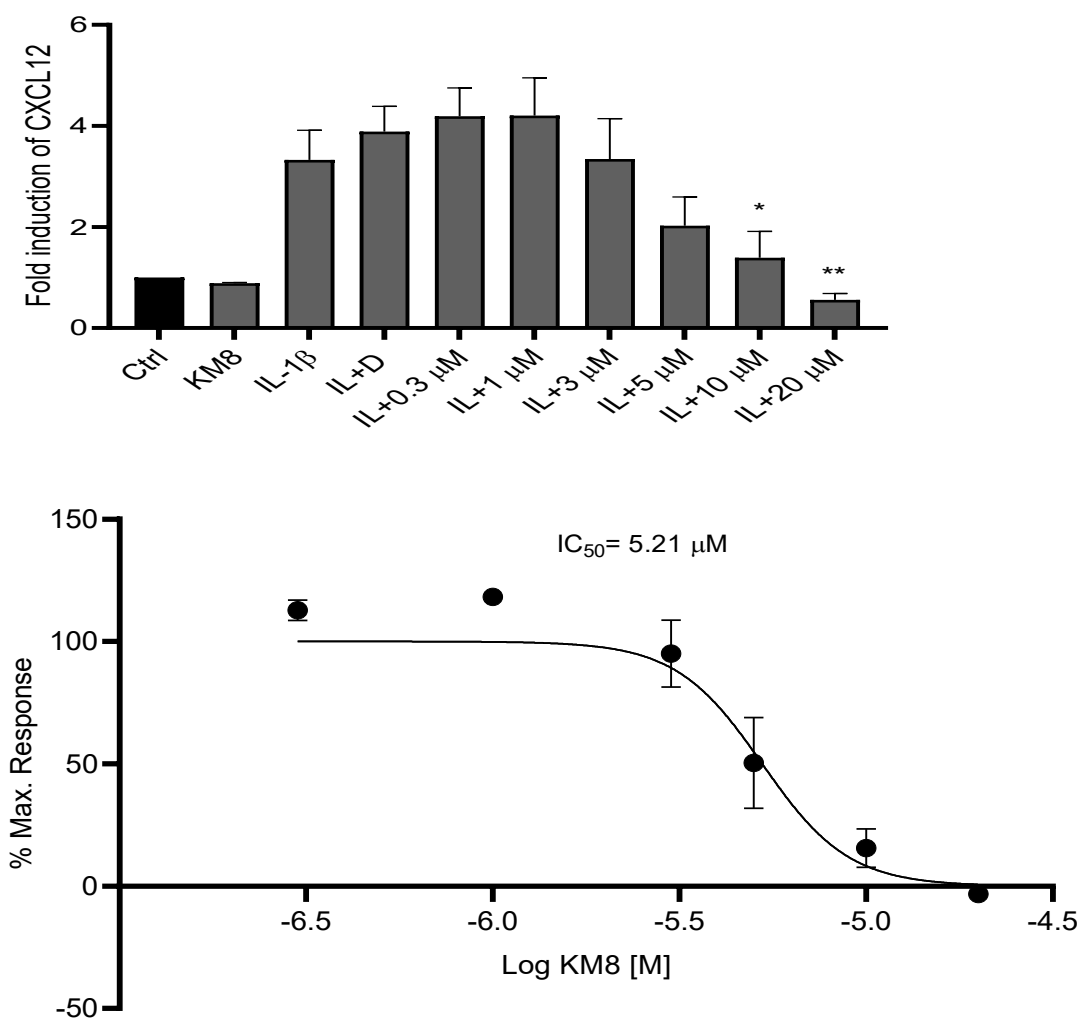


Figure 5. 4 The effect of KM8 upon IL-1β-induced CXCL12 activity in U2OS cells.

Cells were pre-treated with increasing concentrations of KM8 for 1h before stimulation with IL-1β (IL,10 ng/mL) for a further 6 h. Cell lysates were then measured for luciferase activity as previously described in Section 2.5.1. Data shown expressed as fold induction, and each value represents the mean \pm SEM of three independent experiments. Data was analysed using a one-way ANOVA test, **P<0.01, *P<0.05 vs. IL-1β, and DMSO as an agonist-stimulated control.

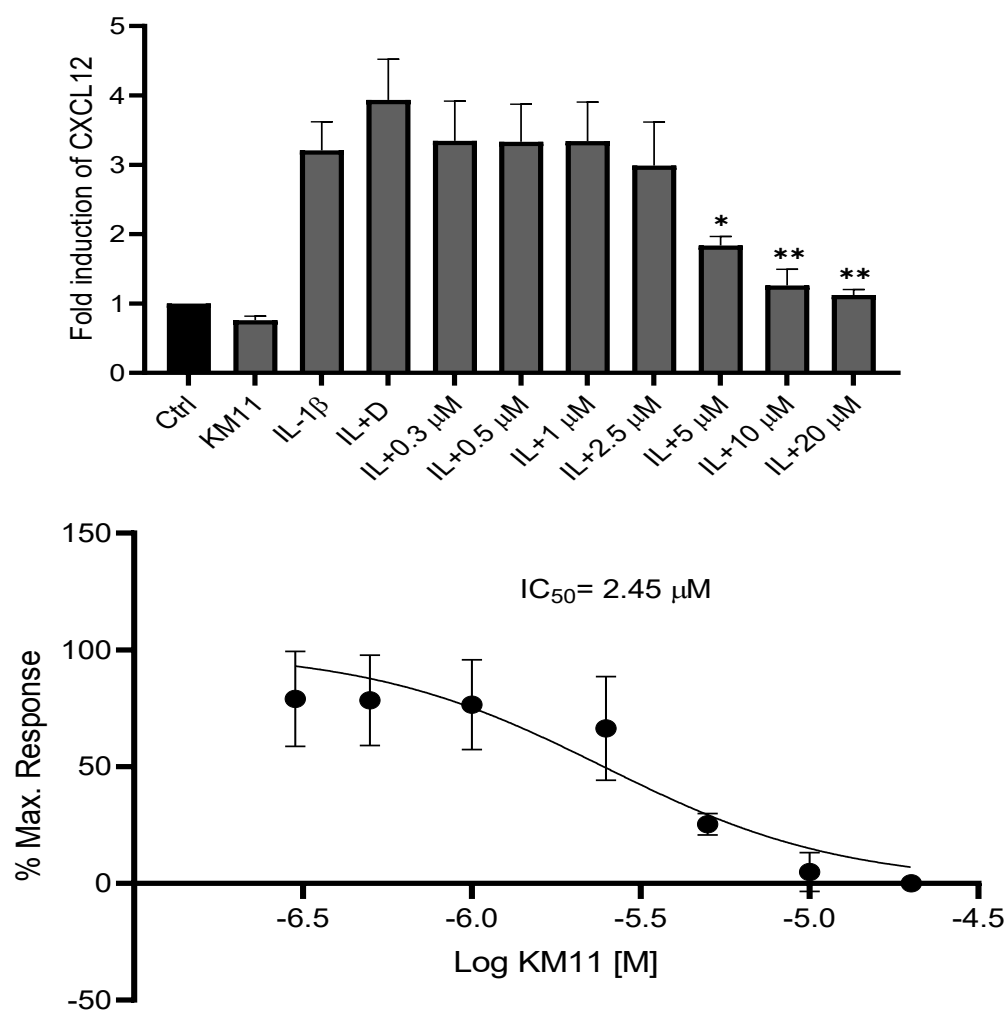


Figure 5. 5 The effect of KM11 upon IL-1 β -induced CXCL12 activity in U2OS cells.

Cells were pre-treated with increasing concentrations of KM11 for 1h before stimulation with IL-1 β (IL,10 ng/mL) for a further 6 h. Cell lysates were then measured for luciferase activity as previously described in Section 2.5.1. Data shown expressed as fold induction, and each value represents the mean \pm SEM of three independent experiments. Data was analysed using a one-way ANOVA test, **P<0.01, *P<0.05 vs. IL-1 β , and DMSO as an agonist-stimulated control.

5.3 Effect of novel KM compounds on luciferase enzyme activity

To exclude the direct effect of KM compounds **KM8** and **KM11** on luciferase enzyme activity, the compounds were assessed post-stimulation. Following 6 hours of stimulation, KM8 and KM11 were added to IL-1 β -stimulated lysates 7 min before reading the absorbance. Figure 5.6 (A) shows a non-significant effect of KM8 at a concentration range between 5-20 μ M, with little impact on luciferase enzyme activity at 40 μ M concentration. Additionally, Figure 5.6 (B) showed no significant reduction in luciferase enzyme activity over a concentration range of KM11. These results suggest *bona fide* effects of both compounds on IL-1 β -induced CXCL12 activity.

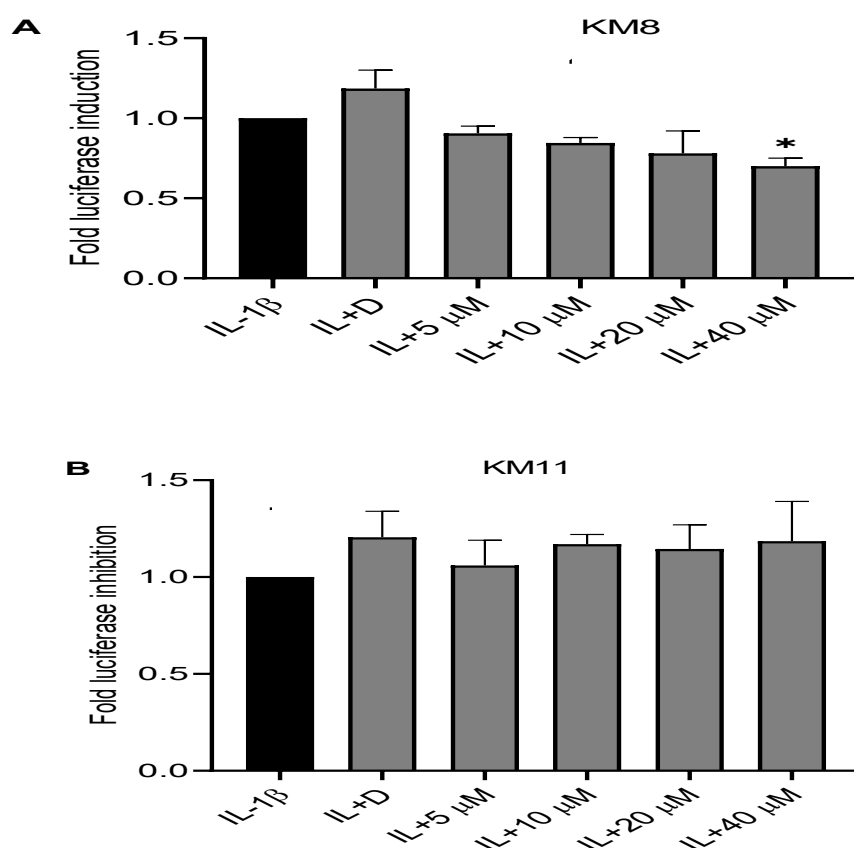


Figure 5. 6 The effect of KM compounds on luciferase enzyme activity in U2OS Cells.

Cells were stimulated with IL-1 β (IL,10 ng/mL) for 6 h. Stimulated cell lysates were treated with KM compounds for 7 min, then the luciferase activity was measured as previously described in Section 2.5.3. Data shown expressed as luciferase fold induction for A) KM8 and B) KM11, and each value represents the mean \pm SEM of three independent experiments. Data was analysed using a one-way ANOVA test, *P<0.05 vs IL-1 β as an agonist-stimulated control.

5.4 Effect of novel CXCL12 inhibitors on U2OS cell viability using MTT assay

The effects of the KM8 and KM11 compounds on U2OS cell integrity and viability were assessed using an MTT assay. Cells were treated with increasing concentrations of the compounds and incubated for different periods, as shown in Figures 5.7 (KM8) and 5.8 (KM11). The results illustrated the effect of both KM compounds on U2OS cell viability at 20 μ M, reducing control levels by approximately 9 % for KM8 and 14 % for KM11 (% cell viability = 91 %, 86 %, respectively), with no effect over the lower micromolar range (1-10 μ M).

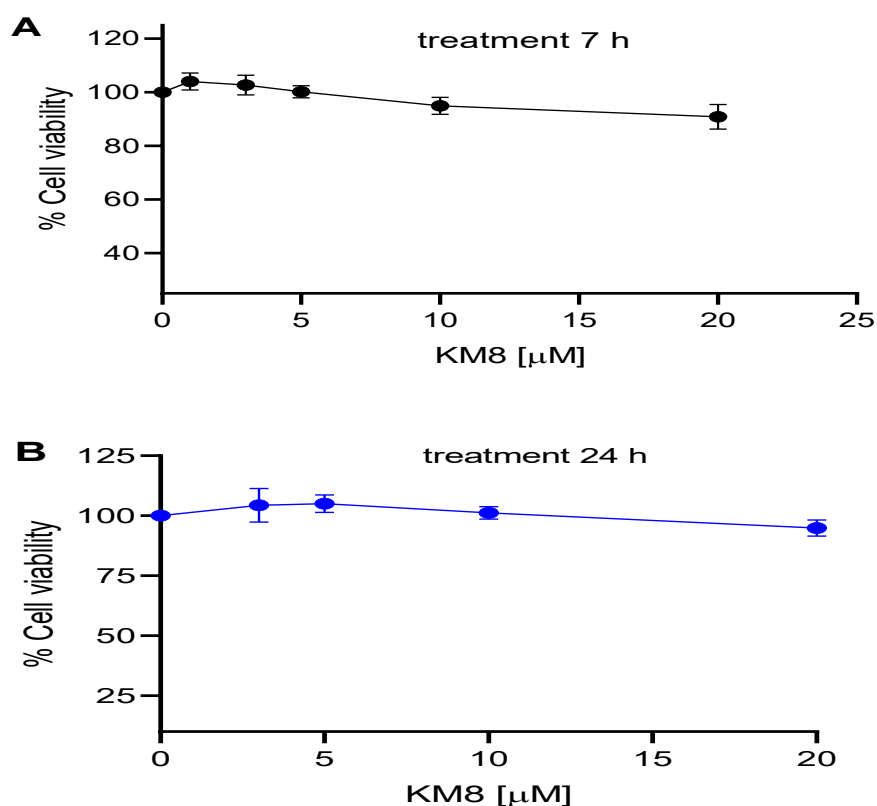


Figure 5. 7 Effect of KM8 on U2OS cell viability.

Cells were grown in 96-well plates and examined with the MTT assay as previously described in Section 2.6, using various concentrations of KM8 (1-20 μ M) for 7 h (A) and (3-20 μ M) for 24 h (B). U2OS cells treated with DMSO provided a negative control, and H₂O₂ (400 μ M) acted as a positive control. Triplicates were used for each experiment. Data shown expressed as U2OS cell viability of three independent experiments. The results were normalised to treated control and plotted on a log scale as a percentage of the control relative to absorbance.

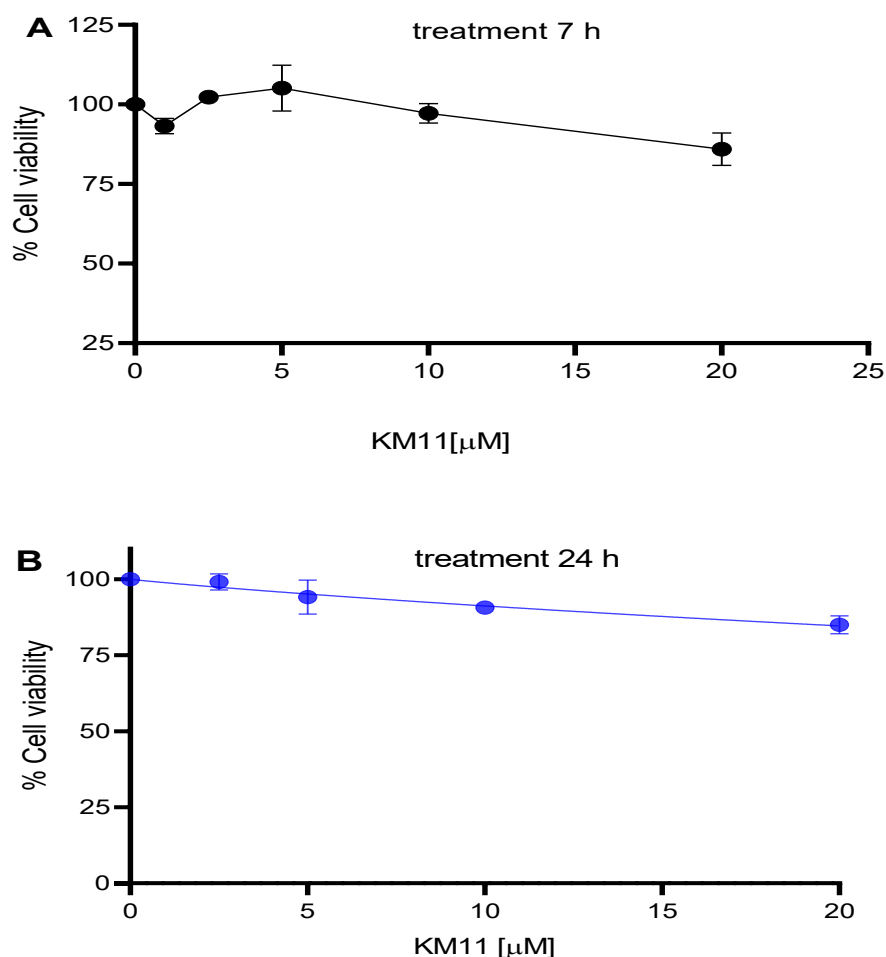


Figure 5. 8 Effect of KM11 on U2OS cell viability.

Cells were grown in 96-well plates and examined with the MTT assay as previously described in Section 2.6, using various concentrations of KM11 (1-20 μ M) for 7 h (A) and (3-20 μ M) for 24 h (B). U2OS cells treated with DMSO provided a negative control, and H_2O_2 (400 μ M) acted as a positive control. Triplicates were used for each experiment. Data shown expressed as U2OS cell viability of three independent experiments. The results were normalised to treated control and plotted on a log scale as a percentage of the control relative to absorbance.

5.5 Effect of novel CXCL12 inhibitors on IL-1 β -induced CXCL12 protein expression in U2OS cells

The luciferase reporter activity data suggested differences in CXCL12 activity in response to IL-1 β used in this study and the impact of two novel compounds, KM8 and KM11, in regulating this expression. Therefore, the effect of KM8 and KM11 in CXCL12 regulation was verified using an ELISA assay.

5.5.1 Effect of KM8 on IL-1 β -Induced CXCL12 Protein Expression using ELISA in U2OS cells.

The effect of KM8 in regulating CXCL12 induction was examined. Following 6 h stimulation, IL-1 β produced a more than 45-fold increase in CXCL12 protein expression at 10 ng/mL (Fold expression = 46.58 ± 4.27 , $P < 0.0001$). As shown in Figure 5.9, this response was significantly inhibited by KM8, IL-1 β stimulation was reduced markedly between 10-20 μ M (Fold expression for IL-1 β + 10 μ M KM8 - 14.50 ± 2.80 , IL-1 β + 20 μ M - 5.25 ± 1.82 , $P > 0.0001$). This result strongly confirms the inhibitory effect of KM8 on CXCL12 expression induced by IL-1 β .

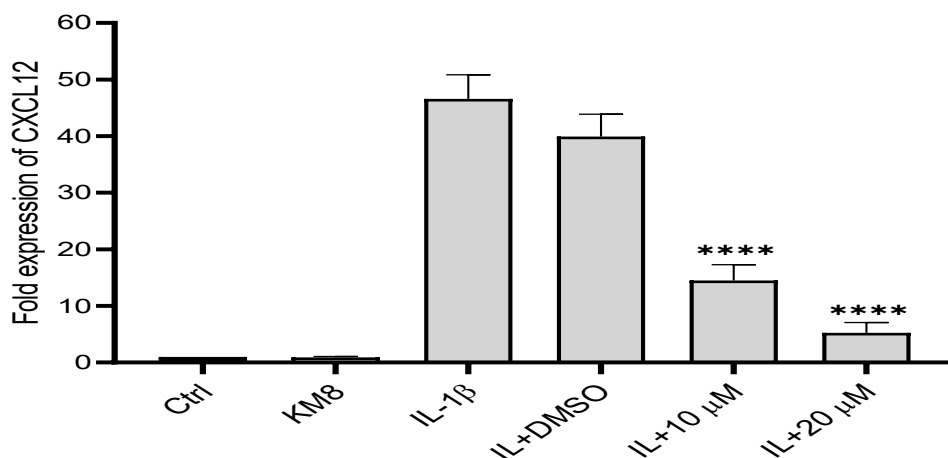


Figure 5. 9 The effect of KM8 upon CXCL12 protein levels in U2OS cells.

Cells were seeded in 6-well plates and pre-treated with increasing concentrations of KM8 for 1 h before stimulation with IL-1 β (IL, 10 ng/mL) for a further 6 h. Supernatants were collected, and the CXCL12 protein levels were assessed by ELISA assay, as outlined in Section 2.7. Three independent experiments were performed in duplicate, and the results expressed as means \pm SEM. Data was analysed using a one-way ANOVA test. **** $P < 0.0001$ vs agonist-stimulated control.

5.5.2 Effect of KM11 Compound on IL-1 β -Induced CXCL12 Protein Expression using ELISA in U2OS cells.

Following 6 h stimulation, IL-1 β produced a more than 45-fold increase in CXCL12 protein expression at 10 ng/mL (Fold expression = 46.58 ± 4.27 , $P < 0.0001$). This response was significantly inhibited by KM11, as shown in Figure 5.10, where IL-1 β stimulation reduced at 10 μ M (Fold expression for IL-1 β + 10 μ M- 26.33 ± 4.16 , $P < 0.05$), with strongest inhibition at 20 μ M (Fold expression for IL-1 β + 20 μ M- 20.03 ± 4.13 , $P < 0.001$). This result strongly confirms the inhibitory effect of KM11 on CXCL12 expression induced by IL-1 β .

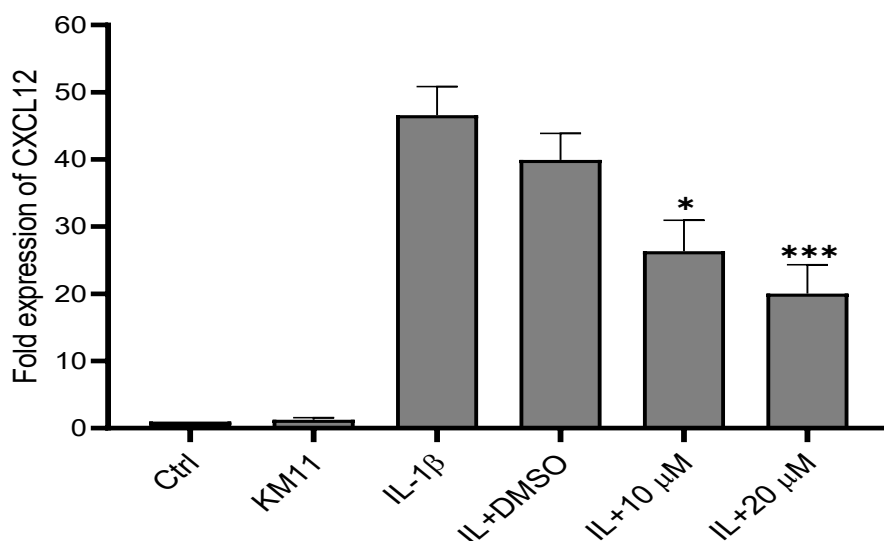


Figure 5. 10 The effect of KM11 upon CXCL12 protein levels in U2OS cells.

Cells were seeded in 6-well plates and pre-treated with increasing concentrations of KM11 for 1 h before stimulation with IL-1 β (IL, 10 ng/mL) for a further 6 h. Supernatants were collected, and the CXCL12 protein levels were assessed by ELISA assay, as outlined in Section 2.7. Three independent experiments were performed in duplicate, and the results expressed as means \pm SEM. Data was analysed using a one-way ANOVA test. *** $P < 0.001$, * $P < 0.05$ vs agonist stimulated control.

5.5.3 Effect of Novel CXCL12 Inhibitors on IL-1 β -Induced IL8 Protein Expression in U2OS Cells

In order to confirm and extend the results obtained from the luciferase reporter assay and the CXCL12 ELISA assay on the impact of KM compounds, KM8 and KM11, the effect of both compounds on IL-8 protein expression induced by IL-1 β was examined.

5.5.3.1 Effect of KM8 on IL-1 β -induced IL8 protein expression in U2OS Cells

Following 24 h stimulation, IL-1 β produced an approximately 30-fold increase in IL-8 protein expression at 10 ng/mL (Fold expression = 30.02 ± 3.79 , $P < 0.05$). Figure 5.11 shows that KM8 had no significant effect on IL-8 and slightly increased IL-8 expression with increasing concentration compared to IL-1 β -stimulated cells. This result robustly confirmed the targeting effect of KM8 against CXCL12 expression induced by IL-1 β in U2OS cells.

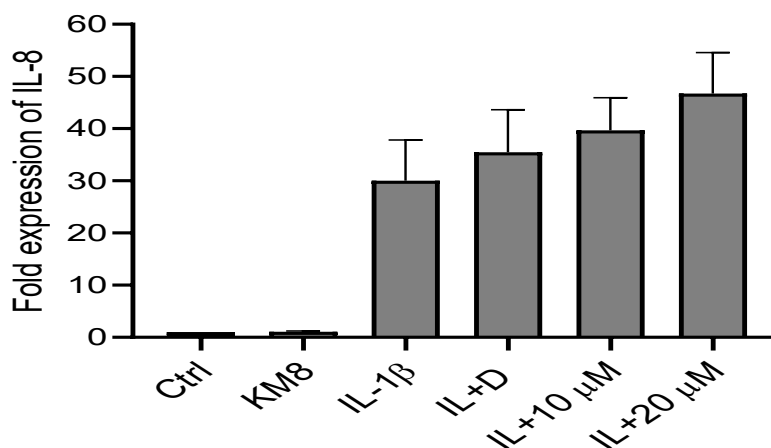


Figure 5. 11 The effect of KM8 upon IL-8 protein levels in U2OS cells.

Cells were seeded in 6-well plates and pre-treated with increasing concentrations of KM8 for 1 h before stimulation with IL-1 β (IL,10 ng/mL) for a further 24 h. Supernatants were collected, and the IL-8 protein levels were assessed by ELISA assay as outlined in Section 2.7. Three independent experiments were performed in duplicate, and the results expressed as means \pm SEM. Data was analysed using a one-way ANOVA test, ns, non-significant vs agonist-stimulated control.

5.5.3.2 Effect of KM11 Compound on IL-1 β -Induced IL8 Protein Expression in U2OS Cells

The effect of KM11 on IL-8 induction was examined using 10 and 20 μ M concentrations of the compound. Following 24 h stimulation, IL-1 β produced an approximately 25-fold increase in IL-8 protein expression at 10 ng/mL (Fold expression = 25.35 ± 3.37 , $P < 0.01$). Figure 5.12 showed no effect of **KM11** on IL8 expression at 10 μ M concentration, with a slight increase in protein expression at 20 μ M concentration compared to the IL-1 β -stimulated control.

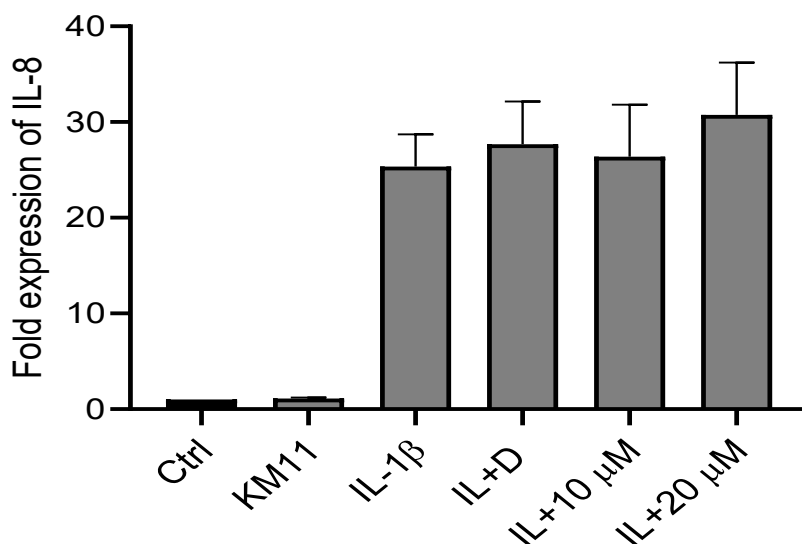


Figure 5. 12 The effect of KM11 upon IL-8 protein levels in U2OS cells.

Cells were seeded in 6-well plates and pre-treated with increasing concentrations of KM11 for 1 h before stimulation with IL-1 β (IL, 10 ng/mL) for a further 24 h. Supernatants were collected, and the IL-8 protein levels were assessed by ELISA assay, as outlined in Section 2.7. Three independent experiments were performed in duplicate, and the results expressed as means \pm SEM. Data was analysed using a one-way ANOVA test.

5.6 Effect of Novel CXCL12 Inhibitors (KM Compounds) on IL-1 β -induced MAPK Signalling in U2OS Cells

5.6.1 Effect of KM8 Compound on IL-1 β -Induced JNK Phosphorylation in U2OS Cells

The previous results in this study showed that a significant effect of KM8 and KM11 on CXCL12 activity highlighted further experiments to demonstrate their impact on the signalling pathways. Both KM compounds were tested on IL-1 β -induced cellular signalling, starting with the MAPK pathway, mainly JNK, a downstream signalling component. As shown in Figure **5.13**, IL-1 β induced more than a 20-fold increase in JNK phosphorylation in U2OS cells (Fold stims = 25.97 ± 1.62 , $P < 0.0001$) compared to non-stimulated cells. Pre-treatment of the cells in a concentration-dependent manner for KM8 (1-20 μ M) did not alter this response.

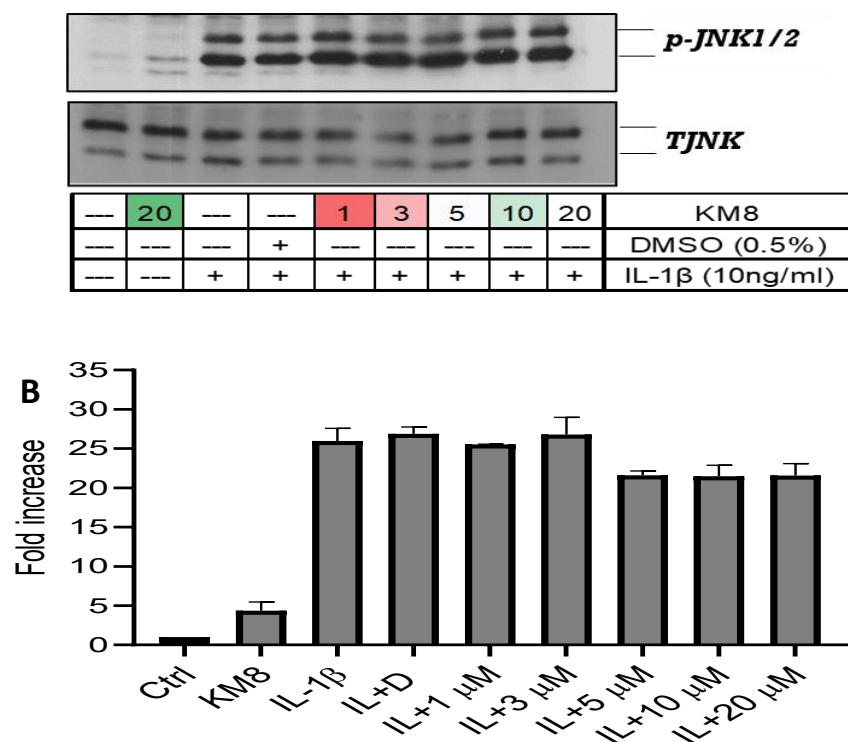


Figure 5. 13 Effect of KM8 on IL-1 β -induced phosphorylation of JNK in U2OS cells.

Cells were pre-treated with increasing concentrations of KM8 for 1 h before stimulation with IL-1 β (IL,10 ng/mL) for a further 30 min. Whole-cell extracts were assessed for A) pJNK phosphorylation (46,54 kDa) and total JNK (54,46 kDa), which was used as a loading control. Blots were semi-quantified by scanning densitometry, and the result was expressed as a fold increase relative to control for B) pJNK. Each value represents the mean \pm SEM of three independent experiments. Data was analysed using a one-way ANOVA test.

5.6.2 Effect of novel CXCL12 inhibitors upon IL-1 β -Induced Canonical NF- κ B Signalling in U2OS Cells

5.6.2.1 Effect of KM8 Compound on IL-1 β -Induced Cellular I κ B- α loss and Phosphorylation of p65 in U2OS Cells.

The effect of the KM8 compound was then tested on the two main components of the canonical NF- κ B pathway, cellular I κ B α loss and phosphorylation of p65, in response to IKK β activation. Figure 5.14 showed that IL-1 β induced significant I κ B α degradation by about 94% (% basal I κ B α expression = 6, $P < 0.0001$) compared to the basal. Pre-treatment of the cells in a concentration-dependent manner for KM8 (1-20 μ M) did not abolish the cellular I κ B α loss in stimulated cells.

Furthermore, following a 40-fold increase in p65 phosphorylation induced by IL-1 β at 30 min (Fold stim = 41.17, $P < 0.0001$), KM8 had no inhibitory effect on p65 phosphorylation.

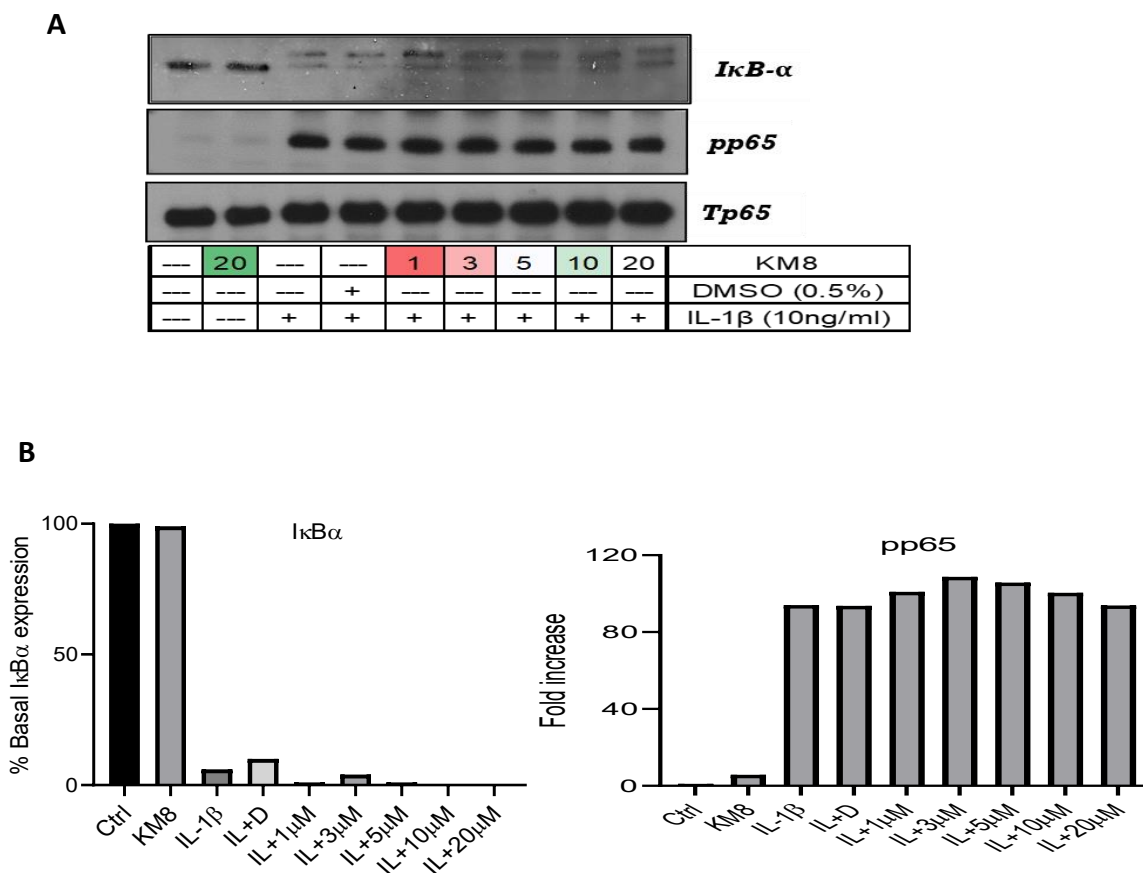


Figure 5. 14 Effect of KM8 on IL-1 β -induced cellular I κ B α loss and phosphorylation of p65 in U2OS cells.

Cells were pre-treated with increasing concentrations of KM8 for 1 h before stimulation with IL-1 β (IL, 10 ng/mL) for a further 30 min. Whole-cell extracts were assessed for A) I κ B α loss (39 kDa), p65 phosphorylation (65 kDa), and total p65 (65 kDa), which was used as a loading control. Blots were semi-quantified by scanning densitometry, and the result expressed as a fold increase relative to control for B) I κ B α and p-p65. Each value represents two experiments.

5.6.3 Effect of Novel CXCL12 Inhibitors on IL-1 β -Induced Non-Canonical NF- κ B Signalling in U2OS Cells.

5.6.3.1 Effect of KM8 Compound on IL-1 β -Induced p100 Phosphorylation and p52 Formation in U2OS Cells

The same experiment was done for the non-canonical NF- κ B pathway to assess the effect of both KM compounds on p100 phosphorylation. Figure **5.15** showed that IL-1 β induced a more than 3-fold increase in p100 phosphorylation at 30 min compared to non-stimulated cells (Fold stims = 3.39 ± 0.83 , $P < 0.001$). Following pretreatment with the KM8 compound in the micromolar range (1-20 μ M), the phosphorylation of p100 was increased gradually at concentrations of 1-5 μ M, with a non-significant reduction at 10-20 μ M compared to the stimulated control. Moreover, compared to the control, KM8 did not affect p100/p52 levels in pretreated cells.

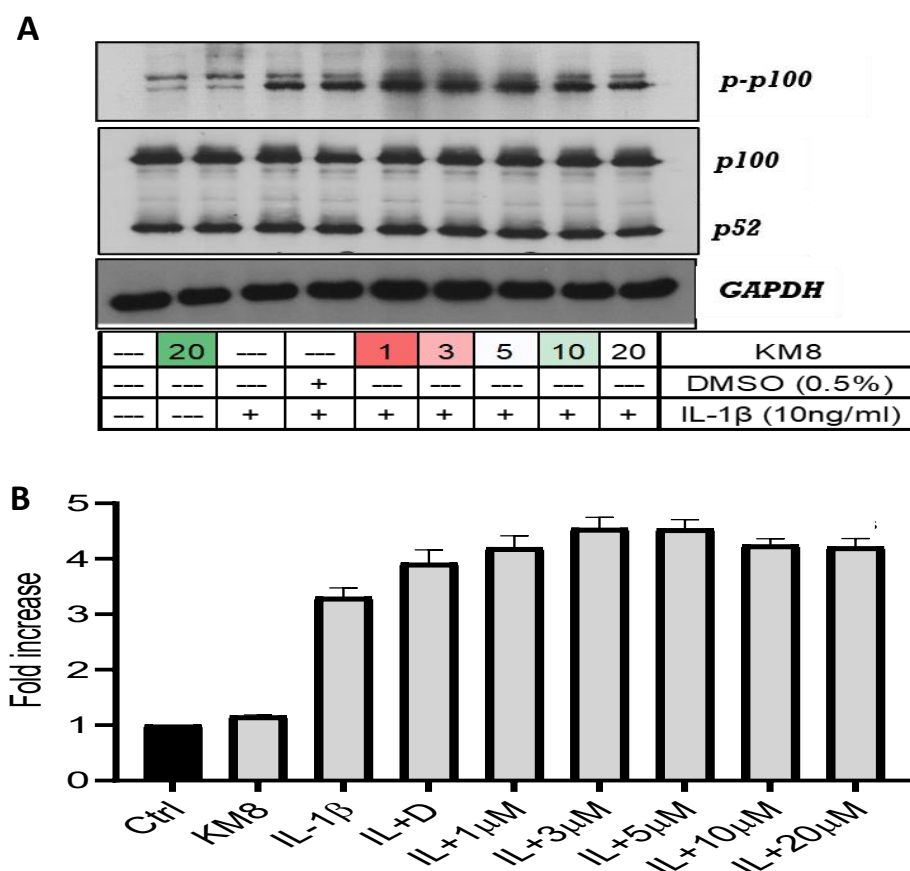


Figure 5. 15 Effect of KM8 on IL-1 β -induced phosphorylation of p100 in U2OS cells.

Cells were pre-treated with KM8 for 1 h before stimulation with IL-1 β (IL, 10 ng/mL) for a further 30 min. Whole-cell extracts were assessed for A) p100 phosphorylation (100 kDa), p52 (52 kDa), and GAPDH (37 kDa), which was used as a loading control. Blots were semi-quantified by scanning densitometry, and the results expressed as a fold increase relative to control for B) p-p100. Each value represents the mean \pm SEM of three independent experiments. Data was analysed using a one-way ANOVA test.

5.7 Effect of KM11 on IL-1 β -Induced signalling pathways in U2OS cells

5.7.1 Effect of KM11 on IL-1 β -induced JNK phosphorylation in U2OS cells

The same experiment was carried out for KM11. Figure 5.16 showed that IL-1 β -induced more than a 20-fold increase in JNK phosphorylation in U2OS cells (Fold stim= 21.44, $P < 0.0001$) compared to control. Pre-treatment of the cells with KM11 (1-20 μ M) had no inhibitory effect on this response. The results revealed that both KM compounds have no effect on IL-1 β -induced JNK phosphorylation-mediated MAPK pathway in U2OS cells.

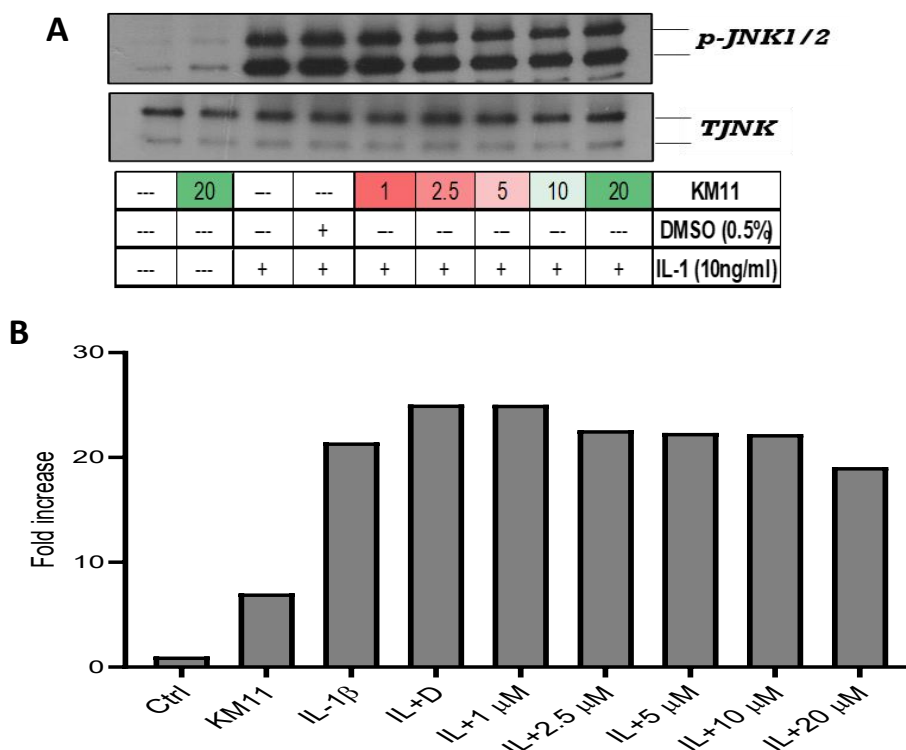


Figure 5. 16 Effect of KM11 on IL-1 β -induced phosphorylation of JNK in U2OS cells.

Cells were pre-treated with increasing concentrations of KM11 for 1 h before stimulation with IL-1 β (IL,10 ng/mL) for a further 30 min. Whole-cell extracts were assessed for A) JNK phosphorylation (46,54 kDa) and total JNK (46,54 kDa), which was used as a loading control. Blots were semi-quantified by scanning densitometry, and the results expressed as a fold increase relative to control for B) pJNK. Each value represents two independent experiments.

5.7.2 Effect of KM11 on IL-1 β -induced NF κ B pathway in U2OS Cells

The effect of the KM11 compound was also tested on the canonical IKK β -dependent pathway. Figure 5.17 showed that IL-1 β -induced significant I κ B α degradation by approximately 93% (% basal I κ B α expression = 7, $P < 0.0001$) compared to the basal. Pre-treatment of the cells in a concentration-dependent manner with KM11 (1-20 μ M) did not reverse the cellular I κ B α loss in stimulated cells. Furthermore, KM11 alone did not significantly affect basal expression of I κ B α .

Furthermore, whilst IL-1 β -induced a 3-fold increase in p65 phosphorylation at 30 min (Fold stim = 3.17 ± 0.68 , $P < 0.001$), KM11 had no impact on p65 phosphorylation. These results reveal that KM8 and KM11 compounds have no inhibitory effect on the IKK β -dependent NF- κ B pathway in U2OS cells.

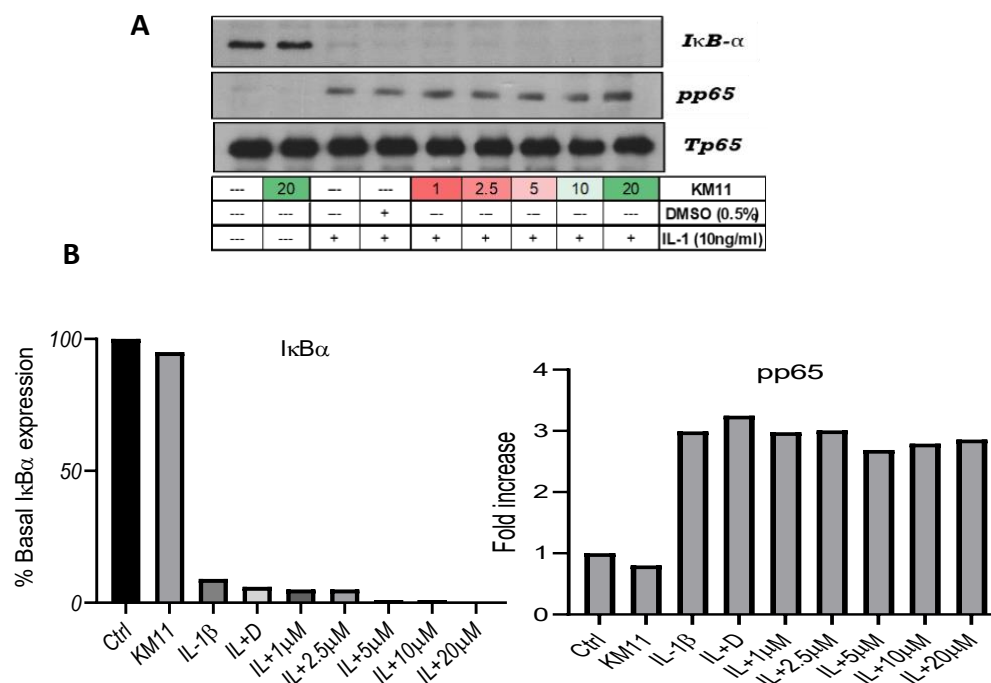


Figure 5. 17 Effect of KM11 on IL-1 β -induced cellular I κ B α loss and phosphorylation of p65 in U2OS cells.

Cells were pre-treated with increasing concentrations of KM11 for 1 h before stimulation with IL-1 β (IL, 10 ng/mL) for a further 30 min. Whole-cell extracts were assessed for A) I κ B α loss (39 kDa), p65 phosphorylation (65 kDa), and total p65 (65 kDa), which was used as a loading control. Blots were semi-quantified by scanning densitometry, and the results expressed as a fold increase relative to control for B) I κ B α and p-p65. Each value represents two independent experiments.

5.7.3 Effect of KM11 on IL-1 β -Induced p100 phosphorylation and p52 Formation in U2OS cells

Next, the effect of KM11 was examined on IKK α signalling. Figure 5.18 showed that IL-1 β -induced a more than 3-fold increase in p100 phosphorylation at 30 min compared to non-stimulated cells (Fold stim= 3.54 ± 1.03 , $P < 0.001$). Pre-treatment with the KM11 compound across micromolar range (1-20 μ M), do not affect the agonist response. Moreover, there was no alteration in p100/p52 levels in pre-treated cells compared to the control. These findings show that KM8 and KM11 compounds have no inhibitory effect on IKK α within the non-canonical NF- κ B pathway in U2OS cells stimulated by IL-1 β .

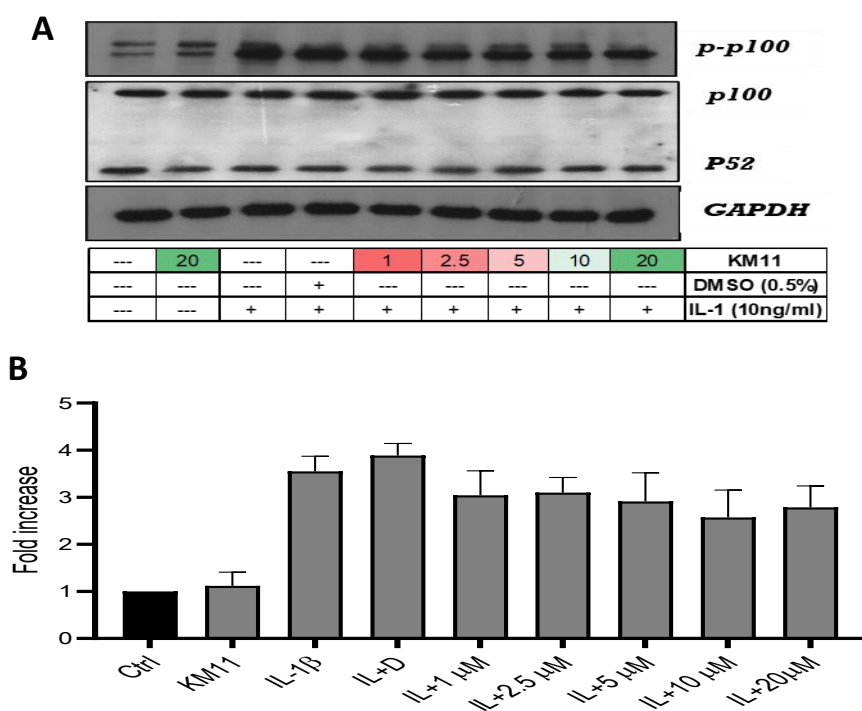


Figure 5. 18 Effect of KM11 on IL-1 β -induced phosphorylation of p100 in U2OS cells.

Cells were pre-treated with KM11 for 1 h before stimulation with IL-1 β (IL, 10 ng/mL) for 30 min. Whole-cell extracts were assessed for A) p100 phosphorylation (100 kDa), p52 (52 kDa), and GAPDH (37 kDa), which was used as a loading control. Blots were semi-quantified by scanning densitometry, and the results expressed as a fold increase relative to control for B) p-p100. Data shown expressed as fold increase, and each value represents the mean \pm SEM of three independent experiments. Data was analysed using a one-way ANOVA test.

5.8 Discussion

This chapter explored the effects of novel compounds and their ability to inhibit IL-1 β -induced signalling and CXCL12 induction. This was based on the identification of a number of hits from a preliminary screening of 5000 commercial compounds on CXCL12 reporter activity carried out by BioAscent, ESC. The screening results showed the potential to target CXCL12 induction in addition to the use of CXCR4 antagonists in chemotherapeutic treatment, for example, Plerixafor (AMD3100), approved by the FDA, and MSX-122 (Bao et al., 2023; Ghasemi & Ghasemi, 2022). As discussed in Chapter One, these antagonists are used in cancer treatment and have shown limitations in clinical trials.

A promising strategy for treating cancer is the development of targeted medicines against the CXCL12 expression. Various studies have shown that many advanced therapies have been developed against the effect of CXCL12, which work with radiation and chemotherapy (Bobbin & Rossi, 2016; Giordano et al., 2024). The optimisation of CXCL12 inhibition strategies remains the central area of the current study. To date, no effective strategy for inhibiting CXCL12 induction has been developed despite the fact that CXCL12 release in the TME is significant.

The initial evaluation of KM compounds using the reporter assay found that most KM compounds had no significant effect on IL-1 β -induced CXCL12 activity. However, some compounds inhibited CXCL12 activity only at high concentrations up to 50 μ M, which obviously affected cell integrity and viability (Figure 5.3). While such compound limitations can be discouraging in the context of therapy, it is informative for compound optimisation using a future structure-activity relationship. Previous findings from an experimental study of CXCR4 antagonists suggested that at higher concentrations, these antagonists exhibited inhibition, coupled with cytotoxicity, a common obstacle to drug development (Sun et al., 2003). Nevertheless, more potent, less toxic drugs were subsequently developed from this starting point.

Notably, interesting results were obtained for the first time using KM8 and KM11, which were considered the most active compounds in this examination study. KM8 showed effective inhibition of CXCL12 induction across the 10-20 μ M range (Figure 5.4), while KM11 was slightly more potent (Figure 5.5). Both compounds were effective at concentrations well below the cytotoxic

level observed these and for other KM compounds. The values are higher than those of other reported CXCR4 antagonists (Mercurio et al., 2016; Zabel et al., 2009).

While the reporter assay showed significant reduction in CXCL12 activity, the luciferase enzyme activity validated the selectivity of these effects and confirmed reduced CXCL12 level with close to no impact on the enzyme itself, especially for KM11, confirming that the downregulation of the supernatant protein is a selective modulation of CXCL12 expression and not targeted towards the enzyme (Figure 5.6). Both compounds had a favourable cytotoxicity profile as a distinguishing feature, the adverse effect on cell viability using an MTT study at concentrations up to 20 μ M, was found to be very minor (Figures 5.7 and 5.8). This highlights the favourable drug-like properties of both compounds.

The ELISA data provided critical confirmation of the findings in the reporter assay for the tested KM compounds and also pointed towards selective inhibition. KM8 and KM11 effectively inhibited IL-1 β -induced CXCL12 protein expression at micromolar concentrations (Figures 5.9 and 5.10), but did not significantly affect IL-1 β -mediated production of IL-8, with a slight increase in its expression (Figures 5.11 and 5.12), further emphasising a unique activity of the compounds specific to CXCL12 expression.

These findings link to the understanding of signalling pathways driving CXCL12 induction, examined in this thesis, and IL-8 production. KM8 and KM11 were ineffective against IL-1 β -induced MAP kinase and NF κ B pathways, supporting the notion that a different signalling pathway is involved for CXCL12 induction, one which KM8 and KM11 have the potential to inhibit, for example, NLK or MEKK3. If time had allowed, kinase profiling of the KM compounds, or individual kinase assays might have revealed the effect of these compounds on MEKK3, NLK or other kinases.

In contrast, IL-8 induction has been shown to be controlled by both MAP (p38, ERK1/2) and NF κ B kinases in various cells, including cancer cells (He et al., 2013; Hwang et al., 2004; Matsumoto et al., 1998; Mukaida, 2003). Given that both KM compounds were not effective against these pathways in U2OS cells, the finding that they do not inhibit IL-8 fits with these

results. The fact that these compounds are ineffective again indicates a degree of selectivity but also a lack of off-target effects.

Based on the obtained data in this chapter, KM8 and KM11 are novel CXCL12 inhibitors in U2OS cells with undiscovered, independent of classic regulatory mechanisms (IKK α and IKK β) of IL-1 β -induced CXCL12 expression. These findings are consistent with prior data establishing that inhibition of CXCL12, in general, principally blocks multiple signalling cascades in various cancer cells (Chinni et al., 2006; X. Liu et al., 2014; Yin et al., 2019).

Chapter Six

General Discussion and Conclusion

6.1 General Discussion and Future Work

The chemokine, CXCL12 (SDF-1), is highly expressed by bone marrow stromal cells and CAFs (Nagasawa, Hirota, et al., 1996; Orimo et al., 2005). It plays a role in controlling immune cell trafficking (Bernardini et al., 2008), and organ vascular development (Ara et al., 2005), through CXCR4 signalling. It also profoundly affects cancer progression due to its effects on cells within the tumour microenvironment. Osteosarcoma is a common type of bone cancer, mainly affecting adolescents and accounts for approximately 40% of primary malignant bone cancer (Ziyu Ji et al., 2023). The pathogenesis of OS includes many genetic mutations that identify the conversion of normal cells to cancerous ones, such as mesenchymal stem/stromal cells (MSCs) or osteoblast precursor lineages (Czarnecka et al., 2020). Significantly, chemokines and their receptor, CXCR4 are now recognised as critical mediators influencing tumour growth and metastasis in various cancers, including osteosarcoma. Experimental studies evidenced this role through a consistent increase in specific CXC chemokines, which was observed in pediatric OS patients (Li et al., 2011). A dysregulated pattern of chemokine receptor expression was examined in OS tumours, suggesting signalling cascades that enhance malignancy (Von Luetichau et al., 2008). CXCR4/CXCL12 signalling is examined as a key pathway and functionally involved in OS hallmarks through inducing proliferation, survival, and homing (Perissinotto et al., 2005). Preliminary treatment strategies have concentrated on directly targeting this pathway. A number of inhibitors for the CXCL12 receptor, CXCR4, have been developed for the treatment of certain cancers (Zhou et al., 2019). For example, research employing AMD3100 (Plerixafor), a particular CXCR4 antagonist, has demonstrated promising results in reducing tumour burden and metastasis in a number of cancer models (Y. X. Liao et al., 2015; Scala, 2015). However, these drugs showed limited clinical success with an unknown safety profile (Bao et al., 2023; Ghasemi & Ghasemi, 2022).

Today, all the researchers worldwide are competing to discover a new way to find a drug that treats cancer with minimal side effects. Crystallographic and computational studies using structural insights have enabled rational drug design models for improving inhibitor specificity and pharmacokinetics (Kumar et al., 2018). The use of computational chemistry techniques, such as

molecular docking, has provided detailed data on the inhibitor binding mode (Prieto-Martínez et al., 2019). The 3D structure of CXCL12 has been recently examined (R. Janssens et al., 2018). Thus, the potential of CXCL12 in the drug design field was demonstrated to be viable.

In addition, novel inhibitors of CXCL12 induction have been synthesised, which can target CXCL12 induction rather than the CXCR4 receptor, thereby maximising the activity and reducing the off-target effect. Recently, the University of Dundee reported that a number of compounds were of interest, having been identified through screening commercial compounds against the CXCL12 gene expression induced by IL-1 β . For these reasons, our study aimed to identify chemical structures that can effectively inhibit CXCL12 signalling by abolishing its expression. Some reported compounds (KM6, KM10, and KM11) demonstrated in Table 3.1 were successfully synthesised in the Jamieson lab using various approaches. Their temperature stability were also examined as described in Chapter Three. If time had allowed, a further QSAR study for these compounds would have been conducted to determine the pharmacophore essential in chemical stability and molecular activity to compare them with the lead compounds during pharmacological testing.

Next, the role of these KM compounds in CXCL12 induction and IL-1 β -mediated signalling pathways activation was examined after the investigation and characterisation of IL-1 β -induced signalling cascades. This concept will be demonstrated in detail shortly.

As mentioned previously, studies have shown that various cellular factors, including proinflammatory cytokines, hypoxia, and growth factors, induced CXCL12 expression (Kryczek et al., 2005; Liu et al., 2020; Yu et al., 2017). Regulation of this expression within the tumour microenvironment is associated with the development of tumour hallmarks in various cancer cells (Scotton et al., 2002; Yang et al., 2023). These increased levels of CXCL12 were due to activation of various signalling cascades, such as MAPK and NF- κ B pathways, in response to proinflammatory cytokines, as reported in some experimental studies using cancer cell lines (Madge et al., 2008; Yu et al., 2018).

Specifically, studies focused on IL-1 β -induced CXCL12 expression in U373 glioma cells through specific binding motifs located on the CXCL12 promoter region (García-Moruja et al., 2005). This finding highlights the need to evaluate the promoter region in osteosarcoma U2OS cells, which revealed its active usage in a cell cycle-dependent manner in our work.

Initially, in five independent experiments using a luciferase reporter assay described in Chapter four, it was shown that IL-1 β treatment resulted in a 4-fold increase of CXCL12 expression at 6-8 h. Therefore, this cell line is ideal for studying cell signalling parameters with respect to CXCL12 induction. Then, the signalling experiments sought to focus on the MAP kinase pathway, where the CXCL12 promoter is known to have a c/EBP β site within the promoter region (Calonge et al., 2010). Studies have shown that c/EBP β phosphorylation is essential for action as a transcription factor that increases CXCL12 activity upon treatment with IL-1 β or cellular confluence (Calonge et al., 2010; Kim et al., 2007). Studies show that this is controlled principally by ERK through phosphorylation on threonine 235 or 188 residues (Hungness et al., 2002; Park et al., 2004; Raymond et al., 2006). The initial finding did not support the idea of ERK activation as a significant pathway for CXCL12 induction in this cell type; ERK activity was negligible relative to other cell studies where the relationship between ERK and c/EBP β has been studied. Indeed, additional experiments showed some increased phosphorylation of c/EBP β , but that was well out with the time span for CXCL12 induction. Interesting to note that, unlike some studies in osteosarcoma cells, in which IL-1 β was effective in activating ERK (Huang et al., 2009), this differential pattern of activation in the two pathways proposed engagement of the selective MAPK pathway, as earlier proposed by (Pyrillou et al., 2020).

The results in this study showed that IL-1 β was able to activate JNK, a well-recognised signalling cassette downstream of IL-1 receptor activation. This pathway needs investigation in other cancer cell types, such as breast or pancreatic cancer cells, to confirm its role related to CXCL12 induction. The role of ERK/cEBP in the regulation of CXCL12 by virtue of a lack of ERK activity, having questioned, and an examination of the NF κ B pathway was indicated. Whilst no putative NF κ B sites are featured in the CXCL12 promotion, is it possible that the pathway plays an indirect role, as yet uncharacterised.

Previous studies showed the significant inhibition of IL-1 β -induced I κ B α loss (Baxter et al., 2004; Kishore et al., 2003), including some from our laboratory, which showed reversal of I κ B α loss, albeit at high concentrations of inhibitor (McIntosh et al., 2023). Effective reversal of I κ B α loss was found most convincingly using DN IKK β adenovirus (Craig et al., 2025). Our results showed that IL-1 β strongly stimulated the canonical NF κ B pathway, as assessed by examining the loss of I κ B α and phosphorylation of p65. However, identifying a role for IKK β remained difficult. While IKK β rundown using siRNA was successful, the effect on I κ B α loss was negligible, and a high concentration of the IKK β inhibitor used was only partially effective.

While some studies suggest IKK α can function as a substitute for IKK β in the canonical NF κ B pathway in various cells (Adli et al., 2010; Prescott et al., 2022). This may not occur in U2OS cells. Preliminary experiments showed minimal I κ B α reversal following siRNA IKK β in combination with SU1261. This result indicates either incomplete IKK β inhibition by the compound or that only minimal active IKK β is needed for amplification.

Studies have shown that TAK-1 operates as a regulatory kinase upstream of IKK β in the canonical cascade. Indeed, preincubation with the TAK-1 inhibitor, 5Z-7oxo, was able to fully reverse the loss in I κ B α in response to IL-1 β . This aligns with a number of studies in immune and cancer models, which show that many stimuli, such as IL-1 β and TNF, activate and phosphorylate TAK-1, resulting in IKK complex phosphorylation, particularly IKK β , which directly phosphorylates I κ B α and enhances its proteasomal degradation (Mukhopadhyay & Lee, 2020; Sakurai, 2012). However, TAK-1 siRNA knockdown could not cause reversals in IL-1 β -induced I κ B α loss, and the degree of inhibition of IKK β phosphorylation was limited to 66%. Therefore, it is again possible that residual IKK beta activity is sufficient to cause activation of the canonical NF κ B pathway.

A second and striking aspect of IL-1 β -induced signalling is related to “non-canonical” NF κ B signalling. Previous findings in endothelial cells (Craig et al., 2025), and in U2OS and DU145 cell lines (McIntosh et al., 2023); demonstrated that IL-1 β -induced p100 phosphorylation was transient and not associated with the formation of p52, a phenomenon usually associated with non-canonical NF κ B signalling, driven by agonists such as LIGHT, LT, CD40L and others (Cildir et al., 2016;

Sun, 2011, 2017). Our findings in Chapter four showed that IL-1 β mediated a strong increase in the phosphorylation of p100 NF κ B2. In the previous study in U2OS cells, CRISPR induced the deletion of IKK α , which significantly reduced p100 phosphorylation (McIntosh et al., 2023). Our results also confirmed that pre-incubation with IKK α siRNA or pre-treatment with SU1261, a selective IKK alpha inhibitor, effectively reduced p100 phosphorylation. In contrast, IKK β siRNA had no effect on IL-1 β -induced p100 phosphorylation, suggesting that this mode of phosphorylation is indeed IKK α -dependent.

Regarding the non-canonical NF κ B pathway, it has been shown that the upstream MAP3K NIK has a predominant role. Studies show that following activation of NIK by TNF family members (CD40L, BAFF) and others, NIK directly phosphorylates human IKK α at specific residues (Ser176/180) in biochemical experiments, activating its kinase activity as reported in an *in vitro* kinase assay (Ling et al., 1998). Similarly, Xiao and coworkers demonstrated the importance of NIK in the non-canonical NF κ B pathway activation through p100 phosphorylation; they showed that wild-type NIK expression in NIK-deficient cells restored the activation of IKK α and p100 phosphorylation with p52 formation (Xiao et al., 2004; Xiao et al., 2001). Another experimental study showed that whilst pharmacological inhibition of NIK using CW15337 compound could inhibit LT or LIGHT-induced p100 phosphorylation in either U2OS cells or HUVECs, the compound did not affect the IL-1 β response. This suggests that NIK is not required to bring IKK α into proximity with p100 as has been suggested by previous studies (Craig et al., 2025; McIntosh et al., 2023).

As we discussed in Chapter Four, NIK is well recognised to be essential for the degradation of p100 and the formation of p52 (Xiao et al., 2004; Xiao et al., 2001), resulting in nuclear translocation and regulating target genes through p52/RelB dimers (Sun, 2017). Huge studies have evidenced that NIK knockout in B cells, fibroblasts, or Human embryonic kidney cells blocked p100 phosphorylation and p52 generation by preventing IKK α phosphorylation (Sun, 2017; Xiao et al., 2001). Experiments identified TAK-1 as being essential for p100 phosphorylation. Pre-treatment of cells with the TAK-1 inhibitor, 5Z-7oxo, results in a concentration-dependent inhibition of p100 phosphorylation, whereas treatment with TAK-1 siRNA causes a significant,

albeit partial, inhibition. Additional experiments showed that IL-1 β induction of pIKK α was also reduced by TAK-1 inhibition. Taken together, this would suggest that TAK-1-mediated phosphorylation of p100 in turn mediates the phosphorylation of IKK α .

TAK-1 inhibition has been shown to regulate MAP kinase signalling, and the canonical NF κ B pathway (Marine et al., 2022; Wang et al., 2022). Our results in this thesis showed similar findings, with JNK and p38 phosphorylation being highly sensitive to TAK-1 knockdown. However, despite the data from several studies demonstrating multiple functions for TAK-1, there is no evidence to support the idea that TAK-1 may be directly involved in regulating p100, for example, by bringing IKK α into contact with p100 to facilitate phosphorylation. If time allowed, TAK-1 immunoprecipitation experiments may have revealed binding of TAK-1 to p100, functioning as a substitute for NIK.

Further preliminary experiments were conducted to assess any additional aspects of co-regulation of the pathway. One MAP3 kinase studied was MEKK3. MEKK3 has been shown to work in concert with TAK-1 in regulating NF κ B signalling in response to IL-1 β and infection (Di et al., 2008; Sokolova et al., 2014; Zhang et al., 2019). However, siRNA strategies that significantly reduced MEKK3 protein expression were ineffective either alone or in combination with TAK-1 knockdown.

As mentioned previously, MEKK3 has been shown to act as a central signalling site activated by upstream receptors or stressors such as TNF- α . Instead, it acts primarily by phosphorylation and activation of kinases downstream signalling, such as IKKs or MAP4Ks, triggering various signalling cascades, implications for inflammation, including the NF- κ B pathway (Sokolova et al., 2014; Zhang et al., 2019). However, MEKK3 did not substitute MAPK signalling-mediated IL-1 β -induced JNK and p38 activation, nor did NF- κ B signalling mediate IKK α and p100 phosphorylation in U2OS cells. Further experiments, including CRISPR or genetic studies, are required to investigate the downstream signalling cascades mediated by MEKK3 activation.

Having established the signalling that is stimulated in response to IL-1 β in U2OS cells, such as activation of JNK and p38 signalling (Chen et al., 2019) and NF- κ B activation (Craig et al., 2025) (McIntosh et al., 2023; Vertegaal et al., 2000), the role of each cascade was examined.

Our result from treatment with SB203580 indicates that it inhibits CXCL12 reporter activity by approximately 30%. This was a caveat in our experimental findings. Recent studies have shown that SB203580 inhibits Nemo-like kinase (NLK) (Coulombe & Meloche, 2007). Later studies expand NLK's role in regulating cellular processes through downstream signalling cascades described in Chapter Four. However, depending on previous studies that illustrated the crosstalk of NLK with MAPK (Ohnishi et al., 2010) and NF- κ B signalling (Li et al., 2014), a preliminary additional experiment using pharmacological inhibition showed that NLK had no effect on MAPK and NF- κ B signalling induced by IL-1 β . A study by Zhang and coworkers demonstrated the crosstalk of NLK with TAK-1-c/EBP β activation induced via IL-1 β , involving ATF5 stabilisation; however, this finding was not replicated in our study (Zhang et al., 2015). If time allowed, studies using NLK siRNA may have been useful to determine if this kinase played a role in CXCL12 induction.

Other experiments focused on the role of IKK α in regulating CXCL12 induction. Initially, pharmacological evidence pointed to a role for IKK α in the regulation of CXCL12 reporter activity, as the IL-1 β response was sensitive to the selective IKK α inhibitor SU1261. SU1261 has been shown to be selective with respect to inhibition of agonist stimulation of the non-canonical NF- κ B pathway (Anthony et al., 2017) and IL-1 β stimulation in HUVECs (Craig et al., 2025). However, no studies have examined the long-term effect of SU1261, and there is the possibility of off-target effects. This idea was supported by the finding that siIKK α did not affect reporter activity or protein synthesis and release as assessed by ELISA. Indeed, a combination of siRNA and SU1261 strongly supported the notion of an off-target effect; SU1261 was effective in IKK α knockdown cells. Furthermore, pre-treating cells with TAK-1 siRNA showed a moderate effect on CXCL12 at the level of reporter activity and ELISA.

As we mentioned in Chapter Four, the off-target effects of SU1261 and other tested compounds remain to be fully characterised. Given that such effects are a well-documented source of efficacy and toxicity, as reported in Imatinib and SB203580, future studies must address this effect (Cismowski, 2007; Lali et al., 2000; Sadri, 2023).

The assessment of TAK-1's role is complicated by pharmacological limitations. The inhibitor 7-oxo showed time-dependent potency and a high concentration was required for efficacy, which can induce apoptosis and complicate the interpretation of specific pathway inhibition, as demonstrated previously in hematological cancer models (Wu et al., 2013). This difference is highlighted by the contrast between strong initial pharmacological evidence for the role of TAK-1 in CXCL12 induction and the lack of inhibition observed by siRNA.

The kinase IKK α is a regulator of inflammation, demonstrating cell and stimulus-specific functions. It can act as either an activator or a repressor of classic proinflammatory cytokines, as mentioned previously (Lawrence et al., 2005; Yang et al., 2008). Furthermore, IKK α plays a nuclear role in the non-canonical NF- κ B pathway, where it is recruited to promoters by ligands such as LIGHT to drive the expression of genes including ICAM-1 and VCAM-1 in endothelial cells (Madge et al., 2008; M. J. Wolf et al., 2010). This functional flexibility highlights the importance of defining the specific context when determining the contribution of IKK α to a biological process.

Initial data as explained in Chapter Four, using USOS cells, revealed a distinct inflammatory effect in response to IL-1 β , characterised by a lack of VCAM-1 and ICAM-1 induction but evidence of TAK-1 and NF- κ B-dependent IL-8 production (Roccaro et al., 2014; Waugh & Wilson, 2008). Given that IL-8 expression is strongly associated with AP-1 and MAPK signalling rather than IKK α , this result may explain the absence of adhesion molecule upregulation (Russo et al., 2014; Waugh & Wilson, 2008). Ultimately, the use of IKK α siRNA would be required to definitively confirm that its role in this pathway is negligible.

Finally, and interestingly, our findings showed for the first time the potential for MEKK3 to regulate the induction of CXCL12. Both CXCL12 reporter activity and CXCL12 protein level were inhibited via siRNA knockdown as assessed by reporter and ELISA assays. Equivalent studies assessing IL-8 level showed no effect, suggesting that the selective impact is toward the CXCL12 gene and not a general inflammatory response. Additionally, the inhibitor Ponatinib demonstrated potent inhibition of CXCL12 at low micromolar concentrations, which is recognised to be a multi-

kinase inhibitor, including MEKK3 inhibition, as shown *in vitro* and *in vivo* models with kinase assay (Choi et al., 2018; Gozgit et al., 2012).

As discussed above, MEKK3 significantly inhibited CXCL12 induction. However, a comprehensive investigation of NF- κ B and MAPK signalling induced by IL-1 β revealed no effect of MEKK3 on either NF- κ B or MAPK, or in combination with siRNA TAK-1, suggesting a MEKK3-independent pathway, which stands in clear contrast to earlier research that exhibited involvement of MEKK3 in IL-1 β -induced NF- κ B and JNK activation in fibroblasts and cancer cells (Qin et al., 2006; Yao et al., 2007; Zhang et al., 2019). A similar study confirmed the role of MEKK3 in NF- κ B activation during *H. pylori* infection (Sokolova et al., 2014). If time allowed, MEK5/ERK5 signalling may have been used to investigate it further as downstream signalling for MEKK3 (Drew et al., 2012; Wang & Tournier, 2006).

As mentioned in Chapter Three, preliminary studies reported the assay of 5,000 compounds in U2OS cells transfected with the CXCL12 promoter to assess their effect on promoter activity using a reporter assay. The screening results showed that some of these compounds significantly affect the IL- β -induced CXCL12 expression, and these findings highlighted the importance of discovering and investigating the novel targets that could replace the existing pathway for CXCR4 antagonists in chemotherapeutic treatment. As discussed in Chapter One, these antagonists are used in cancer treatment and have shown drawbacks in clinical trials. The synthesis and temperature stability analysis of the KM compounds were successfully evaluated. KM10 and KM11 compounds showed good chemical stability under various storage conditions for up to 7 days, particularly at 25 °C and 37 °C.

At 50 °C, slight fluctuations in the readings were observed, but they remained within acceptable limits, indicating its relative tolerance to high temperatures in the short term. In contrast, the KM6 compound exhibited reduced stability with mild degradation in its chemical composition. An analytical evaluation suggests that further experimental replication and investigation are required.

Our study focused on inhibiting CXCL12 expression induced via IL-1 β to create more potent targeted therapies using the osteosarcoma U2OS cell line model.

In this study, different experimental approaches were utilised to elucidate the mechanism of action of a new class of CXCL12 inhibitors (KM) compounds and their ability to modulate CXCL12 expression. To date, no published studies have investigated and characterised these compounds' effect on CXCL12 induction mediated via proinflammatory cytokines, including IL-1 β or TNF- α .

The initial evaluation of KM compounds using the reporter assay found that most KM compounds had no significant effect on IL-1 β -induced CXCL12 activity, indicating that these compounds do not interfere with CXCL12 expression pathways. However, some compounds inhibited CXCL12 activity only at high concentrations up to 50 μ M, which obviously affected cell integrity and viability. While such compound inaction can be disheartening in the context of therapy, it is informative for compound optimisation using a future structure-activity relationship.

Notably, an interesting result was obtained from the novel examination of KM8 and KM11 compounds, which were considered the most active compounds in this study. These compounds demonstrated effective inhibition across the low micromolar range in IL-1 β -induced CXCL12 activity, well below the cytotoxic threshold observed for other KM compounds. The observed values showed higher efficacy than those of other reported CXCR4 antagonists (Mercurio et al., 2016; Zabel et al., 2009). Its novel mechanism of inhibiting CXCL12 expression represents a significant deviation from established approaches.

Our data revealed two critical findings: first, the suppression of CXCL12 is a result of selective expression modulation rather than direct enzyme inhibition; second, the novel compounds, particularly KM11, exhibited a highly favourable cytotoxicity profile with minimal impact on cell viability as determined by an MTT study at concentrations up to 20 μ M. This effect clarifies a beneficial distinction from earlier generations of CXCL12/CXCR4 antagonists, which often showed considerable cytotoxicity at clinically relevant concentrations in cancer patients (Ghasemi & Ghasemi, 2022).

The ELISA data provided critical confirmation of the findings in the reporter assay for the tested KM compounds. As previously discussed, IL-1 β significantly induced CXCL12 protein levels. KM8 and KM11 effectively inhibited IL-1 β -induced CXCL12 protein expression at a moderate

micromolar range. These findings are strongly compatible with the reporter results in reduced CXCL12 activity.

Furthermore, KM8 and KM11 did not significantly affect IL-1 β -mediated production of IL-8 protein levels, with a slight increase in its expression, further emphasising a unique activity specific to CXCL12 expression. Such selectivity is striking given that previous studies had shown many chemokine inhibitors to be pan-active (Cambier et al., 2023; Matsuo et al., 2009). These findings suggest, for the first time, that KM8 and KM11 are novel compounds that selectively inhibit CXCL12 expression induced by proinflammatory cytokines, IL-1 β .

In the current investigation on the signalling pathways induced via IL-1 β , and to determine if both KM8 and KM11 impact these signalling, at the same time, MAPK and NF- κ B (canonical and non-canonical) activation have been established in Chapter Four. The mechanistic analysis revealed that neither KM8 nor KM11 impacted IL-1 β -stimulated JNK phosphorylation, suggesting their mechanism of action is independent of MAPK signalling. This result strongly aligns with the previously discussed data for the involvement of MAPK signalling in CXCL12 regulation. Also, neither compound significantly affected canonical (I κ B α degradation, p65 phosphorylation) or non-canonical (p100 phosphorylation) NF- κ B signalling pathways induced via IL-1 β . This finding also aligns with the results from chapter four that IL-1 β -induced CXCL12 upregulation is IKK α and IKK β independent, and MEKK3 signalling is a new regulated pathway involved in U2OS cells. The mechanistic data for KM compounds support what we get from the previous signalling study for IL-1 β stimulation pathways. A schematic diagram in Figure 6.1 summarises our findings in respect to signalling pathways mediated by IL-1 β -induced CXCL12 expression and the impact of KM compounds on CXCL12 induction. If time had allowed, kinase screening for KM compounds, siRNA NLK, and MEKK3 immunoblotting experiments might have revealed the effect of these compounds on MEKK3 or another kinase such as NLK.

Our results identify KM8 and KM11 as novel inhibitors of IL-1 β -induced CXCL12 expression in U2OS osteosarcoma cells. Their mechanism of action is independent of classic IKK α and IKK β regulatory pathways. This finding aligns with prior evidence establishing that inhibition of CXCL12 generally involves blocking multiple signalling cascades in cancer cells (Chinni et al.,

2006). Moreover, their novel biological activities and favourable toxicity profiles make KM8 and KM11 attractive candidates for further development, particularly in investigating their exact molecular target(s) for potential therapeutic applications.

Future studies might focus on understanding the precise mechanism by which MEKK3 regulates CXCL12 expression, and whether c/EBP β still has a role in this regulation pattern or not and whether NLK is involved in CXCL12 induction using siRNA NLK, exploring the therapeutic potential of targeting this pathway in cancer and inflammatory diseases. Furthermore, other cancer cells, such as those from breast and prostate cancers, may be examined to investigate the signalling pathways induced by IL-1 β in comparison to those from bone cancer cells. Regarding KM compounds, QSAR studies for KM8 and KM11 are necessary to investigate the importance of their pharmacophore in biological activity. Further LC-MS and NMR investigation studies are required for KM6 to determine the exact degradation mechanism.

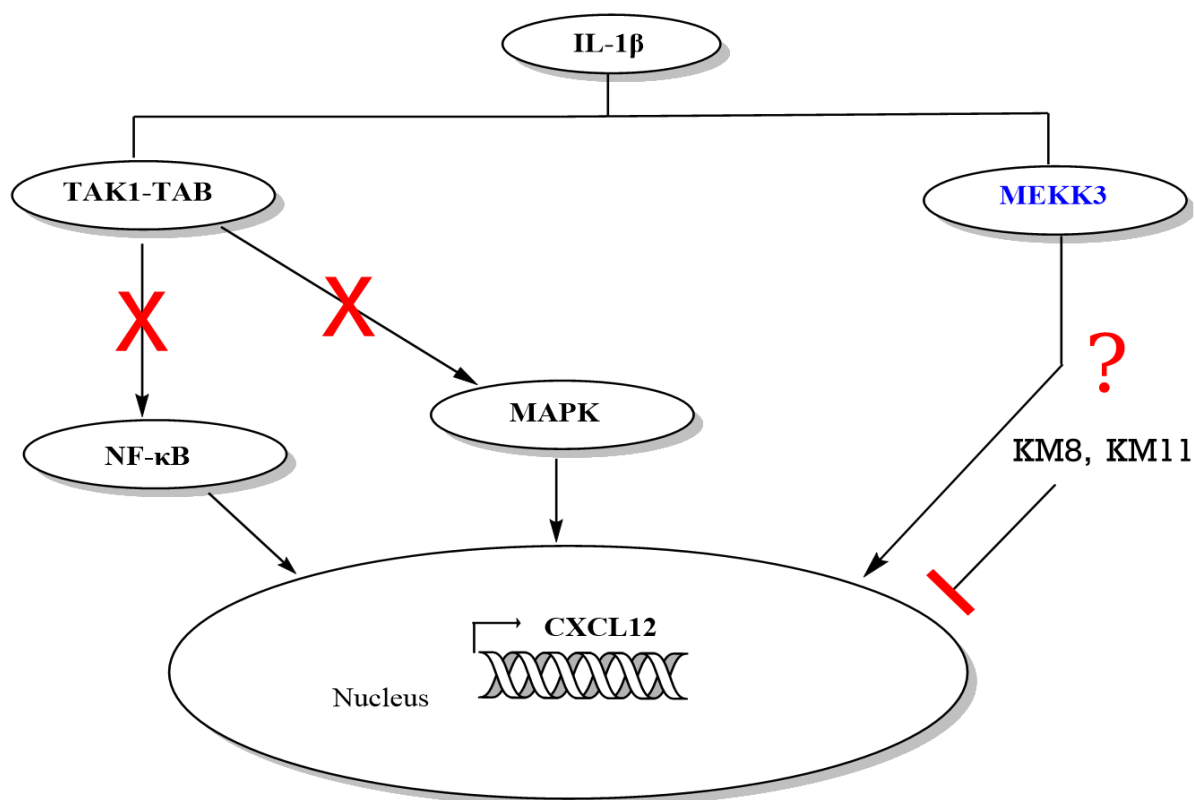


Figure 6. 1 A schematic diagram shows the effect of IL-1 β -induced CXCL12 expression via the MAPK, NF- κ B, and MEKK3 pathways—role of KM compounds in inhibiting CXCL12 activity in U2OS cells.

6.2 Conclusion

The targeted compounds KM6, KM10, and KM11 were synthesised successfully, and the HPLC stability analysis showed their resistance to degradation at elevated temperatures, except KM6. IL-1 β is a potent inducer of CXCL12 expression in U2OS osteosarcoma cells, increasing reporter activity and protein expression. IL-1 β activated several signalling cascades, including MAP kinases, and both canonical and non-canonical NF- κ B pathways. MEKK3 was identified as a specific and novel regulator of CXCL12 expression, independent of classical inflammatory signalling pathways. KM8 and KM11 are novel inhibitors for IL-1 β -induced CXCL12 expression in U2OS cells through upstream MEKK3 signalling. These findings open a new way for therapeutic intervention in conditions where CXCL12 plays a pathological role.

References

- Abarrategi, A., Tornin, J., Martinez-Cruzado, L., Hamilton, A., Martinez-Campos, E., Rodrigo, J. P., González, M. V., Baldini, N., Garcia-Castro, J., & Rodriguez, R. (2016). Osteosarcoma: cells-of-origin, cancer stem cells, and targeted therapies. *Stem cells international*, 2016(1), 3631764.
- Adams, J. M., & Cory, S. (2007). The Bcl-2 apoptotic switch in cancer development and therapy. *Oncogene*, 26(9), 1324-1337.
- Adelaja, A., Taylor, B., Sheu, K. M., Liu, Y., Luecke, S., & Hoffmann, A. (2021). Six distinct NF κ B signaling codons convey discrete information to distinguish stimuli and enable appropriate macrophage responses. *Immunity*, 54(5), 916-930. e917.
- Adli, M., Merkhofer, E., Cogswell, P., & Baldwin, A. S. (2010). IKK α and IKK β each function to regulate NF- κ B activation in the TNF-induced/canonical pathway. *PLoS one*, 5(2), e9428.
- Ajibade, A. A., Wang, H. Y., & Wang, R.-F. (2013). Cell type-specific function of TAK1 in innate immune signaling. *Trends in immunology*, 34(7), 307-316.
- Alcamo, E., Hacohen, N., Schulte, L. C., Rennert, P. D., Hynes, R. O., & Baltimore, D. (2002). Requirement for the NF- κ B family member RelA in the development of secondary lymphoid organs. *Journal of Experimental Medicine*, 195(2), 233-244.
- Alessi, D. R., James, S. R., Downes, C. P., Holmes, A. B., Gaffney, P. R., Reese, C. B., & Cohen, P. (1997). Characterization of a 3-phosphoinositide-dependent protein kinase which phosphorylates and activates protein kinase B α . *Current biology*, 7(4), 261-269.
- Alkalay, I., Yaron, A., Hatzubai, A., Orian, A., Ciechanover, A., & Ben-Neriah, Y. (1995). Stimulation-dependent I kappa B alpha phosphorylation marks the NF-kappa B inhibitor for degradation via the ubiquitin-proteasome pathway. *Proceedings of the National Academy of Sciences*, 92(23), 10599-10603.
- Amanolahi, F., Mohammadi, A., Oskuee, R. K., Nassirli, H., & Malaekheh-Nikouei, B. (2017). A simple, sensitive and rapid isocratic reversed-phase high-performance liquid chromatography method for determination and stability study of curcumin in pharmaceutical samples. *Avicenna journal of phytomedicine*, 7(5), 444.
- Amara, A., Lorthioir, O., Valenzuela, A., Magerus, A., Thelen, M., Montes, M., Virelizier, J.-L., Delepiepierre, M., Baleux, F., & Lortat-Jacob, H. (1999). Stromal cell-derived factor-1 α associates with heparan sulfates through the first β -strand of the chemokine. *Journal of Biological Chemistry*, 274(34), 23916-23925.
- An, X.-D., & Yu, S. (2015). Direct synthesis of nitriles from aldehydes using an O-benzoyl hydroxylamine (BHA) as the nitrogen source. *Organic Letters*, 17(20), 5064-5067.

- Anest, V., Hanson, J. L., Cogswell, P. C., Steinbrecher, K. A., Strahl, B. D., & Baldwin, A. S. (2003). A nucleosomal function for IkappaB kinase-alpha in NF-kappaB-dependent gene expression. *Nature*, 423(6940), 659-663. <https://doi.org/10.1038/nature01648>
- Annunziata, C. M., Davis, R. E., Demchenko, Y., Bellamy, W., Gabrea, A., Zhan, F., Lenz, G., Hanamura, I., Wright, G., & Xiao, W. (2007). Frequent engagement of the classical and alternative NF-kB pathways by diverse genetic abnormalities in multiple myeloma. *Cancer cell*, 12(2), 115-130.
- Anthony, N. G., Baiget, J., Berretta, G., Boyd, M., Breen, D., Edwards, J., Gamble, C., Gray, A. I., Harvey, A. L., Hatzieremia, S., Ho, K. H., Huggan, J. K., Lang, S., Llona-Minguez, S., Luo, J. L., McIntosh, K., Paul, A., Plevin, R. J., Robertson, M. N.,...Mackay, S. P. (2017). Inhibitory Kappa B Kinase α (IKK α) Inhibitors That Recapitulate Their Selectivity in Cells against Isoform-Related Biomarkers. *J Med Chem*, 60(16), 7043-7066. <https://doi.org/10.1021/acs.jmedchem.7b00484>
- Ara, T., Tokoyoda, K., Okamoto, R., Koni, P. A., & Nagasawa, T. (2005). The role of CXCL12 in the organ-specific process of artery formation. *Blood*, 105(8), 3155-3161.
- Arwert, E. N., Harney, A. S., Entenberg, D., Wang, Y., Sahai, E., Pollard, J. W., & Condeelis, J. S. (2018). A unidirectional transition from migratory to perivascular macrophage is required for tumor cell intravasation. *Cell reports*, 23(5), 1239-1248.
- Asai, T., Tomita, Y., Nakatsuka, S. i., Hoshida, Y., Myoui, A., Yoshikawa, H., & Aozasa, K. (2002). VCP (p97) regulates NFkB signaling pathway, which is important for metastasis of osteosarcoma cell line. *Japanese journal of cancer research*, 93(3), 296-304.
- Asgarova, A., Asgarov, K., Godet, Y., Peixoto, P., Nadaradjane, A., Boyer-Guittaut, M., Galaine, J., Guenat, D., Mougey, V., & Perrard, J. (2018). PD-L1 expression is regulated by both DNA methylation and NF-kB during EMT signaling in non-small cell lung carcinoma. *Oncoimmunology*, 7(5), e1423170.
- Assi, K., Pillai, R., Gómez-Muñoz, A., Owen, D., & Salh, B. (2006). The specific JNK inhibitor SP600125 targets tumour necrosis factor- α production and epithelial cell apoptosis in acute murine colitis. *Immunology*, 118(1), 112-121.
- Avnet, S., Di Pompo, G., Chano, T., Errani, C., Ibrahim-Hashim, A., Gillies, R. J., Donati, D. M., & Baldini, N. (2017). Cancer-associated mesenchymal stroma fosters the stemness of osteosarcoma cells in response to intratumoral acidosis via NF-kB activation. *International journal of cancer*, 140(6), 1331-1345.
- Avraham, S., Korin, B., Aviram, S., Shechter, D., Shaked, Y., & Aronheim, A. (2019). ATF3 and JDP2 deficiency in cancer associated fibroblasts promotes tumor growth via SDF-1 transcription. *Oncogene*, 38(20), 3812-3823.

- Baeriswyl, V., & Christofori, G. (2009). The angiogenic switch in carcinogenesis. *Seminars in cancer biology*,
- Baertschi, S. (2016). *Pharmaceutical stress testing: predicting drug degradation*. google.com.
- Bahar, M. E., Kim, H. J., & Kim, D. R. (2023). Targeting the RAS/RAF/MAPK pathway for cancer therapy: from mechanism to clinical studies. *Signal transduction and targeted therapy*, 8(1), 455.
- Baker, C., & Mansfield, Z. (2023). Cancer statistics for England, Commons Library research briefing. *House of Commons Library, London*, 1-29.
- Baker, K. J., Houston, A., & Brint, E. (2019). IL-1 family members in cancer; two sides to every story. *Frontiers in immunology*, 10, 459981.
- Balkwill, F. (2004). Cancer and the chemokine network. *Nature Reviews Cancer*, 4(7), 540-550.
- Bao, S., Darvishi, M., H Amin, A., Al-Haideri, M. T., Patra, I., Kashikova, K., Ahmad, I., Alsaikhan, F., Al-Qaim, Z. H., & Al-Gazally, M. E. (2023). CXCR4 chemokine receptor 4 (CXCR4) blockade in cancer treatment. *Journal of cancer research and clinical oncology*, 149(10), 7945-7968.
- Barbieri, F., Thellung, S., Würth, R., Gatto, F., Corsaro, A., Villa, V., Nizzari, M., Albertelli, M., Ferone, D., & Florio, T. (2014). Emerging Targets in Pituitary Adenomas: Role of the CXCL12/CXCR4-R7 System. *International journal of endocrinology*, 2014(1), 753524.
- Baumhoer, D., Smida, J., Zillmer, S., Rosemann, M., Atkinson, M. J., Nelson, P. J., Jundt, G., Luettichau, I. v., & Nathrath, M. (2012). Strong expression of CXCL12 is associated with a favorable outcome in osteosarcoma. *Modern Pathology*, 25(4), 522-528.
- Baxter, A., Brough, S., Cooper, A., Floettmann, E., Foster, S., Harding, C., Kettle, J., McNally, T., Martin, C., & Mobbs, M. (2004). Hit-to-lead studies: the discovery of potent, orally active, thiophenecarboxamide IKK-2 inhibitors. *Bioorganic & medicinal chemistry letters*, 14(11), 2817-2822.
- Bayani, J., Zielenska, M., Pandita, A., Al-Romaih, K., Karaskova, J., Harrison, K., Bridge, J. A., Sorensen, P., Thorner, P., & Squire, J. A. (2003). Spectral karyotyping identifies recurrent complex rearrangements of chromosomes 8, 17, and 20 in osteosarcomas. *Genes, Chromosomes and Cancer*, 36(1), 7-16.
- Beider, K., Begin, M., Abraham, M., Wald, H., Weiss, I. D., Wald, O., Pikarsky, E., Zeira, E., Eizenberg, O., & Galun, E. (2011). CXCR4 antagonist 4F-benzoyl-TN14003 inhibits leukemia and multiple myeloma tumor growth. *Experimental hematology*, 39(3), 282-292.
- Beider, K., Bitner, H., Leiba, M., Gutwein, O., Koren-Michowitz, M., Ostrovsky, O., Abraham, M., Wald, H., Galun, E., & Peled, A. (2014). Multiple myeloma cells recruit tumor-supportive

- macrophages through the CXCR4/CXCL12 axis and promote their polarization toward the M2 phenotype. *Oncotarget*, 5(22), 11283.
- Ben-Neriah, Y., & Karin, M. (2011). Inflammation meets cancer, with NF- κ B as the matchmaker. *Nature immunology*, 12(8), 715-723.
- Bennett, B. L., Sasaki, D. T., Murray, B. W., O'Leary, E. C., Sakata, S. T., Xu, W., Leisten, J. C., Motiwala, A., Pierce, S., & Satoh, Y. (2001). SP600125, an anthrapyrazolone inhibitor of Jun N-terminal kinase. *Proceedings of the National Academy of Sciences*, 98(24), 13681-13686.
- Bennett, S. R., Carbone, F. R., Karamalis, F., Flavell, R. A., Miller, J. F., & Heath, W. R. (1998). Help for cytotoxic-T-cell responses is mediated by CD40 signalling. *Nature*, 393(6684), 478-480.
- Bernardini, G., Sciume, G., Bosisio, D., Morrone, S., Sozzani, S., & Santoni, A. (2008). CCL3 and CXCL12 regulate trafficking of mouse bone marrow NK cell subsets. *Blood, the Journal of the American Society of Hematology*, 111(7), 3626-3634.
- Berx, G., & Van Roy, F. (2009). Involvement of members of the cadherin superfamily in cancer. *Cold Spring Harbor perspectives in biology*, 1(6), a003129.
- Bhandoola, A., & Sambandam, A. (2006). From stem cell to T cell: one route or many? *Nature Reviews Immunology*, 6(2), 117-126.
- Bielack, S. S., Kempf-Bielack, B., Delling, G., Exner, G. U., Flege, S., Helmke, K., Kotz, R., Salzer-Kuntschik, M., Werner, M., Winkelmann, W., Zoubek, A., Jürgens, H., & Winkler, K. (2002). Prognostic Factors in High-Grade Osteosarcoma of the Extremities or Trunk: An Analysis of 1,702 Patients Treated on Neoadjuvant Cooperative Osteosarcoma Study Group Protocols. *Journal of Clinical Oncology*, 20(3), 776-790. <https://doi.org/10.1200/jco.2002.20.3.776>
- Blasco, M. A. (2005). Telomeres and human disease: ageing, cancer and beyond. *Nature Reviews Genetics*, 6(8), 611-622.
- Bleul, C. C., Fuhlbrigge, R. C., Casasnovas, J. M., Aiuti, A., & Springer, T. A. (1996). A highly efficacious lymphocyte chemoattractant, stromal cell-derived factor 1 (SDF-1). *The Journal of experimental medicine*, 184(3), 1101-1109.
- Bobbin, M. L., & Rossi, J. J. (2016). RNA Interference (RNAi)-Based Therapeutics: Delivering on the Promise? *Annu Rev Pharmacol Toxicol*, 56, 103-122. <https://doi.org/10.1146/annurev-pharmtox-010715-103633>
- Borges, R., Pelosine, A. M., de Souza, A. C. S., Machado Jr, J., Justo, G. Z., Gamarra, L. F., & Marchi, J. (2022). Bioactive glasses as carriers of cancer-targeted drugs: Challenges and opportunities in bone cancer treatment. *Materials*, 15(24), 9082.

- Bourgeois, C., Rocha, B., & Tanchot, C. (2002). A role for CD40 expression on CD8+ T cells in the generation of CD8+ T cell memory. *Science*, 297(5589), 2060-2063.
- Brassart-Pasco, S., Brézillon, S., Brassart, B., Ramont, L., Oudart, J.-B., & Monboisse, J. C. (2020). Tumor microenvironment: extracellular matrix alterations influence tumor progression. *Frontiers in oncology*, 10, 397.
- Bray, F., Laversanne, M., Sung, H., Ferlay, J., Siegel, R. L., Soerjomataram, I., & Jemal, A. (2024). Global cancer statistics 2022: GLOBOCAN estimates of incidence and mortality worldwide for 36 cancers in 185 countries. *CA: a cancer journal for clinicians*, 74(3), 229-263.
- Burger, J., & Peled, A. (2009). CXCR4 antagonists: targeting the microenvironment in leukemia and other cancers. *Leukemia*, 23(1), 43-52.
- Burger, J. A., & Kipps, T. J. (2006). CXCR4: a key receptor in the crosstalk between tumor cells and their microenvironment. *Blood*, 107(5), 1761-1767.
- Burkhardt, D. L., & Sage, J. (2008). Cellular mechanisms of tumour suppression by the retinoblastoma gene. *Nature Reviews Cancer*, 8(9), 671-682.
- Burns, J. M., Summers, B. C., Wang, Y., Melikian, A., Berahovich, R., Miao, Z., Penfold, M. E., Sunshine, M. J., Littman, D. R., & Kuo, C. J. (2006). A novel chemokine receptor for SDF-1 and I-TAC involved in cell survival, cell adhesion, and tumor development. *The Journal of experimental medicine*, 203(9), 2201-2213.
- Calonge, E., Alonso-Lobo, J., Escandón, C., González, N., Bermejo, M., Santiago, B., Mestre, L., Pablos, J., Caruz, A., & Alcamí, J. (2010). c/EBP β Is a Major Regulatory Element Driving Transcriptional Activation of the CXCL12 Promoter. *Journal of molecular biology*, 396(3), 463-472.
- Cambier, S., Gouwy, M., & Proost, P. (2023). The chemokines CXCL8 and CXCL12: molecular and functional properties, role in disease and efforts towards pharmacological intervention. *Cellular & Molecular Immunology*, 20(3), 217-251.
- Campolo, M., Lanza, M., Casili, G., Paterniti, I., Filippone, A., Caffo, M., Cardali, S. M., Puliafito, I., Colarossi, C., & Raciti, G. (2020). TAK1 inhibitor enhances the therapeutic treatment for glioblastoma. *Cancers*, 13(1), 41.
- Carnero, A., Blanco-Aparicio, C., Renner, O., Link, W., & Leal, J. F. (2008). The PTEN/PI3K/AKT signalling pathway in cancer, therapeutic implications. *Current cancer drug targets*, 8(3), 187-198.
- Carter, M., & Shieh, J. (2010). Biochemical assays and intracellular signaling. *Guide to research techniques in neuroscience*, 297-329.
- Cause, G., & Age, S. (2020). by Country and by Region, 2000–2019. *World Health Organization*.

- Chandhanayingyong, C., Kim, Y., Staples, J. R., Hahn, C., & Lee, F. Y. (2012). MAPK/ERK signaling in osteosarcomas, ewing sarcomas and chondrosarcomas: therapeutic implications and future directions. *Sarcoma*, 2012(1), 404810.
- Chang, F., Steelman, L., Lee, J., Shelton, J., Navolanic, P., Blalock, W. L., Franklin, R., & McCubrey, J. (2003). Signal transduction mediated by the Ras/Raf/MEK/ERK pathway from cytokine receptors to transcription factors: potential targeting for therapeutic intervention. *Leukemia* (08876924), 17(7).
- Chen, C.-G., Malliaros, J., Katerelos, M., D'Apice, A. J., & Pearce, M. J. (1996). Inhibition of NF- κ B activation by a dominant-negative mutant of I κ B α . *Molecular immunology*, 33(1), 57-61.
- Chen, F., Bi, D., Cheng, C., Ma, S., Liu, Y., & Cheng, K. (2019). Bone morphogenetic protein 7 enhances the osteogenic differentiation of human dermal-derived CD105+ fibroblast cells through the Smad and MAPK pathways. *International journal of molecular medicine*, 43(1), 37-46.
- Chen, F. E., Huang, D.-B., Chen, Y.-Q., & Ghosh, G. (1998). Crystal structure of p50/p65 heterodimer of transcription factor NF- κ B bound to DNA. *Nature*, 391(6665), 410-413.
- Chen, H.-J., Lin, C.-M., Lee, C.-Y., Shih, N.-C., Peng, S.-F., Tsuzuki, M., Amagaya, S., Huang, W.-W., & Yang, J.-S. (2013). Kaempferol suppresses cell metastasis via inhibition of the ERK-p38-JNK and AP-1 signaling pathways in U-2 OS human osteosarcoma cells. *Oncology reports*, 30(2), 925-932.
- Chen, X.-Y., Zhou, J., Luo, L.-P., Han, B., Li, F., Chen, J.-Y., Zhu, Y.-F., Chen, W., & Yu, X.-P. (2015). Black rice anthocyanins suppress metastasis of breast cancer cells by targeting RAS/RAF/MAPK pathway. *BioMed Research International*, 2015.
- Chen, Y., McAndrews, K. M., & Kalluri, R. (2021). Clinical and therapeutic relevance of cancer-associated fibroblasts. *Nature reviews Clinical oncology*, 18(12), 792-804.
- Chen, Z., Gao, Z., Xia, L., Wang, X., Lu, L., & Wu, X. (2021). Dysregulation of DPP4-CXCL12 balance by TGF- β 1/SMAD pathway promotes CXCR4+ inflammatory cell infiltration in Keloid scars. *Journal of inflammation research*, 4169-4180.
- Cheng, J. W., Sadeghi, Z., Levine, A. D., Penn, M. S., von Recum, H. A., Caplan, A. I., & Hijaz, A. (2014). The role of CXCL12 and CCL7 chemokines in immune regulation, embryonic development, and tissue regeneration. *Cytokine*, 69(2), 277-283.
- Cheng, N., Chytil, A., Shyr, Y., Joly, A., & Moses, H. L. (2008). Transforming growth factor- β signaling-deficient fibroblasts enhance hepatocyte growth factor signaling in mammary carcinoma cells to promote scattering and invasion. *Molecular Cancer Research*, 6(10), 1521-1533.

- Chinni, S. R., Sivalogan, S., Dong, Z., Filho, J. C., Deng, X., Bonfil, R. D., & Cher, M. L. (2006). CXCL12/CXCR4 signaling activates Akt-1 and MMP-9 expression in prostate cancer cells: the role of bone microenvironment-associated CXCL12. *Prostate*, 66(1), 32-48. <https://doi.org/10.1002/pros.20318>
- Choi, J., Wang, R., Yang, X., Wang, X., Wang, L., Ting, K., Foley, M., Cogger, V., Yang, Z., & Liu, F. (2018). Ponatinib (AP24534) inhibits MEKK3-KLF signaling and prevents formation and progression of cerebral cavernous malformations. *Sci Adv* 4 (11): eaau0731. In.
- Chow, M. T., & Luster, A. D. (2014). Chemokines in cancer. *Cancer immunology research*, 2(12), 1125-1131.
- Cildir, G., Low, K. C., & Tergaonkar, V. (2016). Noncanonical NF- κ B signaling in health and disease. *Trends in molecular medicine*, 22(5), 414-429.
- Cismowski, M. J. (2007). Imatinib. In *xPharm: The Comprehensive Pharmacology Reference* (pp. 1-7). Elsevier Inc.
- Claudio, E., Brown, K., Park, S., Wang, H., & Siebenlist, U. (2002). BAFF-induced NEMO-independent processing of NF- κ B2 in maturing B cells. *Nature immunology*, 3(10), 958-965.
- Collares, D. M. (2019). *An alternative way to look at diffuse large B-cell lymphoma: the impact of frequent engagement of RelB NF- κ B subunit on cell survival and patient outcome* [Université Sorbonne Paris Cité].
- Colvin, L., & Fallon, M. (2008). Challenges in cancer pain management—bone pain. *European Journal of Cancer*, 44(8), 1083-1090.
- Conley-LaComb, M. K., Semaan, L., Singareddy, R., Li, Y., Heath, E. I., Kim, S., Cher, M. L., & Chinni, S. R. (2016). Pharmacological targeting of CXCL12/CXCR4 signaling in prostate cancer bone metastasis. *Molecular Cancer*, 15, 1-13.
- Connors, K. A. (1986). *Chemical stability of pharmaceuticals: a handbook for pharmacists*. John Wiley & Sons.
- Coope, H., Atkinson, P., Huhse, B., Belich, M., Janzen, J., Holman, M., Klaus, G., Johnston, L., & Ley, S. (2002). CD40 regulates the processing of NF- κ B2 p100 to p52. *The EMBO journal*.
- Costa, A., Kieffer, Y., Scholer-Dahirel, A., Pelon, F., Bourachot, B., Cardon, M., Sirven, P., Magagna, I., Fuhrmann, L., & Bernard, C. (2018). Fibroblast heterogeneity and immunosuppressive environment in human breast cancer. *Cancer cell*, 33(3), 463-479. e410.

- Coulombe, P., & Meloche, S. (2007). Atypical mitogen-activated protein kinases: structure, regulation and functions. *Biochim Biophys Acta*, 1773(8), 1376-1387. <https://doi.org/10.1016/j.bbamcr.2006.11.001>
- Coussens, L. M., & Werb, Z. (2002). Inflammation and cancer. *Nature*, 420(6917), 860-867.
- Craig, R., McIntosh, K., Ho, K. H., McCulloch, A., Riley, C., Lawson, C., Mackay, S. P., Paul, A., Coats, P., & Plevin, R. (2025). IL-1 β stimulates a novel axis within the NF κ B pathway in endothelial cells regulated by IKK α and TAK-1. *Biochemical Pharmacology*, 232, 116736.
- Crump, M. P., Gong, J. H., Loetscher, P., Rajarathnam, K., Amara, A., Arenzana-Seisdedos, F., Virelizier, J. L., Baggiolini, M., Sykes, B. D., & Clark-Lewis, I. (1997). Solution structure and basis for functional activity of stromal cell-derived factor-1; dissociation of CXCR4 activation from binding and inhibition of HIV-1. *The EMBO journal*.
- Cuesta-Gomez, N., Graham, G. J., & Campbell, J. D. (2021). Chemokines and their receptors: predictors of the therapeutic potential of mesenchymal stromal cells. *Journal of Translational Medicine*, 19(1), 1-10.
- Czarnecka, A. M., Synoradzki, K., Firlej, W., Bartnik, E., Sobczuk, P., Fiedorowicz, M., Grieb, P., & Rutkowski, P. (2020). Molecular Biology of Osteosarcoma. *Cancers (Basel)*, 12(8). <https://doi.org/10.3390/cancers12082130>
- Daams, R., & Massoumi, R. (2020). Nemo-Like Kinase in Development and Diseases: Insights from Mouse Studies. *Int J Mol Sci*, 21(23). <https://doi.org/10.3390/ijms21239203>
- Dai, J.-m., Sun, K., Li, C., Cheng, M., Guan, J.-h., Yang, L.-n., & Zhang, L.-w. (2023). Cancer-associated fibroblasts contribute to cancer metastasis and apoptosis resistance in human ovarian cancer via paracrine SDF-1 α . *Clinical and Translational Oncology*, 25(6), 1606-1616.
- Dales, N., Fonarev, J., Fu, J., Kamboj, R., Kodumururu, V., Liu, S., Pokrovskaja, N., Raina, V., Sun, S., & Zhang, Z. (2008). *Organic compounds (WO 2008/127349 A2)*. . <https://patents.google.com/patent/WO2008127349A2/en>, Accessed 24/4/2025
- Davies, M., & Samuels, Y. (2010). Analysis of the genome to personalize therapy for melanoma. *Oncogene*, 29(41), 5545-5555.
- Décaillot, F. M., Kazmi, M. A., Lin, Y., Ray-Saha, S., Sakmar, T. P., & Sachdev, P. (2011). CXCR7/CXCR4 heterodimer constitutively recruits β -arrestin to enhance cell migration. *Journal of Biological Chemistry*, 286(37), 32188-32197.
- Dejardin, E., Droin, N. M., Delhase, M., Haas, E., Cao, Y., Makris, C., Li, Z.-W., Karin, M., Ware, C. F., & Green, D. R. (2002). The lymphotoxin- β receptor induces different patterns of gene expression via two NF- κ B pathways. *Immunity*, 17(4), 525-535.

- Demchenko, Y. N., Glebov, O. K., Zingone, A., Keats, J. J., Bergsagel, P. L., & Kuehl, W. M. (2010). Classical and/or alternative NF- κ B pathway activation in multiple myeloma. *Blood, the Journal of the American Society of Hematology*, 115(17), 3541-3552.
- Demchenko, Y. N., & Kuehl, W. M. (2010). A critical role for the NF κ B pathway in multiple myeloma. *Oncotarget*, 1(1), 59.
- DeNardo, D. G., Andreu, P., & Coussens, L. M. (2010). Interactions between lymphocytes and myeloid cells regulate pro-versus anti-tumor immunity. *Cancer and Metastasis Reviews*, 29(2), 309-316.
- Dergham, S. T., Dugan, M. C., Kucway, R., Du, W., Kamarauskiene, D. S., Vaitkevicius, V. K., Crissman, J. D., & Sarkar, F. H. (1997). Prevalence and clinical significance of combined K-ras mutation and p53 aberration in pancreatic adenocarcinoma. *International journal of pancreatology*, 21(2), 127-143.
- Deshpande, A., Sicinski, P., & Hinds, P. W. (2005). Cyclins and cdks in development and cancer: a perspective. *Oncogene*, 24(17), 2909-2915.
- Devignes, C.-S., Aslan, Y., Brenot, A., Devillers, A., Schepers, K., Fabre, S., Chou, J., Casbon, A.-J., Werb, Z., & Provot, S. (2018). HIF signaling in osteoblast-lineage cells promotes systemic breast cancer growth and metastasis in mice. *Proceedings of the National Academy of Sciences*, 115(5), E992-E1001.
- Di, Y., Li, S., Wang, L., Zhang, Y., & Dorf, M. E. (2008). Homeostatic interactions between MEKK3 and TAK1 involved in NF- κ B signaling. *Cellular Signalling*, 20(4), 705-713.
- Dobrzanski, P., Ryseck, R.-P., & Bravo, R. (1993). Both N-and C-terminal domains of RelB are required for full transactivation: role of the N-terminal leucine zipper-like motif. *Molecular and cellular biology*, 13(3), 1572-1582.
- Dong, R., Wang, Q., He, X., Chu, Y., Lu, J., & Ma, Q. (2007). Role of nuclear factor kappa B and reactive oxygen species in the tumor necrosis factor- α -induced epithelial-mesenchymal transition of MCF-7 cells. *Brazilian Journal of Medical and Biological Research*, 40, 1071-1078.
- Drew, B. A., Burow, M. E., & Beckman, B. S. (2012). MEK5/ERK5 pathway: the first fifteen years. *Biochimica et Biophysica Acta (BBA)-Reviews on Cancer*, 1825(1), 37-48.
- Edeiken, J., Raymond, A. K., Ayala, A. G., Benjamin, R. S., Murray, J. A., & Carrasco, H. C. (1987). Small-cell osteosarcoma. *Skeletal Radiol*, 16(8), 621-628. <https://doi.org/10.1007/bf00357110>
- Elbashir, S. M., Harborth, J., Lendeckel, W., Yalcin, A., Weber, K., & Tuschl, T. (2001). Duplexes of 21-nucleotide RNAs mediate RNA interference in cultured mammalian cells. *Nature*, 411(6836), 494-498.

- Farhood, B., Najafi, M., & Mortezaee, K. (2019). Cancer-associated fibroblasts: Secretions, interactions, and therapy. *Journal of cellular biochemistry*, 120(3), 2791-2800.
- Feig, C., Jones, J. O., Kraman, M., Wells, R. J., Deonaraine, A., Chan, D. S., Connell, C. M., Roberts, E. W., Zhao, Q., & Caballero, O. L. (2013). Targeting CXCL12 from FAP-expressing carcinoma-associated fibroblasts synergizes with anti-PD-L1 immunotherapy in pancreatic cancer. *Proceedings of the National Academy of Sciences*, 110(50), 20212-20217.
- Ferguson, W. S., & Goorin, A. M. (2001). Current treatment of osteosarcoma. *Cancer Invest*, 19(3), 292-315. <https://doi.org/10.1081/cnv-100102557>
- Ferreiro, D. U., & Komives, E. A. (2010). Molecular mechanisms of system control of NF- κ B signaling by I κ B α . *Biochemistry*, 49(8), 1560-1567.
- Flavell, R. A., Sanjabi, S., Wrzesinski, S. H., & Licona-Limón, P. (2010). The polarization of immune cells in the tumour environment by TGF β . *Nature Reviews Immunology*, 10(8), 554-567.
- Freeman, G. J., Long, A. J., Iwai, Y., Bourque, K., Chernova, T., Nishimura, H., Fitz, L. J., Malenkovich, N., Okazaki, T., & Byrne, M. C. (2000). Engagement of the PD-1 immunoinhibitory receptor by a novel B7 family member leads to negative regulation of lymphocyte activation. *The Journal of experimental medicine*, 192(7), 1027-1034.
- Freshney, R. I. (2015). *Culture of animal cells: a manual of basic technique and specialized applications*. John Wiley & Sons.
- Friedl, P., & Wolf, K. (2008). Tube travel: the role of proteases in individual and collective cancer cell invasion. *Cancer Research*, 68(18), 7247-7249.
- Friedl, P., & Wolf, K. (2010). Plasticity of cell migration: a multiscale tuning model. *Journal of Cell Biology*, 188(1), 11-19.
- Fumarola, C., Bonelli, M. A., Petronini, P. G., & Alfieri, R. R. (2014). Targeting PI3K/AKT/mTOR pathway in non small cell lung cancer. *Biochemical pharmacology*, 90(3), 197-207.
- Gabrilovich, D. I., Ostrand-Rosenberg, S., & Bronte, V. (2012). Coordinated regulation of myeloid cells by tumours. *Nature Reviews Immunology*, 12(4), 253-268.
- Gao, D., Tang, T., Zhu, J., Tang, Y., Sun, H., & Li, S. (2019). CXCL12 has therapeutic value in facial nerve injury and promotes Schwann cells autophagy and migration via PI3K-AKT-mTOR signal pathway. *International journal of biological macromolecules*, 124, 460-468.
- Gao, W., Gao, J., Chen, L., Ren, Y., & Ma, J. (2019). Targeting XIST induced apoptosis of human osteosarcoma cells by activation of NF- κ B/PUMA signal. *Bioengineered*, 10(1), 261-270.

- García-Moruja, C., Alonso-Lobo, J. M., Rueda, P., Torres, C., González, N., Bermejo, M., Luque, F., Arenzana-Seisdedos, F., Alcamí, J., & Caruz, A. (2005). Functional characterization of SDF-1 proximal promoter. *Journal of molecular biology*, 348(1), 43-62.
- Geindreau, M., Bruchard, M., & Végan, F. (2022). Role of cytokines and chemokines in angiogenesis in a tumor context. *Cancers*, 14(10), 2446.
- Geng, F., Guo, J., Guo, Q.-Q., Xie, Y., Dong, L., Zhou, Y., Liu, C.-L., Yu, B., Wu, H., & Wu, J.-X. (2019). A DNA vaccine expressing an optimized secreted FAP α induces enhanced anti-tumor activity by altering the tumor microenvironment in a murine model of breast cancer. *Vaccine*, 37(31), 4382-4391.
- Ghasemi, K., & Ghasemi, K. (2022). MSX-122: Is an effective small molecule CXCR4 antagonist in cancer therapy? *International Immunopharmacology*, 108, 108863.
- Ghebranious, N., & Donehower, L. A. (1998). Mouse models in tumor suppression. *Oncogene*, 17(25), 3385-3400.
- Ghosh, S., May, M. J., & Kopp, E. B. (1998). NF- κ B and Rel proteins: evolutionarily conserved mediators of immune responses. *Annual review of immunology*, 16(1), 225-260.
- Gilmore, T. D. (2006). Introduction to NF- κ B: players, pathways, perspectives. *Oncogene*, 25(51), 6680-6684.
- Giordano, F. A., Layer, J. P., Leonardelli, S., Friker, L. L., Turiello, R., Corvino, D., Zeyen, T., Schaub, C., Müller, W., Sperk, E., Schmeel, L. C., Sahm, K., Oster, C., Kebir, S., Hambsch, P., Pietsch, T., Bisdas, S., Platten, M., Glas, M.,...Hölzel, M. (2024). L-RNA aptamer-based CXCL12 inhibition combined with radiotherapy in newly-diagnosed glioblastoma: dose escalation of the phase I/II GLORIA trial. *Nat Commun*, 15(1), 4210. <https://doi.org/10.1038/s41467-024-48416-9>
- Giordano, F. A., Link, B., Glas, M., Herrlinger, U., Wenz, F., Umansky, V., Brown, J. M., & Herskind, C. (2019). Targeting the post-irradiation tumor microenvironment in glioblastoma via inhibition of CXCL12. *Cancers*, 11(3), 272.
- Gonçalves, E. S., Poulsen, L., & Ogilby, P. R. (2007). Mechanism of the temperature-dependent degradation of polyamide 66 films exposed to water. *Polymer Degradation and Stability*, 92(11), 1977-1985.
- Gozgit, J. M., Wong, M. J., Moran, L., Wardwell, S., Mohemmad, Q. K., Narasimhan, N. I., Shakespeare, W. C., Wang, F., Clackson, T., & Rivera, V. M. (2012). Ponatinib (AP24534), a multitargeted pan-FGFR inhibitor with activity in multiple FGFR-amplified or mutated cancer models. *Molecular cancer therapeutics*, 11(3), 690-699.

- Greten, F. R., Eckmann, L., Greten, T. F., Park, J. M., Li, Z.-W., Egan, L. J., Kagnoff, M. F., & Karin, M. (2004). IKK β links inflammation and tumorigenesis in a mouse model of colitis-associated cancer. *cell*, 118(3), 285-296.
- Griffith, J. W., Sokol, C. L., & Luster, A. D. (2014). Chemokines and chemokine receptors: positioning cells for host defense and immunity. *Annual review of immunology*, 32, 659-702.
- Grivennikov, S. I., Greten, F. R., & Karin, M. (2010). Immunity, inflammation, and cancer. *Cell*, 140(6), 883-899.
- Guan, S., Lu, J., Zhao, Y., Woodfield, S. E., Zhang, H., Xu, X., Yu, Y., Zhao, J., Bieerkehazhi, S., & Liang, H. (2017). TAK1 inhibitor 5Z-7-oxozeaenol sensitizes cervical cancer to doxorubicin-induced apoptosis. *Oncotarget*, 8(20), 33666.
- Guideline, I. H. T. (2005). Validation of analytical procedures: text and methodology. *Q2 (R1)*, 1(20), 05.
- Guillemot, E., Karimjee-Soilihi, B., Pradelli, E., Benchetrit, M., Goguet-Surmenian, E., Millet, M., Larbret, F., Michiels, J., Birnbaum, D., & Alemanno, P. (2012). CXCR7 receptors facilitate the progression of colon carcinoma within lung not within liver. *British journal of cancer*, 107(12), 1944-1949.
- Hacker, H., & Karin, M. (2006). Regulation and function of IKK and IKK-related kinases. *Science's STKE*, 2006(357), re13-re13.
- Häcker, H., & Karin, M. (2006). Regulation and function of IKK and IKK-related kinases. *Sci STKE*, 2006(357), re13. <https://doi.org/10.1126/stke.3572006re13>
- Hall, J. M., & Korach, K. S. (2003). Stromal cell-derived factor 1, a novel target of estrogen receptor action, mediates the mitogenic effects of estradiol in ovarian and breast cancer cells. *Molecular endocrinology*, 17(5), 792-803.
- Han, Z.-J., Li, Y.-B., Yang, L.-X., Cheng, H.-J., Liu, X., & Chen, H. (2021). Roles of the CXCL8-CXCR1/2 axis in the tumor microenvironment and immunotherapy. *Molecules*, 27(1), 137.
- Hanahan, D., & Folkman, J. (1996). Patterns and emerging mechanisms of the angiogenic switch during tumorigenesis. *Cell*, 86(3), 353-364.
- Hanahan, D., & Weinberg, R. A. (2000). The hallmarks of cancer. *cell*, 100(1), 57-70.
- Hanahan, D., & Weinberg, R. A. (2011). Hallmarks of cancer: the next generation. *Cell*, 144(5), 646-674.
- Harada, A., Sekido, N., Akahoshi, T., Wada, T., Mukaida, N., & Matsushima, K. (1994). Essential involvement of interleukin-8 (IL-8) in acute inflammation. *Journal of leukocyte biology*, 56(5), 559-564.

- Haselager, M., Thijssen, R., West, C., Young, L., Van Kampen, R., Willmore, E., Mackay, S., Kater, A., & Eldering, E. (2021). Regulation of Bcl-XL by non-canonical NF- κ B in the context of CD40-induced drug resistance in CLL. *Cell Death & Differentiation*, 28(5), 1658-1668.
- Hattermann, K., Held-Feindt, J., Lucius, R., Mürköster, S. S., Penfold, M. E., Schall, T. J., & Mentlein, R. (2010). The chemokine receptor CXCR7 is highly expressed in human glioma cells and mediates antiapoptotic effects. *Cancer Research*, 70(8), 3299-3308.
- Hayden, M. S., & Ghosh, S. (2008). Shared principles in NF- κ B signaling. *cell*, 132(3), 344-362.
- Hayden, M. S., & Ghosh, S. (2012). NF- κ B, the first quarter-century: remarkable progress and outstanding questions. *Genes & development*, 26(3), 203-234.
- He, W., Qu, T., Yu, Q., Wang, Z., Lv, H., Zhang, J., Zhao, X., & Wang, P. (2013). LPS induces IL-8 expression through TLR 4, M y D 88, NF-kappa B and MAPK pathways in human dental pulp stem cells. *International endodontic journal*, 46(2), 128-136.
- Hernandez, L., Magalhaes, M. A., Coniglio, S. J., Condeelis, J. S., & Segall, J. E. (2011). Opposing roles of CXCR4 and CXCR7 in breast cancer metastasis. *Breast Cancer Research*, 13(6), 1-17.
- Hiscott, J., Nguyen, T., Arguello, M., Nakhaei, P., & Paz, S. (2006). Manipulation of the nuclear factor- κ B pathway and the innate immune response by viruses. *Oncogene*, 25(51), 6844-6867.
- Hoang, B. H., Dyke, J. P., Koutcher, J. A., Huvos, A. G., Mizobuchi, H., Mazza, B. A., Gorlick, R., & Healey, J. H. (2004). VEGF expression in osteosarcoma correlates with vascular permeability by dynamic MRI. *Clin Orthop Relat Res*(426), 32-38. <https://doi.org/10.1097/01.blo.0000141492.52166.20>
- Holderfield, M., Deuker, M. M., McCormick, F., & McMahon, M. (2014). Targeting RAF kinases for cancer therapy: BRAF-mutated melanoma and beyond. *Nature Reviews Cancer*, 14(7), 455-467.
- Hollander, M. C., Blumenthal, G. M., & Dennis, P. A. (2011). PTEN loss in the continuum of common cancers, rare syndromes and mouse models. *Nature Reviews Cancer*, 11(4), 289-301.
- Huang, C. Y., Lee, C. Y., Chen, M. Y., Yang, W. H., Chen, Y. H., Chang, C. H., Hsu, H. C., Fong, Y. C., & Tang, C. H. (2009). Stromal cell-derived factor-1/CXCR4 enhanced motility of human osteosarcoma cells involves MEK1/2, ERK and NF- κ B-dependent pathways. *Journal of cellular physiology*, 221(1), 204-212.
- Huang, K., Chen, Y., Zhang, R., Wu, Y., Ma, Y., Fang, X., & Shen, S. (2018). Honokiol induces apoptosis and autophagy via the ROS/ERK1/2 signaling pathway in human osteosarcoma cells in vitro and in vivo. *Cell death & disease*, 9(2), 157.

- Huang, S., Wa, Q., Pan, J., Peng, X., Ren, D., Huang, Y., Chen, X., & Tang, Y. (2017). Downregulation of miR-141-3p promotes bone metastasis via activating NF- κ B signaling in prostate cancer. *Journal of Experimental & Clinical Cancer Research*, 36, 1-13.
- Huang, Y., Yang, Y., He, Y., & Li, J. (2015). The emerging role of Nemo-like kinase (NLK) in the regulation of cancers. *Tumour Biol*, 36(12), 9147-9152. <https://doi.org/10.1007/s13277-015-4159-7>
- Hungness, E. S., Pritts, T. A., Luo, G.-J., Hershko, D. D., Robb, B. W., & Hasselgren, P.-O. (2002). IL-1 β activates C/EBP- β and δ in human enterocytes through a mitogen-activated protein kinase signaling pathway. *The international journal of biochemistry & cell biology*, 34(4), 382-395.
- Huvos, A. G., Rosen, G., Bretsky, S. S., & Butler, A. (1982). Telangiectatic osteogenic sarcoma: a clinicopathologic study of 124 patients. *Cancer*, 49(8), 1679-1689. [https://doi.org/10.1002/1097-0142\(19820415\)49:8<1679::aid-cnrcr2820490824>3.0.co;2-2](https://doi.org/10.1002/1097-0142(19820415)49:8<1679::aid-cnrcr2820490824>3.0.co;2-2)
- Hwang, Y. S., Jeong, M., Park, J. S., Kim, M. H., Lee, D. B., Shin, B. A., Mukaida, N., Ellis, L. M., Kim, H. R., & Ahn, B. W. (2004). Interleukin-1 β stimulates IL-8 expression through MAP kinase and ROS signaling in human gastric carcinoma cells. *Oncogene*, 23(39), 6603-6611.
- Inoue, J. i., Gohda, J., Akiyama, T., & Semba, K. (2007). NF- κ B activation in development and progression of cancer. *Cancer science*, 98(3), 268-274.
- Ishitani, T., Kishida, S., Hyodo-Miura, J., Ueno, N., Yasuda, J., Waterman, M., Shibuya, H., Moon, R. T., Ninomiya-Tsuji, J., & Matsumoto, K. (2003). The TAK1-NLK mitogen-activated protein kinase cascade functions in the Wnt-5a/Ca(2+) pathway to antagonize Wnt/beta-catenin signaling. *Mol Cell Biol*, 23(1), 131-139. <https://doi.org/10.1128/mcb.23.1.131-139.2003>
- Israël, A. (2000). The IKK complex: an integrator of all signals that activate NF- κ B? *Trends in cell biology*, 10(4), 129-133.
- Italiano, A., Mir, O., Mathoulin-Pelissier, S., Penel, N., Piperno-Neumann, S., Bompas, E., Chevreau, C., Duffaud, F., Entz-Werlé, N., Saada, E., Ray-Coquard, I., Lervat, C., Gaspar, N., Marec-Berard, P., Pacquement, H., Wright, J., Toulmonde, M., Bessede, A., Crombe, A.,...Blay, J. Y. (2020). Cabozantinib in patients with advanced Ewing sarcoma or osteosarcoma (CABONE): a multicentre, single-arm, phase 2 trial. *Lancet Oncol*, 21(3), 446-455. [https://doi.org/10.1016/s1470-2045\(19\)30825-3](https://doi.org/10.1016/s1470-2045(19)30825-3)
- Izumi, D., Ishimoto, T., Miyake, K., Sugihara, H., Eto, K., Sawayama, H., Yasuda, T., Kiyozumi, Y., Kaida, T., & Kurashige, J. (2016). CXCL12/CXCR4 activation by cancer-associated fibroblasts promotes integrin β 1 clustering and invasiveness in gastric cancer. *International journal of cancer*, 138(5), 1207-1219.

- Izumi, D., Ishimoto, T., Sugihara, H., Kojiro, E., Sawayama, H., Miyake, K., Kiyozumi, Y., Kosumi, K., Tokunaga, R., & Harada, K. (2015). CXCL12/CXCR4 activation by cancer-associated fibroblasts promotes integrin β 1 clustering and invasive ability in gastric cancer. In: AACR.
- Janssens, R., Mortier, A., Boff, D., Vanheule, V., Gouwy, M., Franck, C., Larsen, O., Rosenkilde, M. M., Van Damme, J., & Amaral, F. A. (2016). Natural nitration of CXCL12 reduces its signaling capacity and chemotactic activity in vitro and abrogates intra-articular lymphocyte recruitment in vivo. *Oncotarget*, 7(38), 62439.
- Janssens, R., Struyf, S., & Proost, P. (2018). The unique structural and functional features of CXCL12. *Cell Mol Immunol*, 15(4), 299-311. <https://doi.org/10.1038/cmi.2017.107>
- Janssens, R., Struyf, S., & Proost, P. (2018). The unique structural and functional features of CXCL12. *Cellular & molecular immunology*, 15(4), 299-311.
- Ji, Z., Shen, J., Lan, Y., Yi, Q., & Liu, H. (2023). Targeting signaling pathways in osteosarcoma: Mechanisms and clinical studies. *MedComm*, 4(4), e308.
- Ji, Z., Shen, J., Lan, Y., Yi, Q., & Liu, H. (2023). Targeting signaling pathways in osteosarcoma: Mechanisms and clinical studies. *MedComm* (2020), 4(4), e308. <https://doi.org/10.1002/mco2.308>
- Jiang, B. H., & Liu, L. Z. (2009). PI3K/PTEN signaling in angiogenesis and tumorigenesis. *Advances in cancer research*, 102, 19-65.
- Jung, Y., Wang, J., Schneider, A., Sun, Y.-X., Koh-Paige, A., Osman, N., McCauley, L., & Taichman, R. (2006). Regulation of SDF-1 (CXCL12) production by osteoblasts; a possible mechanism for stem cell homing. *Bone*, 38(4), 497-508.
- Jurida, L., Soelch, J., Bartkuhn, M., Handschick, K., Müller, H., Newel, D., Weber, A., Dittrich-Breiholz, O., Schneider, H., & Bhujju, S. (2015). The activation of IL-1-induced enhancers depends on TAK1 kinase activity and NF- κ B p65. *Cell reports*, 10(5), 726-739.
- Kadariya, Y., Menges, C. W., Talarchek, J., Cai, K. Q., Klein-Szanto, A. J., Pietrofesa, R. A., Christofidou-Solomidou, M., Cheung, M., Mossman, B. T., & Shukla, A. (2016). Inflammation-related IL1 β /IL1R signaling promotes the development of asbestos-induced malignant mesothelioma. *Cancer Prevention Research*, 9(5), 406-414.
- Kaewlert, W., Sakonsinsiri, C., Lert-Itthiporn, W., Mahalapbutr, P., Ali, S., Rungrotmongkol, T., Jusakul, A., Armartmuntree, N., Pairojkul, C., & Feng, G. (2024). Buparlisib and ponatinib inhibit aggressiveness of cholangiocarcinoma cells via suppression of IRS1-related pathway by targeting oxidative stress resistance. *Biomedicine & Pharmacotherapy*, 180, 117569.

- Kalluri, R. (2016). The biology and function of fibroblasts in cancer. *Nature Reviews Cancer*, 16(9), 582-598.
- Karin, M. (2006). Nuclear factor- κ B in cancer development and progression. *Nature*, 441(7092), 431-436.
- Karin, M., & Lin, A. (2002). NF- κ B at the crossroads of life and death. *Nature immunology*, 3(3), 221-227.
- Kelly, A., Gunaltay, S., McEntee, C. P., Shuttleworth, E. E., Smedley, C., Houston, S. A., Fenton, T. M., Levison, S., Mann, E. R., & Travis, M. A. (2018). Human monocytes and macrophages regulate immune tolerance via integrin $\alpha\beta 8$ -mediated TGF β activation. *Journal of Experimental Medicine*, 215(11), 2725-2736.
- Kendellen, M. F., Bradford, J. W., Lawrence, C. L., Clark, K. S., & Baldwin, A. S. (2014). Canonical and non-canonical NF- κ B signaling promotes breast cancer tumor-initiating cells. *Oncogene*, 33(10), 1297-1305.
- Kennedy, S. G., Wagner, A. J., Conzen, S. D., Jordan, J., Bellacosa, A., Tsichlis, P. N., & Hay, N. (1997). The PI 3-kinase/Akt signaling pathway delivers an anti-apoptotic signal. *Genes & development*, 11(6), 701-713.
- Khan, H. (2017). Analytical method development in pharmaceutical research: Steps involved in HPLC method development. *Asian Journal of Pharmaceutical Research*, 7(3), 203-207.
- Khongthong, P., Roseweir, A. K., & Edwards, J. (2019). The NF- κ B pathway and endocrine therapy resistance in breast cancer. *Endocrine-related cancer*, 26(6), R369-R380.
- Kim, C. H., & Broxmeyer, H. E. (1998). In vitro behavior of hematopoietic progenitor cells under the influence of chemoattractants: stromal cell-derived factor-1, steel factor, and the bone marrow environment. *Blood, The Journal of the American Society of Hematology*, 91(1), 100-110.
- Kim, H., Yoo, S., Zhou, R., Xu, A., Bernitz, J. M., Yuan, Y., Gomes, A. M., Daniel, M. G., Su, J., Demicco, E. G., Zhu, J., Moore, K. A., Lee, D. F., Lemischka, I. R., & Schaniel, C. (2018). Oncogenic role of SFRP2 in p53-mutant osteosarcoma development via autocrine and paracrine mechanism. *Proc Natl Acad Sci U S A*, 115(47), E11128-e11137. <https://doi.org/10.1073/pnas.1814044115>
- Kim, K.-E., Gu, C., Thakur, S., Vieira, E., Lin, J. C., & Rabson, A. B. (2000). Transcriptional regulatory effects of lymphoma-associated NFKB2/lyt10 protooncogenes. *Oncogene*, 19(10), 1334-1345.
- Kim, K., Kim, H. H., Kim, J. H., Choi, Y. H., Kim, Y. H., & Cheong, J. (2007). Chemokine stromal cell-derived factor-1 induction by C/EBP β activation is associated with all-trans-retinoic acid-induced leukemic cell differentiation. *Journal of Leucocyte Biology*, 82(5), 1332-1339.

- Kim, S. Y., Lee, C. H., Midura, B. V., Yeung, C., Mendoza, A., Hong, S. H., Ren, L., Wong, D., Korz, W., & Merzouk, A. (2008). Inhibition of the CXCR4/CXCL12 chemokine pathway reduces the development of murine pulmonary metastases. *Clinical & Experimental Metastasis*, 25(3), 201-211.
- Kim, S. Y., Lee, C. H., Midura, B. V., Yeung, C., Mendoza, A., Hong, S. H., Ren, L., Wong, D., Korz, W., Merzouk, A., Salari, H., Zhang, H., Hwang, S. T., Khanna, C., & Helman, L. J. (2008). Inhibition of the CXCR4/CXCL12 chemokine pathway reduces the development of murine pulmonary metastases. *Clin Exp Metastasis*, 25(3), 201-211. <https://doi.org/10.1007/s10585-007-9133-3>
- Kimura, Y., Tomihara, K., Tachinami, H., Imaue, S., Nakamori, K., Fujiwara, K., Suzuki, K., Yasuda, T., Miwa, S., & Nakayama, E. (2017). Conventional osteosarcoma of the mandible successfully treated with radical surgery and adjuvant chemotherapy after responding poorly to neoadjuvant chemotherapy: a case report. *Journal of medical case reports*, 11, 1-6.
- Kishore, N., Sommers, C., Mathialagan, S., Guzova, J., Yao, M., Hauser, S., Huynh, K., Bonar, S., Mielke, C., & Albee, L. (2003). A selective IKK-2 inhibitor blocks NF- κ B-dependent gene expression in interleukin-1 β -stimulated synovial fibroblasts. *Journal of Biological Chemistry*, 278(35), 32861-32871.
- Kitamura, T., Qian, B.-Z., Soong, D., Cassetta, L., Noy, R., Sugano, G., Kato, Y., Li, J., & Pollard, J. W. (2015). CCL2-induced chemokine cascade promotes breast cancer metastasis by enhancing retention of metastasis-associated macrophages. *Journal of Experimental Medicine*, 212(7), 1043-1059.
- Kohli, K., Pillarisetty, V. G., & Kim, T. S. (2022). Key chemokines direct migration of immune cells in solid tumors. *Cancer gene therapy*, 29(1), 10-21.
- Kohno, M., & Pouyssegur, J. (2003). Pharmacological inhibitors of the ERK signaling pathway: application as anticancer drugs. *PROGRESS IN CELL CYCLE RESEARCH*, 5, 219-224.
- Kolch, W. (2000). Meaningful relationships: the regulation of the Ras/Raf/MEK/ERK pathway by protein interactions. *Biochemical Journal*, 351(2), 289-305.
- Kondoh, A., Oishi, M., Tezuka, H., & Terada, M. (2020). Development of chiral organosuperbase catalysts consisting of two different organobase functionalities. *Angewandte Chemie International Edition*, 59(19), 7472-7477.
- Kortlever, R. M., Sodir, N. M., Wilson, C. H., Burkhart, D. L., Pellegrinet, L., Swigart, L. B., Littlewood, T. D., & Evan, G. I. (2017). Myc cooperates with Ras by programming inflammation and immune suppression. *cell*, 171(6), 1301-1315. e1314.
- Krempski, J., Karyampudi, L., Behrens, M. D., Erskine, C. L., Hartmann, L., Dong, H., Goode, E. L., Kalli, K. R., & Knutson, K. L. (2011). Tumor-infiltrating programmed death receptor-1+ dendritic cells

- mediate immune suppression in ovarian cancer. *The Journal of Immunology*, 186(12), 6905-6913.
- Kryczek, I., Lange, A., Mottram, P., Alvarez, X., Cheng, P., Hogan, M., Moons, L., Wei, S., Zou, L., & Machelon, V. (2005). CXCL12 and vascular endothelial growth factor synergistically induce neoangiogenesis in human ovarian cancers. *Cancer research*, 65(2), 465-472.
- Kucharzewska, P., Maracle, C. X., Jeucken, K. C. M., van Hamburg, J. P., Israelsson, E., Furber, M., Tas, S. W., & Olsson, H. K. (2019). NIK-IKK complex interaction controls NF- κ B-dependent inflammatory activation of endothelium in response to LT β R ligation. *J Cell Sci*, 132(7). <https://doi.org/10.1242/jcs.225615>
- Kuhne, M. R., Mulvey, T., Belanger, B., Chen, S., Pan, C., Chong, C., Cao, F., Niekro, W., Kempe, T., & Henning, K. A. (2013). BMS-936564/MDX-1338: a fully human anti-CXCR4 antibody induces apoptosis in vitro and shows antitumor activity in vivo in hematologic malignancies. *Clinical cancer research*, 19(2), 357-366.
- Kumar, S., Stecher, G., Li, M., Knyaz, C., & Tamura, K. (2018). MEGA X: molecular evolutionary genetics analysis across computing platforms. *Molecular biology and evolution*, 35(6), 1547-1549.
- Lakins, M. A., Ghorani, E., Munir, H., Martins, C. P., & Shields, J. D. (2018). Cancer-associated fibroblasts induce antigen-specific deletion of CD8⁺ T Cells to protect tumour cells. *Nature communications*, 9(1), 948.
- Lali, F. V., Hunt, A. E., Turner, S. J., & Foxwell, B. M. (2000). The pyridinyl imidazole inhibitor SB203580 blocks phosphoinositide-dependent protein kinase activity, protein kinase B phosphorylation, and retinoblastoma hyperphosphorylation in interleukin-2-stimulated T cells independently of p38 mitogen-activated protein kinase. *Journal of Biological Chemistry*, 275(10), 7395-7402.
- Larue, L., & Bellacosa, A. (2005). Epithelial–mesenchymal transition in development and cancer: role of phosphatidylinositol 3' kinase/AKT pathways. *Oncogene*, 24(50), 7443-7454.
- Lawrence, T., Bebie, M., Liu, G. Y., Nizet, V., & Karin, M. (2005). IKK α limits macrophage NF- κ B activation and contributes to the resolution of inflammation. *Nature*, 434(7037), 1138-1143. <https://doi.org/10.1038/nature03491>
- Leach, D. R., Krummel, M. F., & Allison, J. P. (1996). Enhancement of antitumor immunity by CTLA-4 blockade. *Science*, 271(5256), 1734-1736.
- Lenardo, M. J., & Baltimore, D. (1989). NF- κ B: a pleiotropic mediator of inducible and tissue-specific gene control. *cell*, 58(2), 227-229.

- Levoye, A., Balabanian, K., Baleux, F., Bachelier, F., & Lagane, B. (2009). CXCR7 heterodimerizes with CXCR4 and regulates CXCL12-mediated G protein signaling. *Blood, The Journal of the American Society of Hematology*, 113(24), 6085-6093.
- Li, B., Wang, Z., Wu, H., Xue, M., Lin, P., Wang, S., Lin, N., Huang, X., Pan, W., & Liu, M. (2018). Epigenetic regulation of CXCL12 plays a critical role in mediating tumor progression and the immune response in osteosarcoma. *Cancer research*, 78(14), 3938-3953.
- Li, D.-k., & Wang, G.-h. (2022). Asiaticoside reverses M2 phenotype macrophage polarization-evoked osteosarcoma cell malignant behaviour by TRAF6/NF- κ B inhibition. *Pharmaceutical Biology*, 60(1), 1635-1645.
- Li, H., Wolfe, A., Septer, S., Edwards, G., Zhong, X., Bashar Abdulkarim, A., Ranganathan, S., & Apte, U. (2012). Deregulation of Hippo kinase signalling in human hepatic malignancies. *Liver International*, 32(1), 38-47.
- Li, L., & Hong, Z. (2016). IL-1 β /NF- κ B signaling promotes colorectal cancer cell growth through miR-181a/PTEN axis. *Archives of biochemistry and biophysics*, 604, 20-26.
- Li, R., Shi, Y., Zhao, S., Shi, T., & Zhang, G. (2019). NF- κ B signaling and integrin- β 1 inhibition attenuates osteosarcoma metastasis via increased cell apoptosis. *International journal of biological macromolecules*, 123, 1035-1043.
- Li, S. Z., Zhang, H. H., Liang, J. B., Song, Y., Jin, B. X., Xing, N. N., Fan, G. C., Du, R. L., & Zhang, X. D. (2014). Nemo-like kinase (NLK) negatively regulates NF- κ B activity through disrupting the interaction of TAK1 with IKK β . *Biochim Biophys Acta*, 1843(7), 1365-1372. <https://doi.org/10.1016/j.bbamcr.2014.03.028>
- Li, Y., Flores, R., Yu, A., Okcu, M. F., Murray, J., Chintagumpala, M., Hicks, J., Lau, C. C., & Man, T. K. (2011). Elevated expression of CXC chemokines in pediatric osteosarcoma patients. *Cancer*, 117(1), 207-217.
- Liang, C., Zhang, M., & Sun, S.-C. (2006). β -TrCP binding and processing of NF- κ B2/p100 involve its phosphorylation at serines 866 and 870. *Cellular Signalling*, 18(8), 1309-1317.
- Liao, D., Zhong, L., Duan, T., Zhang, R.-H., Wang, X., Wang, G., Hu, K., Lv, X., & Kang, T. (2015). Aspirin suppresses the growth and metastasis of osteosarcoma through the NF- κ B pathway. *Clinical cancer research*, 21(23), 5349-5359.
- Liao, G., Zhang, M., Harhaj, E. W., & Sun, S.-C. (2004). Regulation of the NF- κ B-inducing kinase by tumor necrosis factor receptor-associated factor 3-induced degradation. *Journal of Biological Chemistry*, 279(25), 26243-26250.

- Liao, W., Overman, M. J., Boutin, A. T., Shang, X., Zhao, D., Dey, P., Li, J., Wang, G., Lan, Z., & Li, J. (2019). KRAS-IRF2 axis drives immune suppression and immune therapy resistance in colorectal cancer. *Cancer cell*, 35(4), 559-572. e557.
- Liao, Y.-X., Fu, Z.-Z., Zhou, C.-H., Shan, L.-C., Wang, Z. Y., Yin, F., Zheng, L.-P., Hua, Y.-Q., & Cai, Z.-D. (2015). AMD3100 reduces CXCR4-mediated survival and metastasis of osteosarcoma by inhibiting JNK and Akt, but not p38 or Erk1/2, pathways in in vitro and mouse experiments. *Oncology reports*, 34(1), 33-42.
- Liao, Y. X., Fu, Z. Z., Zhou, C. H., Shan, L. C., Wang, Z. Y., Yin, F., Zheng, L. P., Hua, Y. Q., & Cai, Z. D. (2015). AMD3100 reduces CXCR4-mediated survival and metastasis of osteosarcoma by inhibiting JNK and Akt, but not p38 or Erk1/2, pathways in in vitro and mouse experiments. *Oncol Rep*, 34(1), 33-42. <https://doi.org/10.3892/or.2015.3992>
- Lin, A., Giuliano, C. J., Palladino, A., John, K. M., Abramowicz, C., Yuan, M. L., Sausville, E. L., Lukow, D. A., Liu, L., & Chait, A. R. (2019). Off-target toxicity is a common mechanism of action of cancer drugs undergoing clinical trials. *Science translational medicine*, 11(509), eaaw8412.
- Lin, C.-H., Shih, C.-H., Lin, Y.-C., Yang, Y.-L., & Chen, B.-C. (2018). MEKK1, JNK, and SMAD3 mediate CXCL12-stimulated connective tissue growth factor expression in human lung fibroblasts. *Journal of Biomedical Science*, 25(1), 1-11.
- Ling, L., Cao, Z., & Goeddel, D. V. (1998). NF- κ B-inducing kinase activates IKK- α by phosphorylation of Ser-176. *Proceedings of the National Academy of Sciences*, 95(7), 3792-3797.
- Liou, H. C., & Hsia, C. Y. (2003). Distinctions between c-Rel and other NF- κ B proteins in immunity and disease. *Bioessays*, 25(8), 767-780.
- Liu, C.-F., Liu, S.-Y., Min, X.-Y., Ji, Y.-Y., Wang, N., Liu, D., Ma, N., Li, Z.-F., & Li, K. (2014). The prognostic value of CXCR4 in ovarian cancer: a meta-analysis. *PloS one*, 9(3), e92629.
- Liu, J.-F., Chen, P.-C., Chang, T.-M., & Hou, C.-H. (2020). Monocyte Chemoattractant Protein-1 promotes cancer cell migration via c-Raf/MAPK/AP-1 pathway and MMP-9 production in osteosarcoma. *Journal of Experimental & Clinical Cancer Research*, 39, 1-16.
- Liu, J.-j., Liu, S., Wang, J.-g., Zhu, W., Hua, Y.-q., Sun, W., & Cai, Z.-d. (2013). Telangiectatic osteosarcoma: a review of literature. *OncoTargets and therapy*, 593-602.
- Liu, L., Xu, Y., Reiter, R. J., Pan, Y., Chen, D., Liu, Y., Pu, X., Jiang, L., & Li, Z. (2016). Inhibition of ERK1/2 signaling pathway is involved in melatonin's antiproliferative effect on human MG-63 osteosarcoma cells. *Cellular Physiology and Biochemistry*, 39(6), 2297-2307.
- Liu, T., Zhang, L., Joo, D., & Sun, S.-C. (2017). NF- κ B signaling in inflammation. *Signal transduction and targeted therapy*, 2(1), 1-9.

- Liu, X., Xiao, Q., Bai, X., Yu, Z., Sun, M., Zhao, H., Mi, X., Wang, E., Yao, W., & Jin, F. (2014). Activation of STAT3 is involved in malignancy mediated by CXCL12-CXCR4 signaling in human breast cancer. *Oncology reports*, 32(6), 2760-2768.
- Lopez-Haber, C., Barrio-Real, L., Casado-Medrano, V., & Kazanietz, M. G. (2016). Heregulin/ErbB3 signaling enhances CXCR4-driven Rac1 activation and breast cancer cell motility via hypoxia-inducible factor 1 α . *Molecular and cellular biology*, 36(15), 2011-2026.
- Lounsbury, N. (2020). Advances in CXCR7 modulators. *Pharmaceuticals*, 13(2), 33.
- Lu, J., Hu, Z., Deng, Y., Wu, Q., Wu, M., & Song, H. (2021). MEKK2 and MEKK3 orchestrate multiple signals to regulate Hippo pathway. *Journal of Biological Chemistry*, 296.
- Lu, J., Luo, Y., Rao, D., Wang, T., Lei, Z., Chen, X., Zhang, B., Li, Y., Liu, B., & Xia, L. (2024). Myeloid-derived suppressor cells in cancer: therapeutic targets to overcome tumor immune evasion. *Experimental Hematology & Oncology*, 13(1), 39.
- Lu, Y., Xiang, T., Bartberger, M. D., Bernard, C., Bostick, T., Huang, L., Liu, L., Siegmund, A., Sukay, G., & Guo, G. (2006). An efficient one-pot construction of substituted pyrimidinones. *Tetrahedron*, 62(50), 11714-11723.
- Luker, K. E., Lewin, S. A., Mihalko, L. A., Schmidt, B. T., Winkler, J. S., Coggins, N. L., Thomas, D. G., & Luker, G. D. (2012). Scavenging of CXCL12 by CXCR7 promotes tumor growth and metastasis of CXCR4-positive breast cancer cells. *Oncogene*, 31(45), 4750-4758.
- Luo, J., Manning, B. D., & Cantley, L. C. (2003). Targeting the PI3K-Akt pathway in human cancer: rationale and promise. *Cancer cell*, 4(4), 257-262.
- Ma, J., Liang, W., Qiang, Y., Li, L., Du, J., Pan, C., Chen, B., Zhang, C., Chen, Y., & Wang, Q. (2021). Interleukin-1 receptor antagonist inhibits metastatic potential by down-regulating CXCL12/CXCR4 signaling axis in colorectal cancer. *Cell Communication and Signaling*, 19(1), 1-13.
- Madge, L. A., Kluger, M. S., Orange, J. S., & May, M. J. (2008). Lymphotoxin-alpha 1 beta 2 and LIGHT induce classical and noncanonical NF-kappa B-dependent proinflammatory gene expression in vascular endothelial cells. *J Immunol*, 180(5), 3467-3477. <https://doi.org/10.4049/jimmunol.180.5.3467>
- Mahato, R., Qin, B., & Cheng, K. (2011). Blocking IKK α expression inhibits prostate cancer invasiveness. *Pharmaceutical research*, 28, 1357-1369.
- Mamessier, E., Sylvain, A., Thibault, M.-L., Houvenaeghel, G., Jacquemier, J., Castellano, R., Gonçalves, A., André, P., Romagné, F., & Thibault, G. (2011). Human breast cancer cells enhance self

- tolerance by promoting evasion from NK cell antitumor immunity. *The Journal of clinical investigation*, 121(9), 3609-3622.
- Mantovani, A., Marchesi, F., Malesci, A., Laghi, L., & Allavena, P. (2017). Tumour-associated macrophages as treatment targets in oncology. *Nature reviews Clinical oncology*, 14(7), 399-416.
- Marine, T., Melina, M., Zoe, W., Wei, T. L., Lucas, R., Mark, H., Joshua, H., Fangfang, L., Julyanne, B., & Yicong, L. (2022). Mesenchymal Progenitors set the homeostatic inflammatory milieu via the TAK1-NFkB axis. *bioRxiv*, 2022.2012.2011.519940.
- Mascaux, C., Iannino, N., Martin, B., Paesmans, M., Berghmans, T., Dusart, M., Haller, A., Lothaire, P., Meert, A.-P., & Noel, S. (2005). The role of RAS oncogene in survival of patients with lung cancer: a systematic review of the literature with meta-analysis. *British journal of cancer*, 92(1), 131-139.
- Massagué, J. (2008). TGFβ in cancer. *cell*, 134(2), 215-230.
- Matsumoto, K., Hashimoto, S., Gon, Y., Nakayama, T., & Horie, T. (1998). Proinflammatory cytokine-induced and chemical mediator-induced IL-8 expression in human bronchial epithelial cells through p38 mitogen-activated protein kinase-dependent pathway. *Journal of allergy and clinical immunology*, 101(6), 825-831.
- Matsuo, Y., Ochi, N., Sawai, H., Yasuda, A., Takahashi, H., Funahashi, H., Takeyama, H., Tong, Z., & Guha, S. (2009). CXCL8/IL-8 and CXCL12/SDF-1α co-operatively promote invasiveness and angiogenesis in pancreatic cancer. *International journal of cancer*, 124(4), 853-861.
- McIntosh, K., Khalaf, Y. H., Craig, R., West, C., McCulloch, A., Waghmare, A., Lawson, C., Chan, E. Y., Mackay, S., & Paul, A. (2023). IL-1β stimulates a novel, IKKα-dependent, NIK-independent activation of non-canonical NFκB signalling. *Cellular Signalling*, 107, 110684.
- Mercurio, L., Ajmone-Cat, M. A., Cecchetti, S., Ricci, A., Bozzuto, G., Molinari, A., Manni, I., Pollo, B., Scala, S., Carpinelli, G., & Minghetti, L. (2016). Targeting CXCR4 by a selective peptide antagonist modulates tumor microenvironment and microglia reactivity in a human glioblastoma model. *J Exp Clin Cancer Res*, 35, 55. <https://doi.org/10.1186/s13046-016-0326-y>
- Micalizzi, D. S., Farabaugh, S. M., & Ford, H. L. (2010). Epithelial-mesenchymal transition in cancer: parallels between normal development and tumor progression. *Journal of mammary gland biology and neoplasia*, 15(2), 117-134.
- Michelini, S., Sarajlic, M., Duschl, A., & Horejs-Hoeck, J. (2018). IL-1β induces expression of costimulatory molecules and cytokines but not immune feedback regulators in dendritic cells. *Human Immunology*, 79(8), 610-615.

- Michielsen, A. J., Hogan, A. E., Marry, J., Tusetto, M., Cox, F., Hyland, J. M., Sheahan, K. D., O'Donoghue, D. P., Mulcahy, H. E., & Ryan, E. J. (2011). Tumour tissue microenvironment can inhibit dendritic cell maturation in colorectal cancer. *PLoS one*, 6(11), e27944.
- Mirabello, L., Troisi, R. J., & Savage, S. A. (2009). Osteosarcoma incidence and survival rates from 1973 to 2004: data from the Surveillance, Epidemiology, and End Results Program. *Cancer*, 115(7), 1531-1543. <https://doi.org/10.1002/cncr.24121>
- Mohammad, R. M., Muqbil, I., Lowe, L., Yedjou, C., Hsu, H.-Y., Lin, L.-T., Siegelin, M. D., Fimognari, C., Kumar, N. B., & Dou, Q. P. (2015). Broad targeting of resistance to apoptosis in cancer. *Seminars in cancer biology*,
- Moldoveanu, S. C., & David, V. (2022). *Essentials in modern HPLC separations*. Elsevier.
- Moll, N. M., & Ransohoff, R. M. (2010). CXCL12 and CXCR4 in bone marrow physiology. *Expert review of hematology*, 3(3), 315-322.
- Morgan, M. J., & Liu, Z.-g. (2011). Crosstalk of reactive oxygen species and NF- κ B signaling. *Cell research*, 21(1), 103-115.
- Morgan, T. M., Koreckij, T. D., & Corey, E. (2009). Targeted therapy for advanced prostate cancer: inhibition of the PI3K/Akt/mTOR pathway. *Current cancer drug targets*, 9(2), 237-249.
- Mortezaee, K. (2020). CXCL12/CXCR4 axis in the microenvironment of solid tumors: A critical mediator of metastasis. *Life sciences*, 249, 117534.
- Mota, F. L., Carneiro, A. P., Queimada, A. J., Pinho, S. P., & Macedo, E. A. (2009). Temperature and solvent effects in the solubility of some pharmaceutical compounds: Measurements and modeling. *European journal of pharmaceutical sciences*, 37(3-4), 499-507.
- Mukaida, N. (2003). Pathophysiological roles of interleukin-8/CXCL8 in pulmonary diseases. *American Journal of Physiology-Lung Cellular and Molecular Physiology*, 284(4), L566-L577.
- Mukhopadhyay, H., & Lee, N. Y. (2020). Multifaceted roles of TAK1 signaling in cancer. *Oncogene*, 39(7), 1402-1413.
- Mulero, M. C., Wang, V. Y.-F., Huxford, T., & Ghosh, G. (2019). Genome reading by the NF- κ B transcription factors. *Nucleic acids research*, 47(19), 9967-9989.
- Müller, A., Homey, B., Soto, H., Ge, N., Catron, D., Buchanan, M. E., McClanahan, T., Murphy, E., Yuan, W., & Wagner, S. N. (2001). Involvement of chemokine receptors in breast cancer metastasis. *nature*, 410(6824), 50-56.

- Murad, H. A., Rafeeq, M. M., & Alqurashi, T. M. (2021). Role and implications of the CXCL12/CXCR4/CXCR7 axis in atherosclerosis: still a debate. *Annals of medicine*, 53(1), 1598-1612.
- Muta, T. (2006). I κ B- ζ : an inducible regulator of nuclear factor- κ B. *Vitamins & Hormones*, 74, 301-316.
- Nagasawa, T., Hirota, S., Tachibana, K., Takakura, N., Nishikawa, S.-i., Kitamura, Y., Yoshida, N., Kikutani, H., & Kishimoto, T. (1996). Defects of B-cell lymphopoiesis and bone-marrow myelopoiesis in mice lacking the CXC chemokine PBSF/SDF-1. *Nature*, 382(6592), 635-638.
- Nagasawa, T., Nakajima, T., Tachibana, K., Iizasa, H., Bleul, C. C., Yoshie, O., Matsushima, K., Yoshida, N., Springer, T. A., & Kishimoto, T. (1996). Molecular cloning and characterization of a murine pre-B-cell growth-stimulating factor/stromal cell-derived factor 1 receptor, a murine homolog of the human immunodeficiency virus 1 entry coreceptor fusin. *Proceedings of the National Academy of Sciences*, 93(25), 14726-14729.
- Nakajima, H., Sim, F. H., Bond, J. R., & Unni, K. K. (1997). Small cell osteosarcoma of bone: review of 72 cases. *Cancer: Interdisciplinary International Journal of the American Cancer Society*, 79(11), 2095-2106.
- Napetschnig, J., & Wu, H. (2013). Molecular basis of NF- κ B signaling. *Annual review of biophysics*, 42(1), 443-468.
- Narducci, M. G., Scala, E., Bresin, A., Caprini, E., Picchio, M. C., Remotti, D., Ragone, G., Nasorri, F., Frontani, M., & Arcelli, D. (2006). Skin homing of Sezary cells involves SDF-1-CXCR4 signaling and down-regulation of CD26/dipeptidylpeptidase IV. *Blood*, 107(3), 1108-1115.
- Neophytou, C. M., Trougakos, I. P., Erin, N., & Papageorgis, P. (2021). Apoptosis deregulation and the development of cancer multi-drug resistance. *Cancers*, 13(17), 4363.
- Nervi, B., Ramirez, P., Rettig, M. P., Uy, G. L., Holt, M. S., Ritchey, J. K., Prior, J. L., Piwnica-Worms, D., Bridger, G., & Ley, T. J. (2009). Chemosensitization of acute myeloid leukemia (AML) following mobilization by the CXCR4 antagonist AMD3100. *Blood, The Journal of the American Society of Hematology*, 113(24), 6206-6214.
- Neumann, M., & Naumann, M. (2007). Beyond I κ Bs: alternative regulation of NF- κ B activity. *The FASEB Journal*, 21(11), 2642-2654.
- Ninomiya-Tsuji, J., Kajino, T., Ono, K., Ohtomo, T., Matsumoto, M., Shiina, M., Mihara, M., Tsuchiya, M., & Matsumoto, K. (2003). A resorcylic acid lactone, 5Z-7-oxozeaenol, prevents inflammation by inhibiting the catalytic activity of TAK1 MAPK kinase kinase. *Journal of Biological Chemistry*, 278(20), 18485-18490.

- Nishikori, M. (2005). Classical and alternative NF- κ B activation pathways and their roles in lymphoid malignancies. *Journal of clinical and experimental hematopathology*, 45(1), 15-24.
- Nouri, H., Maitigue, M. B., Abid, L., Nouri, N., Abdelkader, A., Bouaziz, M., & Mestiri, M. (2015). Surface osteosarcoma: Clinical features and therapeutic implications. *Journal of bone oncology*, 4(4), 115-123.
- Novack, D. V., Yin, L., Hagen-Stapleton, A., Schreiber, R. D., Goeddel, D. V., Ross, F. P., & Teitelbaum, S. L. (2003). The I κ B function of NF- κ B2 p100 controls stimulated osteoclastogenesis. *Journal of Experimental Medicine*, 198(5), 771-781.
- O'connell, J., O'Sullivan, G. C., Collins, J. K., & Shanahan, F. (1996). The Fas counterattack: Fas-mediated T cell killing by colon cancer cells expressing Fas ligand. *Journal of Experimental Medicine*, 184(3), 1075-1082.
- Oeckinghaus, A., & Ghosh, S. (2009). The NF- κ B family of transcription factors and its regulation. *Cold Spring Harbor perspectives in biology*, 1(4), a000034.
- Ohnishi, E., Goto, T., Sato, A., Kim, M.-s., Iemura, S.-i., Ishitani, T., Natsume, T., Ohnishi, J., & Shibuya, H. (2010). Nemo-like kinase, an essential effector of anterior formation, functions downstream of p38 mitogen-activated protein kinase. *Molecular and cellular biology*, 30(3), 675-683.
- Orimo, A., Gupta, P. B., Sgroi, D. C., Arenzana-Seisdedos, F., Delaunay, T., Naeem, R., Carey, V. J., Richardson, A. L., & Weinberg, R. A. (2005). Stromal fibroblasts present in invasive human breast carcinomas promote tumor growth and angiogenesis through elevated SDF-1/CXCL12 secretion. *cell*, 121(3), 335-348.
- Östman, A., & Augsten, M. (2009). Cancer-associated fibroblasts and tumor growth—bystanders turning into key players. *Current opinion in genetics & development*, 19(1), 67-73.
- Özdemir, B. C., Pentcheva-Hoang, T., Carstens, J. L., Zheng, X., Wu, C.-C., Simpson, T. R., Laklai, H., Sugimoto, H., Kahlert, C., & Novitskiy, S. V. (2014). Depletion of carcinoma-associated fibroblasts and fibrosis induces immunosuppression and accelerates pancreas cancer with reduced survival. *Cancer cell*, 25(6), 719-734.
- Pallegar, N. K., & Christian, S. L. (2020). Adipocytes in the tumour microenvironment. *Tumor microenvironment: non-hematopoietic cells*, 1-13.
- Park, B.-H., Qiang, L., & Farmer, S. R. (2004). Phosphorylation of C/EBP β at a consensus extracellular signal-regulated kinase/glycogen synthase kinase 3 site is required for the induction of adiponectin gene expression during the differentiation of mouse fibroblasts into adipocytes. *Molecular and cellular biology*, 24(19), 8671-8680.

- Parri, M., & Chiarugi, P. (2010). Rac and Rho GTPases in cancer cell motility control. *Cell communication and signaling*, 8, 1-14.
- Paruch, K., Carbain, B., Havel, S., Vsiansky, V., Nikulenkov, F., & Krejci, L. (2019). *Substituted propanamides as inhibitors of nucleases* (WO2019/201867A1). <https://patentscope.wipo.int/search/en/detail.jsf?docid=WO201920187> Accessed 24/4/2025
- Patil, T. R., Patil, V. G., Pawar, S. P., Dhankani, M. A., & Dhankani, A. R. (2023). A COMPREHENSIVE REVIEW ON STABILITY INDICATING METHOD DEVELOPMENT USING UHPLC.
- Pauken, K. E., & Wherry, E. J. (2015). SnapShot: T cell exhaustion. *cell*, 163(4), 1038-1038. e1031.
- Pavlidis, E. T., & Pavlidis, T. E. (2013). Role of bevacizumab in colorectal cancer growth and its adverse effects: a review. *World journal of gastroenterology: WJG*, 19(31), 5051.
- Payne, A. S., & Cornelius, L. A. (2002). The role of chemokines in melanoma tumor growth and metastasis. *Journal of Investigative Dermatology*, 118(6), 915-922.
- Peltier, L. F. (1993). *Orthopedics: a history and iconography*. Norman publishing.
- Perissinotto, E., Cavalloni, G., Leone, F., Fonsato, V., Mitola, S., Grignani, G., Surrenti, N., Sangiolo, D., Bussolino, F., & Piacibello, W. (2005). Involvement of chemokine receptor 4/stromal cell-derived factor 1 system during osteosarcoma tumor progression. *Clinical cancer research*, 11(2), 490-497.
- Petit, I., Jin, D., & Rafii, S. (2007). The SDF-1-CXCR4 signaling pathway: a molecular hub modulating neo-angiogenesis. *Trends Immunol*, 28(7), 299-307. <https://doi.org/10.1016/j.it.2007.05.007>
- Picci, P. (2007). Osteosarcoma (Osteogenic sarcoma). *Orphanet Journal of Rare Diseases*, 2(1), 6. <https://doi.org/10.1186/1750-1172-2-6>
- Pignochino, Y., Grignani, G., Cavalloni, G., Motta, M., Tapparo, M., Bruno, S., Bottos, A., Gammaitoni, L., Migliardi, G., & Camussi, G. (2009). Sorafenib blocks tumour growth, angiogenesis and metastatic potential in preclinical models of osteosarcoma through a mechanism potentially involving the inhibition of ERK1/2, MCL-1 and ezrin pathways. *Molecular Cancer*, 8, 1-17.
- Plitas, G., & Rudensky, A. Y. (2020). Regulatory T cells in cancer. *Annual Review of Cancer Biology*, 4(1), 459-477.
- Prescott, J. A., Balmanno, K., Mitchell, J. P., Okkenhaug, H., & Cook, S. J. (2022). IKK α plays a major role in canonical NF- κ B signalling in colorectal cells. *Biochemical Journal*, 479(3), 305-325.

- Prieto-Martínez, F. D., López-López, E., Juárez-Mercado, K. E., & Medina-Franco, J. L. (2019). Computational drug design methods—current and future perspectives. *In silico drug design*, 19-44.
- Pyrillou, K., Burzynski, L. C., & Clarke, M. C. (2020). Alternative pathways of IL-1 activation, and its role in health and disease. *Frontiers in immunology*, 11, 613170.
- Qian, B.-Z., Li, J., Zhang, H., Kitamura, T., Zhang, J., Campion, L. R., Kaiser, E. A., Snyder, L. A., & Pollard, J. W. (2011). CCL2 recruits inflammatory monocytes to facilitate breast-tumour metastasis. *Nature*, 475(7355), 222-225.
- Qian, B.-Z., & Pollard, J. W. (2010). Macrophage diversity enhances tumor progression and metastasis. *Cell*, 141(1), 39-51.
- Qiao, N., Wang, L., Wang, T., & Li, H. (2016). Inflammatory CXCL12-CXCR4/CXCR7 axis mediates G-protein signaling pathway to influence the invasion and migration of nasopharyngeal carcinoma cells. *Tumor Biology*, 37(6), 8169-8179.
- Qin, J., Yao, J., Cui, G., Xiao, H., Kim, T. W., Fraczek, J., Wightman, P., Sato, S., Akira, S., & Puel, A. (2006). TLR8-mediated NF- κ B and JNK activation are TAK1-independent and MEKK3-dependent. *Journal of Biological Chemistry*, 281(30), 21013-21021.
- Quail, D. F., & Dannenberg, A. J. (2019). The obese adipose tissue microenvironment in cancer development and progression. *Nature Reviews Endocrinology*, 15(3), 139-154.
- Quail, D. F., & Joyce, J. A. (2013). Microenvironmental regulation of tumor progression and metastasis. *Nature medicine*, 19(11), 1423-1437.
- Ray, P., Stacer, A. C., Fenner, J., Cavnar, S. P., Meguiar, K., Brown, M., Luker, K. E., & Luker, G. D. (2015). CXCL12- γ in primary tumors drives breast cancer metastasis. *Oncogene*, 34(16), 2043-2051.
- Raymond, L., Eck, S., Mollmark, J., Hays, E., Tomek, I., Kantor, S., Elliott, S., & Vincenti, M. (2006). Interleukin-1 beta induction of matrix metalloproteinase-1 transcription in chondrocytes requires ERK-dependent activation of CCAAT enhancer-binding protein-beta. *Journal of cellular physiology*, 207(3), 683-688.
- Raynaud, C. M., Hernandez, J., Llorca, F. P., Nuciforo, P., Mathieu, M.-C., Commo, F., Delaloge, S., Sabatier, L., André, F., & Soria, J.-C. (2010). DNA damage repair and telomere length in normal breast, preneoplastic lesions, and invasive cancer. *American journal of clinical oncology*, 33(4), 341-345.
- Raza, A., Franklin, M. J., & Dudek, A. Z. (2010). Pericytes and vessel maturation during tumor angiogenesis and metastasis. *American journal of hematology*, 85(8), 593-598.

- Razani, B., Reichardt, A. D., & Cheng, G. (2011). Non-canonical NF- κ B signaling activation and regulation: principles and perspectives. *Immunological reviews*, 244(1), 44-54.
- Redondo, A., Cruz, J., Lopez-Pousa, A., & Barón, F. (2013). SEOM clinical guidelines for the treatment of osteosarcoma in adults-2013. *Clinical and Translational Oncology*, 15, 1037-1043.
- Reiners Jr, J. J., Lee, J.-Y., Clift, R. E., Dudley, D. T., & Myrand, S. P. (1998). PD98059 is an equipotent antagonist of the aryl hydrocarbon receptor and inhibitor of mitogen-activated protein kinase kinase. *Molecular pharmacology*, 53(3), 438-445.
- Ridker, P. M., Everett, B. M., Thuren, T., MacFadyen, J. G., Chang, W. H., Ballantyne, C., Fonseca, F., Nicolau, J., Koenig, W., & Anker, S. D. (2017). Antiinflammatory therapy with canakinumab for atherosclerotic disease. *New England Journal of Medicine*, 377(12), 1119-1131.
- Rigo, A., Gottardi, M., Zamò, A., Mauri, P., Bonifacio, M., Krampera, M., Damiani, E., Pizzolo, G., & Vinante, F. (2010). Macrophages may promote cancer growth via a GM-CSF/HB-EGF paracrine loop that is enhanced by CXCL12. *Molecular cancer*, 9(1), 1-13.
- Riley, C., Ammar, U., Alsouk, A., Anthony, N. G., Baiget, J., Berretta, G., Breen, D., Huggan, J., Lawson, C., & McIntosh, K. (2024). Design and synthesis of novel aminoindazole-pyrrolo [2, 3-b] pyridine inhibitors of IKK α that selectively perturb cellular non-canonical NF- κ B signalling. *Molecules*, 29(15), 3515.
- Ritt, D. A., Abreu-Blanco, M. T., Bindu, L., Durrant, D. E., Zhou, M., Specht, S. I., Stephen, A. G., Holderfield, M., & Morrison, D. K. (2016). Inhibition of Ras/Raf/MEK/ERK pathway signaling by a stress-induced phospho-regulatory circuit. *Molecular cell*, 64(5), 875-887.
- Roccaro, A. M., Sacco, A., Jimenez, C., Maiso, P., Moschetta, M., Mishima, Y., Aljawai, Y., Sahin, I., Kuhne, M., & Cardarelli, P. (2014). C1013G/CXCR4 acts as a driver mutation of tumor progression and modulator of drug resistance in lymphoplasmacytic lymphoma. *Blood, the Journal of the American Society of Hematology*, 123(26), 4120-4131.
- Rueda, P., Balabanian, K., Lagane, B., Staropoli, I., Chow, K., Levoye, A., Laguri, C., Sadir, R., Delaunay, T., & Izquierdo, E. (2008). The CXCL12 γ chemokine displays unprecedented structural and functional properties that make it a paradigm of chemoattractant proteins. *PloS one*, 3(7), e2543.
- Rueda, P., Richart, A., Récalde, A., Gasse, P., Vilar, J., Guérin, C., Lortat-Jacob, H., Vieira, P., Baleux, F., & Chretien, F. (2012). Homeostatic and tissue reparation defaults in mice carrying selective genetic invalidation of CXCL12/proteoglycan interactions. *Circulation*, 126(15), 1882-1895.
- Ruscher, K., Kuric, E., Liu, Y., Walter, H. L., Issazadeh-Navikas, S., Englund, E., & Wieloch, T. (2013). Inhibition of CXCL12 signaling attenuates the postischemic immune response and improves

- functional recovery after stroke. *Journal of Cerebral Blood Flow & Metabolism*, 33(8), 1225-1234.
- Russo, R. C., Garcia, C. C., Teixeira, M. M., & Amaral, F. A. (2014). The CXCL8/IL-8 chemokine family and its receptors in inflammatory diseases. *Expert review of clinical immunology*, 10(5), 593-619.
- Sadri, A. (2023). Is Target-Based Drug Discovery Efficient? Discovery and "Off-Target" Mechanisms of All Drugs. *J Med Chem*, 66(18), 12651-12677. <https://doi.org/10.1021/acs.jmedchem.2c01737>
- Sakurai, H. (2012). Targeting of TAK1 in inflammatory disorders and cancer. *Trends in pharmacological sciences*, 33(10), 522-530.
- Salcedo, R., & Oppenheim, J. J. (2003). Role of chemokines in angiogenesis: CXCL12/SDF-1 and CXCR4 interaction, a key regulator of endothelial cell responses. *Microcirculation*, 10(3-4), 359-370.
- Salmon, H., Franciszkiewicz, K., Damotte, D., Dieu-Nosjean, M.-C., Validire, P., Trautmann, A., Mami-Chouaib, F., & Donnadieu, E. (2012). Matrix architecture defines the preferential localization and migration of T cells into the stroma of human lung tumors. *The Journal of clinical investigation*, 122(3), 899-910.
- Santarpia, L., Lippman, S. M., & El-Naggar, A. K. (2012). Targeting the MAPK–RAS–RAF signaling pathway in cancer therapy. *Expert opinion on therapeutic targets*, 16(1), 103-119.
- Santini, D., Schiavon, G., Vincenzi, B., Gaeta, L., Pantano, F., Russo, A., Ortega, C., Porta, C., Galluzzo, S., & Armento, G. (2011). Receptor activator of NF- κ B (RANK) expression in primary tumors associates with bone metastasis occurrence in breast cancer patients. *PloS one*, 6(4), e19234.
- Santoro, M. G., Rossi, A., & Amici, C. (2003). NF- κ B and virus infection: who controls whom. *The EMBO journal*.
- Sarkar, M., Nguyen, T., Gundre, E., Ogunlusi, O., El-Sobky, M., Giri, B., & Sarkar, T. R. (2023). Cancer-associated fibroblasts: The chief architect in the tumor microenvironment. *Frontiers in cell and developmental biology*, 11, 1089068.
- Scala, S. (2015). Molecular Pathways: Targeting the CXCR4-CXCL12 Axis--Untapped Potential in the Tumor Microenvironment. *Clin Cancer Res*, 21(19), 4278-4285. <https://doi.org/10.1158/1078-0432.Ccr-14-0914>
- Schmitz, M. L., Kracht, M., & Saul, V. V. (2014). The intricate interplay between RNA viruses and NF- κ B. *Biochimica et Biophysica Acta (BBA)-Molecular Cell Research*, 1843(11), 2754-2764.
- Scotton, C. J., Wilson, J. L., Scott, K., Stamp, G., Wilbanks, G. D., Fricker, S., Bridger, G., & Balkwill, F. R. (2002). Multiple actions of the chemokine CXCL12 on epithelial tumor cells in human ovarian cancer. *Cancer Res*, 62(20), 5930-5938.

- Sen, R., & Baltimore, D. (1986). Multiple nuclear factors interact with the immunoglobulin enhancer sequences. *cell*, 46(5), 705-716.
- Sever, R., & Brugge, J. S. (2015). Signal transduction in cancer. *Cold Spring Harbor perspectives in medicine*, 5(4), a006098.
- Sevilla, J., Schiavello, E., Madero, L., Pardeo, M., Guggiari, E., Baragaño, M., Luksch, R., & Massimino, M. (2012). Priming of hematopoietic progenitor cells by plerixafor and filgrastim in children with previous failure of mobilization with chemotherapy and/or cytokine treatment. *J Pediatr Hematol Oncol*, 34(2), 146-150. <https://doi.org/10.1097/MPH.0b013e31821c2cb8>
- Shi, H., Ju, Q., Mao, Y., Wang, Y., Ding, J., Liu, X., Tang, X., & Sun, C. (2021). TAK1 phosphorylates RASSF9 and inhibits esophageal squamous tumor cell proliferation by targeting the RAS/MEK/ERK axis. *Advanced Science*, 8(5), 2001575.
- Shi, S., Ou, X., Liu, C., Li, R., Zheng, Q., & Hu, L. (2025). NF-κB signaling and the tumor microenvironment in osteosarcoma: implications for immune evasion and therapeutic resistance. *Frontiers in immunology*, 16, 1518664.
- Shi, Y., Riese, D. J., & Shen, J. (2020a). The role of the CXCL12/CXCR4/CXCR7 chemokine axis in cancer. *Frontiers in pharmacology*, 1969.
- Shi, Y., Riese, D. J., & Shen, J. (2020b). The role of the CXCL12/CXCR4/CXCR7 chemokine axis in cancer. *Frontiers in pharmacology*, 11, 574667.
- Shih, V. F.-S., Tsui, R., Caldwell, A., & Hoffmann, A. (2011). A single NFκB system for both canonical and non-canonical signaling. *Cell research*, 21(1), 86-102.
- Shimizu, S., Brown, M., Sengupta, R., Penfold, M. E., & Meucci, O. (2011). CXCR7 protein expression in human adult brain and differentiated neurons. *PloS one*, 6(5), e20680. <https://doi.org/10.1371/journal.pone.0020680>
- Shirozu, M., Nakano, T., Inazawa, J., Tashiro, K., Tada, H., Shinohara, T., & Honjo, T. (1995). Structure and chromosomal localization of the human stromal cell-derived factor 1 (SDF1) gene. *Genomics*, 28(3), 495-500.
- Siegel, R. L., Miller, K. D., Fuchs, H. E., & Jemal, A. (2022). Cancer statistics, 2022. *CA: a cancer journal for clinicians*.
- Singh, A. K., Arya, R. K., Trivedi, A. K., Sanyal, S., Baral, R., Dormond, O., Briscoe, D. M., & Datta, D. (2013). Chemokine receptor trio: CXCR3, CXCR4 and CXCR7 crosstalk via CXCL11 and CXCL12. *Cytokine & growth factor reviews*, 24(1), 41-49.

- Smyth, M. J., Cretney, E., Kelly, J. M., Westwood, J. A., Street, S. E., Yagita, H., Takeda, K., Van Dommelen, S. L., Degli-Esposti, M. A., & Hayakawa, Y. (2005). Activation of NK cell cytotoxicity. *Molecular immunology*, 42(4), 501-510.
- Snyder, L. R. (2011). *Introduction to modern liquid chromatography* Wiley.
- Sokolova, O., Maubach, G., & Naumann, M. (2014). MEKK3 and TAK1 synergize to activate IKK complex in *Helicobacter pylori* infection. *Biochimica et Biophysica Acta (BBA)-Molecular Cell Research*, 1843(4), 715-724.
- Solt, L. A., Madge, L. A., Orange, J. S., & May, M. J. (2007). Interleukin-1-induced NF- κ B activation is NEMO-dependent but does not require IKK β . *Journal of Biological Chemistry*, 282(12), 8724-8733.
- Son, M. H., Kang, E. S., Kim, D. H., Lee, S. H., Yoo, K. H., Sung, K. W., Koo, H. H., Kim, D. W., Kim, J. Y., & Cho, E. J. (2013). Efficacy and toxicity of plerixafor for peripheral blood stem cell mobilization in children with high-risk neuroblastoma. *Pediatr Blood Cancer*, 60(8), E57-59. <https://doi.org/10.1002/pbc.24506>
- Song, L., Liu, D., Wang, B., He, J., Zhang, S., Dai, Z., Ma, X., & Wang, X. (2015). miR-494 suppresses the progression of breast cancer in vitro by targeting CXCR4 through the Wnt/ β -catenin signaling pathway. *Oncology reports*, 34(1), 525-531.
- Stacer, A. C., Fenner, J., Cavnar, S. P., Xiao, A., Zhao, S., Chang, S. L., Salomonsson, A., Luker, K. E., & Luker, G. D. (2016). Endothelial CXCR7 regulates breast cancer metastasis. *Oncogene*, 35(13), 1716-1724.
- Steelman, L. S., Franklin, R. A., Abrams, S. L., Chappell, W., Kempf, C. R., Bäsecke, J., Stivala, F., Donia, M., Fagone, P., & Nicoletti, F. (2011). Roles of the Ras/Raf/MEK/ERK pathway in leukemia therapy. *Leukemia*, 25(7), 1080-1094.
- Steiner, F., Paul, C., & Dong, M. (2019). HPLC autosamplers: perspectives, principles, and practices.
- Stockhammer, G., Poewe, W., Burgstaller, S., Deisenhammer, F., Muigg, A., Kiechl, S., Schmutzhard, E., Maier, H., Felber, S., & Schumacher, P. (2000). Vascular endothelial growth factor in CSF: a biological marker for carcinomatous meningitis. *Neurology*, 54(8), 1670-1676.
- Stylianou, A., Gkretsi, V., Louca, M., Zacharia, L. C., & Stylianopoulos, T. (2019). Collagen content and extracellular matrix cause cytoskeletal remodelling in pancreatic fibroblasts. *Journal of the Royal Society Interface*, 16(154), 20190226.
- Sudarsanam, S., & Johnson, D. E. (2010). Functional consequences of mTOR inhibition. *Curr Opin Drug Discov Devel*, 13(1), 31-40.

- Sugiyama, T., Kohara, H., Noda, M., & Nagasawa, T. (2006). Maintenance of the hematopoietic stem cell pool by CXCL12-CXCR4 chemokine signaling in bone marrow stromal cell niches. *Immunity*, 25(6), 977-988.
- Sun, S.-C. (2011). Non-canonical NF- κ B signaling pathway. *Cell research*, 21(1), 71-85.
- Sun, S.-C. (2017). The non-canonical NF- κ B pathway in immunity and inflammation. *Nature Reviews Immunology*, 17(9), 545-558.
- Sun, X., Cheng, G., Hao, M., Zheng, J., Zhou, X., Zhang, J., Taichman, R. S., Pienta, K. J., & Wang, J. (2010). CXCL12/CXCR4/CXCR7 chemokine axis and cancer progression. *Cancer and Metastasis Reviews*, 29(4), 709-722.
- Sun, Y.-X., Pedersen, E. A., Shiozawa, Y., Havens, A. M., Jung, Y., Wang, J., Pienta, K. J., & Taichman, R. S. (2008). CD26/dipeptidyl peptidase IV regulates prostate cancer metastasis by degrading SDF-1/CXCL12. *Clinical & Experimental Metastasis*, 25(7), 765-776.
- Sun, Y. X., Fang, M., Wang, J., Cooper, C. R., Pienta, K. J., & Taichman, R. S. (2007). Expression and activation of $\alpha\beta 3$ integrins by SDF-1/CXC12 increases the aggressiveness of prostate cancer cells. *The Prostate*, 67(1), 61-73.
- Sun, Y. X., Wang, J., Shelburne, C. E., Lopatin, D. E., Chinnaiyan, A. M., Rubin, M. A., Pienta, K. J., & Taichman, R. S. (2003). Expression of CXCR4 and CXCL12 (SDF-1) in human prostate cancers (PCa) in vivo. *J Cell Biochem*, 89(3), 462-473. <https://doi.org/10.1002/jcb.10522>
- Taichman, R., & Emerson, S. (1996). Human osteosarcoma cell lines MG-63 and SaOS-2 produce G-CSF and GM-CSF: identification and partial characterization of cell-associated isoforms. *Experimental hematology*, 24(4), 509-517.
- Takahashi, H., Ogata, H., Nishigaki, R., Broide, D. H., & Karin, M. (2010). Tobacco smoke promotes lung tumorigenesis by triggering IKK β -and JNK1-dependent inflammation. *Cancer cell*, 17(1), 89-97.
- Taniguchi, K., & Karin, M. (2018). NF- κ B, inflammation, immunity and cancer: coming of age. *Nature Reviews Immunology*, 18(5), 309-324.
- Taub, D., & Oppenheim, J. (1994). Chemokines, inflammation and the immune system. *Therapeutic immunology*, 1(4), 229-246.
- Taube, J. M., Anders, R. A., Young, G. D., Xu, H., Sharma, R., McMiller, T. L., Chen, S., Klein, A. P., Pardoll, D. M., & Topalian, S. L. (2012). Colocalization of inflammatory response with B7-h1 expression in human melanocytic lesions supports an adaptive resistance mechanism of immune escape. *Science translational medicine*, 4(127), 127ra137-127ra137.

- Teicher, B. A., & Fricker, S. P. (2010). CXCL12 (SDF-1)/CXCR4 pathway in cancer. *Clinical cancer research*, 16(11), 2927-2931.
- Teng, F., Tian, W.-Y., Wang, Y.-M., Zhang, Y.-F., Guo, F., Zhao, J., Gao, C., & Xue, F.-X. (2016a). Cancer-associated fibroblasts promote the progression of endometrial cancer via the SDF-1/CXCR4 axis. *Journal of hematology & oncology*, 9(1), 1-15.
- Teng, F., Tian, W.-Y., Wang, Y.-M., Zhang, Y.-F., Guo, F., Zhao, J., Gao, C., & Xue, F.-X. (2016b). Cancer-associated fibroblasts promote the progression of endometrial cancer via the SDF-1/CXCR4 axis. *Journal of hematology & oncology*, 9, 1-15.
- Topalian, S. L., Hodi, F. S., Brahmer, J. R., Gettinger, S. N., Smith, D. C., McDermott, D. F., Powderly, J. D., Carvajal, R. D., Sosman, J. A., & Atkins, M. B. (2012). Safety, activity, and immune correlates of anti-PD-1 antibody in cancer. *New England Journal of Medicine*, 366(26), 2443-2454.
- Totze, J., Gurbani, D., Raphemot, R., Hughes, P. F., Bodoor, K., Carlson, D. A., Loiselle, D. R., Bera, A. K., Eibschutz, L. S., & Perkins, M. M. (2017). Takinib, a selective TAK1 inhibitor, broadens the therapeutic efficacy of TNF- α inhibition for cancer and autoimmune disease. *Cell chemical biology*, 24(8), 1029-1039. e1027.
- Towbin, H., Staehelin, T., & Gordon, J. (1979). Electrophoretic transfer of proteins from polyacrylamide gels to nitrocellulose sheets: procedure and some applications. *Proceedings of the National Academy of Sciences*, 76(9), 4350-4354.
- Turner, N. C., & Reis-Filho, J. S. (2012). Genetic heterogeneity and cancer drug resistance. *The lancet oncology*, 13(4), e178-e185.
- Vallabhapurapu, S., Matsuzawa, A., Zhang, W., Tseng, P.-H., Keats, J. J., Wang, H., Vignali, D. A., Bergsagel, P. L., & Karin, M. (2008). Nonredundant and complementary functions of TRAF2 and TRAF3 in a ubiquitination cascade that activates NIK-dependent alternative NF- κ B signaling. *Nature immunology*, 9(12), 1364-1370.
- Vara, J. Á. F., Casado, E., de Castro, J., Cejas, P., Belda-Iniesta, C., & González-Barón, M. (2004). PI3K/Akt signalling pathway and cancer. *Cancer treatment reviews*, 30(2), 193-204.
- Verkaar, F., van der Doelen, A. A., Smits, J. F., Blankesteyn, W. M., & Zaman, G. J. (2011). Inhibition of Wnt/ β -catenin signaling by p38 MAP kinase inhibitors is explained by cross-reactivity with casein kinase I δ/ϵ . *Chemistry & biology*, 18(4), 485-494.
- Verstrepen, L., Bekaert, T., Chau, T.-L., Tavernier, J., Chariot, A., & Beyaert, R. (2008). TLR-4, IL-1R and TNF-R signaling to NF- κ B: variations on a common theme. *Cellular and molecular life sciences*, 65, 2964-2978.

- Vertegaal, A. C., Kuiperij, H. B., Yamaoka, S., Courtois, G., van der Eb, A. J., & Zantema, A. (2000). Protein kinase C- α is an upstream activator of the I κ B kinase complex in the TPA signal transduction pathway to NF- κ B in U2OS cells. *Cellular Signalling*, 12(11-12), 759-768.
- Viennois, E., Chen, F., & Merlin, D. (2013). NF- κ B pathway in colitis-associated cancers. *Translational gastrointestinal cancer*, 2(1), 21.
- Vilgelm, A. E., & Richmond, A. (2019). Chemokines modulate immune surveillance in tumorigenesis, metastasis, and response to immunotherapy. *Frontiers in immunology*, 10, 333.
- Von Luetichau, I., Segerer, S., Wechselberger, A., Notohamiprodjo, M., Nathrath, M., Kremer, M., Henger, A., Djafarzadeh, R., Burdach, S., & Huss, R. (2008). A complex pattern of chemokine receptor expression is seen in osteosarcoma. *BMC cancer*, 8, 1-10.
- Voronov, E., Shouval, D. S., Krelin, Y., Cagnano, E., Benharroch, D., Iwakura, Y., Dinarello, C. A., & Apte, R. N. (2003). IL-1 is required for tumor invasiveness and angiogenesis. *Proceedings of the National Academy of Sciences*, 100(5), 2645-2650.
- Vose, J. M., Ho, A. D., Coiffier, B., Corradini, P., Khouri, I., Sureda, A., Van Besien, K., & Dpersio, J. (2009). Advances in mobilization for the optimization of autologous stem cell transplantation. *Leukemia & lymphoma*, 50(9), 1412-1421.
- Wald, O., Izhar, U., Amir, G., Kirshberg, S., Shlomai, Z., Zamir, G., Peled, A., & Shapira, O. M. (2011). Interaction between neoplastic cells and cancer-associated fibroblasts through the CXCL12/CXCR4 axis: Role in non-small cell lung cancer tumor proliferation. *The Journal of thoracic and cardiovascular surgery*, 141(6), 1503-1512.
- Walkley, C. R., Qudsi, R., Sankaran, V. G., Perry, J. A., Gostissa, M., Roth, S. I., Rodda, S. J., Snay, E., Dunning, P., & Fahey, F. H. (2008). Conditional mouse osteosarcoma, dependent on p53 loss and potentiated by loss of Rb, mimics the human disease. *Genes & development*, 22(12), 1662-1676.
- Wan, F., Anderson, D. E., Barnitz, R. A., Snow, A., Bidere, N., Zheng, L., Hegde, V., Lam, L. T., Staudt, L. M., & Levens, D. (2007). Ribosomal protein S3: a KH domain subunit in NF- κ B complexes that mediates selective gene regulation. *cell*, 131(5), 927-939.
- Wang, C., Chen, W., & Shen, J. (2018). CXCR7 targeting and its major disease relevance. *Frontiers in pharmacology*, 9, 641.
- Wang, J., Kan, X., Li, X., Sun, J., & Xu, X. (2022). Porcine epidemic diarrhoea virus (PEDV) infection activates AMPK and JNK through TAK1 to induce autophagy and enhance virus replication. *Virulence*, 13(1), 1697-1712.

- Wang, J., Loberg, R., & Taichman, R. S. (2006). The pivotal role of CXCL12 (SDF-1)/CXCR4 axis in bone metastasis. *Cancer and Metastasis Reviews*, 25(4), 573-587.
- Wang, L., Zhang, F., Cui, J.-Y., Chen, L., Chen, Y.-T., & Liu, B.-W. (2018). CAFs enhance paclitaxel resistance by inducing EMT through the IL-6/JAK2/STAT3 pathway. *Oncology reports*, 39(5), 2081-2090.
- Wang, M., Zhao, J., Zhang, L., Wei, F., Lian, Y., Wu, Y., Gong, Z., Zhang, S., Zhou, J., & Cao, K. (2017). Role of tumor microenvironment in tumorigenesis. *Journal of Cancer*, 8(5), 761.
- Wang, X., & Tournier, C. (2006). Regulation of cellular functions by the ERK5 signalling pathway. *Cellular Signalling*, 18(6), 753-760.
- Waterman, K. C. (2005). Accelerated aging: Prediction of chemical stability of pharmaceuticals. *International Journal of Pharmaceutics*, , 101–125.
- Waugh, D. J., & Wilson, C. (2008). The interleukin-8 pathway in cancer. *Clinical cancer research*, 14(21), 6735-6741.
- Weber, A., Wasiliew, P., & Kracht, M. (2010). Interleukin-1 (IL-1) pathway. *Science signaling*, 3(105), cm1-cm1.
- Wei, Y., Zhou, R., Wang, Q., Beibei, F., Jing, W., & Wang, H. (2016). Expression and function of TAK1 in osteosarcoma tissue. *Int J Clin Exp Med*, 9(6), 10891-10898.
- Wertz, I., & Dixit, V. (2010). Regulation of death receptor signaling by the ubiquitin system. *Cell Death & Differentiation*, 17(1), 14-24.
- Wieczorek, M., Abualrous, E. T., Sticht, J., Álvaro-Benito, M., Stolzenberg, S., Noé, F., & Freund, C. (2017). Major histocompatibility complex (MHC) class I and MHC class II proteins: conformational plasticity in antigen presentation. *Frontiers in immunology*, 8, 292.
- Wilkes, M. C., Siva, K., Chen, J., Varetta, G., Youn, M., Chae, H., Ek, F., Olsson, R., Lundbäck, T., & Dever, D. (2020). Diamond Blackfan anemia is mediated by hyperactive Nemo-like kinase. *Nature communications*, 11(1), 3344. <https://www.nature.com/articles/s41467-020-17100-z.pdf>
- Wolf, D., Sopper, S., Pircher, A., Gastl, G., & Wolf, A. M. (2015). Treg (s) in cancer: friends or foe? *Journal of cellular physiology*, 230(11), 2598-2605.
- Wolf, M., Seleznik, G., Zeller, N., & Heikenwalder, M. (2010). The unexpected role of lymphotoxin β receptor signaling in carcinogenesis: from lymphoid tissue formation to liver and prostate cancer development. *Oncogene*, 29(36), 5006-5018.

- Wolf, M. J., Seleznik, G. M., Zeller, N., & Heikenwalder, M. (2010). The unexpected role of lymphotoxin beta receptor signaling in carcinogenesis: from lymphoid tissue formation to liver and prostate cancer development. *Oncogene*, 29(36), 5006-5018. <https://doi.org/10.1038/onc.2010.260>
- Wu, J., Powell, F., Larsen, N. A., Lai, Z., Byth, K. F., Read, J., Gu, R.-F., Roth, M., Toader, D., & Saeh, J. C. (2013). Mechanism and in vitro pharmacology of TAK1 inhibition by (5 Z)-7-oxozeaenol. *ACS chemical biology*, 8(3), 643-650.
- Xiao, G., Cui, Y., Ducey, P., Karsenty, G., & Franceschi, R. T. (1997). Ascorbic acid-dependent activation of the osteocalcin promoter in MC3T3-E1 preosteoblasts: requirement for collagen matrix synthesis and the presence of an intact OSE2 sequence. *Molecular endocrinology*, 11(8), 1103-1113.
- Xiao, G., Fong, A., & Sun, S.-C. (2004). Induction of p100 processing by NF- κ B-inducing kinase involves docking I κ B kinase α (IKK α) to p100 and IKK α -mediated phosphorylation. *Journal of Biological Chemistry*, 279(29), 30099-30105.
- Xiao, G., Harhaj, E. W., & Sun, S.-C. (2001). NF- κ B-inducing kinase regulates the processing of NF- κ B2 p100. *Molecular cell*, 7(2), 401-409.
- Xie, P., Browning, D. D., Hay, N., Mackman, N., & Ye, R. D. (2000). Activation of NF- κ B by bradykinin through a G α_q -and G $\beta\gamma$ -dependent pathway that involves phosphoinositide 3-kinase and Akt. *Journal of Biological Chemistry*, 275(32), 24907-24914.
- Xu, X., Peng, Q., Jiang, X., Tan, S., Yang, Y., Yang, W., Han, Y., Chen, Y., Oyang, L., & Lin, J. (2023). Metabolic reprogramming and epigenetic modifications in cancer: from the impacts and mechanisms to the treatment potential. *Experimental & molecular medicine*, 55(7), 1357-1370.
- Xu, Y.-R., & Lei, C.-Q. (2021). TAK1-TABs complex: a central signalosome in inflammatory responses. *Frontiers in immunology*, 11, 608976.
- Yang, D., Guo, P., He, T., & Powell, C. A. (2021). Role of endothelial cells in tumor microenvironment. *Clinical and Translational Medicine*, 11(6), e450.
- Yang, J., Shay, C., Saba, N. F., & Teng, Y. (2024). Cancer metabolism and carcinogenesis. *Experimental Hematology & Oncology*, 13(1), 10.
- Yang, L., Pang, Y., & Moses, H. L. (2010). TGF- β and immune cells: an important regulatory axis in the tumor microenvironment and progression. *Trends in immunology*, 31(6), 220-227.
- Yang, S., & Liu, G. (2017). Targeting the Ras/Raf/MEK/ERK pathway in hepatocellular carcinoma. *Oncology letters*, 13(3), 1041-1047.

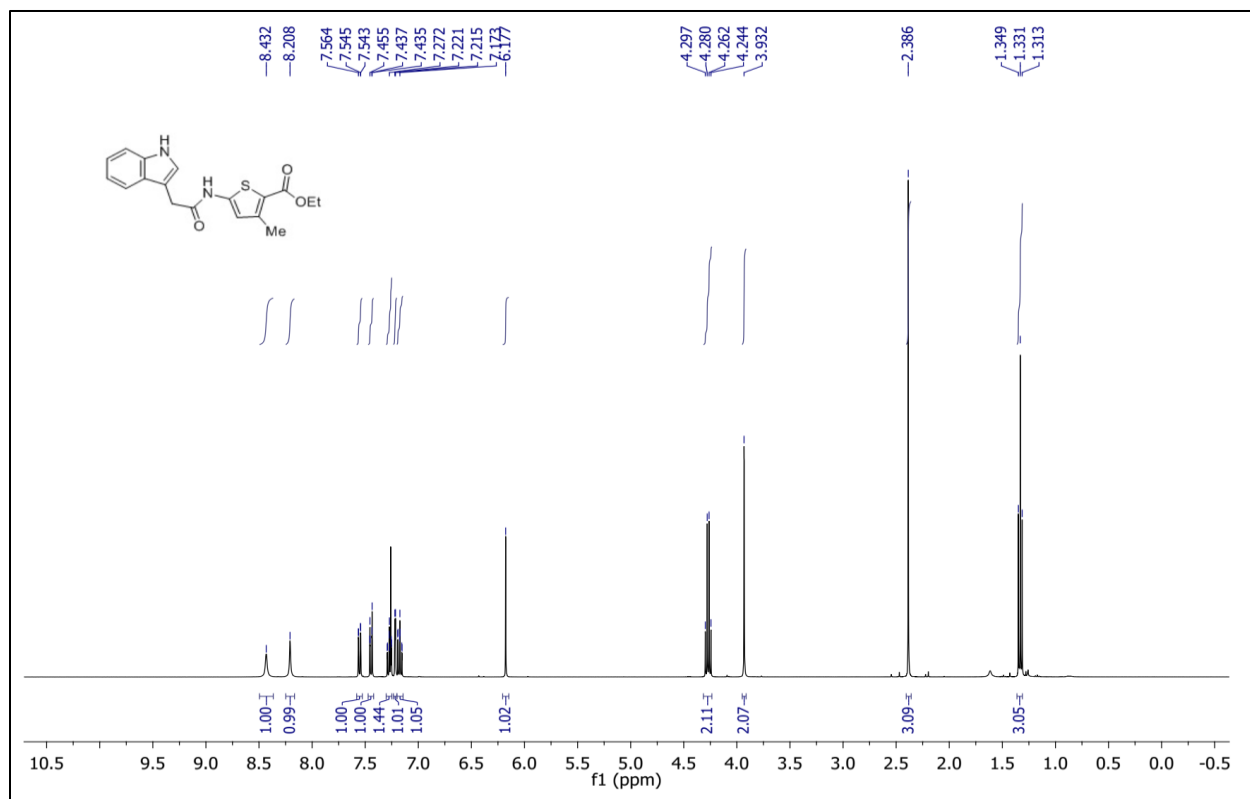
- Yang, S. R., Valvo, S., Yao, H., Kode, A., Rajendrasozhan, S., Edirisinghe, I., Caito, S., Adenuga, D., Henry, R., Fromm, G., Maggirwar, S., Li, J. D., Bulger, M., & Rahman, I. (2008). IKK alpha causes chromatin modification on pro-inflammatory genes by cigarette smoke in mouse lung. *Am J Respir Cell Mol Biol*, 38(6), 689-698. <https://doi.org/10.1165/rcmb.2007-0379OC>
- Yang, Y., Li, J., Lei, W., Wang, H., Ni, Y., Liu, Y., Yan, H., Tian, Y., Wang, Z., Yang, Z., Yang, S., Yang, Y., & Wang, Q. (2023). CXCL12-CXCR4/CXCR7 Axis in Cancer: from Mechanisms to Clinical Applications. *Int J Biol Sci*, 19(11), 3341-3359. <https://doi.org/10.7150/ijbs.82317>
- Yao, J., Kim, T. W., Qin, J., Jiang, Z., Qian, Y., Xiao, H., Lu, Y., Qian, W., Gulen, M. F., & Sizemore, N. (2007). Interleukin-1 (IL-1)-induced TAK1-dependent versus MEKK3-dependent NFκB activation pathways bifurcate at IL-1 receptor-associated kinase modification. *Journal of Biological Chemistry*, 282(9), 6075-6089.
- Yao, J., Weng, Y., Yan, S., Hou, M., Wang, H., Shi, Q., & Zuo, G. (2015). NOV inhibits proliferation while promoting apoptosis and migration in osteosarcoma cell lines through p38/MAPK and JNK/MAPK pathways. *Oncology reports*, 34(4), 2011-2021.
- Ye, R. D. (2001). Regulation of nuclear factor κB activation by G-protein-coupled receptors. *Journal of leukocyte biology*, 70(6), 839-848.
- Yin, X., Liu, Z., Zhu, P., Wang, Y., Ren, Q., Chen, H., & Xu, J. (2019). CXCL12/CXCR4 promotes proliferation, migration, and invasion of adamantinomatous craniopharyngiomas via PI3K/AKT signal pathway. *Journal of cellular biochemistry*, 120(6), 9724-9736.
- Yu, L., Cecil, J., Peng, S.-B., Schrementi, J., Kovacevic, S., Paul, D., Su, E. W., & Wang, J. (2006). Identification and expression of novel isoforms of human stromal cell-derived factor 1. *Gene*, 374, 174-179.
- Yu, P., Huang, Y., Xu, C., Lin, L., Han, Y., Sun, W., Hu, G., Rabson, A., Wang, Y., & Shi, Y. (2017). Downregulation of CXCL12 in mesenchymal stromal cells by TGFβ promotes breast cancer metastasis. *Oncogene*, 36(6), 840-849.
- Yu, Z., Han-Bo, C., Wen-Jun, L., & Li, Z. (2018). The CXCL12 (SDF-1)/CXCR4 chemokine axis: Oncogenic properties, molecular targeting, and synthetic and natural product CXCR4 inhibitors for cancer therapy. *Chinese journal of natural medicines*, 16(11), 801-810.
- Zabel, B. A., Wang, Y., Lewén, S., Berahovich, R. D., Penfold, M. E., Zhang, P., Powers, J., Summers, B. C., Miao, Z., Zhao, B., Jalili, A., Janowska-Wieczorek, A., Jaen, J. C., & Schall, T. J. (2009). Elucidation of CXCR7-mediated signaling events and inhibition of CXCR4-mediated tumor cell transendothelial migration by CXCR7 ligands. *J Immunol*, 183(5), 3204-3211. <https://doi.org/10.4049/jimmunol.0900269>

- Zhang, M., Qiu, L., Zhang, Y., Xu, D., Zheng, J. C., & Jiang, L. (2017). CXCL12 enhances angiogenesis through CXCR7 activation in human umbilical vein endothelial cells. *Scientific Reports*, 7(1), 8289.
- Zhang, W., Borchering, N., & Kolb, R. (2020). IL-1 signaling in tumor microenvironment. *Tumor Microenvironment: The Role of Interleukins—Part A*, 1-23.
- Zhang, Y., Wang, S.-S., Tao, L., Pang, L.-J., Zou, H., Liang, W.-H., Liu, Z., Guo, S.-L., Jiang, J.-F., & Zhang, W.-J. (2019). Overexpression of MAP3K3 promotes tumour growth through activation of the NF- κ B signalling pathway in ovarian carcinoma. *Scientific Reports*, 9(1), 8401.
- Zhang, Z. Y., Li, S. Z., Zhang, H. H., Wu, Q. R., Gong, J., Liang, T., Gao, L., Xing, N. N., Liu, W. B., Du, R. L., & Zhang, X. D. (2015). Stabilization of ATF5 by TAK1-Nemo-like kinase critically regulates the interleukin-1 β -stimulated C/EBP signaling pathway. *Mol Cell Biol*, 35(5), 778-788. <https://doi.org/10.1128/mcb.01228-14>
- Zhao, H., Guo, L., Zhao, H., Zhao, J., Weng, H., & Zhao, B. (2014). CXCR4 over-expression and survival in cancer: a system review and meta-analysis. *Oncotarget*, 6(7), 5022.
- Zhao, X., Wu, Q., Gong, X., Liu, J., & Ma, Y. (2021). Osteosarcoma: a review of current and future therapeutic approaches. *BioMedical Engineering OnLine*, 20(1), 24. <https://doi.org/10.1186/s12938-021-00860-0>
- Zhou, W., Guo, S., Liu, M., Burow, M. E., & Wang, G. (2019). Targeting CXCL12/CXCR4 Axis in Tumor Immunotherapy. *Curr Med Chem*, 26(17), 3026-3041. <https://doi.org/10.2174/0929867324666170830111531>
- Zinatizadeh, M. R., Schock, B., Chalbatani, G. M., Zarandi, P. K., Jalali, S. A., & Miri, S. R. (2021). The Nuclear Factor Kappa B (NF- κ B) signaling in cancer development and immune diseases. *Genes & diseases*, 8(3), 287-297.
- Zlotnik, A., & Yoshie, O. (2000). Chemokines: a new classification system and their role in immunity. *Immunity*, 12(2), 121-127.
- Zou, W., Machelon, V., Coulomb-L'Hermin, A., Borvak, J., Nome, F., Isaeva, T., Wei, S., Krzysiek, R., Durand-Gasselin, I., & Gordon, A. (2001). Stromal-derived factor-1 in human tumors recruits and alters the function of plasmacytoid precursor dendritic cells. *Nature medicine*, 7(12), 1339-1346.

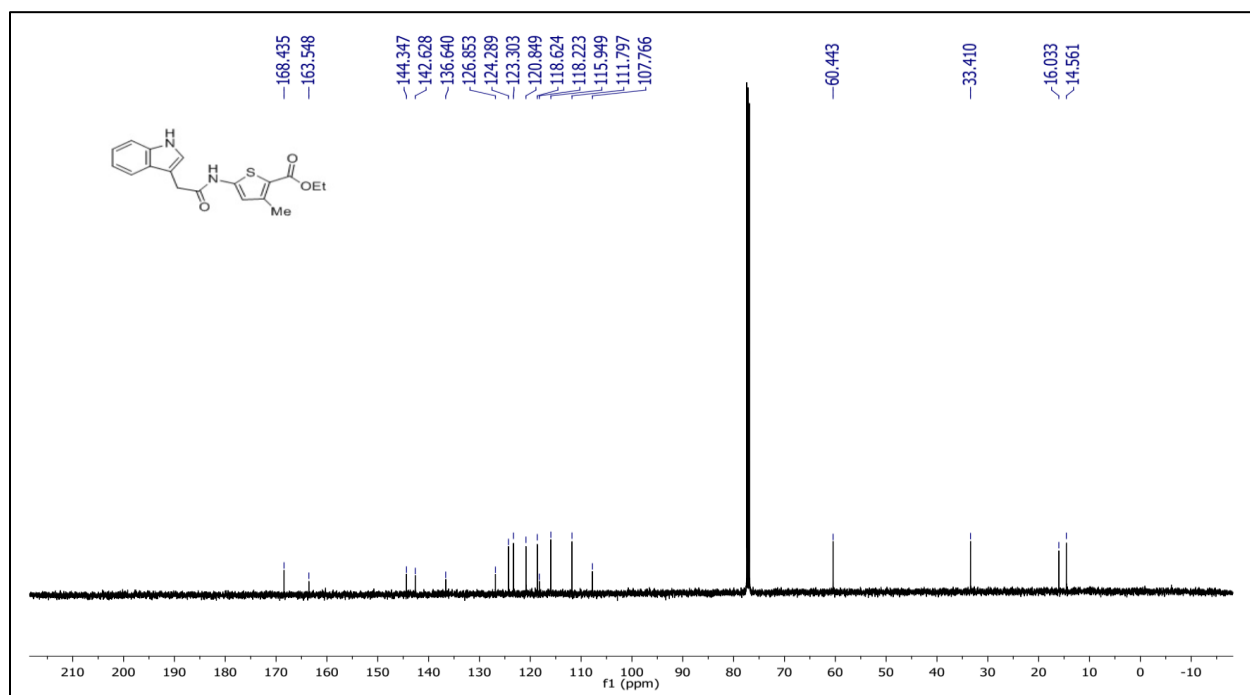
Appendix Seven

NMR and IR Data for KM Compounds and AMG548

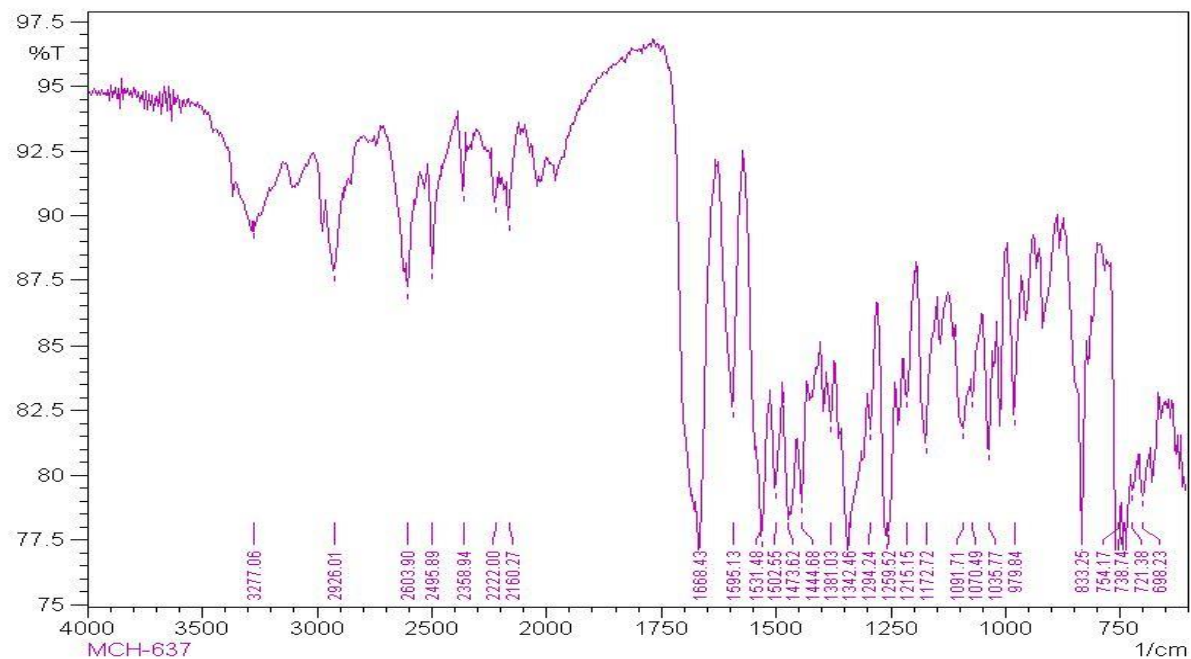
7.1 NMR and IR data for KM6



7.1.1 ¹H NMR for KM6

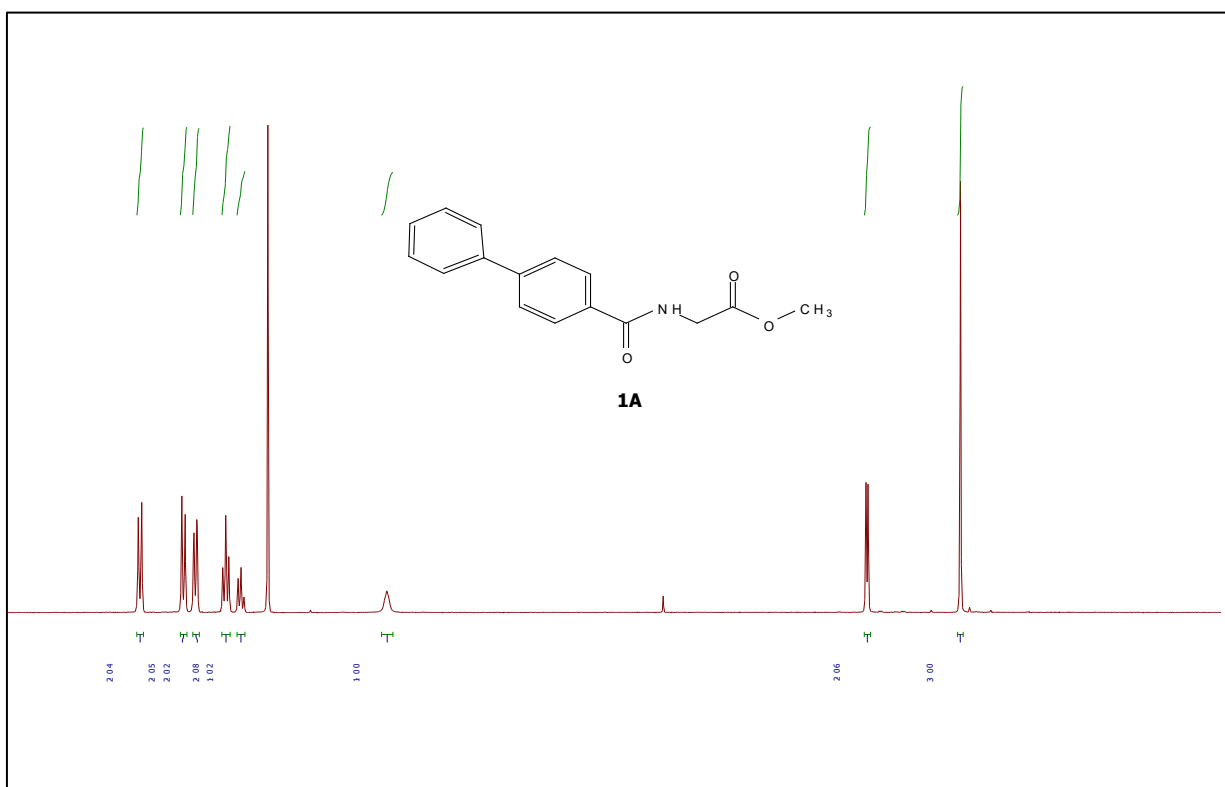


7.1.2 ¹³C NMR for KM6

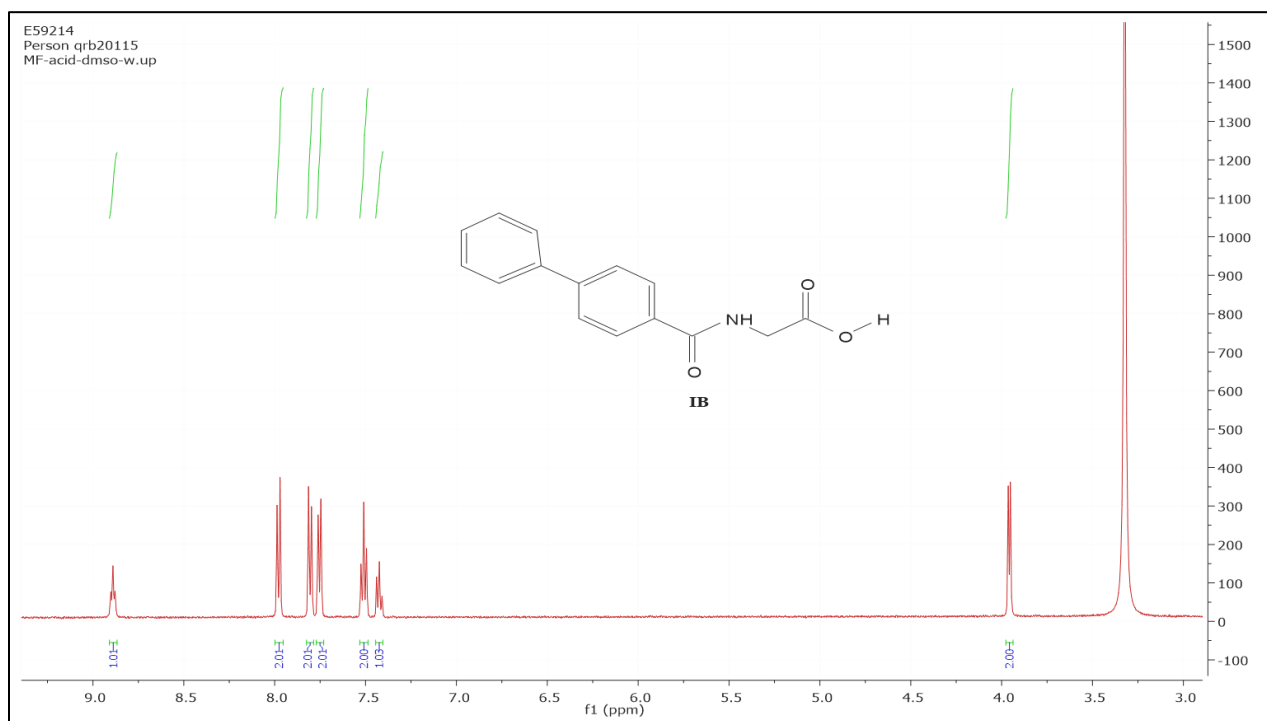


7.1.3 IR for KM6

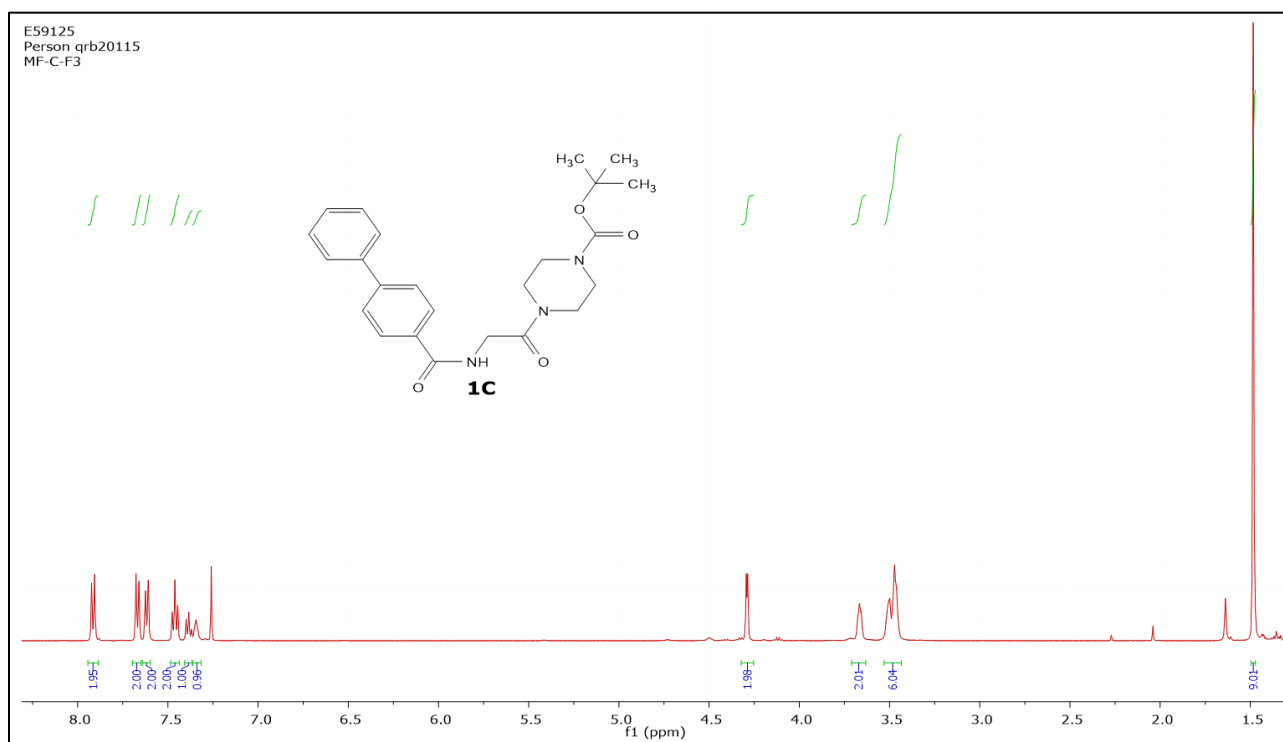
7.2 NMR and IR data for KM10



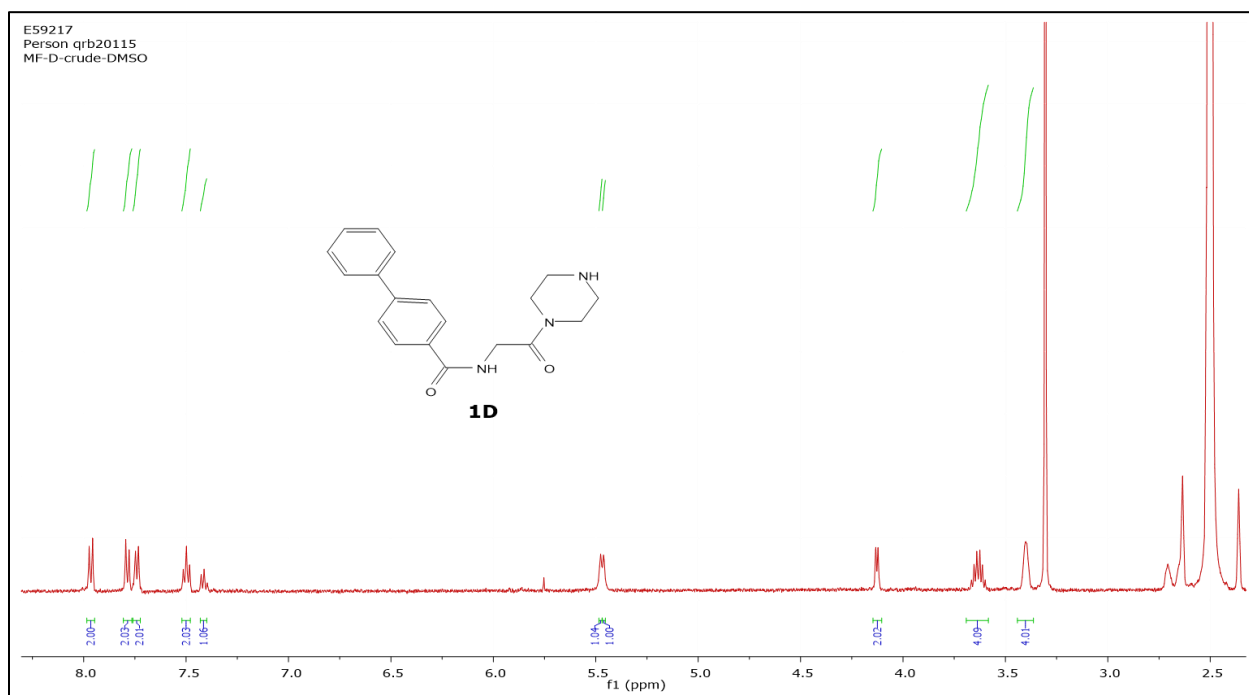
7.2.1 ¹H NMR of Compound 1A



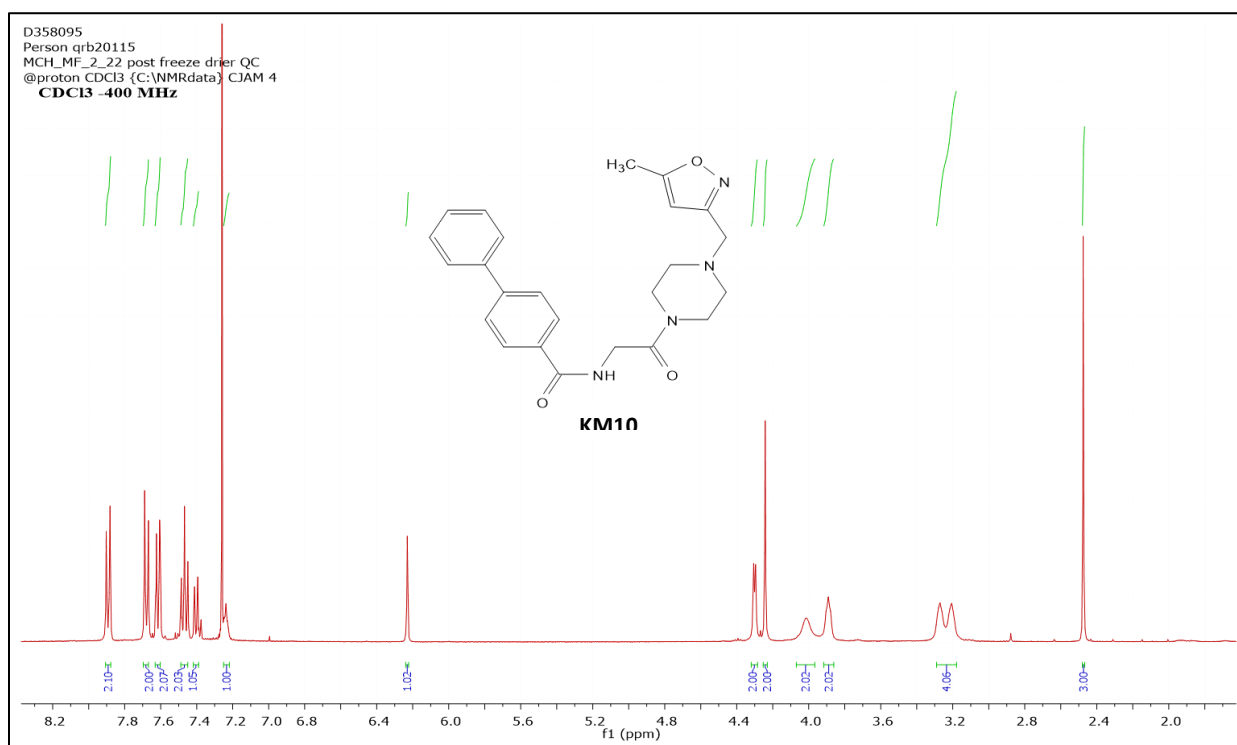
7.2.2 ¹H NMR of Compound 1B



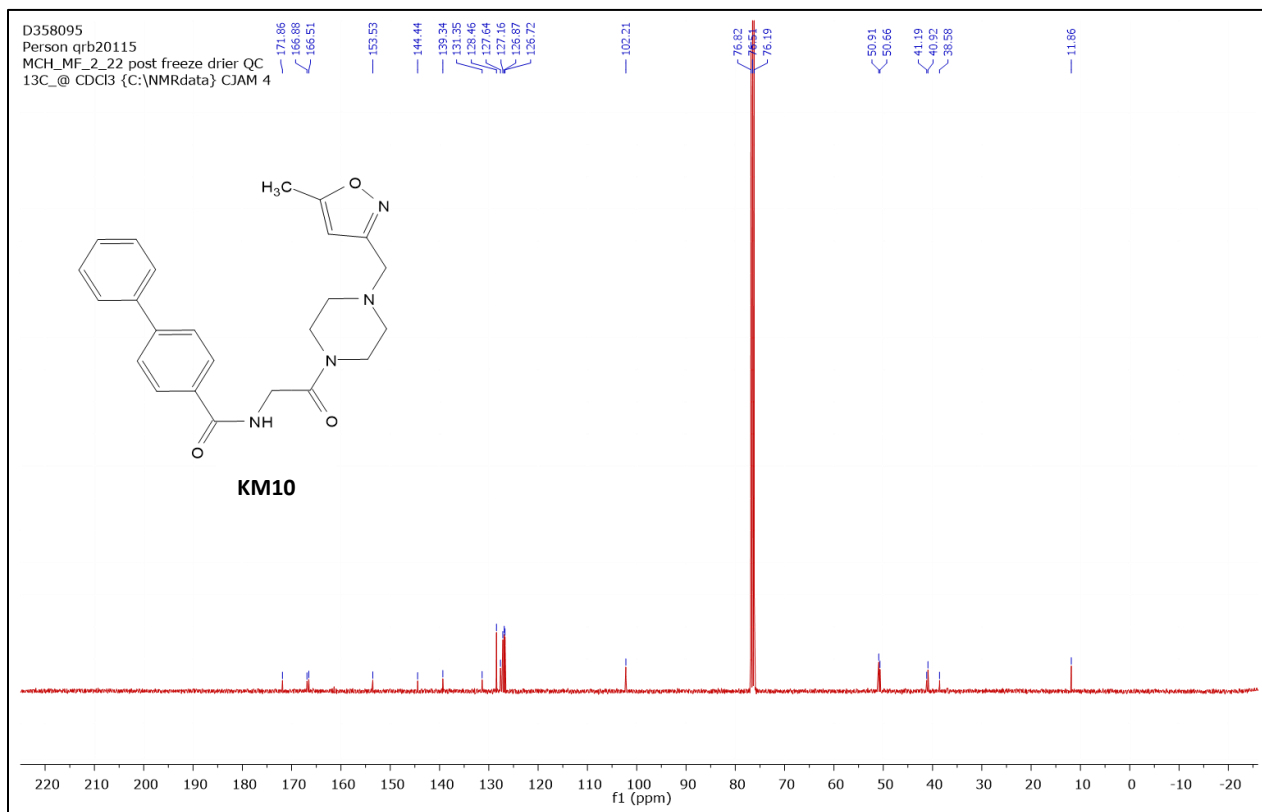
7.2.3 ¹H NMR of Compound 1C



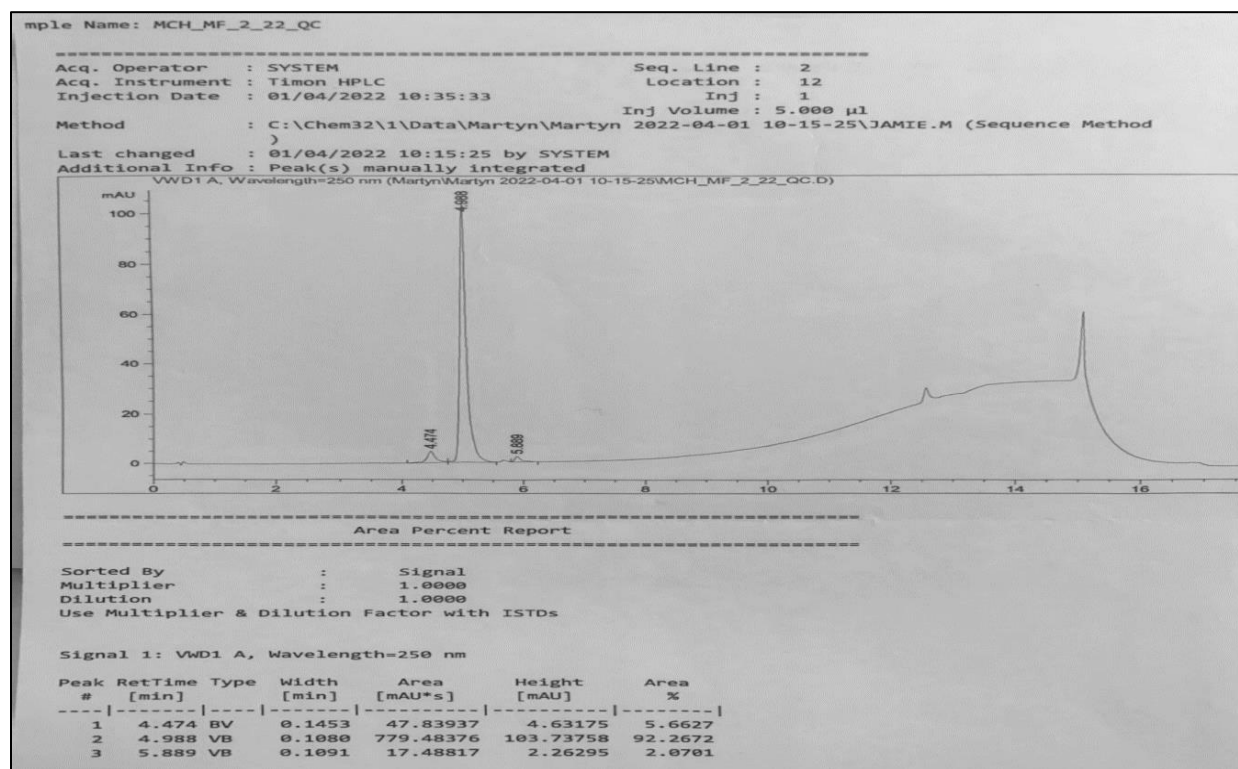
7.2.4 ¹H NMR of Compound 1D



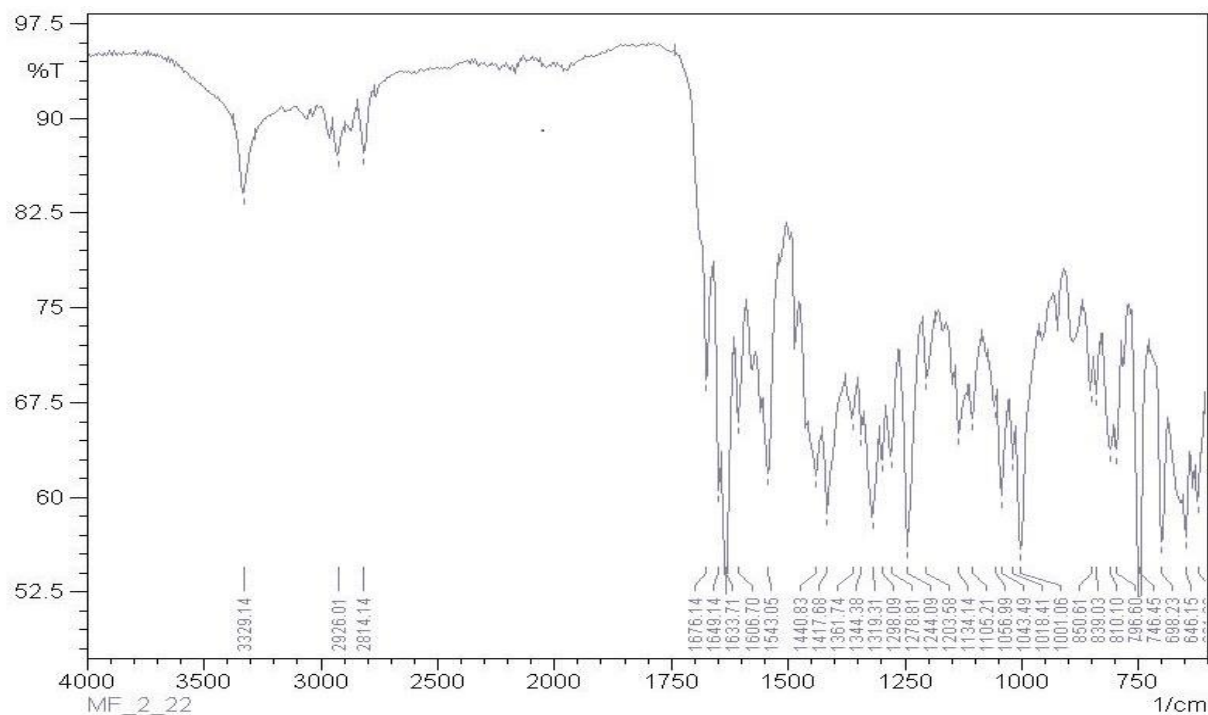
7.2.5 ¹H NMR for KM10



7.2.6 ¹³C NMR for KM10

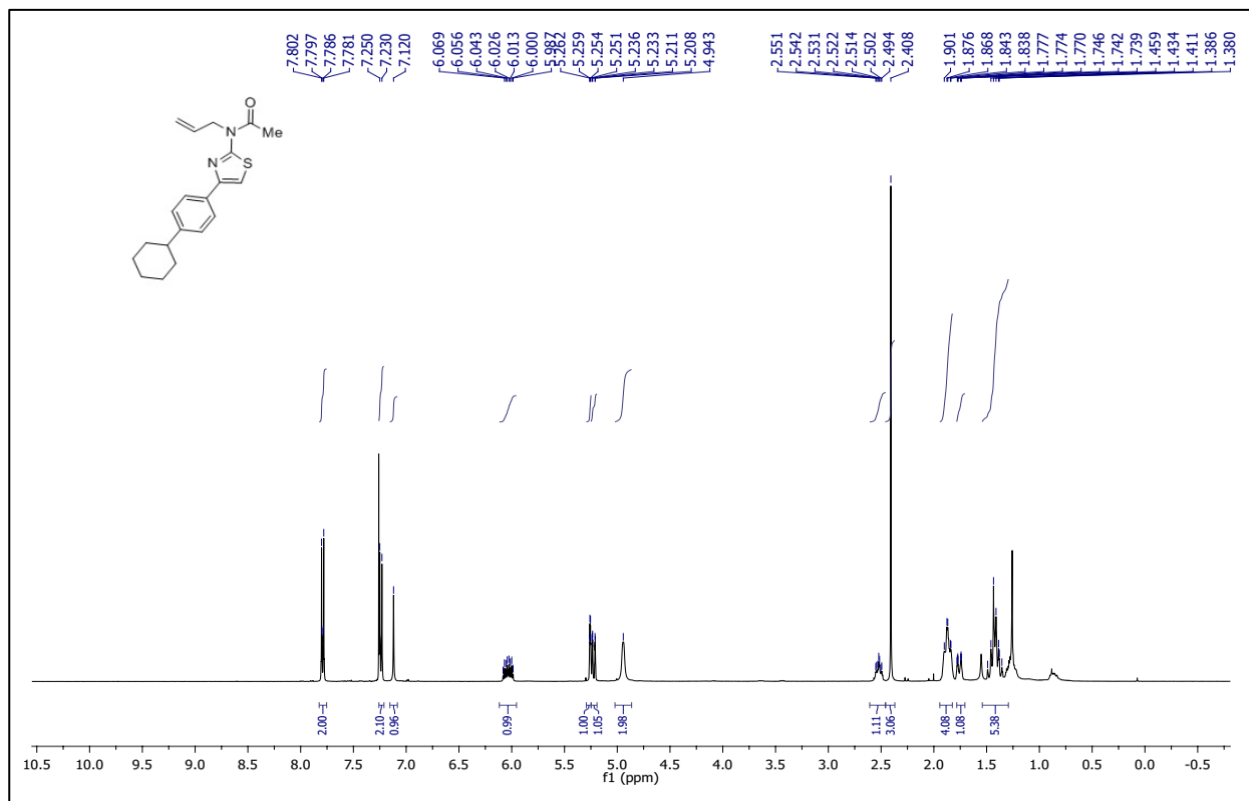


7.2.7 HPLC for KM10

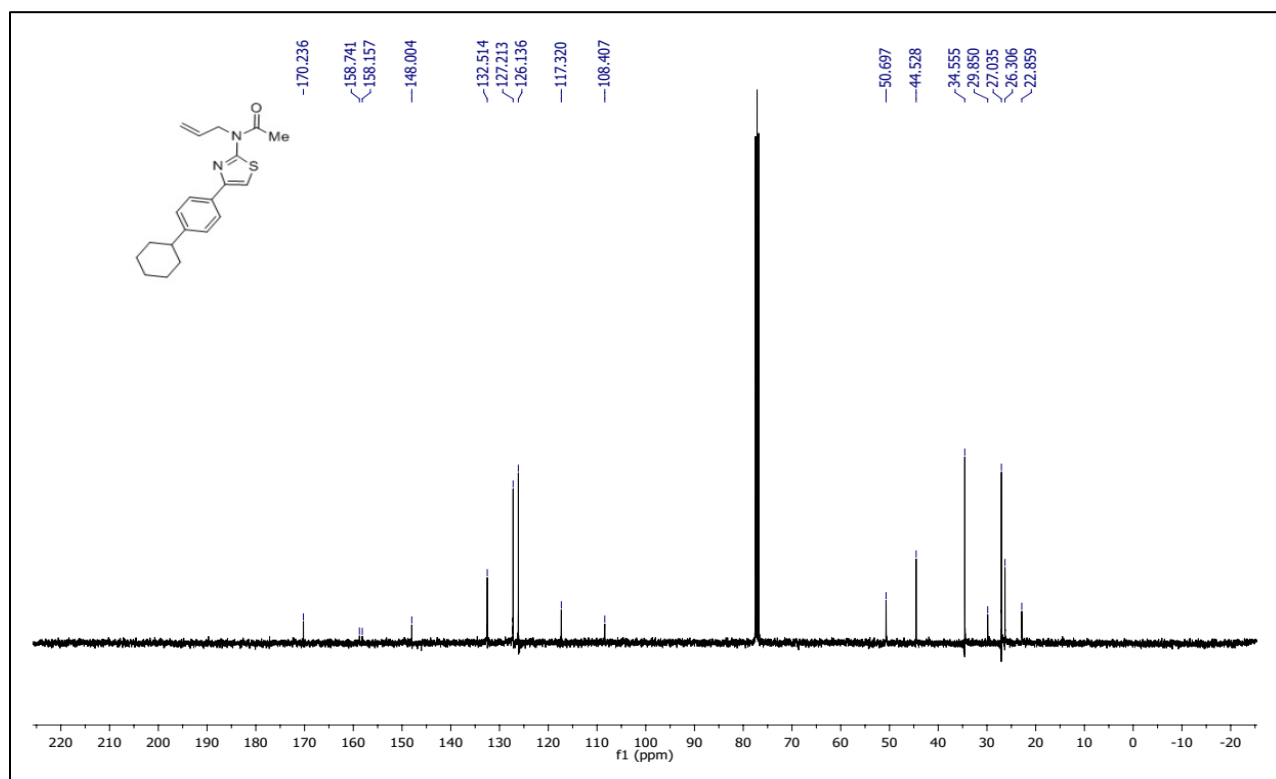


7.2.8 IR for KM10

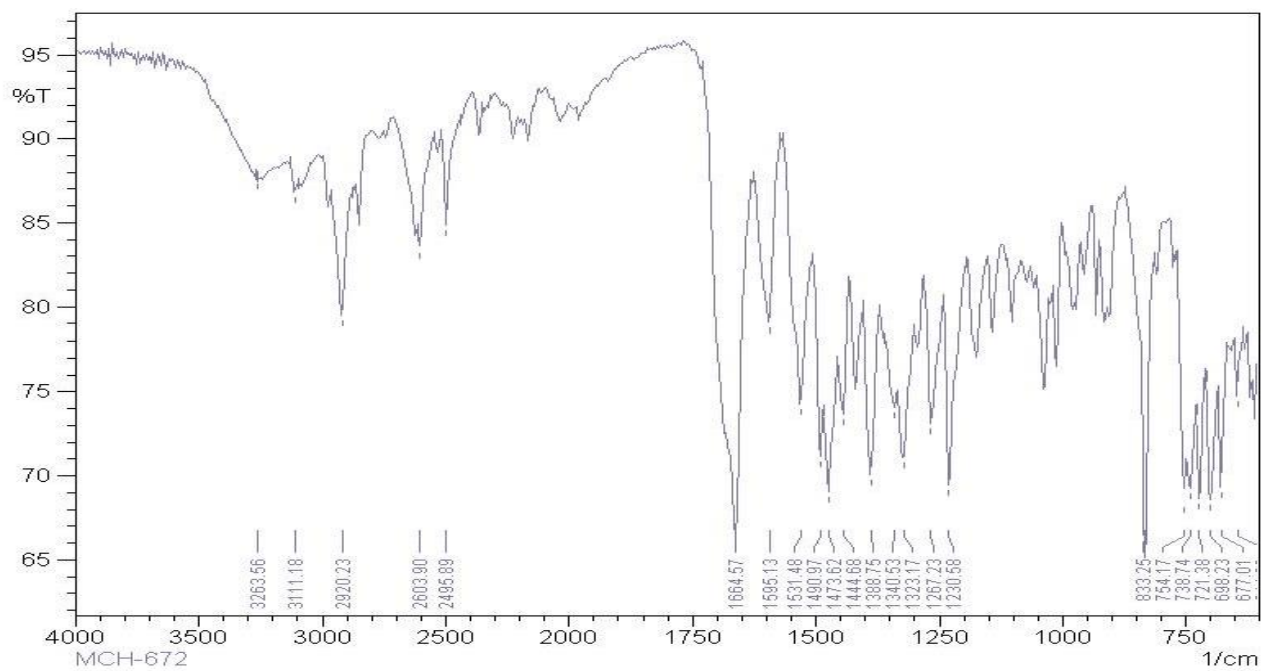
7.3 NMR and IR data for KM11



7.3.1 ¹H NMR for KM11

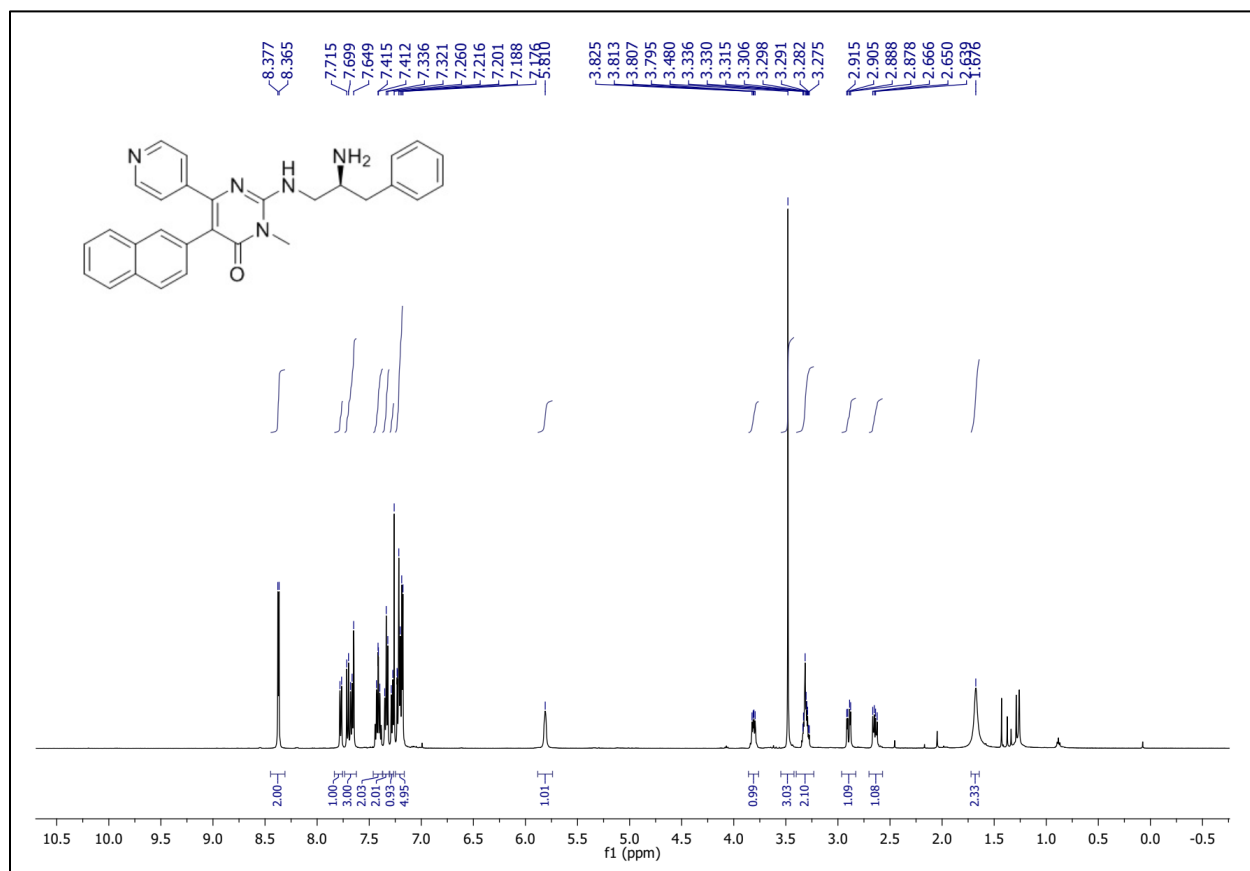


7.3.2 ¹³C NMR for KM11

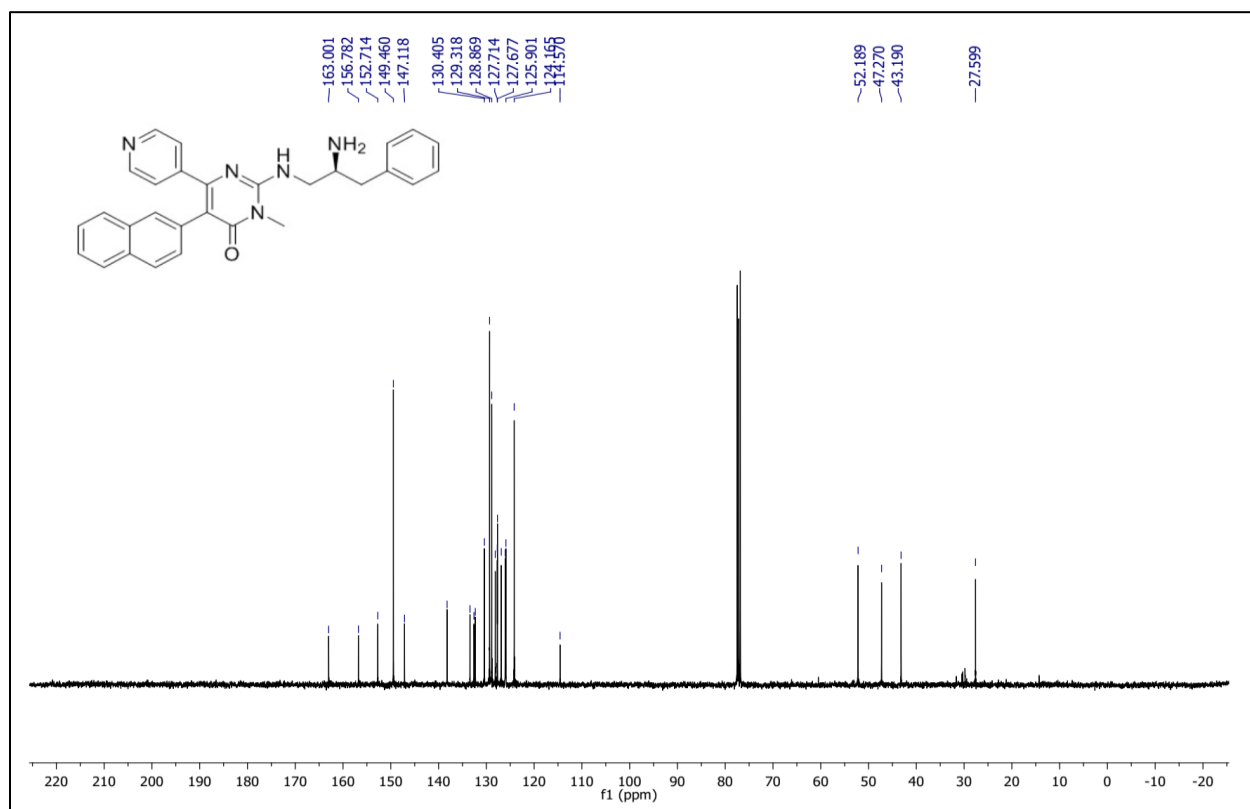


7.3.3 IR for KM11

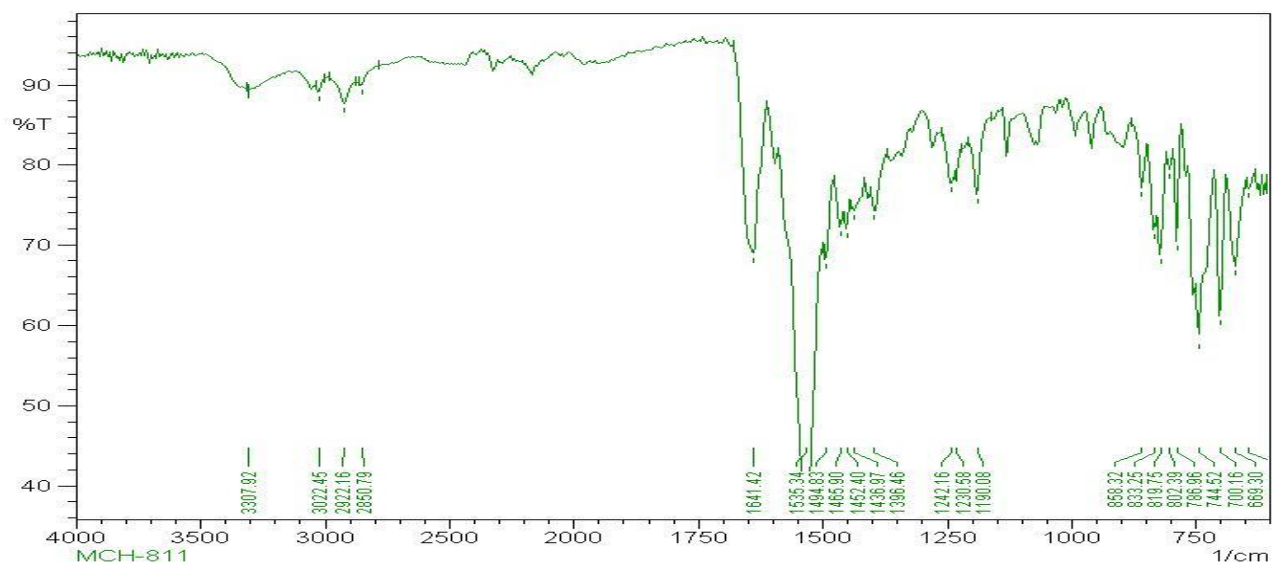
7.4 NMR and IR data for AMG-548



7.4.1 ¹HNMR for AMG-548



7.4.2 ¹³CNMR for AMG-548



7.4.3 IR for AMG-548